首都大学東京 博士 (理学) 学位論文 (課程博士)

論文名 フィリピンにおける総観スケールから十年スケールまでの降雨変動に関する気候学的研究（英文）

著者　リンドン マーク パヤナイ オラゲラ

審査担当者

主査

委員

委員

上記の論文を合格と判定する

平成　　年　　月　　日

首都大学東京大学院都市環境科学研究科教授会

研究科

DISSERTATION FOR A DEGREE OF

DOCTOR OF PHILOSHOPHY (SCIENCE)

TOKYO METROPOLITAN UNIVERSITY

TITLE: A climatological study of the rainfall variability in the Philippines: from synoptic to decadal-scale aspects

AUTHOR: Lyndon Mark P. OLAGUERA

EXAMINED BY

Chief examiner:

Examiner:

Examiner:

QUALIFED BY THE GRADUATE SCHOOL OF

URBAN ENVIROMENT SCIENCES

TOKYO METROPOLITAN UNVERSITY

Dean:

Date:

A Climatological Study of the Rainfall Variability in the Philippines: from Synoptic to Decadal-Scale Aspects

Lyndon Mark P. OLAGUERA

Department of Geography

Graduate School of Urban and Environmental Sciences

Tokyo Metropolitan University

September 2019

Table of Contents

List of Figures

the topography of the Philippines. The open circles are the stations used by PAGASA in their operational onset, while the stars are the three additional stations used for discussion in this study. The black crosses indicate the seven stations used for the monsoon break detection.

Figure 3.2. Annual variations of daily rainfall climatology (1998–2012) for: (a) Basco; (b) Vigan; (c) Laoag; (d) Baguio; (e) Cabanatuan; (f) Dagupan; (g) Science Garden; and (h) Coron. The red solid line represents the smoothed curve obtained by adding the first 18 Fourier harmonics of the daily rainfall time series.

Figure 3.3. Spatial distribution of the lag composites of TRMM rainfall (mm day^{-1}; shaded), 850 hPa *HGT* (HGT_{850hPa}; m; contours), and 850 hPa winds ($WINDS_{850hPa}$; m s^{-1}; vectors) for: (a) Lag –20; (b) Lag –12; (c) Lag –5; (d) Lag 0; (e) Lag +5; (f) Lag +7; (g) Lag +12; and (h) Lag +18. The scale of the wind vectors is 5 m s^{-1}. The contour interval of the HGT_{850hPa} is 5 m between 1, 500 and 1, 520 m.

Figure 3.4. As in Fig. 3.3 but for the 200 hPa winds ($WINDS_{200hPa}$; vectors; m s^{-1}) and 200 hPa geopotential height (HGT_{200hPa}) only. The scale of the wind vectors is 20 m s^{-1}. The contour interval of the HGT_{200hPa} is 10 m, between 12, 470 and 12, 500 m.

Figure 3.5. As in Fig. 3.3 but for the 500 hPa vertical velocity ($\times 10^{-2}$ Pa s^{-1}). The contour interval is 2×10^{-2} Pa s^{-1}.

Figure 3.6. Time series of: (a) vertically integrated moisture flux convergence (*VIMFC*; orange line; $\times 10^{-6}$ kg m^{-2} s^{-1}) and zonal wind at 850 hPa (U_{850hPa}; green line; m s^{-1}) over Luzon Island (120–122.5°E., 12.5–22°N). (b) As in (a) but for the geopotential height (HGT_{850hPa}; blue lines; m) and vertical zonal wind shear (*USHEAR*; U_{200hPa} minus U_{850hPa}; red line; m s^{-1}). The solid horizontal line in (a) indicates the 0

VIMFC and U_{850hPa}. The solid horizontal line in (b) indicates the 1, 500-m HGT_{850hPa} and 0 *USHEAR*. Shaded lag days indicate the monsoon break period.

Figure 3.7. (a) As in Fig. 3.6a but for the perturbation kinetic energy (*PKE*; $m^2\ s^{-2}$) only. (b) As in Fig.3.3 but for Lag –2 only.

Figure 3.8. (a) Time series of mean sea level pressure (*MSLP*; hPa; red line) and net shortwave radiation (*NSWR*; W m^{-2}; blue line) over Luzon Island (120–122.5°E, 12.5–22°N). (b) As in (a) but for the temperature at 850 hPa only ($TEMP_{850hPa}$; K). Shaded lag days indicate the monsoon break period.

Figure 3.9. Schematic diagram illustrating the three-phase onset process of the summer monsoon over the Philippines: (a) Phase I (Onset Phase; mid to late May); (b) Phase II (Break Phase; early June); and (c) Phase III (Monsoon Revival Phase; mid-June). Phases I, II, and III correspond to the periods before and during Lag –12, Lag 0 to Lag +5, after Lag +5, in Figs. 3.3, 3.4, and 3.5, respectively. Stippled areas correspond to dry areas. The red broken line and "A" indicates the location of the anticyclonic circulation at 200 hPa.

Figure 4.1. Horizontal winds at 925 hPa ($WINDS_{925hPa}$; shades and contours; m s^{-1}) on: (a) 06 UTC January 16, 2017; and (b) its corresponding climatology (06 UTC January 16; 1981–2010). Anomalies of the 925 hPa: (c) zonal (U_{925hPa}; shades and contours; m s^{-1}); and (d) meridional (V_{925hPa}; shades and contours; m s^{-1}) winds. Shadings in (a) and (b) indicate the magnitude of the $WINDS_{925hPa}$. The contour interval in (c) and (d) is 2 m s^{-1}.

Figure 4.2. Surface weather charts provided by the Japan Meteorological Agency for: (a) 06 UTC January 15, 2017; (b) 12 UTC January 15, 2017; (c) 18 UTC January 15,

2017; (d) 00 UTC January 16, 2017; (e) 06 UTC January 16, 2017; and (f) 12 UTC January 16, 2017.

Figure 4.3. As in Fig. 4.2 but for the distribution of rainfall from the Tropical Rainfall Measuring Mission (TRMM) 3B42 version 7 (shades; mm hr^{-1}) and 925 hPa winds ($WINDS_{925hPa}$; streams; m s^{-1}). The cyclonic and anticyclonic circulations are denoted as "C" and "A", respectively.

Figure 4.4. Spatial distribution of the 925 hPa: (a) meridional equivalent potential temperature gradient (θe_{925hPa}; shades; × 10^{-5} K s^{-1}); (b) stretching deformation (STD_{925hPa}; shades; × 10^{-5} s^{-1}); (c) shearing deformation (SHD_{925hPa}; shades; × 10^{-5} s^{-1}); and (d) total deformation ($TDef_{925hPa}$; shades; × 10^{-5} s^{-1}) on 06 UTC January 16, 2017. The 925 hPa wind anomalies (streams; m s^{-1}) are superimposed for discussion. The black star indicates the location of the deformation zone. The "A" and "C" are similar to those in Fig. 4.3.

Figure 4.5. Spatial distribution of vertically integrated moisture flux convergence (Q; shades; ×10^{-4} kg m^{-2} s^{-1}), velocity potential (χ_Q; contours; × 10^6 kg s^{-1}), and the divergent component of Q (Q_D; vectors; kg m^{-1} s^{-1}) for: (a) 18 UTC January 15, 2017; (b) 00 UTC January 16, 2017; (c) 06 UTC January 16, 2017; and (d) 12 UTC January 16, 2017. The contour interval of χ_Q is 100 × 10^6 kg s^{-1}, while the scale of the vectors is 1000 kg m^{-1} s^{-1}.

Figure 4.6. Vertical profile of the equivalent potential temperature anomaly (shades; K) and relative humidity anomaly (contours; %) averaged from 122–127°E for: (a) 12 UTC January 15, 2017; (b) 18 UTC January 15, 2017; (c) 00 UTC January 16, 2017; (d) 06 UTC January 16, 2017; (e) 12 UTC January 16, 2017; and (f) 18 UTC January

16, 2017. The vectors are the meridional and vertical velocity anomalies (m s^{-1}; scale is 20 m s^{-1}). The anomalies are relative to the 1981–2010 mean.

Figure 4.7. The location of the 34 non-tropical cyclone related heavy rainfall/flood (HRF) events from November to March over the Philippines from 1979–2017 based on the Dartmouth Flood Observatory archive.

Figure 4.8. Lag composite anomalies of mean sea level pressure (shades; hPa), 925 hPa winds (streams; m s^{-1}) for: (a) Lag –3; (b) Lag 0; (c) Lag +1; (d) Lag +3; (e) Lag +5; and (f) Lag +15. Lag 0 refers to the time when the area-averaged vertically integrated moisture flux convergence (*VIMFC*) of the recorded HRF event over Mindanao Island is maximum. Note that the reanalysis data is 6-hourly so that Lag –3 (+3) means 18 hours before (after) the peak *VIMFC*.

Figure 4.9. Composite anomalies of: (a) 925 hPa meridional wind (V_{925hPa}; shades and contours; m s^{-1}); and (b) 925 hPa zonal winds (U_{925hPa}; shades and contours; m s^{-1}) averaged from 122–127.5°E. The contour interval is 0.5 m s^{-1}.

Figure 4.10. Spatial distribution of composite anomalies of vorticity tendency (ζ_t; $\times 10^{-10}$ s^{-2}), its advection term (ζ_{adv}; $\times 10^{-10}$ s^{-2}), and stretching term ($\zeta_{stretch}$; $\times 10^{-10}$ s^{-2}) for: Lag –3 (a, b, c); Lag 0 (d, e, f); and Lag +1 (g, h, i), respectively. The 925 hPa wind anomalies (m s^{-1}) are superimposed for discussion.

Figure 4.11. As in Fig. 4.10 but for: Lag +3 (a, b, c); Lag +5 (d, e, f); and Lag +15 (g, h, i).

Figure 4.12. Schematic diagram of the possible mechanism leading to the winter HRF over the Mindanao Island (southern Philippines). The cyclonic and anticyclonic

circulations are denoted as “C” and “A”, respectively. The dot-dashed line indicates the location of the shearline.

Figure 5.1. Location of the seven meteorological stations of the Philippine Atmospheric, Geophysical and Astronomical Services Administration (PAGASA; blue circles), Climate Prediction Center Merged Analysis of Precipitation (CMAP) grid points (+ markings), and the topography of the Philippines above 250 m (gray contour lines). The contour interval of the topography is 250 m. The red triangles indicate the nearest five CMAP grid points to the location of the PAGASA stations.

Figure 5.2. Rainfall distribution (mm day^{-1}) from 1979–2008 averaged across the: (a) seven PAGASA stations; and (b) five nearest CMAP grid points to the PAGASA stations. The rainfall distributions are smoothed by 1–2–1 filter in both x- and y-axis. The two vertical lines in (a) and (b) indicates P25 (start of May) and P29 (climatological summer monsoon onset based on Akasaka, 2010), respectively. The horizontal lines in (a) and (b) indicate 1994.

Figure 5.3. (a) Smoothed (1–2–1 filter) pentad-mean rainfall between ES1 (1979–1993) and ES2 (1994–2008) averaged across the seven PAGASA stations on the western coast of the Philippines; and (b) their epochal difference. Shaded pentads in (a) and gray bars in (b) indicate statistically significant difference above the 95 % confidence level using the Student’s *t*-test.

Figure 5.4. (a) Pentad-mean rainfall time series during 1992 (black line; mm day^{-1}) and its equivalent smoothed time series (blue line) obtained by adding the first four Fourier harmonics of the original time series; and (b) time series of annual peak pentads, defined as the maximum of the smoothed time series, from 1979 to 2008.

Figure 5.5. Epochal difference (ES2 minus ES1) in the spatially smoothed (1–2–1 filter; both longitudinal and latitudinal direction) CMAP rainfall (mm day^{-1}) during P45–P50. Cross (+) markings indicate statistical significance at the 95 % confidence level.

Figure 5.6. Time series of area-averaged vertically integrated moisture flux divergence (*VIMFD*; $\times 10^{-4}$ kg m^{-2} s^{-1}) over 117.5–122.5°E and 10–20°N during P45–P50. The blue (red) line is the unfiltered (1–2–1 filtered) time series. Dashed horizontal lines indicate the epochal means.

Figure 5.7. Smoothed (1–2–1 filter) vertically integrated moisture flux (*VIMF*; vectors; kg m^{-1} s^{-1}), moisture flux divergence (*VIMFD*; shades; $\times 10^{-4}$ kg m^{-2} s^{-1}), and 850 hPa geopotential height (HGT_{850hPa}; contours; m) for P45–P50 during: (a) ES1 (1979–1993); (b) ES2 (1994–2008); and their (c) epochal difference (ES2 minus ES1). (a–c) The contour interval is 10 m. Shaded areas, black arrows, and purple contours in (c) indicate statistical significance at the 95 % confidence level. The scale of the vectors is indicated on the lower-left corner of each figure.

Figure 5.8. Epochal difference (1994–2008 minus 1979–1993) in smoothed (1–2–1 filter): (a) 850 hPa relative vorticity ($\times 10^{-6}$ s^{-1}); and (b) 850 hPa zonal winds (U_{850hPa}; m s^{-1}). Cross (+) markings indicate statistical significance at the 95 % confidence level.

Figure 5.9. Tropical cyclone (TC) track frequency (per year) in P45–P50 interpolated onto a 5° × 5° grid for: (a) ES1 (1979–1993); and (b) ES2 (1994–2008) based on JTWC track dataset. As in (a) but for TC tracks and location of 5, 870-m contour line of the 500 hPa geopotential height (HGT_{500hPa}; dashed blue line) for: (c) ES1 and (d) ES2. Dashed boxes in (a) and (b) indicates the Philippine Area of Responsibility (PAR;

115–135°E and 5–25°N). The genesis locations in (c) and (d) are indicated by the red markings.

Figure 5.10. As in Fig. 5.5 but for: (a) 500 hPa vertical velocity (ω; $\times 10^{-2}$ Pa s^{-1}); (b) 700 hPa relative humidity (*RHUM*; %); (c) vertical zonal wind shear ($U_{200\text{hPa}}$ minus $U_{850\text{hPa;}}$ m s^{-1}); and (d) 850 hPa perturbation kinetic energy (*PKE*; m^2 s^{-2}). Cross (+) markings indicate statistical significance at the 95 % confidence level.

Figure 5.11. Schematic diagram showing the possible mechanism leading to the decrease in rainfall over the Philippines from early August to early September occurring in the mid-1990s (1993/1994).

Figure 5.12. Epochal difference (1994–2008 minus 1979–1993) in smoothed sea surface temperature (SST; °C) during: (a) June; (b) July; (c) August; and (d) September. Dotted areas indicate statistical significance at the 95 % confidence level by Student's *t*-test. The SST data came from monthly Hadley Center sea ice and sea surface temperature data set (HadISST version 1.1; Rayner *et al*., 2003).

Figure 5.13. Epochal difference (1994–2008 minus 1979–1993) in smoothed (1–2–1 filter) 200 hPa winds (U_{200hPa}). Bold vectors are statistically significant at the 95 % confidence level by Student's *t*-test.

Figure 6.1. The location of the 32 stations from the Philippine Atmospheric, Geophysical and Astronomical Serviced Station (PAGASA) and the topography of the Philippines (shades; m). The colors of the circles indicate the climate types based on Villafuerte *et al*. (2017).

Figure 6.2. Average monthly rainfall (mm day^{-1}) distribution of the stations that belong to: (a) Climate Type I; (b) Climate Type II; and (c) Climate Type III from the period

1961 to 2008. The black solid line in each figure represents the mean rainfall time series of the different stations in each climate type.

Figure 6.3. Time series of average monthly rainfall (mm day^{-1}) of Climate Type II stations from 1961 to 2008 for: (a) November; (b) December; (c) January; (d) February; and (e) March. The red vertical lines in (b) indicate the significant change points around 1976/1977 and 1992/1993 that divides the time series into three epochs: EW1 (1961–1976); EW2 (1977–1992); and EW3 (1993–2008). The green line indicates the 9-year running average.

Figure 6.4. Time series of tau statistics from the moving Student's *t*-test with varying time windows for: (a) November; (b) December; (c) January; (d) February; and (e) March. The horizontal lines from (a) to (e) indicate the statistical significance at the 95 % and 99 % confidence level for each time window. The red vertical lines in (b) indicate the significant change points around 1976/1977 and 1992/1993 that divides the time series into three epochs: EW1 (1961–1976); EW2 (1977–1992); and EW3 (1993–2008).

Figure 6.5. Differences in interpolated rainfall (contours) during December between: (a) EW1 (1961–1976) and EW2 (1977–1992) (EW2 minus EW1); and (b) EW2 and EW3 (1993–2008) (EW3 minus EW2) across the 32 PAGASA stations (stars). Negative (positive) contours are indicated by dashed (solid) lines. The contour interval is 2 mm day^{-1}. Yellow shaded stars indicate a significant difference at the 95 % confidence level by bootstrapping. The stars with red outlines indicate the 13 stations with significant difference in both (a) and (b).

Figure 6.6. The epochal means of 850 hPa winds ($WINDS_{850hPa}$; streamlines; m s^{-1}), 850 hPa zonal winds (U_{850hPa}; shades; m s^{-1}), and 850 hPa geopotential height (HGT_{850hPa}; contours; m) during December for: (a) EW1 (1961–1976); (b) EW2 (1977–1992); and (c) EW3 (1993–2008). The contour interval is 10 meters.

Figure 6.7. The epochal difference in the vertically integrated moisture flux (*VIMF*; vectors; kg m^{-1} s^{-1}) and moisture flux divergence (*VIMFD*; shades; $\times 10^{-4}$ kg m^{-2} s^{-1}) during December between: (a) EW1 (1961–1976) and EW2 (1977–1992) (EW2 minus EW1); and (b) EW2 and EW3 (1993–2008) (EW3 minus EW2). Shaded areas and black vectors indicate statistical significance at the 95 % confidence level by Student's *t*-test. The scale of the wind vectors is indicated on the upper right corner in each plot.

Figure 6.8. Tropical cyclone (TC) track frequency (y^{-1}) interpolated onto a 5° × 5° grid during December, TC tracks (black lines), 600 hPa winds ($WINDS_{600hPa}$; gray streamlines; m s^{-1}), and 600 hPa geopotential height (HGT_{600hPa}; blue contours; m) for: EW1 (1961–1976; a, b); EW2 (1977–1992; c, d); and EW3 (1993–2008; e, f) based on the Joint Typhoon Warning Center (JTWC) track dataset. Dashed boxes in (a), (c), and (e) indicate the Philippine Area of Responsibility (PAR; 115–135°E and 5–25°N). The TC genesis locations in (b), (d), and (f) are indicated by the red markings.

Figure 6.9. Epochal mean of December sea surface temperature (SST; °C) above 26 °C during (a) EW1 (1961–1972); (b) EW2 (1977–1992); and (c) EW3 (1993–2008). The contour interval is 1 °C.

Figure 6.10. Spatial distribution of the mean 850 hPa perturbation kinetic energy (*PKE*; m^2 s^{-2}) during December for: (a) EW1 (1961–1976); (b) EW2 (1977–1992); and (c) EW3 (1993–2008). Epochal difference in *PKE* between (d) EW1 and EW2 (EW2

minus EW1) and (e) EW2 and EW3 (EW3 minus EW2). The contour interval from (a) to (c) is 2 m. Cross markings in (d) and (e) indicate a significant difference at the 95 % confidence level using the Student's *t*-test.

Figure 6.11. Epochal difference in 500 hPa vertical velocity ($\times 10^{-2}$ Pa s^{-1}; a, b), 700 hPa relative humidity (*RHUM*; %; c, d); and vertical zonal wind shear (U_{200hPa} minus U_{850hPa}; m s^{-1}; e, f) during December. Figures 6.11a, c, and e are the differences between EW1 (1961–1976) and EW2 (1977–1992) (EW2 minus EW1). Figures 6.11b, d, and f are the differences between EW2 and EW3 (1993–2008) (EW3 minus EW2). Cross markings indicate statistical significance at the 95 % confidence level using the Student's *t*-test.

Figure 6.12. Epochal difference in sea surface temperature (SST; °C) and 10-m winds ($WINDS_{10m}$; m s^{-1}) in December between: (a) EW1 (1961–1976) and EW2 (1977–1992) (EW2 minus EW1); (b) EW2 and EW3 (1993–2008) (EW3 minus EW2); and (c) EW3 and EW1 (EW3 minus EW1). Stippled areas and vectors in (a), (b), and (c) indicate significant difference at the 95 % confidence level using the Student's *t*-test. The scale of the arrows is indicated on the upper right corner of (a) and (b).

Figure 6.13. Schematic diagram showing the possible mechanisms leading to the decrease in rainfall during December during EW2 (1977–1992) over the Philippines. PDO: Pacific Decadal Oscillation.

Figure 6.14. As in Fig. 6.13 but for the increase in rainfall during EW3 (1993–2008). WNPSH: western North Pacific Subtropical High.

Figure 6.15. Time series of: (a) the December Pacific Decadal Oscillation (PDO); and (b) December SST anomaly (SSTA) over the Niño 3.4 region (5°S–5°N, 170°

E–120°W) from the period 1961 to 2008. The green line indicates the 9-year running average. The red vertical lines indicate the change points around 1976/1977 and 1992/1993 based on the December rainfall time series for reference discussion.

Figure 6.16. Epochal difference in mean sea level pressure (*MSLP*; hPa) during December between: (a) EW1 (1961–1976) and EW2 (1977–1992) (EW2 minus EW1); and (b) EW2 and EW3 (1993–2008) (EW3 minus EW2). Stippled areas indicate statistical significance at the 95 % confidence level using the Student's *t*-test. The boxes indicate the area averaging location for the East Asian winter monsoon index: Siberian high (SH), Aleutian low (AL), and Maritime Continent (MC) low.

Figure 6.17. Time series of the East Asian winter monsoon index (EAWMI) from 1961 to 2008 for: (a) November; (b) December; (c) January; (d) February; and (e) March. The red vertical lines indicate the change points around 1976/1977 and 1992/1993 based on the December rainfall time series for reference discussion. The green line indicates the 9-yr running average.

Figure 6.18. Composite anomalies of the mean sea level pressure (*MSLP*; shades; hPa) and 850 hPa winds ($WINDS_{850hPa}$; streamlines; m s^{-1}) during EW2 for: (a) November; (b) December; (c) January; (d) February; and (e) March. The anomalies are the deviations from the long-term means (1961–2008).

List of Tables

Acronyms

AGCM	Atmospheric General Circulation Model
AMIP	Atmospheric Model Intercomparison Project
APM	Asia Pacific Monsoon
ASM	Asian Summer Monsoon
BoB	Bay of Bengal
BSISO	Boreal Summer Intra-Seasonal Oscillation
CISO	Climatological Intra-Seasonal Oscillation
CMAP	Climate Prediction Center Merged Analysis of Precipitation
DOE	Department of Energy
EASM	East Asian Summer Monsoon
ENSO	El Niño-Southern Oscillation
GAME-IOP	Global Energy and Water Exchanges Asian Monsoon Experiment–Intensive Observation Period
HGT	Geopotential Height
ISO	Intra-Seasonal Oscillation
ISV	Intra-Seasonal Variability
ITCZ	Inter-tropical Convergence Zone
JJA	June-July-August
JMA	Japan Meteorological Agency
JRA55	Japan Meteorological Agency 55-year Reanalysis
JTWC	Joint Typhoon Warning Center
MJO	Madden Julian Oscillation
NCEP	National Centers for Environmental Prediction

NSWR	Net Shortwave Radiation
PAGASA	Philippine Atmospheric, Geophysical and Astronomical Services Administration
PAR	Philippine Area of Responsibility
PDO	Pacific Decadal Oscillation
PJ	Pacific-Japan
PKE	Perturbation Kinetic Energy
PSM	Philippine Summer Monsoon
RHUM	Relative Humidity
RSMC	Regional Specialized Meteorological Center
SAA	South Asian Anticyclone
SC	South China
SCS	South China Sea
SCSMEX	South China Sea Monsoon Experiment
SCSSM	South China Sea Summer Monsoon
SST	Sea Surface Temperature
SSTA	Sea Surface Temperature Anomaly
TC	Tropical Cyclone
TRMM	Tropical Rainfall Measuring Mission
TS	Tropical Storm
VIMF	Vertically Integrated Moisture Flux
VIMFD	Vertically Integrated Moisture Flux Divergence
VIMFC	Vertically Integrated Moisture Flux Convergence
WHI	Wheeler and Hendon (2004) MJO Index
WNP	Western North Pacific

WNPM Western North Pacific Monsoon

WNPSH Western North Pacific Subtropical High

Acknowledgement

Every end marks a new beginning. As my Ph. D. study comes to a halt, I would like to extend my sincerest gratitude to all the people who helped and supported me throughout my study.

First and foremost, I would like to express my deepest gratitude to my advisor Prof. Jun Matsumoto, for his continuous support throughout my Ph.D. study, for his patience despite the countless emails that I sent about my research progress, for his constant encouragement, and immense knowledge. I am also grateful to my thesis examiners, Prof. Hideo Takahashi and Prof. Hiroshi Matsuyama, for their dedication in reading this thesis and for their insightful comments and suggestions that helped improve this thesis.

I would also like to express my sincere gratitude to Dr. Hisayuki Kubota, Dr. Esperanza O. Cayanan, Dr. Flaviana D. Hilario, and Dr. Tomoshige Inoue for their continuous support when I was writing our papers. I would also like to thank Asst. Prof. Hiroshi Takahashi for the stimulating discussions during my first year and for providing me a big monitor and storage devices that I used throughout my study. I am also thankful to all the members of the Laboratory of Climatology, TMU for their valuable comments and suggestions during our laboratory seminars.

Special thanks to Dr. Masato Nodzu and Assoc. Prof. Akira Yoshida for giving me the opportunity to experience *kansoku* at Cape Shionomisaki. It was a very educational trip!

My Ph.D. life would have been boring without my drinking buddies, Japanese tutors, and ramen-eating companions, Dr. Nozomi Kamizawa, Dr. Ko Nakajima, Dr.

Yoshihito Seto, Dr. Trinh Tuan Long, Mr. Satoru Abiko, Mr. Masaharu Tsutsumi, Ms. Moeka Yamaji, Mr. Rakesh Teja Konduro, and Mr. Yuta Matsuzaki. I would also like to thank my roommates in Building 8, Room 729. Although we did not converse that much, their mere presence lessened the loneliness in my heart.

This Ph.D. study would not have been possible without the financial support provided by the Tokyo Metropolitan Government through the "Tokyo Human Resources Fund for City Diplomacy Scholarship Program". The data provided by the Philippine Atmospheric, Geophysical, and Astronomical Services Administration (PAGASA) through Dr. Marcelino Q. Villafuerte and Dr. Hisayuki Kubota, were also crucial in my research. Hence, I would like to extend my sincerest gratitude to all PAGASA staffs who provided me with the scanned copies of the PAGASA reports and historical data sets. I would also like acknowledge the assistance of Ms. Mio Tanahashi, Ms. Tomoko Motokado, and Ms. Yuko Saigusa with my university requirements.

To my very supportive Filipino and international friends in the university who always call me *fat*: Joval, Charles, Ken, Neriezza, Jean, Mike, Daryl, Joan, Julie, Maurice, Foo, Laili, Uji, Rizky, Nico, Kanyapa, Vu, and Rui, thank you for the movie nights, hiking/biking activities, food trips, for the countless laughter, and for making me feel at home.

Words are not enough to express my feelings for my family for their unconditional support in my study. Life here in Japan would be unbearably difficult and colorless without them. Last but not the least, I am extremely grateful to Joyce, Bea, Tita Fao, and Tito Buboy, for always accommodating me whenever I go back to the Philippines.

Abstract

The variability of rainfall in the Philippines occurs over a wide range of spatial and temporal scales. While the interannual, seasonal, and long-term trends in rainfall have been extensively examined in previous studies, very little attention has been given to the variabilities at the sub-seasonal and decadal-to-interdecadal time scales. In addition, different synoptic-scale convective processes have yet to be identified and examined in detail. Identifying these synoptic-scale processes and understanding the mechanisms inducing the sub-seasonal and interdecadal variabilities in rainfall have important ramifications for improved management of water resources in the country. To address these issues, first, the different synoptic-scale convective processes were identified and examined during the pre-summer, summer, and winter monsoon seasons. Then, the decadal-to-interdecadal variability of the summer and winter monsoon seasons are examined.

Intermittent wet events, which accounts for about 23 % of the total pre-summer monsoon days from 1979–2012, were identified from April 1 to the monsoon onset defined by the Philippine Atmospheric, Geophysical and Astronomical Services Administration (PAGASA). The results show that these intermittent wet events are associated with mid-latitude disturbances besides the prevailing easterlies along the southern flank of the western North Pacific Subtropical High (WNPSH). This is the first attempt to clarify such phenomenon and document the role of deformation zones, where the cold front interacts with the easterlies, as another rain-bearing system during the pre-summer monsoon season.

The zonal wedging of the WNPSH was also found to induce a monsoon break over the Philippines during the early summer monsoon season. Using the rainfall data from

PAGASA, the climatology of the first post-onset monsoon break was examined. The results show that this break is very clear in stations located over the north and central Luzon, and occurs climatologically in early June. Composite analysis of the synoptic conditions during the monsoon break period reveals that the westward intrusion of the WNPSH is facilitated, through a cloud-radiation feedback process, by the enhanced rainfall and cloudiness during the onset period. The enhanced rainfall during the onset leads to the cooling of the atmosphere, while the enhanced cloudiness leads to a decrease in the incoming solar radiation. These changes favor the increase of sea level pressure and the westward intrusion of the WNPSH. Furthermore, the impact of deformation zones is more common during the winter monsoon season. In fact, the shearline along the confluence region of these deformation zones induces winter heavy rainfall/flooding events (HRF) over the southern Philippines. Using the flood reports archived by the Dartmouth Flood Observatory from 1979–2017, it was found that about 74 % of such HRF events occur over Mindanao Island that are associated with the interaction of the shearline and a westward propagating cyclonic circulation.

As for the decadal variability, using the rainfall data of the stations located on the western coast of the Philippines from 1979–2008, a robust climate shift was found around 1993/1994 during the mature phase of the summer monsoon season. Compared with 1979–1993 (ES1), the rainfall during 1994–2008 (ES2) is suppressed, which is accompanied by weakened monsoon westerlies, enhanced moisture flux divergence, mid-tropospheric descent, enhanced vertical zonal wind shear, and decreased relative humidity. These changes are unfavorable for synoptic-scale activities during ES2. Finally, for the winter monsoon season, two robust and significant interdecadal shifts that are most remarkable during December, were found around 1976/1977 and 1992/1993. Hence, the analysis period was divided into three epochs: 1961–1976

(EW1), 1977–1992 (EW2), and 1993–2008 (EW3). The mean and interannual variability of rainfall during EW2 is suppressed compared with the two adjoining epochs. The shift around 1976/1977 is related to an El Niño-like sea surface temperature (SST) change over the Pacific basin, while that around 1992/1993 is related to a La Niña-like SST change. A weakened low-level easterly wind, decreased moisture transport, and decreased synoptic-scale activities contributed to the decrease in the mean rainfall during EW2, while the El Niño-like SST change and the weakening of the East Asian winter monsoon during EW2, partly contributed in suppressing the interannual variability of December rainfall in the Philippines.

Chapter 1. Introduction

1.1. Motivational background

It is well-known that the rainfall over the Asia Pacific monsoon (APM) region varies over a wide range of spatial and temporal scales. Identifying the different processes that contributes to rainfall variability and understanding their underlying mechanisms have important ramifications for improved risk management of hydrological resources in agricultural countries such as the Philippines.

The regional differences of the Asian summer monsoon (ASM) was first recognized by Murakami and Matsumoto (1994). They divided the ASM based on the differences in the wet conditions into the western North Pacific monsoon (WNPSM), the Southeast Asian monsoon (SEAM), the northern Australia-Indonesia monsoon (NAIM), and the mid-latitude wet conditions over the Tibetan Plateau (TIBU) and Japan-East China region (Baiu). Then, Wang and Lin (2001) redefined this regional divisions based on the onset, peak, and withdrawal of the rainy season into the Indian summer monsoon (ISM), the East-Asian summer monsoon (EASM), and the WNPSM. The ISM, for example, peaks between June–July, while the WNPSM reaches its peak around August–September. In the recent decades, the differences among these regional monsoon systems are further elucidated with the availability of more meteorological observations.

The Philippines is an archipelago with about 7, 641 islands that is located at the western periphery of the Pacific Ocean and largely influenced by the WNPSM. The temporal variability of rainfall of the WNPSM occurs over a wide range of time-scales from synoptic (e.g., 2–10-day), intraseasonal (e.g., 10–20-day, 20–70-day, etc.),

interannual (e.g., year to year variability and 3–5-year variabilities), and to decadal-to-interdecadal (e.g., ≥10-years) time-scales. There is also interaction among these scales that adds complexity to the monsoon system. For example, the genesis location and track of tropical cyclones (TCs; a synoptic-scale system; Holland, 1993) are highly influenced by the El Niño Southern Oscillation (ENSO), which is a well-known climate driver at the interannual time-scale. In particular, more TCs are generated in the vicinity of the Philippines during La Niña conditions, compared with El Niño conditions, where TCs tend to develop more over the central Pacific (Wang and Chan, 2002).

Besides the TCs, northwestward propagating synoptic-scale wave trains (i.e., alternating cyclonic and anticyclonic circulations) were also found during the summer monsoon season that originate from the equatorial western North Pacific (WNP) and decay off the coast of South China (SC) (Lau and Lau, 1990). The easterly waves are also one of the regulating synoptic-scale systems for the formation of TCs. According to Chen *et al*. (2008) about 80 % of the TC formations over the WNP for the period 1979–2002 are directly and indirectly related to easterly waves. On the intraseasonal time-scale, it has been shown that there are prominent intraseasonal oscillations (ISOs) with periodicities of about 10–20-days/10–25-days and a lower frequency mode with a period of about 20–70-days/25–90-days over the WNP (e.g., Fukutomi and Yasunari, 1999, 2002; Kajikawa and Yasunari, 2005; Kikuchi and Wang, 2010; Kikuchi *et al*., 2012). These ISOs are also known to have strong seasonal dependence. For example, Kemball-Cook and Wang (2001) found that the ISOs during May-June tends to propagate eastward along the equatorial Indian Ocean and WNP compared with those during August-October that exhibits northwestward propagation over the WNP.

On the other hand, the Pacific Decadal Oscillation (PDO; Mantua and Hare, 2002) is a well-known climate driver in the decadal-to-interdecadal time-scale. It is defined

by the leading principal component of the North Pacific (poleward of 20°N) sea surface temperature (SST) anomalies. The SST anomalies are obtained by removing the climatological annual cycle and the global mean SST anomaly from the data. It has a positive and a negative phase that resemble the SST conditions over the WNP during El Niño and La Niña, respectively. In particular, the positive (warm) phase of PDO is characterized by positive SST anomalies over the central and eastern tropical Pacific, and negative SST anomalies over the WNP. The pattern of SST anomalies during the negative (cool) phase of PDO is just the opposite of those during the positive phase. Mantua and Hare (2002) noted that the PDO fluctuations are most energetic at 15–25 and 50–70 years. Nevertheless, the precise origin of PDO is yet to be determined. Moreover, variabilities at the decadal-to-interdecadal time scales have long been thought to modulate higher frequency variabilities such as the El Niño Southern Oscillation (ENSO; e.g., Gershunov and Barnett, 1998; Wang *et al.*, 2008). Wang *et al.* (2008), for example, found that the relationship between ENSO and the East Asian winter monsoon (EAWM) are more pronounced during the negative phase of PDO. In addition, the phase shift of the these decadal-to-interdecadal climate variabilities often leads to distinct climate shifts.

The islands in the Philippines are generally grouped into three major ones: Luzon (northern Philippines), Visayas (central Philippines), and Mindanao (southern Philippines), as shown in Figure 1.1. There is strong seasonality and spatial contrast in the rainfall of the country due to its heterogeneous topography and monsoonal climate. For example, during the summer monsoon season, which is locally known as *Habagat* (i.e., June to September), westerly to southwesterly winds are apparent over the country and rainfall is more pronounced over the western coast due to the blocking effects of the Cordillera and Sierra Madre mountain ranges (Figure 1.1) over Luzon Island. On

the other hand, the eastern coast of the country experiences its rainy season during winter, which is locally known as *Amihan* (i.e., November to March), when the prevailing winds are northeasterlies.

The pre-summer monsoon season (i.e., March to May) is the hottest and driest season in the Philippines. A number of prolonged dry spells and hydro-meteorological droughts have been reported in this season (e.g., Porio *et al*., 2019) that are further aggravated by El Niño, whose effects may persist until the subsequent summer monsoon season. However, very few studies have examined the variability of rainfall during this season. The rainfall during this season are often associated with, but is not limited to, the easterlies along the southern flank of the western North Pacific Subtropical High (WNPSH; Akasaka, 2010). As will be shown later in Chapter 2, mid-latitude disturbances also contribute to the rainfall during this season.

The variability of the winter monsoon season has also received less attention compared with the summer monsoon season. On the contrary, the onset, climatology, interannual variability, and long-term trends of the summer monsoon of the Philippines are well documented (Flores and Balagot, 1969; Akasaka *et al.*, 2007; Moron *et al*., 2009; Akasaka, 2010; Cruz *et al.*, 2013; Villafuerte *et al.*, 2014; Cinco *et al.*, 2014). However, according to Asuncion and Jose (1980), the summer monsoon accounts for about 43 % of the total annual rainfall of the country, while the winter monsoon contributes by about 38 %, indicating that the rainfall contribution from the summer and winter monsoon seasons are equally important.

In general, the important sub-seasonal scale variations (i.e., active-break cycle) during the pre-summer, summer, and winter monsoon seasons in the country are less emphasized in previous studies. In fact, the different rainfall-producing and rainfall-

suppressing synoptic-scale processes in these aforementioned seasons have yet to be identified and examined in detail. Hence, the present study is our initial attempt to fill this research gap.

1.2. Role of synoptic-scale systems on the variability of rainfall in the Philippines

The TC is one of the synoptic-scale systems that contributes to the rainfall variability of the country. From a long-term analysis of TCs that entered the Philippine Area of Responsibility (PAR; dashed black lines in Figure 1.1) from 1951 to 2013, Cinco *et al*. (2016) found that, on the average, about 19–20 TCs enter the PAR annually, 9 of which makes landfall over the Philippines. The PAR is bounded by the following coordinates: (1) 25°N, 120°E; (2) 25°N, 135°E; (3) 5°N, 135°E; (4) 5°N, 115°N; (5) 15°N, 115°E; and (6) 21°N, 120°E. Sometimes, this is simplified to the area within 115–135°N and 5–25°N (e.g., Corporal-Lodangco and Leslie, 2016), which is used throughout this study. The TC warnings are only issued when the TC is located within this region. Moreover, the TC contribution over the country varies spatially, with more TC-induced rainfall generated over the western part (54 %) of the country compared with those areas located on the southern part (i.e., Mindanao Island; 6 %) (e.g., Kubota and Wang, 2009; Bagtasa, 2017). It is known that TCs can enhance the summer monsoon westerlies when it is located to the north or eastern part of the country, which can explain the large contribution of TCs over the western coast (Cayanan *et al*., 2011). The TC activity also exhibits strong seasonality, with more TCs entering the PAR during the summer monsoon season (i.e., June to October) and decreases in the succeeding winter to spring seasons. Of course, this is related to the seasonal migration of the monsoon trough, which provides the ambient conditions necessary for TC activity.

Other synoptic-scale systems that also contributes to the rainfall variability of the Philippines include; the Inter-tropical Convergence Zone (ITCZ) (Yumul *et al*., 2011), the WNPSH (Flores and Balagot, 1969), mid-latitude cold fronts/surges (Faustino-Eslava *et al*., 2011), and westward propagating cold surge vortices during winter (Chen TC *et al*., 2012). The impact of mid-latitude cold fronts/surges is more common during the winter monsoon season (i.e., November to March) (Faustino-Eslava *et al*., 2011; Pullen *et al*., 2015). Locally, this is referred to as the impact of the "tail-end of a cold front" or the *shearline* that develops when the cool and dry northeasterly winds during winter interact with the warm and humid tropical easterlies. In fact, it is also one of the heavy-rainfall/flood (HRF) inducing synoptic-scale processes during winter, besides the TCs. However, most of the previous studies regarding this phenomenon have only examined specific cases (Pullen *et al*., 2015) or carried out impact-based assessments (Faustino-Eslava *et al*., 2011). Its variability in the climatological mean sense as well as the underlying dynamics and mechanism inducing these HRF events have yet to be examined.

The WNPSH is another mid-latitude synoptic system that affects the rainfall of the Philippines. During the pre-summer monsoon season, it extends further west, over the Indochina Peninsula and brings dry weather conditions over the country and the adjacent regions (e.g., Flores and Balagot, 1969; Zhang *et al*., 2004; Akasaka *et al*., 2007; Akasaka, 2010). Between late April to June, the WNPSH retreats eastward, which indicates the onset of the ASM. The WNPSH also provides the mid-tropospheric steering for most TCs over the WNP around its southern and western periphery (e.g., Nguyen-Le and Matsumoto, 2016; Olaguera *et al*., 2018a). As will be shown later in Chapter 3, the zonal wedging of the WNPSH may also suppress the rainfall over the

Philippines after the summer monsoon onset. This makes the onset process of the summer monsoon over the Philippines more complicated than previously thought.

1.3. Decadal-to-interdecadal variability of rainfall in the Philippines

Previous studies have documented significant interdecadal shifts in the summer and winter rainy seasons over the APM region around the late 1970's to early 1980's (Nitta and Yamada, 1989; Inoue and Matsumoto, 2007), early to mid-1990s (Kwon *et al.*, 2007), and late-1990s to early 2000's (Zhu *et al.*, 2011). It has been suggested that the changes in the tropical Indo-Pacific SST have significantly contributed to these interdecadal shifts (Nitta and Yamada, 1989; Gong and Ho, 2002; Wu *et al.*, 2010; Kajikawa and Wang, 2012). The late 1970's shift, for example, features an El Niño-like SST change over the Pacific basin, while the mid to late 1990's and early 2000's shifts feature a La Niña-like SST change. The changes in SST may also affect the variability of TC activities (Kajikawa and Wang, 2012) and the WNPSH (Nguyen-Le and Matsumoto, 2016). For instance, Nguyen-Le and Matsumoto (2016) found that the further westward extension of the WNPSH after the mid-1990's is related to the La Niña-like SST change in the Pacific, which resulted in more TC landfalls over Vietnam and the Philippines. However, most of these aforementioned studies about the decadal-to-interdecadal variability of rainfall, focused on seasonal mean fields. Some studies also found interdecadal shifts that are more significant and robust at the sub-seasonal time scales (e.g., Inoue and Matsumoto, 2007; Ha *et al.*, 2009).

Moreover, to the best of our knowledge, very few studies have examined the decadal-to-interdecadal variability of rainfall in the Philippines (Kubota and Chan, 2009; Villafuerte *et al.*, 2014). Kubota and Chan (2009) first examined the interdecadal variability of landfalling TCs over the country and found a decrease in landfalling TCs

during the positive phase of PDO and El Niño years. However, their study only focused on landfalling TCs. On the other hand, Villafuerte *et al*. (2014) examined the relationship between the PDO and the seasonal extreme precipitation indices (EPIs) over the country. Although they found significant correlation between the maximum 5-day rainfall total during the June-September season and the 11-yr running PDO index in one station (i.e., Iloilo station), their results are still inconclusive and suggested that longer rainfall data sets that covers at least two PDO cycles are needed to establish the relationship between the PDO and the EPI.

1.4. Main objectives

The primary aim of this dissertation is to gain a better understanding of the rainfall variability in the Philippines by identifying the different rainfall-producing and rainfall-suppressing synoptic-scale systems and the potential interdecadal shifts in rainfall during the summer and winter monsoon seasons. In order to achieve the main aim of this study, comprehensive observational analyses are carried out to address the following specific objectives:

1. To examine the different rainfall producing synoptic-scale systems and their climatology during the pre-summer monsoon season over the Philippines;

2. To investigate the role of the WNPSH on the early summer monsoon break over Luzon Island;

3. To investigate the role of shearlines on the winter monsoon heavy rainfall events over the Philippines;

4. To detect whether the summer monsoon season of the Philippines has an interdecadal shift in the mid-1990s;

5. To determine potential interdecadal shifts in rainfall during the winter monsoon season;

6. To determine the possible factors that are inducing these interdecadal shifts in rainfall during the summer and winter monsoon seasons.

1.5. Scope and Limitations of the study

The term "rainfall variability" covers a wide range of spatial and temporal scales. However, due to time constraints, all of these scales cannot be covered in the present study. As such, only the role of several synoptic-scale systems such as the WNPSH and shearlines associated with mid-latitude cold fronts on the rainfall variability, and the interdecadal shifts in rainfall during the summer and winter monsoon seasons are comprehensively analyzed.

1.6. Dissertation Outline

Generally, this dissertation can be divided into two parts: (1) the first three chapters discuss the role of mid-latitude synoptic scale systems on the rainfall variability during the pre-summer, summer, and winter monsoon seasons, while (2) the last two chapters discuss the interdecadal shifts in the summer and winter monsoon season. This dissertation is a compilation of two published articles (Olaguera *et al*., 2018a, b) and three articles that are under review (Olaguera and Matsumoto, 2019; Olaguera *et al*., 2019a, b); hence, each of these independently written articles appears as separate chapters in this dissertation. While the readers may find it odd by repeatedly seeing each part of the article in every chapter, one can easily generate a conclusion by just reading any of the succeeding chapters.

Chapter 2 investigates the climatology of the pre-summer monsoon rainfall of the Philippines from 1979 to 2012. Although this season is relatively dry compared with the other seasons, we found that the intermittent wet episodes during this season were about 23 % of the total pre-summer monsoon days, suggesting its relative importance. The synoptic conditions associated with these wet episodes are discussed. This is the first attempt to clarify the impact of shearlines associated with deformation zones as another rain bearing system during the pre-summer monsoon season of the Philippines. This chapter is based on an article that is currently under review (Olaguera and Matsumoto, 2019).

Chapter 3 investigates the climatological monsoon break following the onset of the summer rainy season from 1998 to 2012. The first post-onset monsoon break is only remarkable in stations located over the northwest and central Luzon Island and occurs climatologically in early June. Composite analysis of the large-scale circulation features during the monsoon break period shows that this is associated with the westward intrusion of the WNPSH. A cloud-radiation feedback mechanism that favors this zonal shifting of the WNPSH is discussed. This is the first attempt to examine the role of the zonal displacement of the WNPSH in inducing a break during the early summer monsoon season, which is a step related to the summer monsoon onset of the Philippines. This chapter is based on an article that is currently under review (Olaguera *et al*., 2019a).

Chapter 4 first investigates a non-TC related winter heavy rainfall event that leads to extensive flooding (HRF) over Mindanao Island in the southern Philippines on January 2017. This extreme event is associated with the interaction of a shearline and a westward propagating low-pressure area over Mindanao Island. Then, the climatology of these winter HRF events over the Philippines are examined from 1979

to 2017. Previous studies on non-TC related winter HRF events over the Philippines focused only on specific cases or carried out impact-based assessments. Hence, this is the first attempt to examine the climatology of these winter HRF events. This chapter is based on an article that is currently under review (Olaguera *et al*., 2019b).

Chapter 5 examines the interdecadal shift in the summer monsoon season of the Philippines in the mid-1990s. Compared with previous studies that analyzed seasonal means for the interdecadal variability of rainfall, the robust interdecadal shift was found to be most remarkable during the mature phase of the summer monsoon season (i.e., from early August to early September) over the Philippines around 1993/1994. The role of the changes in the large-scale circulation features and possible mechanisms inducing this shift are discussed. This chapter is based on a published article in Olaguera *et al.* (2018a).

Chapter 6 extends the interdecadal shift detection in Chapter 5 on the winter monsoon season of the Philippines. Two interdecadal shifts that are most remarkable during December were identified around 1976/1977 and 1992/1993. The mechanisms including the role of the PDO in inducing these shifts are investigated. This chapter is based on a published article in Olaguera *et al*. (2018b).

Chapter 7 summarizes the major findings, limitations, and research questions for future studies. It is followed by the bibliographical references, figures, and tables that are separated from the main chapters following the University's guidelines.

Chapter 2. A climatological study of wet and dry conditions in the pre-summer monsoon season of the Philippines

2.1. Introduction

The agricultural sector of the Philippines, especially those areas located on the western side of the country, relies heavily on the summer monsoon rainfall. While many studies have investigated the onset (Akasaka, 2010; Kubota *et al*., 2017), climatology (Cruz *et al*., 2013), long-term trends (Villafuerte *et al*., 2014), and variability (Akasaka *et al*., 2018; Olaguera *et al*., 2018a) of the summer monsoon season (i.e., June to September), very few studies have examined the climatology and the different convective systems during the pre-summer monsoon season (i.e., March to May). Of course, the rainfall generated during this season is also important for the total annual rainfall of the country, besides the rainfall from the summer or winter monsoon seasons.

Lohar and Pal (1995) recognized the importance of thunderstorms in the pre-monsoon rainfall of West Bengal in India from the rainfall data in one station for the period 1973–1992. They noted two types of thunderstorms over this area. One that is associated with the interaction of the moist southerlies and arid westerlies, which they referred to as a dry line, and another that is triggered by the sea breeze front. In addition, they found decreasing trends in the frequency of these thunderstorms from 1983 to 1992, which they attributed to the land-use change over this region. Ding (1992) and Chen *et al*. (2004) documented prominent double peaks in the annual mean rainfall in some stations over South China (SC) around May-June and in August, which they referred to as the typhoon season. Ding (1992) further noted that the pre-summer monsoon season over SC is initiated by the northward jump of the western North Pacific

Subtropical High (WNPSH) and the onset of the summer monsoon over the South China Sea (SCS). In addition, he also noted three rain-producing synoptic systems during the pre-summer monsoon season, and include cold fronts, convergence zones (i.e., shearlines, monsoon trough, low-level jet, etc.), and the middle to upper level synoptic scale systems (i.e., mid-latitude westerlies, WNPSH, etc.). Matsumoto (1997) found that the onset of the summer monsoon over the Indochina Peninsula commences in mid-May, almost concurrent with the onset timing over the SCS. However, pre-monsoon rainfall already occurred over the inland region of the Indochina Peninsula, while it is under the influence of mid-latitude westerlies. He also pointed out a potential problem in using the northward migration of the equatorial westerlies as an index for the summer monsoon onset such as those proposed by Orgill (1967) over this region, since southwesterly winds are already apparent over this region in early April. Kiguchi and Matsumoto (2005) examined the pre-summer monsoon rainfall over the Indochina Peninsula during the Global Energy and Water Exchanges (GEWEX) Asian Monsoon Experiment–Intensive Observation Period (GAME-IOP) in 1998 and documented the intermittent rainfall episodes induced by the passage of an upper level trough that migrates along the southern edge of the Tibetan Plateau. This finding also revolutionizes the idea that the pre-summer rainfall over the Indochina Peninsula is not a localized phenomenon, but rather it is a synoptic-scale phenomenon. Kiguchi *et al*. (2016) confirmed the passage of the upper trough using a longer data set from 1979 to 2002. They further noted that this upper trough is associated with the mid-latitude cyclone over the Yangtze River basin and that the rainfall amount during the pre-summer monsoon period has no clear relationship with the onset timing of the summer monsoon over the Indochina Peninsula.

According to Flores and Balagot (1969), the summer monsoon over the Philippines originates as trades from the Indian Ocean anticyclone during the Southern Hemisphere winter. As these trades cross the equator, they are veered to the right and generally reach the country as southwesterly streams. The onset of the summer monsoon over the Philippines generally occurs between mid to late May, following the onset of the summer monsoon over the SCS, although rainfall may start to increase as early as in April (Flores and Balagot, 1969; Akasaka *et al*., 2007; Akasaka, 2010). The southward intrusion of mid-latitude fronts has been suggested as an important trigger for the summer monsoon onset over the SCS (Chang and Chen, 1995; Chan *et al*., 2000). For example, Chan *et al*. (2000) examined the summer monsoon onset over the SCS in 1998 and found a midlatitude trough/front (i.e., a cyclonic flow) that migrated southwards toward the SC coast and triggered the onset. They suggested that the northeasterly flow associated with the decaying winter monsoon during the late spring facilitated the increase of instability (i.e., the transfer of heat and moisture) over the SCS. The appearance of the cyclonic flow over the SC coast induces enhanced ascent of warm and moist air over the SCS. The upper level divergence accompanying this change would then force the extension of rainfall in the upper troposphere and release of the convective available potential energy of the warm air mass. This resulted in the enhanced rainfall over the entire SCS, which indicates the onset of the rainy season over there. Knowing the proximity of the Philippines to the SCS, it can be inferred that the southward intrusion of these mid-latitude cold fronts can also induce rainfall over the country. In fact, the rainfall contours of about 5 mm day^{-1} during the summer monsoon onset over the SCS in Figure 15c of Chan *et al*. (2000) extends over the Philippines. Meanwhile, using the Geostationary Meteorological Satellite (GMS) data from 1982 to 1987, Hirasawa *et al*. (1995) found the appearance of deep convective

clouds over Luzon Island in mid to late May, which is part of an eastward propagating cloud band along 30°N (see their Figures 2 and 4). This result indicates the impact of mid-latitude circulations on the pre-summer monsoon rainfall over the Philippines, which has not been examined in previous studies.

The pre-summer monsoon season of the Philippines (i.e., March to May) is the hottest and driest season in the country. Several instances of prolonged dry spell and drought were previously reported during this season and this is further aggravated by the occurrence of El Niño, whose effects may persist until the succeeding summer season (e.g., Porio *et al.* 2019). Both hydrological and meteorological drought are of great concern because of their profound socio-economic impacts. Hence, understanding the different convective systems during this season including their underlying mechanisms is of utmost importance.

The main objectives of this study are therefore to examine first the climatological characteristics of the wet and dry conditions during the pre-summer monsoon season in the Philippines and determine the major synoptic-scale convective systems during this period. The data and methodology used in this study are described in Section 2.1. The analysis of the pre-summer monsoon convection through case studies and composite analysis are presented in Section 2.3. A summary of the results is presented in Section 2.4.

2.2. Data and Methodology

2.2.1. Data

In this study we used the following data sets:

(1) Daily Outgoing Longwave Radiation (*OLR*; Liebmann and Smith, 1996), with 2.5° × 2.5° grid resolution, from 1979 to 2012 provided by the National Oceanic and Atmospheric Administration (NOAA), as a proxy for rainfall.

(2) Daily zonal (*U*) and meridional (*V*) winds, relative humidity (*RHUM*), Temperature (*TEMP*) at multiple levels from the National Centers for Environmental Prediction-Department of Energy (NCEP-DOE) Atmospheric Model Intercomparison Project (AMIP-II), with 2.5° × 2.5° grid resolution (Kanamitsu *et al*., 2002). Specific humidity (*SHUM*) and equivalent potential temperature (θe) at multiple levels were also used and were derived from this data set.

(3) Regional summer monsoon onset dates from the Philippine Atmospheric, Geophysical and Astronomical Services Administration (PAGASA), the country's official weather bureau. The summer monsoon onset is defined based on the stations located over the western coast of the Philippines due to their geographical exposure to the summer monsoon westerlies. PAGASA defines the onset as the beginning of a five-day period between May and July with total rainfall of about 25 mm or more, with three consecutive days having at least 1 mm of rainfall per day. These conditions should be satisfied in at least seven of the stations located over the western coast of the Philippines. PAGASA also has the disposition to include the changes in the large-scale circulations such as the reversal of the low-level winds from easterly to westerly in the onset criteria.

2.2.2. Methodology

The analysis period spans from 1979 to 2012. We focused our analysis over Luzon Island (northern Philippines) since most of the stations used in defining the onset are located here. We defined Luzon Island and its vicinity as the region within 120–122.5°E and 12.5–22°N. We defined the pre-summer monsoon period as the period from April 1 to the onset day, defined by PAGASA, in each year. We excluded March in this definition since the eastern coast of Luzon Island is still under the influence of the northeasterly monsoon. We used the 240 W m^{-2} as the threshold for active convection following Kiguchi *et al*. (2016). Values below (above or equal to) this threshold indicates enhanced (suppressed) convection.

2.3. Results

2.3.1. Climatological characteristics of the pre-summer monsoon convection

In order to examine the climatological characteristics of the convective activities during the pre-summer monsoon, first, we classified the pre-summer monsoon days into two types: (1) wet days (Type W), when the area-averaged *OLR* over Luzon Island is below 240 W m^{-2}, and (2) dry days (Type D), when the *OLR* is above or equal to 240 W m^{-2}. Henceforth, the *number of days* in each type will be referred to as *cases*. Following these criteria, there are 1459 cases (77.11 % of the 1892 pre-summer monsoon cases from 1979 to 2012) that belong to Type D and 433 cases (22.89 %) to Type W, indicating that the pre-summer monsoon period is relatively dry. To further clarify their difference, the composites of *OLR*, winds at 925 hPa ($WINDS_{925hPa}$), and 200 hPa ($WINDS_{200hPa}$) for both types, are shown in Figure 2.1.

Easterly $WINDS_{925hPa}$ are apparent over the Philippines in the composite of the Type D cases (Figure 2.1a) and the entire Philippines is relatively dry, with *OLR* values above 240 W m^{-2}. The WNPSH is centered around 135°W, 30°N and its western ridge is located over the Indochina Peninsula. A narrow convergence region, with enhanced convection, can be seen over the Indochina Peninsula along 105°E, where the monsoon westerlies from the Bay of Bengal converges with the easterlies from the southern flank of the WNPSH. This feature is one of the triggers for the monsoon onset over the Indochina Peninsula, as noted by Zhang *et al*. (2004; see their Figure 12). At 200 hPa, an upper-level anticyclone is located over the SCS in the Type D composite (Figure 2.1b). This upper-level anticyclone is associated with the developing South Asian Anticyclone (SAA; Yanai *et al*., 1992). On the other hand, southeasterlies are apparent over the Philippines in the Type W composite and the WNPSH retreats eastward and centered around 140°W, 30°N (Figure 2.1c). This is accompanied by the enhanced convection over the Indochina Peninsula, the SCS, and the Philippines. The monsoon southwesterlies converge with the southeasterlies from the southern flank of the WNPSH over the SCS. At 200 hPa, the SAA is located around 100°E, 18°N in the Type W composite (Figure 2.1d).

The anomalous differences of the composites are shown in Figures 2.1e and f. Significant southwesterly $WINDS_{925hPa}$ can be seen over the western Indochina Peninsula, the SCS, and the Philippines (Figure 2.1e) that extends to the dateline along 20°N and the equator. This is also accompanied by a significant increase in convection, as indicated by the negative *OLR* in the aforementioned regions. This suggests that the enhanced southwesterly $WINDS_{925hPa}$ significantly contribute to the convection of the Type W composite. At 200 hPa (Figure 2.1f), although the Philippines is under the easterly conditions, the difference is not significant, indicating that the convection

enhancement over this region is largely influenced by the low-level circulations. Nevertheless, significant easterlies can also be seen along 20–40°N between the northern Luzon Island and Japan, indicating the weakening of the westerly jet in this region.

2.3.2. Characteristics of the pre-summer monsoon convection during 1981

The convection enhancement during the summer monsoon onset over the Philippines is usually accompanied by the reversal of winds from easterly to westerly (e.g., Akasaka, 2010). Hence, we examine first the time series of the area-averaged *OLR* and zonal winds at 925hPa (U_{925hPa}) over Luzon Island for a sample year, 1981, as shown in Figure 2.2. This year was chosen arbitrarily and that the circulation features during the pre-summer monsoon period in this year are similar to those in other years (not shown). The onset during this year occurred on June 4, as defined by PAGASA.

The *OLR* is continuously exceeding 240 W m^{-2} between April 21 and May 8, indicating the prevailing dry condition. *OLR* minima is observed around May 11 (Figure 2.2a), which is accompanied by the abrupt reversal of U_{925hPa} from easterly to westerly (Figure 2.2b) over Luzon Island. From May 17 to May 20, the *OLR* decreases again but easterlies reappear over Luzon Island. The *OLR* also decreases to below 240 W m^{-2} on May 24, while the U_{925hPa} winds are easterly/southeasterly. It is worth mentioning that there was no recorded tropical cyclone in the vicinity of the Philippines from April 1 to June 4 in this year. Based on the results above, it seems that convection varies intermittently during the pre-summer monsoon period over Luzon Island that can be associated both with the reversal of winds from easterly to westerly.

To further elucidate the spatial structure of the convection and winds during the pre-summer monsoon period of the aforementioned case study, we illustrate the *OLR* and $WINDS_{925hPa}$ of four selected days in Figure 2.3. On May 1 (Figure 2.3a), easterly $WINDS_{925hPa}$ are apparent over the Philippines and *OLR* is above 240 W m^{-2}. These easterly $WINDS_{925hPa}$ is part of the WNPSH, whose western ridge is located over the Indochina Peninsula. On May 11 (Figure 2.3b), southwesterly $WINDS_{925hPa}$ appeared over the Indochina Peninsula, the SCS, and Luzon Island. This is related to the eastward retreat of the WNPSH, which is a well-known feature of the onset phase of the Asian summer monsoon (e.g., Zhang *et al*., 2004). Moreover, on May 17 (Figure 2.3c), two cyclonic circulations centered around 115°E, 15°N (SCS) and 135°E, 35°N (southern Japan) that are juxtaposed in a southwest-northeast orientation and two anticyclonic circulations centered around 160°W, 30°N (the WNPSH) and 120°E, 30°N (eastern China) that are adjacent to the aforementioned cyclonic circulations, forms a *deformation zone*. A confluence region can be seen over northern Luzon Island between the cyclonic circulation over the SCS and anticyclonic circulation over eastern China. Southerlies on the eastern flank of the cyclonic circulation over the SCS appears over northern Luzon Island. On May 24 (Figure 2.3d), the deformation zone is located just over Luzon Island, where enhanced convection is also apparent, and southeasterly $WINDS_{925hPa}$ can be seen to its southwest.

Based on these results, it can be inferred that the wet condition during the pre-summer monsoon season over the Philippines can either be due to (1) westerlies accompanied by the sudden eastward retreat of the WNPSH or (2) easterlies along the southern flank of the WNPSH. Akasaka (2010) also noted that easterlies are important triggers for the onset of the summer monsoon over the Philippines, since they may also bring rainfall over the country. However, this is the first attempt to clarify that, while

the Philippines is under the influence of easterly winds, convection may sometimes occur that are associated with mid-latitude disturbances. Another interesting result from the above analysis is the appearance of a deformation zone, when a cyclonic circulation is located over southern Japan, an anticyclone follows to its west, while easterlies are still dominant over the Philippines. Of course, the interaction of TCs with these two causes should also be considered. For instance, when a TC is located to the east or north of Luzon Island, it can enhance the monsoon westerlies (Cayanan *et al*., 2011; Kubota *et al*., 2017), while when it is located over the Philippines or the SCS, it can interact with the cold front to the north of the deformation zone, which may further enhance the convection over Luzon Island.

From the kinematic properties of the horizontal wind field in the natural coordinates, the deformation zone (total deformation; *TDef*) can be represented by the combination of the stretching (*STD*) and shearing deformation (*SHD*) (http://www.zamg.ac.at/docu/Manual/SatManu/main.htm?/docu/Manual/SatManu/CMs/Def/backgr.htm). These are calculated as follows:

$$STD = \frac{\partial U}{\partial x} - \frac{\partial V}{\partial y}, \tag{2.1}$$

$$SHD = \frac{\partial V}{\partial x} + \frac{\partial U}{\partial y}, \tag{2.2}$$

$$TDef = \sqrt{STD^2 + SHD^2}, \tag{2.3}$$

where U and V are the zonal and meridional wind components. As an example, we illustrate these parameters for the May 17 case in Figure 2.4. The confluence region (hereafter, referred to as a *shearline*) north of Luzon Island coincides with a region of more positive STD_{925hPa} (i.e., the zonal wind shear, $\partial U_{925hPa}/\partial x$, is high along the

confluence region) that stretches from the Indochina Peninsula to the east of Japan (Figure 2.4a). On the other hand, the SHD_{925hPa} is weaker and can only be depicted along 15°N (Figure 2.4b). This means that the STD_{925hPa} contributes more to the $TDef_{925hPa}$ during this day, as shown in Figure 2.4c.

The impact of deformation zones on the rainfall of the Philippines is more frequent during the winter monsoon season. In fact, some heavy rainfall events during this season are associated with shearlines, which is locally referred to as the effect of the tail-end of the cold front (Faustino-Eslava *et al*., 2011; Yumul *et al*., 2013; Olaguera *et al*., 2019b). Olaguera *et al*. (2019b) examined a winter heavy rainfall event case on January 16, 2017 over Mindanao Island in the southern Philippines and associated it with a shearline that was formed by the interaction of a low-pressure area over Mindanao Island and the enhanced northeasterlies to its north. They further noted that a cold front associated with these northeasterlies interacted with the warm and humid tropical air mass and resulted in the heavy rainfall event. Following their analysis, we also checked whether a cold front can be found around the deformation zone in the historical surface weather charts provided by the Japan Meteorological Agency (JMA; Figure 2.5). An eastward propagating cold front can be depicted to the northeast of Luzon Island from 12 UTC May 16, 1981 to 12 UTC May 17 (Figures 2.5a to c). The mean location of this cold front can also be depicted as the leading edge of the negative meridional equivalent potential temperature gradient (θe_{925hPa}; https://www.wpc.ncep.noaa.gov/sfc/UASfcManualVersion1.pdf) to the north of Luzon Island and north of the deformation zone, as shown in Figure 2.5d. This indicates that although less frequent, the deformation zone is sometimes important for the rain-bearing systems in the pre-monsoon season and its synoptic features will be elaborated further in the following sub-sections.

2.3.3. Synoptic-scale convective processes in the Type W composite

To investigate the different synoptic-scale convective processes during the pre-summer monsoon period of the Philippines, we further classified the Type W cases into two sub-types based on the wind conditions, as summarized in Table 2.1. Type W_W corresponds to the wet days due to westerlies, while Type W_E corresponds to the wet days due to easterlies. There are 160 (36.95 %) and 273 (63.05 %) cases for the Type W_W and W_E, respectively. This indicates that the majority of the pre-summer monsoon convection is brought by the easterlies along the southern periphery of the WNPSH. We also examined a subset of Type W_E cases, which is referred to as Type W_{EDef}, and corresponds to the wet days with a clear deformation zone in the vicinity of the Philippines. In determining the Type W_{EDef} cases, first, we added a condition to the criteria of the Type W_E cases such that the area-averaged $TDef_{925hPa}$ over Luzon Island should be greater than zero. Then, we checked all of the $WINDS_{925hPa}$ chart of the resulting cases and selected those cases with a clear deformation zone in the vicinity of the Philippines. We identified 52 of such cases from 1979 to 2012, in which 11 cases lasted for at least 2 consecutive days (i.e., propagated eastward/southeastward). This indicates that the development of deformation zones varies rapidly both in space and time.

Figure 2.6 shows the composites of Type W_W, Type W_E, and Type W_{EDef}. The *OLR* and $WINDS_{925hPa}$ in Type W_W (Figure 2.6a) shows apparent westerlies over the Indochina Peninsula, the SCS, and the Philippines. In addition, the WNPSH is already located to the east of the Philippines. In the upper level (i.e., 200hPa; Figure 2.6b), the SAA (centered around 100°E, 20°N) is located over the Indochina Peninsula. In general, these features indicate that the onset of the summer monsoon over the Indochina Peninsula and the SCS has already started (e.g., Yanai *et al*., 1992). On the

other hand, easterly to southeasterly *WINDS*$_{925hPa}$ associated with the southern flank of the WNPSH can be seen over the Philippines and the SCS (Figure 2.6c). This is accompanied by enhanced convection in these areas. The southeasterly *WINDS*$_{925hPa}$ converge with the westerly *WINDS*$_{925hPa}$ over the Indochina Peninsula. At 200hPa (Figure 2.6d), the SAA is centered around 105°E, 15°N. For the Type W_{EDef} (Figure 2.6e), the *WINDS*$_{925hPa}$ resembles those of the May 17, 1981 case, as shown in Figure 2.3c, with two cyclonic and two anticyclonic circulations that are juxtaposed in a southwest-northeast and southeast-northwest orientation. The deformation zone is located northeast of the Philippines and the shearline (i.e., the confluence region) extends over northern Luzon Island. Note that easterly *WINDS*$_{925hPa}$ are also apparent over the SCS that converges with the westerlies over the Indochina Peninsula. This indicates that the summer monsoon onset over the SCS has not commenced yet. At 200hPa (Figure 2.6f), an upper level anticyclone is located to the east of the Philippines (centered around 130°E, 10°N).

Based on the above results, it can be inferred that the mid-latitude disturbances such as cold fronts besides the easterlies along the southern periphery of the WNPSH, also contribute to the pre-summer monsoon convection over the Philippines. To the best of our knowledge, this is the first attempt to clarify such phenomenon and document the role of deformation zones as another convective system during the pre-summer monsoon season of the Philippines.

2.3.4. Daily evolution of the deformation zone

In this section, we examine the formation mechanism of the deformation zone through composite analysis of the long-lasting Type W_{EDef} cases. As we have mentioned previously, there are 11 cases that lasted for at least 2 consecutive days out

of the 52 Type W_{EDef} cases from 1979 to 2012. These cases are listed in Table 2.2. Lag 0 indicates the first day of each of the 11 cases and the preceding and succeeding lag days are denoted by a "–" or a "+" sign, respectively.

Figure 2.7 shows the composites of *OLR* and $WINDS_{925hPa}$ for the Type W_{EDef} cases. At Lag –3 (Figure 2.7a), convection seems to be confined south of 15°N of the Philippines. Easterly $WINDS_{925hPa}$ are apparent south of 15°N over the country and higher *OLR* values can be depicted over Luzon Island. These easterlies are associated with the southern flank of the WNPSH that is centered around 150°W, 30°N (A_1). The WNPSH remains stationary in the same location throughout the composites. Two cyclonic circulations are located north of Japan along 55°N and propagates eastward in the succeeding lag days. At Lag –2 (Figure 2.7b), a developing anticyclonic circulation can be depicted around the Tibetan Plateau (A_2) and a deformation zone develops over eastern China. The confluence region on the western side of the deformation zone appears over mainland China. At Lag –1 (Figure 2.7c), the northerly/northeasterly $WINDS_{925hPa}$ associated with A_2, expands southward over the northern SCS. The deformation zone also proceeds southwards along 123°E, 25°N. Another cyclonic circulation develops to the west of Japan and its southern flank extends further south along 25°N. Convection also starts to increase over Luzon Island. At Lag 0 (Figure 2.7d), A_2 proceeds southeastward and accompanied by the southeastward progression of the deformation zone around 130°E, 22°N. At Lag +1 (Figure 2.7e), A_2 is now located over eastern China and convection over Luzon Island is enhanced. The confluence region along the deformation zone is located over northern Luzon Island. At Lag +2 (Figure 2.7f), A_2 proceeds eastward around 130°E, 30°N, while the deformation zone is located to the east of 140°E. Convection over the Philippines starts

to weaken. At Lag +3 (Figure 2.7g), A_2 is now located around 138°E, 30°N and easterlies are apparent over the Philippines. In the succeeding lag days (not shown), A_2 merges with A_1, the deformation zone dissipates, and the convection decreases again over Luzon Island.

In order to show that the convection over Luzon Island is due to the convergence of the easterly winds from the southern flank of the A_1 and the northeasterlies of A_2, we illustrate the composites of the vertically integrated moisture flux and its convergence in Figure 2.8. The integration was carried out from 1000 hPa to 300 hPa. At Lag –3 (Figure 2.8a), no convergence can be depicted over Luzon Island, which is consistent with the high *OLR* values during this period, as shown in Figure 2.7a. At Lag –2 (Figure 2.8b), a weak convergence can be depicted over Luzon Island. Note that northeasterly fluxes start to appear over Taiwan during this period. At Lag –1 (Figure 2.8c), a southwest-northeast oriented convergence region that extends from Luzon Island to Japan, develops. Note that northeasterly fluxes can also be depicted over the northern SCS during this period. At Lag 0 (Figure 2.8d), this southwest-northeast oriented convergence region extends further south over the Indochina Peninsula due to the intensification of the northeasterly fluxes over the SCS. Enhanced convergence can be depicted around 140°E, 35°N, while enhanced divergence is located to its west around 130°E, 30°N. This enhanced divergence is consistent with the intensification of the A_2, as shown in Figure 2.7c. Another feature worthy of note is the relatively weak convergence at the saddle point of the deformation zone, which is consistent with the higher *OLR* values over this region, as shown in Figure 2.7d. In the succeeding lag days, enhanced convergence persisted over Luzon Island until Lag +3 (Figures 2.8e to g). Furthermore, at Lag +3 (Figure 2.8g), the convergence is already weaker and easterlies are apparent over the entire Philippines.

2.3.5. Interaction of the deformation zone and tropical cyclones

As we have mentioned previously, the deformation zone can interact with tropical cyclones in the vicinity of the Philippines. There are only 6 cases out of the 52 Type W_{EDef} cases when a TC is located in the vicinity of the Philippines, which indicates the rarity of these events. This is also substantiated by the fact that fewer TCs appear in the vicinity of the country during April (e.g., Cinco *et al*., 2016). In this section, we examine one Type W_{EDef} case on May 13, 2006, when Typhoon Chanchu (locally known as Caloy) affected the Philippines and a cold front is present north of Luzon Island. According to the best track data from JMA, this typhoon was formed on May 9, made landfall over the Philippines on May 12, and dissipated around May 19. It attained a minimum sea level pressure of about 930 hPa and maximum sustained winds of about 95 knots (49 m s^{-1}).

Figure 2.9a shows the surface weather map from JMA on 12 UTC May 13, 2006. During this time, the TC is located to the west of Luzon Island. Over the north, a cold front can be seen to the east of Japan and a stationary front at its tail end extends over Taiwan. To the east and west of the cold front, two anticyclonic circulations are found, and this pattern formed the deformation zone. The mean $WINDS_{925hPa}$ on May 13, 2006 in Figure 2.9b shows that the mean position of the deformation zone is centered around 130°E, 25°N. In addition, the enhanced convection can be seen south of 15°N around the Philippines (Figure 2.9b). The mean location of the cold front on May 13, 2006 can also be depicted from the meridional θe_{925hPa} gradient, as shown in Figure 2.9c. A southwest-northeast oriented negative meridional θ_{925hPa} gradient can be seen extending from SC to the east of Japan, indicating the location of the cold front. We also checked the mean $TDef_{925hPa}$ on May 13, 2006 around the Philippines, as shown in

Figure 2.9d. The $TDef_{925HPa}$ is enhanced in three areas: (1) southwest of the TC, where the northeasterlies interact with the westerlies along 10°N, (2) east of the TC, where the westerlies along the southern flank of the TC interacts with the easterlies from the Pacific Ocean, and (3) between Luzon Island and Taiwan, where the southeasterlies on the northeastern part of the TC interacts with the cold front. We speculate that the interaction of the TC, which brings warm and humid air, and the cold front reinforces the supply of moisture carried by the TC. However, this should be clarified further through moisture budget analysis, which will not be discussed in the present study. This issue will be addressed in future studies.

2.4. Summary and Discussion

This study investigated the climatological characteristics of the wet/dry conditions in the pre-summer monsoon period of the Philippines through case studies and composite analysis. We defined the pre-summer monsoon period as the period from April 1 to the onset date in each year. The onset dates were based on simultaneous and persistent rainfall occurrences over the western coast of the country and were provided by PAGASA, the country's official weather bureau.

Using *OLR* as a proxy for rainfall, first, we classified the pre-summer monsoon period into wet cases (Type W; $OLR < 240$ W m^{-2}) and dry cases (Type D; $OLR \geq 240$ W m^{-2}). The Type W (Type D) cases account for about 23 % (77 %) of the total pre-summer monsoon cases from 1979 to 2012, suggesting that the pre-summer monsoon period over the Philippines is relatively dry. At 925 hPa, easterly $WINDS_{925hPa}$ were apparent over the Philippines in the Type D composite. In the upper level, the $WINDS_{200hPa}$ featured the developing phase of the SAA, whose center is located over the SCS and westerly $WINDS_{200hPa}$ along its northern flank were apparent over the

Philippines. In contrast, southeasterly $WINDS_{925hPa}$ were apparent over Luzon Island in the Type W composite. At 200 hPa, the SAA is already located over the Indochina Peninsula and northeasterly $WINDS_{200hPa}$ on its eastern edge are apparent over the Philippines. The differences in the Type W and Type D composites featured an enhanced southwesterly $WINDS_{925hPa}$ that significantly contributed to the convection in the Type W composite. No significant difference in the $WINDS_{200hPa}$ were found between the composites over the Philippines, suggesting that the low-level circulations largely affected the pre-summer monsoon *OLR* fields over the country.

Next, we analyzed one case of the Type W cases to determine the different synoptic-scale convective processes during the pre-summer monsoon period. The first case study analyzed is the period from April 1 to June 4, 1981. This is a sample year with no reported TC in the vicinity of the Philippines. Using *OLR* and U_{925hPa} averaged over Luzon Island (120–122.5°E, 12.5–22°N), we identified intermittent wet activities such as those on May 11 that is associated with the reversal of the U_{925hPa} from easterly to westerly, and May 17, when the U_{925hPa} shifted to easterlies again and a deformation zone developed north of Luzon Island. The May 17 case is special since a westward propagating cold front also exists along 30°N during this day. However, in general, easterlies also bring convection over the Philippines (e.g., Akasaka, 2010). Based on these results, we further classified the Type W cases into two sub-types based on the wind conditions, (1) wet conditions associated with westerlies (Type W_W), and (2) easterlies (Type W_E), and created composites. The Type W_E (Type W_W) accounts for about 63.05 % (36.95 %) of the total Type W cases. Another classification was analyzed, which is a subset of Type W_E cases, when a deformation zone developed north of Luzon Island that is accompanied by an eastward propagating cold front, an anticyclone to its west, and another stationary anticyclone over the north Pacific (Type

W_{EDef}). There were only 52 of such cases out of the 273 Type W_E cases from 1979 to 2012, 11 of which lasted for at least 2 consecutive days, indicating its rarity. The interaction of the cold front north of the deformation zone and the warm and humid air from the prevailing easterlies induced enhanced convergence and convection over Luzon Island. Moreover, the Type W_W composites showed apparent southwesterly winds over the Philippines and the WNPSH that is located to the east of the Philippines, indicating that the summer monsoon over the Indochina Peninsula and the SCS has already started. In contrast, the Type W_E composite showed enhanced convection over the Philippines, with apparent southeasterlies that converged with the summer monsoon westerlies over the Indochina Peninsula.

Of course, the impact of TCs on the pre-summer monsoon convection cannot be neglected. Kubota *et al*. (2017) found that TCs located in the vicinity of the Philippines can enhance the moist southwesterly winds resulting to an advanced onset of the summer monsoon over the Philippines. In this study, we also found that TCs located over Luzon Island or over the SCS may interact with the cold front as in the May 13, 2006 case. We speculated that the southerlies on the eastern flank of the TC carries warm and humid air from the tropics and interacts with the cold front. This favors enhanced convergence and the convection generated through this interaction may resupply the moisture carried by the TC. Olaguera *et al*. (2019b) documented such case during the winter season over the southern Philippines, when a westward propagating low-pressure area interacted with the cold front that led to extensive flooding over Cagayan de Oro City in Mindanao Island. Meanwhile, using numerical experiments, Wu *et al*. (2009) examined a winter heavy rainfall event over Taiwan that is associated with the interaction of Typhoon Babs (1998) and the northeast monsoon. When they reduced the size of the typhoon vortex in their simulation, they found that the cold front

north of Taiwan moves southward at a faster pace. They also carried out an experiment without an imposed typhoon vortex and found that the rainfall over northeast Taiwan is greatly reduced compared with the simulation with a reduced typhoon vortex.

In general, the results of this study revealed that aside from the convective activity brought by the easterly $WINDS_{925hPa}$ along the southern flank of the WNPSH, mid-latitude disturbances may also contribute to the pre-summer monsoon convection over the Philippines. For the first time, the role of deformation zones as another convective system during the pre-summer monsoon season over the country was presented. There are still many issues left unaddressed in the present study. For instance, we only showed that the intermittent convective events during the pre-summer monsoon season is a synoptic-scale phenomenon. The contribution of the localized thunderstorms on the pre-summer monsoon convection have yet to be investigated. Also, the percentage contribution of all these aforementioned factors on the total pre-summer monsoon convection of the Philippines should be quantified. For example, the percentage contribution of the different cases presented in Table 2.1 can be quantified by generating composites of rainfall using station data and then getting the ratio of these rainfall composites to the total pre-summer monsoon rainfall of the Philippines. The role of cold fronts in triggering the onset of the summer monsoon over the SCS has long been recognized (Chan *et al*., 2000). In fact, it is one of the factors that makes the onset detection of the summer monsoon over the SCS more complicated (Wang *et al*., 2004). The current available indices in detecting the onset over the SCS such as those proposed by Wang *et al*. (2004) are oversimplified and excludes the impact of these cold fronts. Finally, how these cold fronts can also affect the onset of the summer monsoon over the Philippines is also an interesting issue.

Chapter 3. A climatological analysis of the monsoon break following the summer monsoon onset over Luzon Island, Philippines

3.1. Introduction

The Asian summer monsoon (ASM) is well known for its stepwise evolution, prominent sub-seasonal variabilities—active-break cycles in rainfall, and abrupt changes that has been documented in many studies (e.g., Nakazawa, 1992; Matsumoto, 1992; Yanai *et al*., 1992; Murakami and Matsumoto, 1994; Matsumoto, 1995; Ueda *et al*., 1995; Ueda and Yasunari, 1996; Lau and Yang, 1997; Wang and Xu, 1997; Wu and Wang, 2000, 2001; Lin and Wang, 2002; Wu, 2002; Ueda, 2005; Hung and Hsu, 2008, among others). For instance, Nakazawa (1992) showed the phase-locking feature of the seasonal progression of the ASM in the annual cycle and identified two important stages of rainfall enhancement. According to his study, the first enhancement of rainfall appears over the Indian Ocean in late May to early June, while the second enhancement occurs rather abruptly in late July over the western North Pacific (WNP). Lau and Yang (1997) showed that the summer monsoon starts in the Philippine area from south to north in early to mid-May. Murakami and Matsumoto (1994), Matsumoto (1995), and Wu and Wang (2000, 2001) showed that the onset of the summer rainy season progresses from west to east in mid-May to mid-June over the Philippines before proceeding northeastward in mid to late July.

Wang and Xu (1997) documented the breaks in rainfall during the summer monsoon season over the WNP. They attributed these breaks to the arrival of the dry phase of the Climatological Intra-Seasonal Oscillation (CISO). Matsumoto (1997) also identified a break in the summer rainy season over the Indochina Peninsula using pentad mean rainfall over Thailand. Takahashi and Yasunari (2006) suggested that this

break is associated with a quasi-stationary ridge that is induced by the interaction of the monsoon westerlies and the topography of the Indochina Peninsula. On the other hand, Chen *et al*. (2004) pointed out that the break in the East Asian Summer Monsoon (EASM) occurs during the transition from the Mei-yu to the TC season. An earlier study by Lau et al. (1988) suggested that this break is due to the westward/northwestward shifting of the western North Pacific Subtropical High (WNPSH) over East Asia. So and Chan (1997) investigated the break in rainfall in South China (SC) from April to June using the rainfall data in Hong Kong. They found that the increase in convective clouds during the onset and active periods over the SC region leads to a reduction in solar radiation, decrease in temperature, and an increase in sea level pressure that are favorable for the westward intrusion of the WNPSH. Meanwhile, Ramage (1952) also documented a monsoon break over SC using the rainfall data from Hong Kong, Lungchow, and Taiwan from late June to early July. He suggested that this is related to the northward migration of the WNPSH.

Located in the western rim of the Pacific Ocean, the Philippines is part of the ASM system and its agricultural sector relies heavily on monsoon activity. The start of the planting season, for example, over most parts of the country coincides with the onset of the summer monsoon. In general, the Philippines can be divided into three major island groups, Luzon (Northern Philippines), Visayas (Central Philippines), and Mindanao (Southern Philippines). Luzon Island is the largest island and with mountain ranges with heights of more than 500 m, as shown in Figure 3.1. These mountain ranges along the eastern coast (Sierra Madre) and western coast (Cordillera and Zambales Mountain ranges) of Luzon Island induces monsoon blocking effects such that during the summer monsoon season, the areas along the eastern coast experience its dry season, whereas the areas along the western coast experience its wet season. The

opposite is true during the winter monsoon season. Therefore, the stations located along the western (eastern) coast of Luzon Island or the Philippines, in general, are often used in defining the summer (winter) monsoon season of the country. Flores and Balagot (1969) noted that the summer monsoon over the Philippines (hereafter, PSM following Wang and Xu, 1997) originates as trades from the Indian Ocean Anticyclone during the Southern Hemisphere winter and reaches the country as southwesterlies. The onset of the PSM generally occurs between mid-May to late May and ends in October, although sometimes it may last until November or December (Flores and Balagot, 1969; Moron *et al*., 2009; Akasaka, 2010).

Moreover, the rainfall of the Philippines is influenced by multi-scale systems such as the monsoons, (Akasaka *et al*., 2007), the Inter-tropical Convergence Zone (ITCZ) (Yumul *et al*., 2011), the El Niño Southern Oscillation (ENSO) (Roberts *et al*., 2009; Lyon and Camargo, 2009), Tropical Cyclone (TC) activities (Cayanan *et al*., 2011; Kubota *et al*., 2017), the Intra-seasonal oscillations (ISO) (Pullen *et al*., 2015), the Pacific-Japan (P-J) Pattern (Kubota *et al*., 2016), and the WNPSH (Flores and Balagot, 1969; Lin and Wang, 2002). However, it is only recently that the impacts of these systems on the local climate of the Philippines have been elucidated compared with the adjacent regions (e.g., South China Sea (SCS), Indochina, and South Asia). For example, no onset date isolines are depicted in the classical textbooks such as Ramage (1971) or Tao and Chen (1987), although local onset maps are depicted by Asuncion and Jose (1980) using station-based rainfall.

While several studies such as Akasaka *et al*. (2007), Moron *et al*. (2009), Akasaka (2010), and Cruz *et al*. (2013) have examined the onset, withdrawal, seasonal climatology, and regional differences of the PSM, the important sub-seasonal variations (i.e., active-break cycle) during the life cycle of the summer monsoon season in the

Philippines are less emphasized in these studies. Therefore, the present study is our initial attempt to fill this research gap. In addition, an understanding of these sub-seasonal variations is important for a better understanding of the weather and climate variability of the Philippines.

This paper is organized as follows. The data and methodology used in this study are described in Section 3.2. We identify and characterize the monsoon break including its climatology through a composite analysis and the possible mechanism inducing it in Section 3.3. The summary and discussion are provided in Section 3.4.

3.2. Data Sources and Methodology

3.2.1. Data

The primary datasets analyzed in this study include:

(1) Daily rainfall data at 11 meteorological stations from the Philippine Atmospheric, Geophysical and Astronomical Services Administration (PAGASA), the country's official weather bureau. These stations are shown in Figure 3.1 and the annual variations of the mean daily rainfall of selected stations are shown in Figure 3.2. These stations have relatively complete record during the analysis period. In addition, these stations have the same climate type and commonly used in characterizing the summer monsoon season of the Philippines including its onset (e.g., Cruz *et al.*, 2013; Kubota *et al.*, 2017).

(2) Daily rainfall data from the Tropical Rainfall Measuring Mission Multi-Satellite Precipitation Analysis (TRMM-TMPA) 3B42RT version 7 (Huffman and Bolvin, 2015), with 0.25° × 0.25° resolution.

(3) Daily reanalysis data, with 2.5° × 2.5° horizontal grid resolution, of zonal winds (*U*), meridional winds (*V*), geopotential height (*HGT*), and temperature (*TEMP*) from the National Center for Environmental Prediction-Department of Energy (NCEP-DOE) Atmospheric Model Intercomparison Project (AMIP-II) Reanalysis (Kanamitsu *et al*., 2002) at multiple levels.

3.2.2. Methodology

The analysis period starts from 1998 to 2012. We only focus our analysis around Luzon Island because the monsoon break after the onset is only clear around this region, as will be shown later. According to the Philippine Statistics Authority (PSA, 2016), the largest percentage of total rice production in the Philippines in 2016 came from Luzon Island (59 %), suggesting that it is an important agricultural region in the country.

We define "Luzon Island" and its vicinity as the region within 120°E–122.5°E and 12.5°N–22°N, where for brevity, is simply referred to as "Luzon Island". We also used the summer monsoon onset dates provided by PAGASA. These onset dates were obtained following the criteria indicated in the 2019 memorandum of PAGASA and stated as follows: (1) The beginning of a five-day period (between May and July) with total rainfall of about 25 mm or more, with three consecutive days having at least 1 mm of rainfall per day. These conditions should be satisfied in at least seven stations located over the western coast of the Philippines. These stations include: Laoag, Vigan (Sinait), Dagupan, Iba, San Jose (Mindoro), Metro Manila, Ambulong (Batangas), Iloilo, Nueva Ecija (Muñoz), Clark (Pampanga), Cubi Point (Subic), Coron (Palawan), and Cuyo (Palawan) (open circles in Figure 3.1; for Metro Manila, only the Science Garden

station is shown). For Metro Manila to be included in this criterion, at least three of the four Metro Manila stations (i.e., Science Garden, Sangley Point, Port Area, and NAIA) must have satisfied (1). Additionally, PAGASA has the disposition to include other variables such as prevailing westerly winds (i.e., westerly from surface to 850 hPa level) in the onset criteria. It is important to note that the summer monsoon onset date is taken simultaneously or spatially averaged across the aforementioned stations over the western coast of the Philippines. In this study, we used the Science Garden station as a representative of the stations over Metro Manila (e.g., Cruz *et al*., 2013; Olaguera *et al*., 2018a). We exclude Nueva Ecija (Muñoz) station in the analysis because it has a lot of missing data after 2001. In addition, we used two additional stations that are located over the northern (Basco station) and central Luzon Island (Baguio and Cabanatuan stations).

3.3. Results

3.3.1. Climatological characteristics of the summer monsoon over the Philippines

Figure 3.2 shows the climatological rainfall time series from 1998–2012 of selected 8 stations over Luzon Island. The first rainfall peak, which exceeds 10 mm day^{-1}, occurs around late May to early June in these stations. This indicates the onset of the summer rainy season over the Philippines. A distinct decrease in rainfall below 10 mm day^{-1} follows this first rainfall peak and is very clear in stations located over the north (Basco, Vigan, Laoag, and Baguio; Figures 3.2a to d) and central Luzon Island (Cabanatuan, Dagupan, and Science Garden; Figures 3.2e to g). The stations that are located over the southern Luzon Island such as Coron (Figure 3.2h), Ambulong, and Iloilo stations do not show such remarkable decrease in rainfall compared with those

located in the north and central Luzon Island. The monsoon break is also not clear in Iba station probably because it is located on the windward side of the Zambales mountain range compared with Dagupan and Cabanatuan stations that are in the central plain of Luzon Island. We checked the rainfall time series over Clark (Pampanga) and Cubi Point stations (not shown), respectively. However, the monsoon break is also not clear in these stations. Several decreases in rainfall can also be seen between July and September in all the stations, indicating the regional differences in the climatological monsoon pattern and the large impact of ISOs on the rainfall of the Philippines.

There are no uniform criteria in defining a monsoon break. Chen *et al*. (2004), for example, defined the monsoon break over East Asia as the period when the frontal activity diminishes and rainfall decreases to below 5 mm day^{-1}. On the other hand, Rajeevan *et al*. (2010) defined the monsoon break during the summer monsoon over India as the period when the standardized daily rainfall anomaly is below −1 standard deviation for at least 3 consecutive days. In this study, we define a monsoon break as the period following the onset when rainfall decreases below 5 mm day^{-1} and should last for at least three consecutive days or more. The 5 mm day^{-1} value is based on Moron *et al*. (2009) who noted that the dry season over the western coast of the Philippines usually have rainfall amounts that is less than this value. Since the onset dates are simultaneously obtained in stations located over the western coast of the Philippines, we identified the breaks from the average rainfall across the 7 stations, where the monsoon break is clear, as shown in Figure 3.2 (stations marked with black crosses). These stations include Basco, Vigan, Laoag, Baguio, Cabanatuan, Dagupan, and Science Garden. In addition, we only focus on the first break following the onset in each year. This way, the monsoon break can be treated as a step-related to the onset. The detected first post-onset breaks are summarized in Table 3.1.

The average of the PAGASA onset dates from 1998–2012 is May 22 with standard deviation of about 11 days, while the average starting date of the monsoon break period is June 2, with standard deviation of about 14 days. On the average, the first monsoon break following the onset only lasts for about five days and occurs 12 days after the onset. The earliest monsoon break occurred in 2009 (May 10–13), while the latest occurred in 2006 (June 28–July 4).

3.3.2. Changes in the large-scale conditions

To further depict the development of the first post-onset break, we performed lag composite analysis, where Lag 0 corresponds to the first day of the monsoon break period. The previous and succeeding lag days are denoted with "–" and "+" signs, respectively.

3.3.2.1. *Circulation changes at 850 and 200 hPa levels*

Figure 3.3 shows the lag composites of the TRMM rainfall, 850 hPa winds ($WINDS_{850hPa}$), and 850 hPa *HGT* (HGT_{850hPa}), while Figure 3.4 shows the lag composites of the 200 hPa winds ($WINDS_{200hPa}$) and *HGT* (HGT_{200hPa}). At Lag –20 (Figure 3.3a), the WNPSH, which is indicated by the 1, 500-m HGT_{850hPa}, is located just at the northern tip of Luzon Island and rainfall reaches by about 11 mm day^{-1}. Prior to this day, the WNPSH is located over the Indochina Peninsula and progresses eastward (not shown). This eastward retreat of the WNPSH is a well-known feature of the ASM onset (Lau and Yang, 1997; Zhang *et al*., 2004; Akasaka, 2010). Strong southwesterly $WINDS_{850hPa}$ are apparent over the western Indochina Peninsula that is accompanied by enhanced rainfall of about 20 mm day^{-1}. Matsumoto (1997) first noted that the earliest onset of the ASM starts over the Indochina Peninsula. Zhang *et al*.

(2004) later suggested that this is due to the convergence of southwesterly $WINDS_{850hPa}$ originating from the Bay of Bengal and southeasterly $WINDS_{850hPa}$ from the southern flank of the WNPSH. They also pointed out that the onset is accompanied by the reversal of meridional temperature gradient in the entire troposphere and the establishment of an easterly vertical wind shear over the Indochina Peninsula. Furthermore, southerlies are also apparent over the SCS originating from the southern flank of the WNPSH. The rainfall over the Indian Subcontinent is less than 5 mm day^{-1}, indicating that the summer monsoon has not started yet in this region. Enhanced southwesterly $WINDS_{850hPa}$ can also be seen over SC and the Okinawa region, and rainfall starts to increase to about 11 mm day^{-1} over SC, which indicates the onset of the Mei-yu over this region. The $WINDS_{200hPa}$ (Figure 3.4a) shows an anticyclonic circulation centered around 105°E, 20°N during this period (i.e., the Tibetan/South Asian Anticyclone; SAA). The eastern edge (12470 m HGT_{200hPa}) of this anticyclone stretches further east to the dateline.

Figures 3.3b and 3.4b show the spatial structures of TRMM rainfall, $WINDS_{850hPa}$, HGT_{850hPa} at Lag –12. This period corresponds to the onset of the PSM. The southwesterly $WINDS_{850hPa}$, starts to strengthen and stretches from the western Indochina Peninsula, SCS, Luzon Island, and the Okinawa region. Over the western coast of Luzon Island, the TRMM rainfall increased to about 14 mm day^{-1}. The western edge of the WNPSH is located around 130°E. Westerly $WINDS_{850hPa}$ also starts to strengthen south of 10°N in the southeastern part of the Indian Subcontinent. Westerlies can also be depicted to the west of the Indian Subcontinent. However, rainfall is still around 5 mm day^{-1} over this region. The rainfall over the Okinawa region further intensifies during this period. At 200 hPa (Figure 3.4b), the SAA intensifies and progresses northwestward. Enhanced northeasterly $WINDS_{200hPa}$ appear over the SCS

and southern Luzon Island. The intensification of the SAA has been linked by previous studies to the increase in the diabatic heating following the abrupt expansion of warm air over the Tibetan Plateau (e.g., Yanai *et al*., 1992). Yanai *et al*. (1992) suggested that such warming leads to the reversal of the meridional temperature gradient over the south of the Tibetan Plateau that is favorable for the quick establishment of the southwesterly $WINDS_{850hPa}$ over the tropical Indian Ocean.

At Lag –5 (Figure 3.3c), the WNPSH further retreats eastward (near 135°E), westerly to southwesterly $WINDS_{850hPa}$ is established, and rainfall increases along the equator and 10°N. Enhanced rainfall (~14 mm day^{-1}) can also be seen over the southwestern Indian Subcontinent, SCS, and Luzon Island. An anticyclonic circulation that is centered around 120°E, 35°N can be seen over eastern China and rainfall decreases to about 5 mm day^{-1} over the Korean Peninsula, Taiwan, and the Okinawa region. At 200 hPa (Figure 3.4c), the eastern edge of the SAA is located around 150°E. Northeasterly $WINDS_{200hPa}$ along the eastern edge of this anticyclone can be seen over the central Luzon Island.

At Lag 0 (Figure 3.3d), the WNPSH moves westward and the western edge of the 1, 505-m HGT_{850hPa} contour line is located over Luzon Island. Rainfall also decreases below 5 mm day^{-1} over Luzon Island. Enhanced westerly $WINDS_{850hPa}$ can be seen over the western Indian Subcontinent that is induced by the southward shift of the 1, 500-m HGT_{80hPa} contour line, and the rainfall over this region reaches by about 17 mm day^{-1}. This indicates the onset of the Indian summer monsoon (ISM). On the other hand, the northern part of the WNPSH establishes the Mei-yu/Baiu frontal zone over SC, Taiwan, and the Okinawa region, as indicated by the enhanced rainfall in these regions. Southeasterly $WINDS_{850hPa}$ can also be seen over the equatorial WNP between 120 to

150°E. At 200 hPa (Figure 3.4d), the SAA moves further northwest of the Indochina Peninsula and its center is located around 100°E, 22°N. Easterly/northeasterly $WINDS_{200hPa}$ can be seen over the Philippines during this period.

At Lag +5 (Figure 3.3e), the western edge of the 1, 505-m HGT_{850hPa} contour line is still located over Luzon Island. Southerly $WINDS_{850hPa}$ can be seen over the SCS, while southerly/southeasterly $WINDS_{850hPa}$ are apparent over the Philippines. The rainfall amounts over the western Indian Subcontinent and Indochina Peninsula increases due to the acceleration of moist westerly winds along 10–20°N, and almost reaches by about 30 mm day^{-1}. The southeasterly $WINDS_{850hPa}$ along the southern flank of the WNPSH converges with the westerlies near the equatorial region around 120°E. This indicates the strengthening of the ITCZ. At 200 hPa (Figure 3.4e), the SAA strengthens, expands westward, and progresses further north. Its northern edge is located along 30°N.

At Lag +7 (Figure 3.3f), the 1,505-m HGT_{850hPa} shifts to the east of the Philippines. Southwesterly $WINDS_{850hPa}$ reappears over Luzon Island and rainfall increases again to about 17 mm day^{-1}. At 200 hPa (Figure 3.4f), the SAA continues its northwestward advance. At Lag +12 (Figure 3.3g), the western edge of the WNPSH retreats further eastward, with the 1, 500-m HGT_{850hPa} located over the eastern Luzon Island, and rainfall is reactivated over the Philippines. Southwesterly $WINDS_{850hPa}$ are apparent over Luzon Island. The westerly winds south of 10°N originating from the tropical Indian Ocean further intensify. Southwesterly $WINDS_{850hPa}$ also appear over the southern Philippines. At 200 hPa (Figure 3.4g), enhanced northeasterly $WINDS_{200hPa}$ that are associated with the SAA are apparent over the Philippines, which is consistent with the enhancement of rainfall in this period.

At Lag +18 (Figure 3.3h), the WNPSH progresses northward and a decrease in rainfall can be seen over Taiwan and the Okinawa region, indicating the end of the Mei-yu and Baiu in these regions, respectively. The rainfall over Luzon island appears to be due to the convergence of the monsoon southwesterly $WINDS_{850hPa}$ and the southeasterly $WINDS_{850hPa}$ from the southern flank of the WNPSH. Another remarkable feature is the enhanced southwesterly $WINDS_{850hPa}$ around 10°N at the southern flank of the WNPSH, indicating the northward progression of the ITCZ. In addition, rainfall further intensifies over mainland China and mainland Japan, which indicates the mature phase of the Mei-yu and Baiu in these regions. At 200 hPa (Figure 3.4h), the SAA progresses northwards and its northern flank is located along 35°N.

3.3.2.2. *Circulation changes at 500 hPa level*

How does the westward propagation of WNPSH induces dry weather conditions over Luzon Island? To answer this question, we first look at the lag composites of 500 hPa vertical velocity. Note that negative (positive) values of vertical velocity indicates mid-tropospheric ascent (descent). Mid-tropospheric ascent can be seen over Luzon Island from Lag −20 to Lag −5 (Figures 3.5a to c). This is consistent with the enhanced rainfall, as shown in Figure 3.3 due to the eastward retreat of the WNPSH. During the onset period (i.e., Lag −12), the vertical velocity reaches by about -10×10^{-2} Pa s^{-1} over Luzon Island. At Lag 0, mid-tropospheric descent can be seen over southwestern Philippines. However, the values of the vertical velocity are weak (less than 2×10^{-2} Pa s^{-1}). This is still consistent with the rainfall in stations located over this region, as shown in Figure 3.2, where the rainfall does not decrease remarkably during the break period. Furthermore, during this period, the western edge of the WNPSH is located over Luzon Island (Figure 3.3d). Mid-tropospheric ascent can be seen to the north of Luzon Island

in the same day, which is consistent with the enhanced rainfall due to the convergence of the monsoon southwesterly $WINDS_{850hPa}$ and the southerlies from the western edge of the WNPSH in this area. In the succeeding lag days (Figures 3.5e to h), the location of the descending air shifts to the north, which is consistent with the northward migration of the WNPSH. The values of the vertical velocity between Lag 0 and Lag +5 exceed 2×10^{-2} Pa s^{-1}, especially over the central and northern Luzon Island (not shown). At Lag +5 (Figure 3.5e), the mid-tropospheric descent seems to be confined along 12–15°N, with higher values of vertical velocity over the central and northern Luzon Island. At Lag +7 (Figure 3.5f), weak mid-tropospheric ascent can be seen over Luzon Island, suggesting the reactivation of the summer monsoon over this region. Mid-tropospheric ascent can be seen over Luzon Island in the succeeding lag days (Figures 3.5g and h), which is consistent with the increase in rainfall over this region, as shown in Figures 3.3g and h. In general, the westward intrusion of the WNPSH induces mid-tropospheric descent over Luzon Island. Olaguera *et al*. (2018a) noted that such mid-tropospheric descent is one of the factors that induces unfavorable conditions for synoptic-scale activities over Luzon Island.

3.3.2.3. *Changes in moisture transport*

Moreover, it is known that moisture transported from the Indian Ocean by the monsoon westerlies are essential for the formation of rainfall over the Philippines (e.g., Flores and Balagot, 1969; Olaguera *et al*., 2018a). Therefore, we also examined the time series of the averaged vertically integrated moisture flux convergence (*VIMFC*) over Luzon Island, as shown in Figure 3.6a. The vertical integration was performed from 1000 hPa to 300 hPa following Olaguera *et al*. (2018a, b). The *VIMFC* reaches by about 6×10^{-6} kg m^{-2} s^{-1} during the onset period (Lag −12) and gradually increases to

about 9×10^{-6} kg m^{-2} s^{-1} at Lag –4. This is followed by a sharp decrease in *VIMFC* at Lag –3. Then, the *VIMFC* decreases below 0 at Lag +1 until Lag +5, indicating enhanced divergence during the monsoon break period. In the succeeding lag days, convergence reappears over Luzon Island (between Lag +6 to Lag +20). However, the values are weaker (below 4×10^{-6} kg m^{-2} s^{-1}) compared with those before the monsoon break.

Also shown in Figure 3.6a is the averaged zonal wind at 850 hPa (U_{850hPa}; green line) over Luzon Island. It appears that the enhanced *VIMFC* during the onset is accompanied by enhanced westerly U_{850hPa}, while during the break period, the westerly U_{850hPa}, weakens and easterlies appear over Luzon Island until Lag +5. In the succeeding lag days, the U_{850hPa} remained around +2 m s^{-1} until Lag +16, which is relatively weaker than those during the onset.

3.3.2.4. *Changes in synoptic-scale disturbances*

To explain why such weakening of the $WINDS_{850hPa}$ persisted for a longer time, we checked the averaged HGT_{850hPa} over Luzon Island in Figure 3.6b. During the onset, the WNPSH decreases below 1493 m, which is consistent with Figure 3.3b, where the WNPSH is located to the east of the Philippines. During the break period, the HGT_{850hPa} increased to about 1507 m, which is consistent with the westward intrusion of the WNPSH, as shown in Figures 3.3d and e. From Lag +7 to Lag +12, the values of the HGT_{850hPa} remained below 1, 500-m but not as remarkable compared with those during the onset period. This means that the WNPSH is still located near Luzon Island and has not progressed northwards yet, indicating that the ITCZ is not yet fully developed. This may have hindered the intrusion of westerly $WINDS_{850hPa}$ over Luzon Island. From Lag

+16 to Lag +20, Luzon Island is located just between the 1, 500 and 1, 505-m HGT_{850hPa} contour line, like those features at Lag +18 (Figure 3.3h).

Aside from the low-level divergence, some studies have pointed out that an anticyclone and enhanced vertical zonal wind shear located near the Philippines can suppress the development of synoptic-scale disturbances (e.g., Olaguera *et al*., 2018a). Therefore, we checked the time series of the vertical zonal wind shear (*USHEAR*; U_{200hPa} minus U_{850hPa}) over Luzon Island, as shown in Figure 3.6b. Note that a more negative *USHEAR* indicates stronger westerly U_{850hPa} than easterly U_{200hPa}. The *USHEAR* starts to decrease below 0 around Lag +14, which is consistent with the enhancement of the U_{850hPa}, as shown in Figure 3.6a. Then, the *USHEAR* gradually decreases until Lag 0 (−7 m s^{-1})., The *USHEAR* is enhanced until Lag +5 to about −4 m s^{-1} during the monsoon break period. In the succeeding lag days, it gradually decreases again. This enhanced *USHEAR* during the monsoon break period, together with the enhanced low-level divergence and mid-tropospheric descent, imply that the atmospheric conditions over Luzon Island are unfavorable for synoptic-scale disturbances.

To confirm whether the synoptic-scale disturbances are suppressed during the monsoon break period, we illustrate the time series of the average perturbation kinetic energy (*PKE*) over Luzon Island at 850 hPa in Figure 3.7a. This atmospheric parameter can be used to represent synoptic-scale disturbances including those disturbances that are weaker than TCs (i.e., residual lows, mid-latitude fronts, etc.) (e.g., Olaguera *et al*., 2018a, 2018b). The *PKE* is calculated using the formula: $PKE = \overline{\left(u'^2 + v'^2\right)}/2$, where u' and v' are the perturbations obtained by subtracting an 11-day running mean to the daily U_{850hPa} and V_{850hPa} winds, respectively, while the overbar indicates the daily

means. During the onset period (Lag −12), the *PKE* increases to about 17.5 m^2 s^{-2}, indicating enhanced synoptic scale activities during this period. The *PKE* gradually increases in the succeeding lag days and peaks at Lag –2 (~30 m^2 s^{-2}). Then, it decreases to about 11 m^2 s^{-2} at Lag +1 and remains below 17.5 m^2 s^{-2} until Lag +13. This indicates that the synoptic-scale disturbances are suppressed during the monsoon break period, which corroborates the unfavorable background conditions mentioned previously. The PKE peaks again at Lag +15 and reaches by about 23 m^2 s^{-2}. We confirmed that an enhanced southerly wind, related to the western edge of the WNPSH, appeared over Luzon Island during this period (not shown). We also show the spatial map of TRMM, $WINDS_{850hPa}$, and HGT_{850hPa}, to explain the peak in *PKE* at Lag –2 in Figure 3.7b. Enhanced southwesterly $WINDS_{850hPa}$ can be seen from the Bay of Bengal to the Okinawa region along the northwestern flank of the WNPSH and enhanced rainfall of about 17 mm day^{-1} can be seen around Luzon Island. The WNPSH is also located to the east of Luzon Island. These results suggest that the eastward retreat of the WNPSH favors the enhancement of the synoptic-scale disturbances over Luzon Island.

3.3.3. Possible mechanisms inducing the monsoon break

As mentioned previously, So and Chan (1997) examined the post-onset break over SC during the summer monsoon season for the period 1985–1990 and suggested a cloud-radiation feedback mechanism that facilitated the westward intrusion of the WNPSH. They suggested that the convective clouds during the onset period reduce the incoming solar radiation leading to a decrease in temperature and an increase in the mean sea level pressure (*MSLP*) over the SC region. This increase in *MSLP* leads to a decrease in rainfall and favors the westward intrusion of the WNPSH. Huang and Sun

(1992) also suggested that the decrease in rainfall over the Philippines favors the westward/southward intrusion of the WNPSH.

To confirm this mechanism, we illustrate the *MSLP*, net shortwave radiation flux (*NSWR*), temperature at 850 hPa ($TEMP_{850hPa}$) averaged over Luzon Island in Figure 3.8. It is worth mentioning that higher values of the *NSWR* means more incoming solar radiation, which indicates less cloudiness or convective activity. Prior to the monsoon break, the *MSLP* drops to about 1007 hPa, while the *NSWR* drops to about 200 K (Figure 3.8a). In the same period, the $TEMP_{850hPa}$ is also below 292.6 K (Figure 3.8b). This is consistent with the enhanced rainfall during the onset, which may have cooled the atmosphere, as shown in Figure 3.3. The *MSLP*, *NSWR*, and $TEMP_{850hPa}$ start to increase at Lag −7. At Lag 0, the *MSLP* increases to about 1008.7 hPa, while the $TEMP_{850hPa}$ increases to about 292.8 K. In the same period, the *NSWR* increases to about 220 K. At Lag +5, the *MSLP* begins to decrease again, while the *NSWR* and $TEMP_{850hPa}$ start to decrease after Lag +6. While the values of the *MSLP* remained between 1008.5 hPa and 1009 hPa, the values of the $TEMP_{850hPa}$ gradually decreases in the succeeding lag days. This gradual decrease in $TEMP_{850hPa}$ indicates that frequent rainfall occurrences after the break cools the atmosphere. The increase in *MSLP*, *NSWR*, and $TEMP_{850hPa}$ during the monsoon break period are consistent with the decrease in rainfall and the westward intrusion of the WNPSH. Therefore, the mechanism proposed by So and Chan (1997) for the monsoon break over SC is one potential mechanism that can explain the monsoon break over the Philippines.

3.4. Summary and Discussion

This study investigated the climatology of the first post-onset break in rainfall over Luzon Island (120–122.5°E, 12.5–22°N) from 1998 to 2012. We defined the monsoon

break as the period with rainfall below 5 mm day^{-1} after the onset that lasted for three consecutive days or more. On the average, the examined monsoon breaks lasted for about 5 days and occurred 11 days after the onset. Specifically, the climatological onset date from 1998–2012 is May 22, while the first day of the monsoon break period is June 2.

We also found that the cloud-radiation feedback mechanism proposed by So and Chan (1997) for the monsoon breaks over SC is one potential mechanism that could have facilitated the westward intrusion of the WNPSH over Luzon Island. However, So and Chan (1997) composited all the breaks during the summer monsoon season over SC (i.e., from April to June). Hence, this study is the first attempt to examine the monsoon break as a step related to the onset of the summer monsoon over the Philippines. In addition, this is also the first attempt to clarify the local impact of the WNPSH in the early summer monsoon season of the Philippines. The summer monsoon onset is characterized by enhanced convective activity, cloudiness, decreased *MSLP*, and decreased incoming solar radiation. However, the enhanced convective activity eventually leads to the cooling of the atmosphere and subsequent increase in *MSLP* in the succeeding periods. This, in turn, favors the westward intrusion of the WNPSH. The westward intrusion of the WNPSH induced enhanced divergence, enhanced vertical zonal wind shear, mid-tropospheric descent, weakening of the monsoon westerlies, and subsequent decrease in moisture transport over Luzon Island. These changes are unfavorable for synoptic-scale disturbances, as substantiated by the decreased *PKE* during the monsoon break period.

After the monsoon break period, the magnitudes of the *MSLP* and *NSWR* (1008.5 hPa and 250 W m^{-2}, respectively) are relatively higher compared with those during the

onset period, when their magnitudes decreased to about 1008 hPa and 200 W m^{-2}, respectively. These can be explained by the weaker moisture convergence and monsoon westerlies after the break compared with those during the onset period. The weaker monsoon westerlies can be explained by the fact that the WNPSH is still near Luzon Island, which could have hindered the intrusion of the westerly winds over this region, and that it has not progressed northwards yet. The time-series of the HGT_{850hPa} shows that its magnitude remained between 1, 497 to 1, 500 m after the break compared with those during the onset period, when it decreased to about 1490 m. The PKE also remained weaker until Lag +15, which can be explained by the weaker monsoon westerlies after the break.

The precise controlling mechanism for the zonal displacement of the WNPSH in early summer is not yet known. Some studies used numerical models to explain the mechanisms controlling its zonal displacement during the summer monsoon season (e.g., Lu and Dong, 2001). However, these numerical models have large uncertainties and gave inconsistent results compared with actual observations (e.g., Kawatani *et al*., 2008). For instance, Lu and Dong (2001) used an Atmospheric General Circulation Model (AGCM) to investigate the relationship between the local sea surface temperature (SST) anomalies and the zonal displacement of the WNPSH during the June to August season (JJA). They found that the lower SST anomalies over the warm pool region (110–160°E, 10–20°N) leads to suppressed rainfall, which is favorable for the westward intrusion of the WNPSH. However, the recent observational study by Kawatani *et al*. (2008) revealed inconsistencies in their results, especially for June and July. In particular, Kawatani *et al*. (2008) found that the geopotential height (*HGT*) anomalies over the western Pacific have a nearly barotropic structure, with a poleward tilt with height in these months, while the results of Lu and Dong (2001) shows a

baroclinic structure. They further noted that simulating the SST-rainfall relationship is somewhat challenging and that both the local and remote forcing should be considered in numerical simulations. The inability of AGCMs in correctly simulating the SST-rainfall relationship was also pointed out by Wang *et al*. (2005). On the seasonal timescale, there is a negative relationship between SST and rainfall over the WNP (Wang *et al*., 2005; Kubota *et al*., 2016). However, most AGCMs that ignores the atmosphere-ocean interactions leads to positive SST-rainfall relationship (e.g., Dado and Takahashi, 2017). Wang *et al*. (2005) further showed that an AGCM coupled with an ocean model can better simulate this negative SST-rainfall relationship. Nevertheless, correctly simulating the timing of the monsoon break using numerical models is also of great interest.

Although not presented, we also found that the occurrence of the monsoon breaks after the onset have important implications in the summer monsoon onset detection. We compared the PAGASA onset dates and those obtained using a more objective criteria such as those used by Matsumoto (1997), Cook and Buckley (2009), and Luo and Lin (2017). However, these indices led to delayed onset dates. Therefore, we are advocating that the zonal displacement of the WNPSH should be considered in developing a more robust summer monsoon onset criteria in future studies. Moreover, with the appearance of a monsoon break after the onset, it can be inferred that the early stage of the PSM can be divided into three distinct and abrupt phases, as schematically illustrated in Figure 3.9.

Phase I (Onset Phase; Figure 3.9a) features the eastward retreat of the WNPSH, the northward advance of the Tibetan/South Asian anticyclone (SAA), and the onset of the summer monsoon over the SCS and west coast of the Philippines from mid to late

May. This phase almost corresponds to the period before and during Lag −12 in Figures 3.3, 3.4, and 3.5.

Phase II (Break Phase; Figure 3.9b) features the strengthening of the ITCZ in the equatorial WNP, and the sudden westward intrusion of the WNPSH in the lower level, the northwestward migration and intensification of the SAA in the upper level, and the onset of the ISM. This phase largely corresponds to the period between Lag 0 and Lag +5 in Figures 3.3, 3.4, and 3.5. Following the intensification of the $WINDS_{850hPa}$ south of 10°N is the intensification of the ITCZ in the equatorial WNP. The western ridge of the WNPSH is located over Luzon Island and reduces the moisture and rainfall in this region. The onset of the ISM also occurs in this phase. In the upper-level, the SAA moves northwestward over the northwestern part of the Indochina Peninsula.

Phase III (Monsoon Revival Phase; Figure 3.9c) features the revival of the summer monsoon over the Philippines, further expansion of the SAA in the upper level, intensification of the ITCZ, and the mature phase of the Mei-yu/Baiu over central China and mainland Japan. This phase corresponds to the period after Lag +5 in Figures 3.3, 3.4, and 3.5. The rainfall over the Indian Subcontinent and central Indochina Peninsula intensifies because of the acceleration of moist westerly winds along 10–20°N. The WNPSH shifts to the east of the Philippines and proceeds northward following the intensification of the ITCZ. Southwesterly $WINDS_{850hPa}$ are also apparent over Luzon Island. A monsoon break occurs over Taiwan, following the northward migration of the WNPSH. In the upper level, enhanced northeasterly $WINDS_{200hPa}$ along the eastern flank of the SAA are apparent over Luzon Island, which is consistent with the enhanced $WINDS_{850hPa}$ in this region.

Ueda and Yasunari (1996) suggested that the abrupt seasonal changes in the WNP summer monsoon involve important atmosphere-ocean interactions. They pointed out the importance of ISOs as triggers for the northeastward advance of rainfall from the SCS to the east Philippine Sea and the sub-seasonal changes in the SST over the Indian Ocean and the WNP. Previous studies found that instraseasonal oscillations on the 10–25-day timescale is prominent over the WNP in early summer (BSISO; e.g., Fukutomi and Yasunari, 1999, 2002; Kajikawa and Yasunari, 2005; Kikuchi and Wang, 2010; Kikuchi *et al.*, 2012). The impact of BSISO on the local climate of the Philippines will be examined in future studies. The rainfall contribution of the different rainfall-producing weather disturbances in the three phases will be examined in future studies. In addition, since the analysis period is relatively short, we did not examine the interannual variability of the monsoon break. How the sub-seasonal variabilities in the summer monsoon season of the Philippines, in general, are influenced by ENSO is also another interesting topic for future study.

Chapter 4. Non-tropical cyclone related winter heavy rainfall events over the Philippines: climatology and mechanisms

4.1. Introduction

Heavy rainfall events, which often lead to extreme flooding and related disasters (hereafter, HRF), have profound agricultural and socio-economic impacts. Projections from multiple climate models used in the recent assessment report by the Intergovernmental Panel on Climate Change (Stocker *et al*., 2013) show that the HRF events over the tropical regions are "very likely" to increase in the late 21st century. Located over the western rim of the Pacific Ocean, the Philippines is one of the countries over tropical Southeast Asia that is vulnerable to extreme HRF events. Recent observational studies over the country show increasing trends in extreme rainfall (Cinco *et al*., 2014; Villafuerte *et al*., 2014; Villafuerte *et al*., 2015). Therefore, understanding the mechanisms leading to these HRF events is crucial for disaster management and mitigation.

HRF events over the Philippines occur almost throughout the year. Tropical cyclones (TC) generated over the South China Sea (SCS) and the Pacific Ocean are the primary cause of HRF events in the country, especially during the summer monsoon season (Cayanan *et al*., 2011; Kubota *et al*., 2017). Aside from the rainfall brought by TCs upon landfall, it has been shown that non-landfalling TCs can also enhance the prevailing summer monsoon westerlies that bring more rainfall over the country (Cayanan *et al*., 2011). Nevertheless, the number of landfalling and non-landfalling TCs decreases in the succeeding winter monsoon season (i.e., November to March), with the lowest number around March (Cinco *et al*., 2016). Hence, not all HRF events

are associated with TCs. Such seasonality in the TC influence is related to the seasonal migration of the monsoon trough, which provides ambient condition for TC activity.

The HRF events during winter over the tropical Southeast Asia are often associated with cold surges (Yokoi and Matsumoto, 2008; Faustino-Eslava *et al*., 2011), westward propagating cold surge vortices (CSVs) that is formed from the interaction of the cold surges and easterly waves (Chen TC *et al*., 2012, 2013, 2015a, b), and other sub-seasonal variabilities (Pullen *et al*., 2015; Takahashi *et al*., 2011). Yokoi and Matsumoto (2008) found that the interaction of cold surges and the westward propagating tropical depression (TD)-type disturbances (TDDs) is important for the formation of winter HRF events over Vietnam and that the former, alone, does not contribute much to the total rainfall. Chen TC *et al*. (2012, 2013, 2015a, b) extensively examined the formation mechanism of westward propagating CSVs that induce HRF events over the Philippines, Vietnam, Peninsular Malaysia, and Borneo. They documented two types of CSVs: (1) the Philippine CSV that develops east of the Philippines due to the interaction of cold surge flow and easterly wave and the presence of an island-chain trough, and (2) the Borneo CSV that develops due to the interaction of the SCS cold surge flow, the near equatorial trough, and Borneo's orography.

Frequent non-TC related HRF events during winter often cause heavy flooding over the Philippines. Pullen *et al*. (2015), for example, examined an HRF event during February 2008 and linked this event to the interaction of multi-scale systems such as the Indian Ocean Dipole, the strong La Niña condition, the coincidence with the Madden Julian Oscillation (MJO), and cold surge activity. Faustino-Eslava *et al*. (2011) and Yumul *et al*. (2013) also documented an HRF event over the Mindanao Island in the southern Philippines on January 2009, which they associated with a "tail end of a cold front". According to Yumul *et al*. (2013), the accumulated rainfall during January

2009 over Cagayan de Oro City (CDO; 300–400 mm) is almost four times than its climatological rainfall (50–100 mm). Similar HRF events were reported in other parts of Mindanao Island during January 2009 that led to extensive flooding and multiple landslides. Another HRF event occurred just recently over Mindanao Island, which has been locally associated with the interaction of the "tail end of a cold front" and a Low-Pressure Area (LPA) by the Philippine Atmospheric Geophysical and Astronomical Services Administration (PAGASA), the country's official weather bureau. Henceforth, this event will be referred to as JAN2017 for brevity. This HRF event is discussed further in Section 4.3. Moreover, the JAN2017 HRF event is one of the extreme events recorded in the world in the year 2017 (Hoell *et al*., 2019; Christidis *et al*., 2019). For example, an HRF event was also reported in Peru on March 2017 (Christidis *et al*., 2019).

Several issues arise based on the documented winter HRF events over the Philippines:

(1) Non-TC related HRF events such as cold surges also cause extensive flooding over the Philippines. However, most of the previous studies only examined specific cases (e.g., Pullen *et al*., 2015) or focus on the impacts of these HRF events (e.g., Faustino-Eslava *et al*., 2011). How these non-TC related HRF events affect the country in the climatological mean sense have yet to be described in detail;

(2) As will be shown later, the winter HRF events over the country occur more frequently over Mindanao Island (south of 10°N) from December to March of the succeeding year. This seems to be consistent with seasonal change in rainfall and winds over the country. The winter monsoon of the Philippines

usually occurs from November to March and rainfall over the eastern coast gradually increases from north to south (Chen *et al*., 2015a; Kubota *et al*., 2017), concurrent with the seasonal change in the prevailing summer monsoon southwesterlies to northeasterlies. According to the recent agricultural statistics by the Philippine Statistics Authority (PSA) for the year 2017, a large portion of total corn (50 %) and coconut (60 %) productions came from Mindanao Island, indicating that it is an important agricultural region; therefore, understanding the rainfall variability over this region has important ramifications on the economy of the country;

(3) Another purpose of this study is to describe the atmospheric conditions during the JAN2017 HRF event in detail and to discuss the mechanisms responsible for the HRF event over Mindanao Island.

The rest of the paper is organized as follows. Section 4.2 describes the various data sources and methodology used in this study. We investigated the recent extreme HRF during January 2017 and performed composite analyses to confirm the mechanisms in Sections 4.3 and 4.4, respectively. Section 4.5 presents the summary and discussion.

4.2. Data Sources and Methodology

4.2.1. Data Sources

This study utilized the following data sets:

(1) Surface weather charts provided by the Japan Meteorological Agency and archived by the National Institute of Informatics "Digital Typhoon" from 1979 to 2017 (http://agora.ex.nii.ac.jp).

(2) Global heavy rainfall/flood (HRF) events compiled by the Dartmouth Flood Observatory (DFO) from 1979 to 2017 (http://floodobservatory.colorado.edu).

(3) 6-hourly mean sea level pressure (*MSLP*), zonal (*U*) and meridional (*V*) wind components, relative humidity, and air temperature at multiple levels from the National Centers for Environmental Prediction-Department of Energy (NCEP-DOE) Atmospheric Model Intercomparison Project (AMIP-II) from 1979–2017 (https://www.esrl.noaa.gov/psd; Kanamitsu *et al*., 2002).

(4) 6-hourly TC best track archive from the Joint Typhoon Warning Center (JTWC; https://www.usno.navy.mil/NOOC/nmfc-ph/RSS/jtwc/best_tracks/wpindex.php) from 1979–2017.

(5) 3-hourly rainfall from the Tropical Rainfall Measuring Mission (TRMM; https://disc.gsfc.nasa.gov/datasets/TRMM_3B42_V7/summary) 3B42RT version 7 from January 15–16, 2017 (Huffman *et al*., 2010).

4.2.2. Methodology

First, we examined the large-scale circulation features during the JAN2017 HRF event. For the climatological analysis, we only selected HRF events not categorized as TC-related in the DFO archive and cases without TCs in the vicinity of the Philippines (110–130°E, 5–25°N) from 1979–2017 using the JTWC TC best track data. There are 34 reported HRF events from November to March during the analysis period, 25 of which occurred over Mindanao Island (south of 10°N). We define Mindanao Island and its vicinity as the region within 122–127.5°E and 5–10°N, which for brevity, is simply referred to as “Mindanao Island”. The TRMM rainfall was converted to 6-hourly

intervals to match the reanalysis data set. All anomalies are relative to the 1981–2010 mean.

4.3. The JAN2017 HRF

In this section, we examine the large-scale circulation features during the JAN2017 HRF event. An extreme flooding over CDO (124.63°E, 8.45°N) was reported around the afternoon of January 16, 2017 (between 06 and 12UTC). A weather station by the Weather Philippines Foundation Incorporated, located over CDO recorded a 24-hr accumulated rainfall of about 188.20 mm from 00 UTC January 16, 2017 to 00 UTC January 17, 2017 (https://weather.ph.org/understanding-the-weather-conditions-behind-the-cagayan-de-oro-flooding), which exceeded the climatological daily maximum of January (97.9 mm) from 1979–2008 in one long-term recording weather station of PAGASA in CDO (i.e., Lumba station). The horizontal wind field at 925 hPa ($WINDS_{925hPa}$) during 06 UTC January 16, 2017 (Figure 4.1a) features cyclonic circulations over Mindanao Island and in the broad North Pacific along 20–50°N centered around 45°N, 180°. The magnitude of the $WINDS_{925hPa}$ over the central and northern Philippines is about 10 m s^{-1}, which is twice the climatological wind speed (5 m s^{-1}; Figure 4.1b) in these regions. Such enhanced $WINDS_{925hPa}$ during the JAN2017 HRF event might be due to the enhanced pressure gradient induced by the cyclonic circulation around Mindanao Island and the anticyclonic circulation to its north. The zonal wind anomaly at 925 hPa (U_{925hPa}; Figure 4.1c) features enhanced westerlies over Mindanao Island and enhanced easterlies over the central and northern Philippines. On the other hand, the meridional wind anomaly (V_{925hPa}; Figure 4.1d), shows enhanced northerlies penetrating over northern Borneo and enhanced southerlies over Mindanao

Island. The enhanced westerly and southerly wind anomalies over Mindanao Island might have brought more moisture, resulting in heavier rainfall.

Figure 4.2 shows the synoptic charts from 06 UTC January 15, 2017 to 12 UTC January 16, 2017. Some remarkable features on 06 UTC January 15, 2017 (Figure 4.2a) include the TD located in the south of Vietnam, the LPA that is located in the east of Japan along 40°N, and the southeastern ridge of the anticyclonic circulation located in the north of Luzon Island. On 12 UTC January 15, 2017 and 18 UTC (Figures 4.2b and c), the southeastern ridge of the anticyclonic circulation in the north of Luzon Island extends further southward and the LPA along 40°N further intensify. An LPA developed south of 10°N on 00 UTC January 16, 2017 (Figure 4.2d) and briefly intensified around 06 UTC (Figure 4.2e). Note also that the center of the LPA over Mindanao Island, which is denoted as "L", moved slightly westward (Figures 4.2d to f). On 12 UTC January 16, 2017 (Figure 4.2f), this LPA weakens. As we have mentioned previously, the JAN2017 HRF event was associated with the "tail-end of a cold front" and its interaction with the LPA over Mindanao Island by PAGASA. However, considering the center of the LPA along 40°N as the "head" of the cold front, its "tail" is only depicted east of 160°E on the surface weather charts in Figure 4.2. It seems that using the term "tail-end of a cold front" is not appropriate for this case and needs further clarification.

Figure 4.3 shows the 3-hourly rainfall from TRMM superimposed with the $WINDS_{925hPa}$ from 06 UTC January 15, 2017 to 12 UTC January 16, 2017. There are two anticyclonic circulations centered around 120°E, 35°N (A_1) and 140°W, 30°N (A_2) that are juxtaposed in a northwest-southeast orientation (NW–SE; a similar abbreviation method will be used in the succeeding sections) on 18 UTC January 15,

2017 (Figure 4.3a). The A_1 has a NW–SE orientation, while the A_2 has a SW–NE orientation. In the same figure, two cyclonic circulations centered around 165°E, 40°N (C_1) and 125°E, 8°N (C_2) are also juxtaposed in a SW–NE orientation. In addition, another cyclonic circulation can also be depicted in the south of Vietnam (around 10°N; Figure 4.3a), which is associated with the TD in the synoptic charts in Figure 4.2. Note that on 06 UTC January 16, 2017, the TD has already weakened (Figures 4.2e and 4.3e). In addition, this TD is no longer clear at 925 hPa from 18 UTC January 15, 2017 to 00 UTC January 16, 2017, as shown in Figure 4.3c, although it is still indicated in the surface weather charts until 00 UTC January 16, 2017 (Figures 4.2c and d). This indicates that this dissipating TD is only detectable near the surface level. The northeasterlies from A_1 interact with the easterlies of the TD and C_2, while the southwesterlies on the western flank of A_2 interact with the northwesterlies on the western flank of C_1. The northeasterlies from A_1 bring cool air from the mid-latitudes, while the easterlies from C_2 bring warm and humid air from the tropics. The interaction of these two systems forms a confluence region, which is known as a *shearline* (e.g., Cabanerit, 2016). In general, the shearline is just part of a deformation zone and lies along its axis of dilatation. The total deformation (*TDef*) can be represented, mathematically, as the sum of the stretching (*STD*) and shearing (*SHD*) deformations (http://www.zamg.ac.at/docu/Manual/SatManu/main.htm?/docu/Manual/SatManu/CMs/Def/backgr.htm). These are calculated as follows:

$$STD = \frac{\partial U}{\partial x} - \frac{\partial V}{\partial y}, \tag{4.1}$$

$$SHD = \frac{\partial V}{\partial x} + \frac{\partial U}{\partial y}, \tag{4.2}$$

$$TDef = \sqrt{STD^2 + SHD^2}, \tag{4.3}$$

where U and V are the zonal and meridional wind components, respectively. We illustrate the $STD_{925\text{hPa}}$, SHD_{925hPa}, and $TDef_{925hPa}$ in Figure 4.4 to show the location of the shearline on 06 UTC January 16, 2017. Also shown is the meridional equivalent potential temperature gradient at 925 hPa (θe_{925hPa}) to indicate to mean position of the cold front. During this period, the location of the deformation zone is centered around 155°E,15°N, as indicated by the star in Figure 4.4. The southern edge of A_1 extends further south of 10°N. The cold front is oriented in a southwest-northeast direction from 120°E to 120°W just to the north of the deformation zone (Figure 4.4a). The shearline coincides with the region of more positive STD_{925hPa}, indicating that the horizontal wind gradient/shear (i.e., $\partial U_{925hPa}/\partial x$) is large along this region (Figure 4.4b). On the other hand, the SHD_{925hPa} (Figure 4.4c) is weaker on the western side of the deformation zone but stronger on the eastern side. This suggests that the STD_{925hPa} is more important in inducing the JAN2017 HRF event and that it contributed more to the $TDef_{925hPa}$, as shown in Figure 4.4d. Along the shearline, cold air from A_1 and warm air over the tropics induces enhanced convergence over Mindanao Island, as will be shown later. We also found enhanced mid-tropospheric ascent over the same region since warm air is pushed upwards by the cooler air (not shown).

The rainfall distribution from the TRMM data, as shown in Figure 4.3, depicts a SW–NE oriented band of rainfall from the SCS to the north Pacific along the shearline. On 06 and 12 UTC January 15, 2017 and 12 UTC (Figures 4.3a and b, respectively), this rainfall band is located north of 10°N and rainfall clusters can only be depicted over the central Philippines. On 18 UTC January 15, 2017 and 00 UTC January 16, 2017 (Figures 4.3c and d, respectively), this rainfall band progresses southward, concurrent with the weakening of the TD in the south of Vietnam, and the strengthening

of A_1 and C_1. On 06 and 12 UTC January 16, 2017 (Figures 4.3e and f, respectively), the rainfall clusters over Mindanao Island become well defined, especially along the shearline. Although, no more cyclonic circulation change can be depicted over Mindanao Island, a trough still exists in the same region.

4.3.1. Maintenance of the JAN2017 heavy rainfall event

Rainfall is maintained by the convergence of water vapor flux ($\boldsymbol{Q}$; Chen *et al*., 2013). According to Chen (1985), $\boldsymbol{Q}$ can be split into its rotational ($\boldsymbol{Q_R}$) and divergent ($\boldsymbol{Q_D}$) components:

$$\boldsymbol{Q} = \boldsymbol{Q_R} + \boldsymbol{Q_D}, \tag{4.4}$$

where $\boldsymbol{Q} = (1/g)\int_{P300}^{P1000} \boldsymbol{V}qdp$, g, $\boldsymbol{V}$, p, and q are the water vapor flux (kg m^2 s^{-1}), gravitational constant (m s^{-2}), wind vector (m s^{-1}), pressure (mb), and specific humidity (g g^{-1}), respectively. The $\boldsymbol{Q_R}$ and $\boldsymbol{Q_D}$, can also be expressed in terms of the horizontal gradients of the streamfunction ($\boldsymbol{Q_R} = \mathbf{k} \times \nabla \boldsymbol{\psi_Q}$) and velocity potential $\left(\boldsymbol{Q_D} = \nabla \boldsymbol{\chi_Q}\right)$, respectively. Thus, rainfall ($\boldsymbol{P}$) can be approximated as:

$$\boldsymbol{P} \cong \nabla \cdot \boldsymbol{Q_D} = -\nabla^2 \boldsymbol{\chi_Q}. \tag{4.5}$$

The maintenance of rainfall is illustrated by the spatial plots of $\boldsymbol{\chi_Q}$, $\boldsymbol{Q_D}$, and $\boldsymbol{Q}$ in Figure 4.5, following Chen *et al*. (2013). A prominent north-south contrast of convergent and divergent fluxes during the JAN2017 HRF event can be seen over the tropical southeast Asia. The zero-contour line splits these two opposing circulations along 15°N over the Philippines. The enhanced $\boldsymbol{Q}$ can be seen in the downstream of the northerly fluxes along this zero-contour line (Figure 4.5a), which is consistent with the location of enhanced rainfall, as shown in Figure 4.3. The divergent fluxes originate from the negative $\boldsymbol{\chi_Q}$ center (130°E, 28°N) in the south of Japan, which is part of A_1 in

Figure 4.3. Northerly fluxes appear to be confined along 10°N on 18 UTC January 15, 2017 (Figure 4.5a) and a convergence region is located downstream of these northerly fluxes in the eastern side of Mindanao Island. On 06 UTC January 16, 2017, this convergence region shifts westward (Figures 4.4c and d), which is consistent with Figures 4.3d and e. On 12 UTC January 16, 2017 (Figure 4.5d), the northerly fluxes further intrude the equatorial region and the convergence region near Mindanao Island is located further south over the Indonesian archipelago.

4.3.2. The vertical structure of the shearline

To further clarify the vertical structure of the shearline, we derived the pressure-latitude cross-section of the θe (shades) and relative humidity (contours) anomalies averaged from 122–127.5°E, as shown in Figure 4.5. On 12 UTC January 15, 2017 (Figure 4.6a), the warm θe anomaly is slightly tilted with height to the north and the warmest region is located between 6–18°N, while the relative humidity anomaly appears to be standing below the 300 hPa level. The location of the warmest θe anomaly coincides with the location of the maximum relative humidity anomaly. Ascending anomalies between these latitudes are confined below 600 hPa. From 12 UTC January 15, 2017 (Figure 4.6b) to 00 UTC January 16, 2017 (Figure 4.6c), the cold θe anomaly below 700 hPa expands to the south along 15°N and the ascending anomalies south of this latitude reach 200 hPa. Concurrently, the relative humidity anomaly also increases to about 40 %. Also remarkable are the enhanced descending anomalies in the north of 18°N, indicating an enhanced cold surge activity. On 06 UTC January 16, 2017 (Figure 4.6d), the warm θe anomaly weakens and the cold θe anomaly to its north penetrates 12°N. On 12 UTC January 16, 2017 (Figure 4.6e), the ascending anomalies between 6–12°N weaken, which is consistent with the weakening of rainfall

during this period. In addition, positive relative humidity anomaly starts to extend in the upper levels (i.e., 200 hPa). On 18 UTC January 16, 2017 (Figure 4.6f), the cold θe anomaly below 900 hPa penetrates the equatorial region and the relative humidity anomaly decreases to about 20 %. These changes are consistent with the northeasterly wind intrusion over the Philippines during this period.

4.4. Composite Analysis

Using the flood reports from the DFO, we checked all HRF events from 1979 to 2017 and validated them using the surface weather charts. We only considered those cases that were not categorized as TC-induced (i.e., those cases due to shearlines, etc.) and cases when there was no reported TC within 110–130°E and 5–25°N. There are 34 HRFs over the Philippines satisfying the above criteria, in which 25 cases (74 %) occurred over Mindanao Island. Since most of the cases occurred over Mindanao Island, we focus our analysis over this region in the succeeding sections. We classified the HRFs per month as shown in Figure 4.7. A majority of the cases occurred between December and March. This distribution appears to be consistent with the southward progression of the northeast monsoon over the Philippines (e.g., Kubota *et al*., 2017; Chen *et al*., 2015b). In particular, three cases occurred during December, eight cases during January, nine cases during February, and five cases during March.

4.4.1. Climatology of non-TC related winter HRF events over Mindanao Island

Unfortunately, we do not have a homogenous rainfall data over this area and since we are interested in the climatology of non-TC related HRF events, we need an index to represent them. Note that in the JAN2017 case, the region with enhanced rainfall coincides with the region of enhanced $\boldsymbol{Q}$ over Mindanao Island. Hence, in this study,

we represented the HRF event using $\boldsymbol{Q}$. The duration and the location of the HRF events are included in the DFO archive. We checked the time series of the $\boldsymbol{Q}$ in each of the 25 cases and defined Lag 0 as the time when the area-averaged $\boldsymbol{Q}$ over Mindanao Island of the reported HRF event attains its maximum value. Then, we performed lag-composites to determine the controlling mechanisms of these HRF events.

Figure 4.8 shows the lag composites of $WINDS_{925hPa}$ and *MSLP* anomalies from Lag −3 to Lag +15. A westward propagating cyclonic anomaly can be seen over Mindanao Island. We refer to this cyclonic anomaly over Mindanao Island as "Mindanao vortex" for brevity. Moreover, a westward propagating cyclonic anomaly and an anticyclonic circulation anomaly behind it can be seen along 20–40°N (Figures 4.8a to f). These circulation features resemble those from the JAN2017 case, suggesting that they are common for the winter HRF events over Mindanao Island. Notice that when the center of the anticyclonic circulation anomaly reaches around 160°E (Figure 4.8f), the Mindanao vortex is already located to the west of Mindanao Island. This is also accompanied by the intrusion of the enhanced northeasterlies over the Philippines.

4.4.2. Intensification and westward propagation of the Mindanao vortex

Yokoi and Matsumoto (2008) examined a cold surge (CS) event during November 1999 over central Vietnam that lingered there for several days. They suggested that the strong southerly winds over the central SCS prevented this CS from propagating southwards. The Mindanao vortex did not show southward propagation tendency from the composite anomalies. Therefore, we examine first the time-latitude cross section of the U_{925hPa} and V_{925hPa} in Figure 4.9.

The time-latitude cross section of V_{925hPa} anomaly (Figure 4.9a) shows enhanced southerly winds south of 15°N from Lag –20 to Lag +8. The southerly V_{925hPa} starts to intensify at Lag –5 between 10–15°N. Easterly U_{925hPa} appears along 5–10°N between Lag –7 and Lag –4 (Figure 4.9b). At Lag 0, enhanced southerly V_{925hPa} appears along 5–10°N, which is concurrent with the intensification of westerly U_{925hPa} along the same latitude band. These changes favor the enhancement of the Mindanao vortex. The southerly V_{925hPa} might have also facilitated the transport of warm and humid air from the equatorial region that interacted with the cool and dry northeasterlies. After Lag +1, the southerly V_{925hPa} weakens. These changes favor the southward/southwestward propagation of the Mindanao vortex, as shown in Figure 4.8. At Lag +8, northerly V_{925hPa} and easterly U_{925hPa} begin to penetrate the equatorial region concurrent with the westward propagation of the Mindanao vortex.

On the other hand, Chen *et al*. (2015b) examined the westward propagating CS vortices (CSVs) during the winter monsoon season over the western North Pacific. They used vorticity budget analysis to diagnose the intensification and propagation tendencies of these CSVs. The vorticity tendency can be used to represent such propagation tendencies and can be calculated as follows:

$$\xi_t = -\boldsymbol{V} \cdot \nabla(\xi + f) - (\xi + f)\nabla \cdot \mathbf{V}, \tag{4.6}$$

where f is the Coriolis parameter (s^{-1}) and **V** is the wind vector (m s^{-1}). The first term on the right-hand side of Equation 4.6 denotes the vorticity advection (ξ_{adv}), while the second term indicates the vorticity stretching ($\xi_{stretch}$). Chen *et al*. (2015b) noted that the westward propagation of CSVs is facilitated by a positive ξ_{adv} to the west of the central vortex and larger values of ξ_{adv} compared with the $\xi_{stretch}$.

Figures 4.10 and 4.11 show the ξ_t , ξ_{adv}, $\xi_{stretch}$ anomalies. At Lag –3 (Figures 4.10a to c), the spatial distribution of ξ_{adv} shows favorable conditions (i.e., positive ξ_{adv} to the west of the vortex center) for westward propagation of the Mindanao vortex to the east of Mindanao Island. The magnitudes of ξ_{adv} and $\xi_{stretch}$ are also comparable over the SCS and to the east of the Philippines. At Lag 0 (Figures 4.10d to f), the magnitude of the $\xi_{stretch}$ becomes larger than the ξ_{adv} (almost five times), which inhibits the westward propagation of the cyclonic anomaly over Mindanao Island. This implies that the intensification of the Mindanao vortex is mainly achieved by the vorticity stretching, which is facilitated by the enhanced low-level convergence over this area. The Mindanao vortex starts its west/southwestward propagation when $\xi_{stretch}$ weakens at Lag +1 (Figures 10g to i) together with the weakening of the southerly V_{925hPa} in Figure 4.9a. Northeasterlies invade the southern Philippines in the succeeding lag hours (Figure 4.11). At Lag +3 (Figures 4.11a to c), the Mindanao vortex is located off the eastern coast of Borneo and centered around 120°E, 5°N. At Lag +5 and Lag +15 (Figures 4.11d to i), the center of the vortex becomes undefined.

4.5. Summary and Discussion

This study examined the large-scale circulation features associated with the recent non-TC related heavy rainfall event that led to extensive flooding (HRF) over Cagayan de Oro City (CDO) in Mindanao Island (122–127°E, 5–10°N), Philippines on January 16, 2017 (JAN2017 event). This HRF event is associated with the interaction of a low-pressure area (LPA) in the vicinity of Mindanao Island and a shearline that is associated with an anomalous eastward-propagating cyclonic circulation (cold front) along 20–40°N and its interaction with the tropical easterlies. The maximum moisture convergence during this event was found during 06 UTC January 16, 2017. Enhanced

westerly U_{925hPa} and southerly V_{925hPa} during 06 UTC January 16, 2017 over Mindanao Island might have supplied more warm and humid tropical air that interacted with the cool and dry air from the enhanced northerly V_{925hPa}. This interaction resulted in enhanced moisture convergence and rainfall over Mindanao Island.

Using the flood reports archived by the Dartmouth Flood Observatory, we examined the climatology of non-TC related HRF events over the Philippines from 1979 to 2017. As previously noted, previous studies on non-TC related winter HRF events focused only on specific cases or carried out impact-based studies. Hence, this study is the first attempt to characterize these winter HRF events in a climatological mean sense. We identified 34 cases of such HRF events, 25 (74 %) of which occurred over Mindanao Island (southern Philippines); therefore, we only focused our analysis over Mindanao Island since most of the cases occurred over this region. Using the maximum area-averaged vertically integrated moisture flux convergence of the reported HRF event over Mindanao Island to represent the peak rainfall, we created composites to understand the mechanisms leading to these HRF events. A schematic diagram of the possible mechanism leading to the winter HRF over Mindanao Island is shown in Figure 4.12.

The winter HRF events over Mindanao Island is induced by the interaction of the eastward propagating cyclonic and anticyclonic circulation anomalies along 20–40°N and a westward propagating cyclonic anomaly along 5–10°N (i.e., the Mindanao vortex). A shearline is formed at the trailing end of the cold front associated with the eastward propagating cyclonic and anticyclonic circulation anomalies. The interaction of the shearline and the Mindanao vortex induces HRF events over Mindanao Island. Composite analysis of the large-scale circulation features further revealed that the

enhanced southerly V_{925hPa} in the south of Mindanao Island prevented the Mindanao vortex from progressing southward despite the background northeasterlies. In addition, we also performed vorticity budget analysis to explain the westward propagation tendency of the Mindanao vortex. We decomposed the vorticity tendency into its advection and stretching terms. It turns out that the Mindanao vortex only propagated westward when both the advection and stretching terms were comparable to each other, together with the weakening of the southerly V_{925hPa}. The enhanced convergence over Mindanao Island favored the enhancement of the stretching term, which inhibited the westward propagation of the Mindanao vortex.

Yokoi and Matsumoto (2008) found the importance of westward propagating TDDs associated with an MJO-like convective activity over the maritime continent to the HRF over central Vietnam. Pullen *et al*. (2015) also found the role of MJO on the February 2008 HRF over the Philippines. Using the Wheeler and Hendon (2004) index (hereafter, WHI) for depicting the location and strength of the MJO, we checked the WHI of the 25 cases over Mindanao Island. The WHI defines the MJO component based on a multivariate empirical orthogonal function (EOF) analysis of daily 850 hPa zonal wind, 200 hPa zonal wind, and OLR between 15°S–15°N. Two principal component time series from the EOF analysis are defined as Real-time Multivariate MJO series 1 and 2, RMM1 and RMM2, respectively. The RMM1 and RMM2 are drawn in a phase-space diagram to indicate the magnitude and location of the MJO. The equatorial region is divided into 8 regions: South America to Africa (Phases 1 and 8), Indian Ocean (Phases 2 and 3), Maritime Continent (Phases 4 and 5), and the Pacific Ocean (Phases 6 and 7). Since the MJO propagates eastward, its trajectory on the phase-space diagram is drawn counter-clockwise. The MJO is weak (strong) when the WHI is less (greater) than 1.

There were 12 HRF cases that occurred when the MJO phase is weak, including the JAN2017 case, and only two cases occurred when the MJO is over the maritime continent (not shown). The rest occurred when the MJO is located over the Indian Ocean or the western Pacific. These results suggest that not all winter HRF cases can be associated with MJO and that other factors might be involved. On the other hand, aside from the MJO, Compo *et al*. (1999) found that cold surges south of 25°N also have significant periodicities at the submonthly (i.e., 6–30-days) time scale. Takahashi *et al*. (2011) examined the impact of long lasting northerly cold surges at the submonthly time scale on the TC formation over the tropical region. They found that the long-lasting northerly surges may facilitate the formation of TCs over the SCS during October and November. The role of these intraseasonal northerly surges on the formation and development of the Mindanao vortex will be discussed further in our future study. In addition, this study was limited by the availability of a long-term high temporal rainfall (and other variables) data set. Therefore, it would be interesting to extend the analysis when such data sets are already available in future studies.

Chapter 5. Abrupt climate shift in the mature rainy season of the Philippines in the mid-1990s

5.1. Introduction

Rainfall variability is an important issue in many climate studies because of its profound impact on the economy, especially in agricultural countries such as the Philippines. Generally, the rainfall of the Philippines is influenced by multi-scale systems and their interactions (e.g., tropical cyclone (TC)-enhanced monsoons) such as the monsoons, El Niño Southern Oscillation (ENSO), TC activity, intraseasonal oscillations, and other mesoscale processes (Matsumoto, 1992; Lyon and Camargo, 2009; Cayanan *et al*., 2011; Cruz *et al*., 2013; Pullen *et al*., 2015) that contributes to rainfall variability. In particular, the seasonal transition of the Asian summer monsoon leads to regional differences in the rainfall over the Philippines. The western coast of the country, for example, has a distinct dry season in winter and a wet season in summer, while the eastern coast has no dry season and experience more rainfall in winter (Kintanar, 1984; Akasaka, 2010).

A number of studies, using the long available observation data in the Asian monsoon region, found significant decadal-to-interdecadal shifts, especially in the recent decade (Ding *et al*., 2008; Inoue and Matsumoto, 2007; Villafuerte *et al*., 2014; Cinco *et al*., 2014). For example, a prominent interdecadal shift has been identified after the late 1970s over East Asia (Nitta and Yamada, 1989; Wang B, 1995; Wang HJ, 2001; Ding *et al.*, 2008; Ha *et al.*, 2009). Wang HJ (2001) suggested that the Asian monsoon system has weakened after the 1970s. Some studies have linked this interdecadal shift to the changes in the sea surface temperature (SST) over the tropical Pacific and Indian Ocean (Nitta, 1987; Gong and Ho, 2002; Fu *et al.*, 2009; Ding *et al.*,

2009; Wang *et al.*, 2013). The impact of the snow cover over the Tibetan Plateau in the preceding winter/spring was also suggested (Ding *et al.*, 2009). Quite recently, several studies have found another interdecadal shift in the mid (i.e., 1992/1993 or 1993/1994) to late 1990s (i.e., 1999), especially over East Asia (Kwon *et al.*, 2005, 2007; Wu *et al.*, 2010; Liu *et al.*, 2011; Zhu *et al.*, 2011; Kajikawa and Wang, 2012; Kajikawa *et al.*, 2012). According to Liu *et al.* (2011), the abrupt changes around 1993 features an increase in the summer rainfall over South China (SC), while that around 1999 features a decrease in rainfall over northeast China. Wu *et al.* (2010) found that the increase in rainfall over SC is accompanied by an increase in the low-level convergence, mid-tropospheric ascent, and upper-level divergence, while other studies such as Kwon *et al.* (2007), Kim *et al.* (2012), and Chen J *et al.* (2012) attributed this increase in rainfall to the increase in the number of TCs over the western North Pacific (WNP) in the mid-1990s. The impact of the shifting of the Pacific Decadal Oscillation (PDO) to a negative phase has also been linked to the changes in the summer rainfall over eastern China (Zhu *et al.*, 2011). In addition, some studies have also found interdecadal changes in the intraseasonal variability (ISV) over the WNP (Kajikawa *et al.*, 2009; Kim *et al.*, 2011; Luo and Zhang, 2015; Yamaura and Kajikawa, 2016). For example, Kajikawa *et al*. (2009) found that the periodicity of ISV over the South China Sea (SCS) became shorter after the mid-1990s. Most of these studies on the decadal-to-interdecadal changes in the monsoon system focused on the seasonal mean fields (i.e., average from June to August (JJA)). However, it is known that rainfall also exhibits strong sub-seasonal (i.e., monthly) variabilities (e.g., Inoue and Matsumoto, 2007; Takahashi and Yasunari, 2008; Ha *et al.*, 2009; Kim *et al.*, 2011; Takahashi, 2011; Kajikawa *et al.*, 2012; Luo and Zhang, 2015; Yamaura and Kajikawa, 2016).

The rainfall over the Philippines has also experienced long-term changes (Akasaka, 2010; Cruz *et al.*, 2013; Cinco *et al.*, 2014; Villafuerte *et al.*, 2014; Kubota *et al.*, 2017). For example, Cruz *et al.* (2013) found a significant decreasing rainfall trend in stations located over the western coast of the country from 1961 to 2010 but no detailed mechanisms for the trends were presented. Meanwhile, in analyzing the decadal changes in the East Asian summer monsoon circulation, Kwon *et al.* (2007) found a significant strengthening of upper level (i.e., 200 hPa) convergence over the Philippines around 1993/1994 (see their Figure 2a). However, their analysis used seasonal mean fields (JJA) and mainly focused on East Asia. As such, no detailed mechanisms for the change over the Philippines were presented. Akasaka (2010) found that the variability of the onset of the Philippine summer monsoon (PSM) has increased greatly since the 1970s (see her Figure 7). Early onset dates of the PSM has been linked to the "great approach" of the easterly waves originating from WNP (Cruz *et al.*, 2013) and the presence of TCs in the vicinity of the Philippines that can initiate the moist southwesterly winds over the southwestern portion of the country (Kubota *et al.*, 2017). The onset of the PSM occurs almost five days (P29; 21 May–25 May) following the onset of the summer monsoon over the SCS (SCSSM) (Matsumoto, 1992; Lau and Yang, 1997; Akasaka, 2010; Chen *et al.*, 2017). Recently, Kajikawa and Wang (2012) found a significant advance in the SCSSM onset dates around 1993/1994. It is suggested that the increase in the TC activity in May, changes in ISV (Kajikawa and Wang, 2012), earlier retreat of the western North Pacific Subtropical High (WNPSH) (Yuan and Chen, 2013), and a La Niña-like pattern SST change over the Pacific basin (Xiang and Wang, 2013) are responsible for the advanced SCSSM onset. Other studies such as Kajikawa *et al.* (2012) hypothesized that the variability in the thermal contrast, induced by aerosols and dust, between the Asian landmass and the Indian Ocean is

responsible for the advanced onset over the south and southeastern monsoon regions including the Bay of Bengal (BoB), the Indochina Peninsula, and western Pacific region (120–140°E). The role of natural decadal variability other than anthropogenic forcing in relation to the advanced summer monsoon onset has also been suggested (Xiang and Wang, 2013). Furthermore, Xu and Wang (2014) attributed the changes in TC activity in May to the increase in genesis potential index, maximum potential intensity, and vertical wind shear after the late 1990s over the WNP.

In this study, we addressed the following issues:

(1) With the observed decadal changes in the summer monsoon of the adjacent regions, it is necessary to confirm whether such an interdecadal change can be observed locally over the Philippines. In fact, an inconspicuous rainfall trend can be seen in Figure 1 of Kajikawa *et al.* (2012) using reanalysis datasets over Luzon Island. In particular, the increasing rainfall trend in May (see their Figure 1a) only appears over the central and southern Philippines and the decreasing rainfall trend in June (see their Figure 1b) can only be depicted over the SCS. It is worth mentioning that the complex topography of the Philippines gives rise to four different climate types (Kintanar, 1984). The current resolution of available reanalysis datasets present difficulties in representing the correct sub-regional characteristics of rainfall. Thus, to better capture the changes in rainfall in the sub-regional scale, station-based rainfall data are preferred. In this study, we used the station-based rainfall data and supplemented it by the rainfall estimates from the Climate Prediction Center Merged Analysis of Precipitation (CMAP) during 1979–1993 and 1994–2008 following the change point used by Kwon *et al.* (2007) and Kajikawa and Wang (2012) around 1993/1994. We also investigated other periods with remarkable changes. Additional tests were

performed in both datasets to confirm whether this change point in the mid-1990s is significant or not over the Philippines.

(2) To the best of our knowledge, very few studies have examined the decadal-to-interdecadal changes in rainfall over the Philippines. Previous studies (e.g., Cruz *et al.*, 2013; Villafuerte *et al.*, 2014; Cinco *et al.*, 2014) only focus on long-term trends and variability of seasonal and annual rainfall or temperature. This study is part of our on-going endeavor in understanding the multi-temporal variability of rainfall in the Philippines.

The rest of the paper is organized as follows. The datasets and methodology used in this study are presented in Section 5.2. Section 5.3 investigates the interdecadal shifts in the summer monsoon rainfall of the Philippines and the possible mechanisms leading to these shifts. Summary and discussions are presented in Section 5.4.

5.2. Data sources and Methodology

5.2.1. Data Sources

Daily rainfall data from the Philippine Atmospheric, Geophysical and Astronomical Services Administration (PAGASA) for the seven stations located over the west coast of the Philippines and for the period 1979–2008 were used in this study. The seven stations are Laoag, Baguio, Iba, Dagupan, Science Garden, Ambulong, and Coron stations (blue circles in Figure 5.1). These stations were chosen because they have a relatively complete data during the study period, which is suitable for decadal change analysis. Furthermore, these stations are currently used by PAGASA in monitoring the summer monsoon of the Philippines. According to Cruz *et al.* (2013) the western coast of the Philippines, where these stations are located, receives about

80–90 % of the 30-year mean annual total rainfall (1961–1990) during the summer monsoon season (June–September).

Daily data of zonal (U) and meridional (V) components of winds, geopotential height (*HGT*), vertical velocity (ω), and relative humidity (*RHUM*) at multiple levels from the National Centers for Environmental Prediction-Department of Energy (NCEP-DOE) Atmospheric Model Intercomparison Project (AMIP-II) Reanalysis (hereafter NCEP-R2) (Kanamitsu *et al.*, 2002) with 2.5° × 2.5° grid resolution were used to depict changes in the large-scale conditions. We also used the reanalysis data from the Japan Meteorological Agency (JMA) 55-year reanalysis with 1.25° × 1.25° grid resolution (hereafter, JRA55) (Kobayashi *et al.*, 2015) to test the consistency of the results. Our comparison of the two reanalysis datasets actually yielded the same results. Thus, most figures presented here are based on NCEP-R2 data. Pentad-mean rainfall estimates from CMAP (Xie and Arkin, 1997), with 2.5° × 2.5° grid resolution from 1979 to 2008, were also used to supplement the station-based rainfall.

We also used the best track data provided by the Joint Typhoon Warning Center (JTWC; https://www.usno.navy.mil/NOOC/nmfc-ph/RSS/jtwc/best_tracks/wpindex.php) to depict TC activity. To check the consistency of the results, we compared the JTWC best track data with the TC track data from the Regional Specialized Meteorological Center of the Japan Meteorological Agency (hereafter, RSMC-Tokyo; http://www.jma.go.jp/jma/jma-eng/jma-center/rsmc-hp-pub-eg/trackarchives.html). Due to the difference in TC categories between these two datasets, we only consider TCs above Tropical Storm (TS) category or TCs with maximum wind speeds (Vmax) above 17.5 m s^{-1} (34 knots). In addition, we only considered TCs that entered the Philippine Area of Responsibility (PAR; 115–135°E

and 5–25°N). The genesis location is defined as the location where the TC first attained a TS category (Wang and Chan, 2002; Fudeyasu *et al.*, 2006). It is worth mentioning that the RSMC-Tokyo and JTWC TC datasets yielded similar results. Thus, most of the figures presented in this study are only based on JTWC TC tracks.

5.2.2. Methodology

First, we divided the analysis period into two epochs, namely: 1979–1993 (hereafter, ES1) and 1994–2008 (hereafter, ES2) following Kwon *et al.* (2007) and Kajikawa and Wang (2012). Then, we performed the Pettitt test (Pettitt, 1979) to confirm whether the shift is significant over the western coast of the Philippines. Unless otherwise stated, the daily variables from the reanalysis and PAGASA datasets were converted to five-day consecutive and non-overlapping averages (hereafter, pentads), where the first pentad corresponds to the first five days of January and the last pentad corresponds to the last five days of December. There are 73 pentads in a year. We also applied a running three pentad 1–2–1 filter to reduce the high-frequency fluctuations in all the datasets (Murakami and Matsumoto, 1994; Kim *et al.,* 2011).

The Pettitt test is a non-parametric test that detects the changes in the median of a sequence of observations. This test is commonly used for detecting change points in climatic and hydrological time series (Ha and Ha, 2006; Stone, 2010; Vincent *et al.*, 2011; Salarijasi *et al.*, 2012; Bates *et al.*, 2012; Yeh *et al.*, 2015; Mallakpour and Villarini, 2016). For instance, Ha and Ha (2006) used this test for detecting the climate shift in rainfall over the Korean Peninsula. Bates *et al.* (2012) also used this test for detecting the change points in the North Atlantic Oscillation index, *RHUM* fields, and TC count series. The Pettitt test is performed as follows.

Let T be the length of the time series and t be the probable change point. Then, the single time series can be considered as two samples and represented by $X_1, \ldots, X_t$ and $X_{t+1}, \ldots, X_T$ with distributions $F_1(X)$ and $F_2(X)$, respectively. The null hypothesis of this test is that the two samples are independent and have identical distributions (i.e., $F_1(X) = F_2(X)$). The non-parametric test statistic (K_T) is defined by:

$$K_T = \max\left|U_{t,T}\right|, \;\; 1 \leq t < T, \tag{5.1}$$

where

$$U_{t,T} = \sum_{i=1}^{t} \sum_{j=t+1}^{T} sgn(X_i - X_j); \quad sgn(X_i - X_j) = \begin{cases} -1, & (X_i - X_j) < 1 \\ 0, & (X_i - X_j) = 0 \\ +1, & (X_i - X_j) > 1 \end{cases} \tag{5.2}$$

Here, $U_{t,T}$, is equivalent to the Mann–Whitney statistic for testing whether the two samples belong to the same population. The value of t where the maximum K_T occurs is the estimated change point in the sequence. The significance probability of K_T can be approximated as:

$$p \cong 2\exp\left(\frac{-6K_T^2}{T^3 + T^2}\right). \tag{5.3}$$

A complete description and derivation of this test can be found in Pettitt (1979). We also used the Student's t-test (Wilks, 2011) for testing the significance of the difference plots. It should be noted that we applied a logarithmic transformation to the rainfall data prior to applying Student's t-test since rainfall does not follow a normal distribution.

In generating the TC track density, the TC track data were interpolated onto a 5° × 5° grid boxes (Cinco *et al.*, 2016). The same TC within a grid box is only counted once. Then, we derived the accumulated TC tracks in each grid box and divided it by the total number of years (i.e., 15 years in each epoch) to get the TC frequency in each year.

5.3. Results

5.3.1. Changes in rainfall

Figures 5.2a and b show the smoothed pentad-mean rainfall distribution averaged across the seven PAGASA stations, as shown in Figure 5.1, and CMAP dataset extracted from the nearest five grid (red triangles in Figure 5.1) points to the PAGASA station location from 1979 to 2008, respectively. Climatologically, the rainy season over the western coast of the Philippines starts in mid-May and lasts until September (Akasaka, 2010). The peak of the PSM usually occurs between P41 and P49 (20 July–2 September) based on Wang and Lin (2002), which is concurrent with the peak of the western North Pacific monsoon (WNPM) (Murakami and Matsumoto, 1994; Wang, 1995; Wang and Lin, 2002). Using the rainfall data from the period 1961–2000 and from the 39 synoptic stations across the Philippines, Akasaka (2010) found that the climatological onset date of the PSM is around P29 (May 21–May 25). The onset pentad is indicated by the vertical line in Figures 5.2a and b. The CMAP rainfall dataset was able to capture the changes in rainfall structure although the values are underestimated in most of the pentads. In particular, the CMAP dataset was not able to capture the rainfall above 35 mm day^{-1} despite the high correlation (0.88) between the two datasets (not shown). Such a difference in magnitude of rainfall can be attributed to the coarse resolution of the CMAP dataset (e.g., Matsuyama *et al*., 2002). An obvious

increase in rainfall above 5 mm day^{-1} between P25 and P29 after the mid-1990s can be seen in Figures 5.2a and b. This result is consistent with a recent study by Kubota *et al.* (2017), who also found a tendency for more rainfall occurrence in May after the mid-1990s. A decrease in rainfall occurrence above 25 mm day^{-1} (10 mm day^{-1}) can also be seen between P46 to P50 (14 August to 7 September) in the PAGASA (CMAP) dataset.

Figures 5.3a and b shows the smoothed rainfall time series between the two epochs and their difference, respectively, using the PAGASA dataset. It is worth mentioning that similar features were observed in the CMAP dataset (not shown). We found seven periods with significant rainfall differences (P28–P31, P33–P36, P38–P39, P43–P44, P45–P50, P52–P54, and P59–P60) above the 95 % confidence level, as indicated by the shaded pentads in Figure 5.3a. For instance, an obvious increase in rainfall from P28 to P31 (16 May–4 June) can be seen in Figures 5.3a and b with a peak around P30 (26 May–30 May). The average daily rainfall for P28–P31 in ES1 is about 8 mm day^{-1} (7 mm day^{-1}), while that in ES2 is about 12 mm day^{-1} (13 mm day^{-1}) using the PAGASA (CMAP) dataset. The difference in rainfall between the two epochs is statistically significant above the 95 % confidence level using the Student's *t*-test in both datasets. The increase in rainfall in May is followed by a decrease in rainfall from P33 to P36 (10 June–29 June). The same features were observed by Kajikawa *et al.* (2012), where areas with increasing rainfall in May experience a decreasing rainfall in June (see their Figure 1b) especially over the SCS. They attributed this to the slowing down of the northward propagation of the first ISV. The average daily rainfall for P33–P36 in ES1 is about 16 mm day^{-1} (13 mm day^{-1}), while that in ES2 is about 10 mm day^{-1} (9 mm day^{-1}) using the PAGASA (CMAP) dataset. The difference in rainfall is also significantly above the 95 % confidence level in both datasets. The decrease in

rainfall from early to late June is followed by a sharp increase in rainfall from P38 to P39 (5 July–14 July) in ES2. Climatologically, there is a simultaneous break (grand break) between the Indian summer monsoon (ISM), East Asian summer monsoon (EASM), and the WNPM during this period (Wang and Xu, 1997) from P36 to P39. This break appears shorter in ES2. Additionally, the sharp increase in rainfall from P38 to P39 in ES2 is not significant in the CMAP dataset. An increase in rainfall from P41 to P44 can also be seen in Figures 5.3a and b. However, only the increase in rainfall from P43 to P44 (30 July–8 August) is statistically significant at the 99 % confidence level using the PAGASA dataset. A decrease in rainfall from P45 to P50 is apparent in ES2, which is statistically significant at the 99 % confidence level in both datasets. The average daily rainfall for P45–P50 in ES1 is about 22 mm day^{-1} (15 mm day^{-1}), while that in ES2 is about 16 mm day^{-1} (10 mm day^{-1}) using the PAGASA (CMAP) dataset.

The peak of the summer monsoon in ES1 appears to be shifted earlier in ES2 (Figure 5.3a). To verify this, we estimated the annual rainfall peak using the sum of the first four Fourier harmonics of the pentad-mean rainfall time series (i.e., a smoothed time series) in each year. The first four Fourier harmonics represent the slowly-varying component of rainfall (i.e., low-frequency oscillations with periods longer than 90 days; Wang and Xu, 1997). As a test case, Figure 5.4a shows the pentad-mean rainfall time series during 1992 (black line) and the sum of the first four Fourier harmonics (blue line). The annual peak can then be estimated as the pentad when the smoothed series attains its maximum. During 1992, the annual peak occurred at P48. The time series of annual peaks from 1979 to 2008 using the method above is shown in Figure 5.4b. There are no significant shifts in the annual peaks of rainfall using the Pettitt test. In fact, the average rainfall peak for both epochs is around P44. This result suggests that the decrease in rainfall during P45–P50 is not related to the shifting of the rainfall peak. A

significant increase in rainfall (above the 95 % confidence level) from P52 to P54 (13 September–27 September) follows the decrease in rainfall during P45–P50 in ES2. This increase in rainfall is only significant in the PAGASA dataset. The last period with a significant rainfall difference occurs from P59 to P60 (18 October–27 October), which features a decrease in rainfall in ES2. The rainfall difference is significant at the 99 % confidence level in both datasets. According to Wang and Xu (1997), the last wet spell of the WNPM and PSM usually occurs during this period.

To confirm whether the change point significantly occurred around 1993/1994, we performed the Pettitt test on the smoothed average rainfall time series between the seven periods. The calculated change points are summarized in Table 5.1. Although there is a clear tendency for increased precipitation from P28 to P31 after 1994 (Figure 5.2), the climate shift was found around 1995/1996 in the PAGASA dataset and no significant change point can be detected in the CMAP dataset. These results are still consistent with the earlier results of Kajikawa *et al.* (2012) (see their Figure 1a) using the CMAP data. The climate shift after 1994 cannot be detected in the CMAP dataset because it underestimates the rainfall in ES2. The climate shift for P33–P36 occurred around 1993/1994 and 1992/1993 in the PAGASA and CMAP datasets, respectively. This climate shift is significant at 95 % confidence level. Furthermore, the climate shift during P38–P39 was detected around 1998/1999 in both sets. However, only the shift in the PAGASA dataset is significant at the 95 % confidence level. Additionally, a significant climate shift during P45–P50 was also detected around 1993/1994 in both datasets, while the climate shift during P59–P60 was detected around 1999/2000. Only the periods P45–P50 and P59–P60 show a robust climate shift (i.e., similar change points in the two rainfall datasets) from the mid to late 1990s, respectively. In the succeeding sections, we mainly focus the discussion on the climate shift from P45 to

P50, since the changes in other periods are not robust or occurred later (1999/2000; e.g., P59–P60). Furthermore, P45–P50 coincides with the mature phase of the PSM. Thus, its relative importance outweighs the other periods. We checked and confirmed that the decrease in rainfall from P45 to P50 in ES2 is present at all seven PAGASA stations. Thus, taking the averaged time series across the seven stations can reasonably represent the observed trends over the west coast of the Philippines.

We also performed a running Student's *t*-test with varying time windows following the methodology of Choi *et al.* (2017) to check the robustness of the change points in Table 5.1. A significant change point corresponds to the year with the largest absolute *t*-statistic value exceeding a certain level of significance and should be the same for the different time windows. We found that the change points detected by the running Student's *t*-test (Yin *et al.*, 2015; Choi *et al.*, 2017; Wang *et al.*, 2018) are consistent with the results from the Pettitt test, which suggests that the change points in Table 5.1 are robust. Only the period P28–P31 shows an unclear change point in the running Student's *t*-test because the different time windows resulted in different maximum *t*-statistics. The change point during this period is also insignificant using the Pettitt test. Nonetheless, the focus of the study is the P45–P50 period and we obtained the same change points for both the CMAP and PAGASA datasets.

To further depict the large-scale change in rainfall, we illustrate the epochal difference (ES2 minus ES1) in CMAP rainfall during P45–P50 in Figure 5.5. A significant decrease in rainfall can be seen over the eastern Indochina Peninsula, the Korean Peninsula, Luzon Island, and some parts of Visayan Islands (121–127.5°E; 8–12.5°N) in the Philippines. In contrast, a significant increase in rainfall can be depicted over southeastern China along 25–30°N and Mindanao Island (121–127.5°E; 5–8°N).

The possible mechanisms for the changes in rainfall will be discussed further in the succeeding section.

5.3.2. Possible influencing factors

In this section, we investigate the possible causes leading to the abrupt shift in the rainfall during P45–P50.

5.3.2.1. *Changes in moisture transport*

Moisture transported from the Indian Ocean by the monsoon winds are essential for the formation of rainfall over the Asian monsoon region (Okada and Yamazaki, 2012; Nguyen-Le *et al*., 2016). Thus, we examined first the possible contribution of the changes in the vertically integrated moisture flux (*VIMF*) and vertically integrated moisture flux divergence (*VIMFD*) to the changes in rainfall. The *VIMFD* is calculated as:

$VIMFD = \nabla \cdot \int_{P_s}^{P_{300}} q \frac{V}{g} dp$, where P_s, P_{300}, q, g, and V are the pressure at the surface (mb), the pressure at 300 hPa (mb), specific humidity (g g^{-1}), gravitational acceleration constant (9.8 m s^{-2}), and wind vectors (m s^{-1}), respectively.

Figure 5.6 shows the time series of area-averaged *VIMFD* over Luzon Island (117.5–122.5°E; 10–20°N). The average *VIMFD* in ES1 is about -3×10^{-4} kg m^{-2} s^{-1}, while that in ES2 is about -1×10^{-4} kg m^{-2} s^{-1}. The epochal difference is statistically significant at the 99 % confidence level by Student's *t*-test. This result indicates that the reduction of rainfall in ES2 over Luzon Island can be associated with the weakening of the eastward moisture transport (or moisture convergence) by the summer monsoon.

To further clarify the changes in the moisture transport between the two epochs, we illustrate the spatial patterns of *VIMF* and *VIMFD* including their epochal difference in Figure 5.7. The most remarkable feature is the increase of *VIMFD* over the Philippines in ES2 (Figure 5.7b). In particular, the moisture flux convergence (i.e., negative *VIMFD*), which is centered around 112°E, 20°N and stretches over the western coast the Philippines in ES1 (Figure 5.7a), weakens in ES2. Additionally, a northwest–southeast tilted moisture flux convergence, which corresponds to the monsoon trough, near Taiwan that stretches around 115°E, 25°N to the equatorial WNP (around 150°E, 5°N) can be seen in ES1. In contrast, the monsoon trough appears more southward and stretches from 125°E, 15°N to the equatorial WNP in ES2. The *VIMF* also appears to bifurcate to southwesterly and westerly direction over the Luzon Island in ES2. This bifurcation leads to the strengthening of *VIMFD* over the Luzon Island. On the other hand, the *VIMF* in ES1 is southwesterly over the Philippines and extends eastward up to 140°E along 15°N. These results imply that the monsoon trough near the Philippines has weakened in ES2.

What causes this bifurcation in the moisture flux in ES2? We illustrate the 850 hPa *HGT* (HGT_{850hPa}) in Figures 5.7a and b (blue contours) since the wind vectors generally follow the *HGT* contours. It turns out that the western ridge of the WNPSH has extended further westward during ES2. In particular, the 1, 490-m contour line is located near 120°E in ES2 and crosses the Korean Peninsula. In ES1, this contour line is located near 130°E. Additionally, the 1, 500-m contour line, which is located along 9°N and crosses the northern part of Mindanao Island in ES1, has shifted northwards along the Visayan Islands in ES2. In general, the bifurcation of *VIMF* appears to result from the westward extension of the WNPSH.

We also check the epochal difference in relative vorticity at 850 hPa to confirm the weakening of the monsoon trough (Figure 5.8a) and found significant negative low-level relative vorticity difference (anticyclonic circulation) over the SCS and northeast of the Philippines. The epochal difference in the *VIMFD* in Figure 5.7c also shows significant divergence over the SCS including the western coast and the northeast of the Philippines along 20°N, which indicates a weakening of monsoon westerly/southwesterly winds. To confirm this, we also checked the epochal difference in zonal winds at 850 hPa (U_{850hPa}; Figure 5.8b) and found an apparent decrease between 10 and 20°N, with a significant change over the SCS and eastern Indochina Peninsula. The epochal difference in HGT_{850hPa} in Figure 5.7c shows significant positive difference along 10–30°N, which indicates the strengthening of the WNPSH.

5.3.2.2. *Changes in tropical cyclone activity*

The rainfall peak from August to September in the PSM is usually attributed to TC activity and TC-monsoon interaction (e.g., Cinco *et al.*, 2016; see their Figure 4). Thus, the apparent weakening of rainfall from P45 to P50 might be related to the changes in the TC activity (i.e., changes in TC tracks, genesis location, occurrence frequency, etc.). An earlier study by Kubota and Wang (2009) found that the TC-induced rainfall accounts for about 30–50 % of the total rainfall during the TC season (July to October) in stations located over the eastern coast and the northern Philippines (see their Table 2), while that over the western coast of the Philippines accounts for about 40 % (e.g., Bagtasa, 2017; see his Figure 5c). Aside from landfalling TCs, non-landfalling TCs also contribute to the rainfall over the western coast of the country by enhancing the prevailing summer monsoon system (Cayanan *et al.*, 2011; Kubota *et al.*, 2017). Therefore, in this section, we examine the changes in the TC activity.

Figure 5.9 shows the TC tracks, passage frequency over a 5° × 5° grid, and the mean location of 500 hPa *HGT* (HGT_{500hPa}) in the two epochs during P45–P50. There are 48 (43) TCs that entered the PAR in ES1, while there are 40 (37) TCs in ES2 using the JTWC (RSMC-Tokyo, Japan) dataset. A decrease in the TC activity northeast of Luzon Island during ES2 between 20 and 25°N can be seen in Figure 5.9b. The TC frequency between these latitudes is about 0.5 to 1 y^{-1} in E1. In contrast, an increase in TC frequency can be seen north of Luzon Island around 20°N and 120°E in ES2. Over central Luzon Island and SCS (along 15°N), the TC frequency decreased from 0.3 y^{-1} to 0.1 y^{-1} in ES2 (Figure 5.9b). Furthermore, no TC occurrence can be depicted over the Visayan and Mindanao Islands in ES2 along 10°N. The TC tracks in Figures 5.9c and d show that less TCs made landfall over the Philippines in ES2. There is also a northwestward shift in the genesis location and fewer northeastward recurving TCs in ES2 compared with ES1. The changes in the TC tracks are consistent with a recent study by He *et al.* (2015), who found a decrease in northeastward recurving TCs towards Japan and increase in TC frequency over southeastern China and the Okinawa region during July to October in the late 1990s. The TC tracks in ES2 also appears to be similar to the TC tracks during La Niña years (e.g., see Figure 2d of Fudeyasu *et al.*, 2006). Earlier studies such as Saunders *et al.* (2000) and Zhang *et al.* (2012) found a significant increase in the number of landfalling TCs over the Philippines during the peak of La Niña years because of the shift in the mean genesis location. However, this is not the case in the observed TC tracks in ES2. The changes in the tracks might also be related to the changes in the steering flow pattern. Previous studies such as Choi *et al.* (2010), Hirata and Kawamura (2014), and Yang *et al.* (2015) have shown that the steering flow of TCs is highly influenced by the western ridge of the WNPSH. Thus, we illustrate the location of the WNPSH as represented by the 5870-m HGT_{500hPa}

(dashed contour line) in Figures 5.9c and d. The 5, 870-m contour line expands further westward near 90°E in ES2, whereas its western ridge is located near 125°E in ES1. The westward extension of the WNPSH in ES2 reduced the number of recurving TCs towards Japan and allowed more northwestward moving TCs towards southeastern China. Additionally, the increase in TC frequency north of Luzon Island between 18 and 20°N in ES2 can be attributed to this change in the location of the western ridge of the WNPSH. It is worth mentioning that we observed the same features in the tracks and genesis location using the RSMC-Tokyo dataset, which highlights the consistency of these results.

To quantify the rainfall contribution of TCs to the climate shift during P45–P50, we derived the total TC-induced rainfall (P_{TC}) following the estimation method by Kubota and Wang (2009) and Bagtasa (2017). In these studies, the TC rainfall rate is expressed as a function of the distance of each station to the TC center from the 6-hourly best track data. They classified the rainfall as P_{TC} when the distance between the station and the TC center is less than or equal to 10° (~1000–1100 km). We interpolated the daily rainfall data into six-hourly data in each station to match the best track data by dividing the daily rainfall into 6-hourly intervals. We derived the accumulated P_{TC} during P45–P50 in each station and for each epoch. The remaining rainfall other than P_{TC} was classified as P_{NOTC}. The results are summarized in Table 5.2. The accumulated rainfall (P_{TOTAL}) averaged across the seven PAGASA stations during the entire period (1979–2008) is 558 mm, about 46 % of which (256 mm) comes from P_{TC} using the JTWC dataset and 54 % comes from P_{NOTC}. The average P_{TC} in ES1 is about 352 mm (~54 % of 651 mm) and decreased to about 160 mm (~35 % of 464 mm) during ES2. The difference between the two epochs is significant at the 95 % confidence level by

Student's *t*-test. These results clearly indicate that the decrease in rainfall during ES2 can be partly attributed to the decrease in TC activity.

The changes in the TC activity in the vicinity of the Philippines raises some important issues: (1) there are fewer TCs that made landfall over the Philippines in ES2 than in ES1; and (2) no TC was formed over the western coast of the Philippines in ES2 compared with ES1. To clarify these issues, we examined the changes in the 500 hPa ω, 700 hPa *RHUM*, and vertical zonal wind shear ($U_{200\text{hPa}}$ minus $U_{850\text{hPa}}$) that are essential for the formation of TCs (He *et al.*, 2015; Ha and Zhong, 2015) in Figure 5.10.

The changes in the 500 hPa ω (Figure 5.10a) and 700 hPa *RHUM* (Figure 5.10b) are largely consistent with the changes in rainfall in Figure 5.5. For instance, the epochal difference in the ω features significant mid-tropospheric descent (subsidence) over the Philippines and ascent over southeastern China. A significant mid-tropospheric descent can also be depicted near 160°E. However, the rainfall change over this longitude is not significant. The subsidence over the Philippines is accompanied by a decrease in *RHUM*, as shown in Figure 5.10b. On the other hand, a significant increase in *RHUM* can be depicted over mainland Japan, which resembles a negative Pacific-Japan (PJ) pattern (Kubota *et al.*, 2016). Huang and Sun (1992) and Zhou and Cui (2008) suggested that the weakened convection over the Philippines leads to a southward shifting of the WNPSH, which induces a negative PJ pattern (Nguyen-Le and Matsumoto, 2014; Kubota *et al.*, 2016). On the other hand, an apparent increase in the vertical zonal wind shear (Figure 5.10c) can be seen along 10–20°N west of 140°E, which is also unfavorable for TC activity (He *et al.*, 2015).

Several studies suggest that an anticyclonic circulation over the WNP inhibits the development of TCs (Zhou and Cui, 2008; Du *et al.*, 2011; Wang *et al.*, 2013). Kubota

and Wang (2009) also noted that an anticyclonic circulation located over the Philippine sea causes the TC-induced rainfall to be shifted further eastward, which leads to a decrease in the total rainfall of the Philippines. To confirm whether the synoptic-scale disturbances changed in the vicinity of the Philippines, we derived the perturbation kinetic energy (*PKE*) of the low-level winds (Figure 5.10d). The *PKE* can be used to depict synoptic-scale disturbances including those disturbances weaker than TCs such as residual lows and frontal activities in mid-latitudes (Maloney and Dickinson, 2003; Takahashi and Yasunari, 2006; Kim *et al.*, 2012). The *PKE* can be calculated using the formula: $PKE = \overline{(u'^2 + v'^2)}/2$, where u' and v' are the perturbations obtained by subtracting an 11-day running mean to the daily U_{850hPa} and V_{850hPa} wind components, respectively, while the overbar denotes the epochal mean of the daily *PKE* values. There is an apparent decrease in *PKE* over Luzon Island along 10–18°N with stronger change over the Philippine Sea near 140°E. This result suggests that the low-level divergence and subsidence in the vicinity of the Philippines inhibits the formation of synoptic-scale disturbances. In general, the changes in the ambient environmental conditions became unfavorable for TC development and other synoptic-scale disturbances in the vicinity of the Philippines as substantiated by the decrease in *PKE*.

5.4. Summary and Discussion

This study examined the recent interdecadal shift in the summer monsoon rainfall of the Philippines and investigated the associated changes in the large-scale conditions and TC activity. As noted earlier, many studies found a significant climate shift around the mid-1990s. In this study, we clarified whether such climate shift can be observed locally over the Philippines and examined its robustness (i.e., the same change can be depicted in the station and reanalysis datasets). We provided a schematic diagram to

summarize the interdecadal changes in the large-scale conditions and TC activity, and how they contribute to the decrease in rainfall over the Philippines after the mid-1990s (Figure 5.11).

We found a robust interdecadal shift in rainfall in stations located over the western coast of the Philippines around 1993/1994 from early August to early September, which corresponds to the mature phase of the summer rainy season over this area. In particular, the average daily rainfall during 1994–2008 (ES2; ~16 mm day^{-1}) is significantly lower than during 1979–1993 (ES1; ~22 mm day^{-1}). We also found inconsistent climate shifts in May, June, July, and September between the rainfall data from the stations and the Climate Prediction Center Merged Analysis of Precipitation, which highlights the importance of sub-seasonal analysis in decadal-to-interdecadal climate change studies. Since this decreasing period corresponds to the peak rainy season of the country, this may partly explain the recent rainfall decrease in the Philippines (Cruz *et al.*, 2013).

We examined the plausible role of the changes in the moisture transport and TC activity in suppressing the rainfall during ES2. The results show enhanced low-level moisture flux divergence over the Philippines, which is accompanied by weak monsoon westerlies and less moisture transport. On the other hand, the TC frequency (e.g., less TC landfall and formation) has decreased over the Philippines in ES2. These changes can be attributed to the unfavorable background conditions for synoptic-scale disturbances induced by a mid-tropospheric descent, enhanced vertical zonal wind shear, and decreased low-level relative humidity in the vicinity of the Philippines. This is further substantiated by the decrease in the perturbation kinetic energy, which can represent synoptic-scale disturbances other than TCs. We also found that the averaged TC contribution has significantly decreased by about 20 % in ES2. The steering flow of TCs, which is highly influenced by the western ridge of the WNPSH, has also

changed in ES2. In particular, the WNPSH has extended further westward in ES2 that led to more landfalling TCs over southeastern China and northern Luzon Island. Additionally, the number of recurving TCs towards Japan has decreased in ES2.

Some studies have shown a La Niña-like SST change over the tropical Indo-Pacific region in the recent decade, with cooling over the central eastern Pacific and warming over the western Pacific including the SCS and the equatorial Indian Ocean (Nguyen-Le and Matsumoto, 2016; Kobayashi *et al.*, 2015; He *et al.*, 2015; Choi *et al.*, 2017; Zhang and Karnauskas, 2017; Xu and Lu, 2018). It has been suggested that the warming of the Indian Ocean can induce a lower-level anticyclonic circulation (low-level divergence) over the SCS (Zhou and Cui, 2008; Wu *et al.*, 2010; Du *et al.*, 2011; Wang *et al.*, 2013), which is unfavorable for the development of TCs. Du *et al.* (2011) suggested that the warming of the Indian Ocean induces a northeastward propagating warm Kelvin wave that promotes surface divergence and reduces rainfall over the WNP. On the other hand, He *et al.* (2015) found a significant decrease in TC activity (e.g., Genesis, TC frequency, etc.) over the southern WNP (105–170°E; 5–20°N), which they also attributed to the Indo-Pacific SST warming (see their Figure 11) after the late 1990s. They suggested that the cooling of SST over the central eastern Pacific can shift the Walker cell leading to suppressed convection around 160°E, which, in turn, can induce an anticyclone to the northwest through a Rossby wave response (Gill 1980) and enhanced convection over the maritime continent. We checked the spatial difference of monthly SST (ES2 minus ES1) and found significant warming over the equatorial Indian Ocean during ES2. However, the SST warming appears throughout the summer season (i.e., from June to September; Figure 5.12) and the cooling of SST over the central eastern Pacific is not very clear and insignificant. The decrease in rainfall around 160°E is also not significant (Figure 5.5). It should be noted that the

decrease in rainfall over the Philippines is only limited from early August to early September in E2 and we found no significant rainfall decrease in July and September. Thus, the decrease in rainfall in ES2 cannot be solely explained by the changes in the SST.

In this study, we speculate that the decrease in rainfall is due to the further westward extension of the WNPSH, which resulted in the bifurcation of moisture flux, weakening of the monsoon trough, and enhanced low-level divergence over the Philippines. As noted earlier, these changes inhibit synoptic-scale disturbances. Furthermore, the low-level divergence is reinforced by the anomalous upper-level cyclonic circulation centered around 100°E and 28°N (Figure 5.13) (Kwon *et al.*, 2005, 2007). Kwon *et al.* (2007) suggested that this upper-level cyclonic circulation is a barotropic response from the enhanced convection over southeastern China. They also suggested that the enhanced TC activity after the mid-1990s is partly responsible for the increase in rainfall.

Why is the shift only remarkable from early August to early September? As we have noted earlier, the decrease in rainfall during E2 is associated with the westward extension of the WNPSH. Xiang *et al.* (2013) examined the variability of the WNPSH from 1979 to 2010 and found that the majority of strong WNPSH cases occur during August. They suggested a local-convection-wind-evaporation-SST (CWES) feedback mechanism to explain the intensification of the WNPSH. In particular, the enhanced rainfall over the WNP during August leads to the cooling of SST, which can induce the westward emanation of descending Rossby waves. These descending Rossby waves induce a decrease in rainfall, which, in turn, promotes low-level divergence that favors the intensification of the WNPSH. In addition, Xiang *et al*. (2013) confirmed this mechanism through numerical simulations with prescribed SST cooling over the WNP.

Some studies also found interdecadal changes in the intraseasonal variability (ISV) over the WNP (Kajikawa *et al.*, 2009; Yamaura and Kajikawa, 2016), which has been associated with the changes in SST. For example, Kajikawa *et al.* (2009) found that the periodicity of ISV over the SCS in boreal summer became shorter during 1994–2007 compared with 1979–1993. Additionally, Yamaura and Kajikawa (2016) found that the boreal summer ISO activity has been enhanced after 1998/1999 with most remarkable change during August to October. These two studies suggested the possible role of the changes in the SST over the tropical Indo-Pacific region in modifying the ISV over the WNP. However, how the changes in SST contribute to the interdecadal changes in the ISV is still unclear. Numerical simulations to quantify the contribution of the SST to the changes in ISV is warranted. Additionally, the impact of the changes in ISV on the rainfall of the Philippines will be examined in future studies.

We also found significant climate shifts during early to late June (P33–P36) and during mid to late October (P59–P60) around 1993/1994 and 1999/2000, respectively. As noted earlier, Kajikawa *et al.* (2012) suggested that the decreasing rainfall trend in June may be related to the slowing down of the northward propagating ISV. However, other factors such as the role of the changes in TC activity and the large-scale circulation should also be considered. In addition, October corresponds to the transition from the summer to the winter monsoon over the Philippines. Thus, it is also interesting to examine the interdecadal changes in the transition period of the summer monsoon in future studies. Furthermore, we only found a single shift in the rainfall time series due to limited rainfall data. Whether this shift is permanent or will change in the future is another important issue to address in future studies. The performance of state-of-the-art climate models in simulating these interdecadal variabilities is also of great interest.

Chapter 6. Interdecadal shifts in the winter monsoon rainfall of the Philippines

6.1. Introduction

It is undeniable that rainfall is of paramount importance to agricultural countries such as the Philippines. The country's cropping calendar, for example, relies heavily on the availability of water resources and the timing of the rainy season. However, it is known that rainfall exhibits multi-scale spatio-temporal variabilities that can have devastating impacts on agriculture, food security, and the economy of the country.

In recent decades, a lot of research has been devoted in understanding the decadal-to-interdecadal variabilities of rainfall (Mantua *et al.*, 1997; Nitta and Yamada, 1989; Trenberth, 1990; Wang, 2001; Inoue and Matsumoto, 2007; Kajikawa and Wang, 2012; Nguyen-Le and Matsumoto, 2016; Xiang and Wang, 2013). Variabilities at these time scales can modulate atmospheric circulations at higher frequencies (e.g., interannual) that have important ramifications for the predictability of rainfall (Sen Roy *et al.*, 2003; Goswami, 2006). Sen Roy *et al.* (2003), for example, showed that the positive (negative) phase of the Pacific Decadal Oscillation (PDO), which is a well-known decadal climate variability, reduces (enhances) the monsoon rainfall over India by modulating the effects of the El Niño-Southern Oscillation (ENSO). In addition, Wang *et al.* (2008) showed that the relationship between ENSO and the East Asian winter monsoon (EAWM) is stronger and significant during the negative phase of PDO. Using a combination of long-term records of tropical cyclone (TC) tracks from the Philippine Weather Bureau and the Joint Typhoon Warning Center (JTWC), Kubota and Chan (2009) found that the annual number of landfalling TCs over the Philippines decreases (increases) during the negative phase of PDO and El Niño (La Niña) years. The phase

shift (i.e., from positive to negative or vice versa) of these decadal-to-interdecadal climate variabilities often leads to remarkable shifts in the rainfall time series.

Over the Asia-Pacific monsoon region, many studies have documented significant decadal-to-interdecadal shifts in rainfall. One such prominent shift occurred in the late 1970s, which has been associated with the phase shift of the PDO from a negative phase to a positive phase (Nitta and Yamada, 1989; Trenberth, 1990; Mantua *et al.*, 1997; Wang and An, 2001). Numerical simulations of Wang and An (2001) showed that the properties (i.e., period, amplitude, or spatio-temporal structure) of the ENSO remarkably changed following this shift. They further suggested that the decadal changes in the surface winds and ocean surface layer dynamics altered the ENSO properties. In addition, another interdecadal shift in the Asian summer monsoon has been detected around the mid-1990s, which features a La Niña-like sea surface temperature (SST) change over the Pacific basin (Kajikawa and Wang, 2012; Xiang and Wang, 2013; Nguyen-Le and Matsumoto, 2016). It has been suggested that this SST change in the mid-1990s can partially explain the advanced Asian summer monsoon onset (Kajikawa and Wang, 2012; Xiang and Wang, 2013) and delayed withdrawal of the autumn rainy season in Vietnam (Nguyen-Le and Matsumoto, 2016). Several studies also found interdecadal shifts in the autumn and winter rainfall in the recent decades over East Asia and Vietnam (Hung and Kao, 2010; Zhou and Wu, 2015; Nguyen-Le and Matsumoto, 2016; Choi *et al.*, 2016; Jia and Ge, 2017). For example, Zhou and Wu (2015) found a significant shift in the winter rainfall in northwest China around 1986/1987. They suggested that this shift is associated with the increase in SST over the North Atlantic Ocean after 1987. Meanwhile, Wang and He (2012) reported a weakening of the EAWM-ENSO relationship after the 1970s. They suggested that the Indo-Pacific SST variability was suppressed after the 1970s. Nguyen-Le and

Matsumoto (2016) found a significant interdecadal shift in the rainfall of Vietnam during December around 1992/1993, which led to the delayed withdrawal of its autumn rainy season.

The Philippines, which is located on the western periphery of the Pacific Ocean, is part of the Asia-Pacific monsoon region. The rainfall of the country has a strong seasonality and spatial contrast due to its heterogeneous topography. In particular, the rainy season over the western coast occurs from May to September (summer monsoon) and followed by a dry season, while the eastern coast experiences its rainy season from November to March (winter monsoon) (Akasaka *et al.*, 2007; Moron *et al.*, 2009; Akasaka, 2010; Chen *et al*., 2017). Recently, a number of studies found long-term changes in the rainfall and temperature of the Philippines (Akasaka, 2010; Cruz *et al.*, 2013; Cinco *et al.*, 2014; Villafuerte *et al.*, 2014, 2015; Cinco *et al.*, 2016; Bagtasa, 2017; Akasaka *et al.*, 2018). For example, Cruz *et al.* (2013) found decreasing rainfall trends during the summer monsoon season (June to September) in stations located over the western coast of the country from 1961–2010. A similar drying tendency was reported by Villafuerte *et al.* (2015) but for the January to March season, while Cinco *et al.* (2014) found a warming tendency in the annual mean and daily minimum temperatures across the country. Bagtasa (2017) found increasing annual trends in the tropical cyclone (TC)-induced rainfall since the year 2000. Olaguera *et al.* (2018a) found a significant interdecadal shift in the summer monsoon rainfall over the western coast of the Philippines during its mature phase (i.e., early August to early September) after the mid-1990s. They suggested that the further westward extension of the western North Pacific Subtropical High (WNPSH) during 1994–2008 promotes lower level divergence in the vicinity of the country, which is unfavorable for synoptic-scale disturbances.

In this study, we addressed the following issues:

(1) While there are many studies that have investigated the variability (i.e., long-term trends and interdecadal shift) of the summer monsoon rainfall of the Philippines (Akasaka, 2010; Cruz *et al.*, 2013; Cinco *et al.*, 2014; Villafuerte *et al.*, 2014, 2015; Cinco *et al.*, 2016; Bagtasa, 2017; Akasaka *et al.*, 2018; Olaguera *et al.*, 2018a), the variability of the winter monsoon rainfall has received less attention. According to Asuncion and Jose (1980), the winter monsoon accounts for about 38 % of the total annual rainfall in the Philippines, while the summer monsoon accounts for about 43 %, suggesting that the rainfall contribution of the winter monsoon is equally important with that from the summer monsoon. Thus, this study is part of our ongoing endeavor to fill this research gap.

(2) Previous studies such as Cruz *et al.* (2013) and Villafuerte *et al.* (2014) focused on the changes in the annual and seasonal mean of rainfall and temperature. However, it is known that rainfall also exhibits strong sub-seasonal variabilities (Inoue and Matsumoto, 2007; Olaguera *et al.*, 2018a). For example, Olaguera *et al.* (2018a) found a robust interdecadal shift in the summer monsoon rainfall of the Philippines from early August to early September. They further noted that this interdecadal shift is not robust in other summer monsoon months (i.e., May to July). In this study, we found that the significant interdecadal shifts are most remarkable during December compared with the other winter monsoon months. This month corresponds to the peak of the winter rainy season in stations located above 10°N (see Figure 3d of Kubota *et al.*, 2017) on the eastern coast of the country. This month is also the peak planting season of rice

and maize that are major agricultural products in the Philippines (Gerpacio *et al.*, 2004). Because of the potential vulnerability of these agriculture products to the interdecadal shifts in rainfall, it is thus necessary to investigate the mechanisms leading to these shifts. This is critical for agricultural planning and management of water resources.

The rest of the paper is organized as follows. The datasets and methodology used in this study are presented in Section 6.2. Section 6.3 presents the interdecadal variability of the winter monsoon rainfall in the Philippines and the possible mechanisms leading to such variability. Summary and discussions are presented in Section 6.4.

6.2. Data Sources and Methodology

6.2.1. Data Sources

In this study, we utilized the following datasets:

(1) Daily rainfall data from the period 1961 to 2008 and from the 32 stations of the Philippine Atmospheric, Geophysical, and Astronomical Services Administration (PAGASA) across the Philippines. These stations are illustrated in Figure 6.1. Because of the heterogeneous topography and strong monsoon influence, the climate of the Philippines has been originally divided into four climate types (Coronas, 1920; Kintanar, 1984). The first climate classification of the country was done by Coronas (1920) based on the average monthly rainfall distribution of different stations across the country from 1903 to 1918. He grouped the rainfall distributions into four types: two types under the prevalence of the summer and winter monsoons and two intermediate

types. He considered a dry month as a month with less than 50 mm of rainfall, although a month with more than 100 mm can still be considered as a dry month if it comes after three or more very dry months. Kintanar (1984) adapted the same criteria for climate classification for the period 1951 to 1980 and instead of using the average monthly rainfall, he used the modal of the yearly climate types. That is, the rainfall distribution type for each year is determined and the most frequent type during the 30-year period is considered as the final climate type. He was able to identify four climate types similar to those of Coronas (1920). However, these studies used old datasets and their results may no longer be applicable for the present climate of the Philippines. Recently, Villafuerte *et al.* (2017) performed a climate classification based on hierarchical clustering of the climatological pentad-mean rainfall time series from 1971 to 2013. They found three dominant climate types, as shown in Figure 6.1. We adapted this climate classification because it is more updated. The average monthly rainfall amounts from 1961 to 2008 in each station and climate type are shown in Figure 6.2. Stations that belong to climate Type I (red circles) have a pronounced dry season from November to April and a wet season for the rest of the year, as shown in Figure 6.2a. The rainy season of stations that belong to climate Type II (blue circles) starts around October and lasts until February, as shown in Figure 6.2b, while stations that belong to climate Type III (yellow circles) have no pronounced maximum rainfall periods and rainfall is more or less distributed throughout the year, as shown in Figure 6.2c. Based on this three-climate type classification, Tacloban station belongs to climate Type II. However, based on the Kintanar's (1984) climate classification, this station belongs to climate Type IV (i.e., stations

with no pronounced rainfall peak and rainfall is more or less evenly distributed throughout the year). We also checked the climatological monthly rainfall distribution of this station from 1961 to 2008 and found that it has a similar rainfall distribution with climate Type II stations. These inconsistencies further motivated us to use the classification by Villafuerte *et al.* (2017) instead of the Kintanar's (1984) classification.

(2) Daily Zonal (*U*) and meridional (*V*) components of the winds, vertical velocity, relative humidity (*RHUM*), geopotential height (*HGT*), and specific humidity (*Q*) at multiple levels from the Japan Meteorological Agency (JMA) 55-year reanalysis with 1.25° × 1.25° grid resolution (JRA55) (Kobayashi *et al.*, 2015).

(3) TC best track data from the Joint Typhoon Warning Center (JTWC). We only considered the TC that entered the Philippine Area of Responsibility (PAR; 115–135°E and 5–25°N) and above the tropical storm categories (TS; maximum wind speed is above 17.5 m s^{-1}).

(4) Monthly SST with 1° × 1° grid resolution from the Hadley Center Global Sea Ice Sea Surface Temperature data version 1.1 (HadISST1) (Rayner *et al.*, 2003).

6.2.2. Methodology

In this study, we used the moving Student's *t*-test (Yin *et al.*, 2015; Choi *et al.*, 2016; Wang *et al.*, 2018) with varying time windows (i.e., 9, 10, 12, and 15 years) in detecting the shifts. A significant shift corresponds to the year in which the largest absolute *t*-statistic exceeding the 95 % confidence level occurs and should be consistent with the different time windows. We also used the Energy Divisive (E-Divisive)

method proposed by Matteson and James (2014) to supplement this test. This E-Divisive method is based on hierarchical clustering or hierarchical divisive estimation and detects any distributional changes in a given time series. Multiple change points are estimated by iteratively applying a single detection algorithm in each of the clusters. The distributions of the clusters are compared using a divergence measure based on Euclidian distances, which can determine whether two independent samples are identically distributed. The significance of an estimated change point is determined through a permutation test. The data within each cluster are permuted to construct a new sequence of observations. In this study, we resampled the data by 1000 times for the permutation test. The null hypothesis for the permutation test is that there are no more additional change points. Additional details about this test can be found in Matteson and James (2014). The change points detected by these two tests are the same, suggesting that the detected shifts are robust. Since rainfall does not follow a normal distribution and the data contains missing values, we used a bootstrapped Student's *t*-test (Efron and Tibshirani, 1993) in estimating the significance of the difference in the rainfall means. For the other variables, we used an ordinary Student's *t*-test.

In generating the TC frequency plot in each epoch, we counted the same TC (i.e., similar identification number) in each 5° × 5° grid box only once and divided it by the total number of years (16 years). In addition, the genesis point indicates the location where the TC first attained a TS category.

6.3. Results

6.3.1. Shifts in rainfall

Figure 6.3 shows the average monthly rainfall time series of climate Type II stations, as shown in Figure 6.1, from the period 1961 to 2008 during the winter monsoon season (i.e., November to March). These stations are currently used by PAGASA in monitoring the winter monsoon over the Philippines (Kubota *et al.*, 2017) because of their geographical location or exposure to the prevailing easterly/northeasterly winds during this season. Remarkable interdecadal shifts can be seen during December, as shown in Figure 6.3b, with suppressed rainfall and decreased interannual variation from the late 1970s to the mid-1990s. In particular, we found that the interdecadal shifts occurred around 1976/1977 and 1992/1993. These shifts are significant above the 95 % confidence level, as shown in Figure 6.4. In contrast, the shift around 1976/1977 is not remarkable in other winter monsoon months, as shown in Figures 6.3a, c, d, and e. To confirm this, we also performed the running Student's *t*-test in these months and the results are also illustrated in Figure 6.4. There are no significant change points detected during November, January, and February. During March, however, a change point exceeding the 95 % confidence level occurred around 1996/1997. Note that in this manuscript, we defined a more stringent criterion for the change point detection (i.e., it should exceed the 95 % confidence limit) and this month does not satisfy this condition. These results highlight the importance of sub-seasonal variabilities of rainfall in decadal-to-interdecadal climate studies. In the succeeding sections, we focus our analysis on December since the interdecadal shifts are most remarkable during this month and divide the time series into three epochs: 1961–1976, (hereafter, EW1), 1977–1992 (hereafter, EW2), and 1993–2008 (hereafter, EW3). To

confirm the robustness of these shifts, we also examined the epochal differences in other stations across the country.

Figure 6.5 shows the interpolated epochal difference in rainfall from EW1 to EW2 (EW2 minus EW1), as shown in Figure 6.5a, and from EW2 to EW3 (EW3 minus EW2), as shown in Figure 6.5b. A decrease in rainfall can be depicted over the Philippines except in central Mindanao Island from EW1 to EW2, as shown in Figure 6.5a, and the significant rainfall difference can be depicted in 13 stations (40 % of the total number of stations). On the other hand, all stations show an increase in rainfall from EW2 and EW3 and the significant difference can be depicted in 23 stations, as shown in Figure 6.5b. Interestingly, the differences in rainfall over Catarman and Hinatuan stations (climate Type II stations) are not significant. The large interannual variability of their respective time series (not shown) is probably the reason why the shifts are not significant. The geographical location of the station can also affect the significance of the differences in rainfall. In particular, most of the stations on the western coast of the country do not show significant difference in rainfall. The stations such as Laoag, Dagupan, and Iba are located on the leeward side during the winter monsoon season and have very little rainfall (the average monthly rainfall in these stations from 1961 to 2008 is less than 1 mm day^{-1}). Baguio station, on the other hand, shows a robust signal since it is in an elevated location (~1, 500 m). All of the 13 stations with a significant decrease in rainfall from EW1 to EW2 show a significant increase in rainfall from EW2 to EW3, as shown by the stars with red outlines in Figure 6.5. We confirmed that the time series of December rainfall in each of the 13 stations including their regional average and change points are similar to that in Figure 6.3b (not shown). Thus, in the succeeding sections, we only use these 13 stations in the regional analysis. The average rainfall amounts across these stations during EW1, EW2,

and EW3 are 10.7, 6.2, and 11.8 mm day^{-1}, respectively. The corresponding variances are 27.5, 4.1, and 35.4 mm^2 day^{-2} during EW1, EW2, and EW3, respectively. The difference in rainfall between EW1 and EW2 (EW2 and EW3) is significant at the 95 % (99 %) confidence level by bootstrapping, while the differences in the variances between EW1 and EW2 as well as EW2 and EW3 are both significant at the 99 % confidence level by *F*-test.

6.3.2. Possible influencing factors

In this section, we examine the similarities and differences in the mean circulations between the three epochs and the possible mechanisms leading to the interdecadal shifts in rainfall.

6.3.2.1. *Changes in the low-level winds*

In the climatological mean sense, northeasterly to easterly winds (trades) are apparent between 5–20°N during December (Matsumoto, 1992; Chang *et al.*, 2005; Hattori *et al.*, 2011). Thus, we first compare the epochal means of 850 hPa winds ($WINDS_{850hPa}$) and HGT_{850hPa} in Figure 6.6. During EW1, as shown in Figure 6.6a, strong low-level easterlies (~12 m s^{-1}) can be seen east of 125°E (along 10–20°N). During EW2, as shown in Figure 6.6b, however, the low-level easterlies weaken (~8 m s^{-1}). In addition, northeasterlies appear to dominate over the eastern coast of the Philippines in EW2 compared with EW1. This is partly induced by the eastward extension of the 1, 530-m HGT_{850hPa} near 135°E. Another important feature is the weakening of the equatorial trough as indicated by the 1, 500-m HGT_{850hPa}, which is located further south below 10°N in the same epoch. During EW3, as shown in Figure 6.6c, on the other hand, the low-level easterlies intensify and reach some parts of Luzon

Island, which is consistent with Nguyen-Le and Matsumoto (2016). The northeasterlies over the South China Sea (SCS) also intensify and extend from the northern tip of Luzon Island to the southern Indochina Peninsula. The changes in the zonal winds appear to be a manifestation of the changes in the SST over the Pacific basin. For instance, it is known that the trade winds weaken (intensify) during El Niño (La Niña) conditions. A similar weakening of zonal winds during the summer monsoon was reported by Xiang and Wang (2013; see their Figure 12), which they suggested to be related to the PDO shift after the late 1970s. These points will be further discussed later.

6.3.2.2. *Changes in moisture transport*

Previous studies have shown that the changes in rainfall are directly associated with the changes in moisture transport (Li *et al.*, 2009; Hattori *et al.*, 2011; Olaguera *et al.*, 2018a). Thus, in this section, we examine the possible role of the changes in the vertically integrated moisture flux (*VIMF*) and moisture flux divergence (*VIMFD*).

Figure 6.7 shows the epochal difference in *VIMF* and *VIMFD* integrated from 1000 hPa to 300 hPa. The difference in *VIMF* between EW1 and EW2 (EW2 minus EW1), as shown in Figure 6.7a, features an anticyclonic circulation and enhanced divergence over the SCS along 18°N that can be associated with the increase in HGT_{850hPa} there and a cyclonic circulation change centered around 135°E, 20°N to the east of the Philippines. The Philippines is located just between these two opposing circulation changes. An anticyclonic circulation over the SCS may inhibit synoptic-scale disturbances and meander the TC tracks from the western North Pacific (WNP) (Kubota and Wang, 2009; Wang *et al.*, 2013; Olaguera *et al.*, 2018a). Another remarkable feature in Figure 6.7a is the enhanced cyclonic circulation centered around 122°E, 5°N. This cyclonic circulation is part of the monsoon trough that progressed southwards

during the winter monsoon season (Chen *et al.*, 2013, 2015a, b). It enhanced the divergent winds (i.e., the northerly component of the moisture flux) of the anticyclone over the SCS. In contrast, the epochal difference of *VIMF* between EW2 and EW3 features a cyclonic circulation and enhanced convergence (i.e., negative *VIMFD*) over the SCS and eastern coast of the Philippines above 10°N, which is consistent with Nguyen-Le and Matsumoto (2016), as shown in Figure 6.7b. Nguyen-Le and Matsumoto (2016) further suggested that the background conditions might have been favorable for the enhancement of moisture convergence over this area.

6.3.2.3. *Changes in tropical cyclone activity*

Tropical cyclone activity also contributes to the variability of the winter rainfall over the Philippines (Kubota and Wang, 2009; Bagtasa, 2017). In general, TCs contribute about 20 % to 50 % to the total mean annual rainfall over the eastern coast of the country (Kubota and Wang, 2009; Bagtasa, 2017). Cinco *et al*. (2016) examined the annual trends in the number of TCs that entered the PAR from the period 1951 to 2013 and found decreasing trends in the number of landfalling TCs over the Philippines. Based on their monthly TC frequency analysis, they also showed that, on the average, the number of landfalling TCs during December is larger than that from January to May. Recently, Nguyen-Le and Matsumoto (2016) found that the number of TCs passing through the southern SCS increased during December from 1993 to 2006. Motivated by these findings, we examined the possible role of the changes in the TC activity and determine the possible factors inducing the said changes in this section.

The TC frequency and tracks in each epoch are shown in Figure 6.8. The total number of TCs that entered the PAR are 15, 21, and 25 during EW1, EW2, and EW3, respectively. During EW1, as shown in Figure 6.8a, the number of TCs that made

landfall over the Philippines is around 0.2 to 0.3 per year. During EW2, as shown in Figure 6.8c, the number of TCs increased over the eastern coast of the Philippines (0.3 per year) and along 130°E (0.9 per year). On the other hand, the number of TCs that made landfall in EW3, as shown in Figure 6.8e, increased to about 0.4 to 0.7 per year. The TCs during EW2 appear to be short-lived and less TCs reach the Indochina Peninsula (Figure 6.8b) compared with EW1, as shown in Figure 6.8d, and EW3, as shown in Figure 6.8f. The genesis location of TCs in EW1 mostly occurs near 130°E while that in EW2 and EW3 occurs further east near the dateline. This is probably related to the differences in the location of the warm SST in the equatorial Pacific. We compared the mean SST between the three epochs, as shown in Figure 6.9, and found that the warm SST extends further eastward near 120°W in both EW2 and EW3. In addition, during EW1, four TCs are generated over the SCS, while only one is generated during EW2. The TCs during EW2 recurves more along 130°E compared with EW1 and EW3. Also, more TCs cross the Philippines and SCS between 10–15°N during EW3.

These changes in the TC tracks might be related to the changes in the steering flow. Takahashi and Yasunari (2008) noted that the steering flow is best depicted at 4–5 km (600–500 hPa level). Following their study, we also use the circulations at 600 hPa ($WINDS_{600hPa}$ and HGT_{600hPa}) to depict the TC steering flow in Figures 6.8b, d, and f. The magnitude of the HGT_{600hPa} during EW1 is lower by about 10 meters compared with the other epochs. This strengthening of the WNPSH after the late 1970s has been noted in previous studies (Yun *et al*., 2010). We used the 4, 405-m contour line to represent the WNPSH during EW1, while using the 4, 415-m contour line for EW2 and EW3. During EW1, as shown in Figure 6.8b, the western ridge of the WNPSH is located along 120°E. During EW2, as shown in Figure 6.8d, however, it appears to split

into two cells along 120°E. According to Wu *et al.* (2004; see their Figure 3), such splitting of the WNPSH allows TCs to recurve more towards Japan and the Korean Peninsula and consequently, less TC landfall over the Philippines. During EW3, as shown in Figure 6.8f, the western ridge of WNPSH further extends westward along 115°E, which resulted in more TCs making landfall over the Philippines.

Moreover, synoptic-scale disturbances that are weaker than TCs, such as tropical depressions and extra-tropical cyclones, can also bring rainfall (Takahashi and Yasunari, 2008; Cayanan *et al.*, 2011; Olaguera *et al.*, 2018a). In this study, we used the perturbation kinetic energy (*PKE*) of the low-level winds ($WINDS_{850hPa}$) to represent these disturbances. This also supplements the changes in the TC activity since TCs may be underestimated during the pre-satellite period. The *PKE* is defined as: $PKE = \overline{(u'^2 + v'^2)}/2$, where *u'* and *v'* are the perturbations obtained by subtracting an 11-day running mean from the daily U_{850hPa} and V_{850hPa}, respectively, while the overbar indicates the monthly average of the daily *PKE* values. Generally, synoptic scale disturbances do not last longer than 11 days. Thus, the 11-day running mean can represent the low-frequency component of the kinetic energy equation (Seiki and Takayabu, 2007). The synoptic-scale disturbances can be expressed as the deviation from this low-frequency component, although there are other ways of representing these disturbances, such as the deviation from a bandpass filtered anomaly with periodicities of about 2 to 8 days (Wu *et al.*, 2012).

Figure 6.10 shows the average *PKE* in each epoch and the corresponding epochal differences. During EW1, as shown in Figure 6.10a, the *PKE* over the western coast of the Philippines including the SCS is about 10–14 $m^2\ s^{-2}$, while that over the eastern coast is about 16–20 $m^2\ s^{-2}$. However, during EW2, as shown in Figure 6.10b, the *PKE*

over the western coast decreased, while the *PKE* over the eastern coast increased. The decrease in *PKE* between EW1 and EW2 is significant at the 95 % confidence level, as shown in Figure 6.10d. The changes in *PKE* are also consistent with the TC frequency change in Figure 6.8. On the other hand, during EW3, as shown in Figure 6.10c, the *PKE* increased over the western coast and decreased over the eastern coast, as shown in Figure 6.10e. These changes in the *PKE* over the SCS is consistent with Nguyen-Le and Matsumoto (2016), who reported an increase in the intraseasonal oscillations at different frequencies (e.g., 5, 12–24, and 30–60 day) during 1993–2006.

To further elaborate what induced the observed changes in the synoptic-scale disturbances including the TC activity in the vicinity of the Philippines, we examined the changes in the dynamic and thermodynamic parameters that are essential for TC activity (Olaguera *et al.*, 2018a). Figure 6.11 shows the epochal difference in 500 hPa vertical velocity, 700 hPa *RHUM*, and vertical zonal wind shear, which is defined as the difference between the zonal winds at 200 hPa (U_{200hPa}) and 850 hPa levels (U_{850hPa}). An anomalous descent, as shown in Figure 6.11a, in the vicinity of the Philippines is accompanied by a decrease in *RHUM,* as shown in Figure 6.11c, with the significant change located along a southwest-northeast tilted region from the SCS to Luzon Island and mainland Japan. The difference in the vertical zonal wind shear between EW1 and EW2, as shown in Figure 6.11e shows a significant increase over the Philippines including the SCS and the Indochina Peninsula. In other words, the background conditions became unfavorable for synoptic-scale disturbances during EW2. In contrast, there is an increase in *RHUM* between EW2 and EW3 over the SCS and the Philippines, as shown in Figure 6.11b, which is accompanied by a mid-tropospheric ascent over the same area, as shown in Figure 6.11d, and a decrease in vertical zonal wind shear, as shown in Figure 6.11f, west of 120°E. These results

suggest favorable background conditions for synoptic-scale disturbances during EW3 (Olaguera *et al.*, 2018a).

6.3.2.4. *Impact of sea surface temperature*

It is known that ENSO modulates the interannual variability of rainfall over the Philippines (Ropelewski and Halpert, 1987; Lyon *et al.*, 2006; Kubota and Wang, 2009; Lyon and Camargo, 2009; Villafuerte *et al.*, 2014). For example, Villafuerte *et al.* (2014) found that El Niño (La Niña) events are associated with drier (wetter) conditions over the country especially in seasons close to the mature stage of ENSO. Thus, in this section, we determine the possible role of the changes in SST to the interdecadal shifts in rainfall.

Figures 6.12 shows the epochal differences in SST and 10-m winds ($WINDS_{10m}$). The SST change between EW1 and EW2, as shown in Figure 6.12a, shows an El Niño-like pattern or a positive phase of the PDO, which is consistent with Nitta and Yamada (1989). Warmer SST can be depicted over the equatorial central Pacific and the Indian Ocean, while cooler SST appears over the northern Pacific. This SST change tends to weaken the trade winds as indicated by the enhanced westerlies east of the Philippines, as shown in Figure 6.12a. On the other hand, the SST change between EW2 and EW3, as shown in Figure 6.12b, shows a La Niña-like pattern, with cooler SST over the equatorial central Pacific and warmer SST over the western Pacific similar to previous studies (Xiang and Wang, 2013; Nguyen-Le and Matsumoto, 2016). The SST change over the Indian Ocean shows warming but the change is not as significantly uniform as that between EW1 and EW2. Easterlies can be depicted from the equatorial central and eastern Pacific to the western Pacific including the Philippines. Westerlies strengthen over the equatorial Indian Ocean, which is probably induced by the descending branch

of the strengthened Walker circulation over the western Pacific (Yamaura and Kajikawa, 2016; see their Figure 14).

Another interesting feature worthy of note is that the shift in December rainfall around 1976/1977 is almost symmetric (i.e., appears reversed) to the shift around 1992/1993. In fact, the average rainfall between EW1 (10.7 mm day^{-1}) and EW3 (11.8 mm day^{-1}) are not significantly different. However, we found notable differences in the circulation patterns between these epochs. For example, the epochal difference in December SST in Figure 6.12a is not exactly the reverse of Figure 6.12b, where warming is both observed west of 160°E. The SST difference between EW3 and EW1, as shown in Figure 6.12c, shows significant warmer SST over the Indian Ocean and western Pacific during EW3. In addition, the mean December SST during EW2 and EW3 are both warmer than in EW1 especially over the eastern equatorial Pacific, as shown in Figure 6.9. The warm SST (i.e., the 28 °C contour line) also expands further eastward near 120°W in the same epochs compared with EW1. As previously noted, the WNPSH as well as the zonal winds, are stronger during EW3 compared with EW1.

The El Niño-like SST change over the Pacific basin may also affect TC landfalls. For instance, Wu *et al.* (2004) found that fewer TCs follow a west-northwestward track and consequently, a smaller number of TC landfalls over the Philippines during the late season of El Niño years. They suggested that the southeastward shift of the genesis location over the WNP and a break in the WNPSH around 130°E during El Niño years are favorable for more recurving TCs. As we have noted earlier, we also found a similar splitting tendency of the WNPSH along 120°E in Figure 6.8d. Thus, the El Niño-like SST change over the equatorial Pacific in EW2 can partly explain the observed changes in the steering flow and TC tracks.

6.4. Summary and Discussion

In this study, we investigated the interdecadal shifts in the winter monsoon (November to March) rainfall of the Philippines from 1961 to 2008. Monthly analysis of the winter monsoon rainfall showed that the interdecadal shifts are only robust and significant during December. This month actually coincides with the peak planting season in most parts of the country. Therefore, an understanding of the mechanisms leading to these interdecadal shifts in December rainfall are crucial for agriculture. Furthermore, the significant interdecadal shifts in the December rainfall time series occurred around 1976/1977 and 1992/1993. These shifts are very clear in 40 % of the total stations used in this study. To facilitate the examination of the possible mechanisms leading to these rainfall shifts, we divided the analysis period into three epochs: 1961–1976 (EW1), 1977–1992 (EW2), and 1993–2008 (EW3). The average rainfall and its interannual variability are significantly suppressed (enhanced) during EW2 (EW3). The schematic diagrams summarizing the possible mechanisms leading to the suppressed rainfall during EW2 and enhanced rainfall during EW3 are shown in Figures 6.13 and 6.14, respectively.

The shift around 1976/1977 is probably related to the shifting of the PDO from a negative phase to a positive phase (Mantua and Hare, 2002; Hartmann and Wendler, 2005; Jacques-Coper and Gerreaud, 2015; Kubota *et al.*, 2016). The time series of the PDO index for December is shown in Figure 6.15a, where the shift from negative to positive in the late 1970s is clear. However, the shift in PDO around 1992/1993 is not remarkable, which suggests that a different mechanism induces the shift in the mid-1990s. The positive phase of PDO is characterized by an El Niño-like SST change over the equatorial central Pacific (Nitta and Yamada, 1989). As we have previously noted,

the low-level easterlies (i.e., the surface branch of the Walker circulation) are weaker during El Niño conditions resulting in less moisture transport over the Philippines.

Moreover, the TC frequency has decreased over the SCS in EW2 compared with EW1 and EW3. Liu and Chan (2013) examined the annual TC frequency over the WNP with at least a TS category from the period 1960 to 2011 and found an inactive period during 1975–1988 (see their Figure 1). Thus, the suppressed TC activity identified by Liu and Chan (2013) may be related to the suppressed TC activity found in this study. Their study also showed a remarkable increase in the vertical zonal wind shear during the period 1975–1988, which corroborated the enhanced vertical zonal wind shear during EW2 found in this study. The SST warming over the Indian Ocean can induce a lower-level divergence (anticyclonic circulation) over the SCS, which is also unfavorable for TC formation (Wang *et al.*, 2013). However, the SST warming over the Indian Ocean appears in both of the difference plots in Figure 6.12, suggesting that the decrease in TC activity over the SCS cannot be solely explained by the SST warming over the Indian Ocean. To further clarify this issue, we examined the changes in the vertical velocity, *RHUM*, and vertical zonal wind shear that influences TC activity. In particular, a mid-tropospheric descent, decrease in *RHUM*, and an enhanced vertical zonal wind shear over the SCS and the Philippines, which occurred during EW2. These changes are unfavorable for synoptic-scale disturbances, which is substantiated by the decrease in the perturbation kinetic energy (*PKE*).

What induced these unfavorable background conditions during EW2? The decrease in *RHUM* can be partly attributed to the weakening of the low-level easterly winds. We also checked the changes in the U_{200hPa} and found significant enhancement (weakening) of the upper-level westerlies between the equator and 30°N between EW1

and EW2 (not shown; EW2 and EW3). It should be noted that during El Niño conditions, the Walker circulation is weakened over the western Pacific; that is, an upper-level convergence and lower-level divergence appears over the western Pacific. Thus, the weakened low-level easterlies and enhanced upper-level westerlies can partly explain the enhanced vertical zonal wind shear during EW2. In general, the unfavorable background conditions leading to decreased synoptic-scale disturbances over the Philippines are induced by the El Niño-like SST change during the positive phase of PDO. Moreover, the changes in the TC tracks show fewer TCs reaching the SCS and the Indochina Peninsula and more recurving TCs over the eastern coast of the country in EW2. We found that this is due to the changes in the steering flow, where the WNPSH tended to split into two cells around the Philippines, which is favorable for more recurving TCs towards East Asia.

The shift in rainfall around 1992/1993 is probably a response to the La Niña-like SST change over the Pacific basin, which enhanced the low-level easterly winds and consequently, led to enhanced moisture transport over the eastern coast of the Philippines during EW3 (Nguyen-Le and Matsumoto, 2016; Zhang and Karnauskas, 2017). Using numerical simulations, Zhang and Karnauskas (2017) further noted that the prominent warming contrast between the Pacific, Indian, and Atlantic Oceans play a major role in enhancing the low-level easterly winds. During La Niña conditions, the Walker circulation is enhanced over the western Pacific. We also checked the epochal difference in the U_{200hPa} between EW2 and EW3 and found significant upper-level easterlies (i.e., divergence), which can explain the weakened vertical zonal wind shear during EW3 (not shown). The TC activity also increased during E3. In particular, more TC made landfall over the Philippines due to the westward extension of the WNPSH. Wu *et al.* (2004) noted that the monsoon trough and the WNPSH shifts westward during

La Niña years leading to more westward/northwestward moving TCs. In other words, the La Niña-like SST change during 1992/1993 induced favorable background conditions for increased synoptic-scale disturbances over the Philippines.

Aside from the decrease in the mean rainfall in December, its interannual variability was significantly reduced during EW2 compared with the other epochs. It is well known that ENSO significantly contributes to the interannual variability of rainfall over the Philippines. The epochal difference in SST features an El Niño-like SST change between EW1 and EW2 (EW2 minus EW1) and a La Niña-like SST change between EW2 and EW3 (EW3 minus EW2). Figure 6.12b shows the time series of SST anomaly (SSTA) over the Niño 3.4 region (170°W–120°W, 5°S–5°N). The anomalies are the deviations from the long-term mean (1961–2008). One remarkable feature in the time series of SSTA is that there are fewer occurrences of cold years (i.e., SSTA < 0) and more warm years (SSTA > 0) during EW2 compared with the other epochs. The correlation between the December rainfall and the Niño 3.4 SSTA is high and significant above the 99 % confidence level (r= –0.5, p = 0.0008). This result suggests that the El Niño-like SST change (i.e., more occurrence of warm years) over the Pacific basin partly contributed in suppressing the interannual variability of December rainfall over the Philippines. This is also consistent with the results of Lyon and Camargo (2009), who reported a significant reduction in rainfall over the entire Philippines during the October to December season (OND) and El Niño years. They further noted that an anticyclonic circulation anomaly develops over the SCS, which is accompanied by a weaker monsoon trough.

Wang and He (2012) found a decreasing trend in the interannual variability of the EAWM during the December to February (DJF) season after the mid-1970s. They

further noted a northward propagation of the EAWM-surface air temperature relationship from the tropics to the mid-latitudes, which is favorable for the weakening of the EAWM-ENSO relationship. Wang *et al.* (2008) suggested that this weakening of the EAWM-ENSO relationship is also associated with the phase shift of PDO through the modification of the Pacific-East Asian teleconnection at the low latitudes and the response of the *HGT* anomalies to ENSO. Over the Philippines, Villafuerte *et al.* (2014) found decreasing trends in extreme rainfall events during the January to February (JFM) season and they suggested that this is partly due to the weakening of the EAWM. Thus, the weakening of the interannual variability of the December rainfall found in this study might be related to these aforementioned studies.

To quantify the possible role of the EAWM on the changes in rainfall, we adapted the index proposed by Wang and Chen (2015) (hereafter EAWMI), which is based on the difference between the normalized area-averaged mean sea level pressure (*MSLP*) over Siberia (70–120°E, 40–60°N), North Pacific (140°E–170°W, 30–50°N), and the maritime continent (110–160°E, 20°S–10°N). Positive (negative) EAWMI values indicate strong (weak) EAWM. This index can be decomposed further into the north-south (i.e., Siberian high-Maritime Continent low relationship) and east-west (i.e., Siberian high-Aleutian low relationship) components. In this study, we only used the north-south component since the circulation anomalies below 30°N were found to be stronger when using this index compared with its east-west counterpart (Wang and Chen, 2015). In addition, we checked the epochal difference in the *MSLP* and only found significant changes over Siberia and the Maritime continent, as shown in Figure 6.16. Thus, using the north-south index is reasonable.

Figure 6.17 shows the monthly time series of the EAWMI from November to March. The correlation of the rainfall and the EAWMI during December is significant above the 99 % confidence level using Student's *t*-test (r = 0.5, p-value = 0.00047). This result further reveals that the EAWM also contributes to the interannual variability of the winter monsoon rainfall over the Philippines. The time series of the EAWMI during December, as shown in Figure 6.17b, shows remarkable and strong negative values from the period 1977 to 1992, while it only became clearer after 1987 during January, as shown in Figure 6.17c. These results suggest that the clear weakening of the EAWM during December in the late 1970s can partly explain why the decrease in rainfall is apparent during this month.

How did the weakening of the EAWM contribute to the decrease in rainfall over the Philippines during EW2? It is worth mentioning that the interaction of the northeasterly winds or cold surges from Siberia with the topography of the Philippines partially contributes to the total winter rainfall of the country (Chang *et al.*, 2005). Endo *et al*. (2009) found a significant increasing trend in the annual maximum number of consecutive dry days (CDD) from the 1950s to the mid-2000s, especially over the eastern coast of the Philippines (see their Figure 6). They suggested that this might be due to the weakening of the EAWM and a subsequent decrease in the cold surge activity from Siberia. In fact, we found a significant decrease in the *MSLP* between EW1 and EW2 over Siberia in Figure 6.18, suggesting a weaker Siberian High. In addition, Wang and Zhang (2002) noted that an anomalous anticyclonic circulation (i.e., the western North Pacific anticyclone or WNPAC) develops over the Philippines during the positive phase of PDO (see their Figure 3a). This WNPAC, in turn, weakens the northeast monsoon over the Philippines.

Why are the climate shifts only remarkable during December? Some studies suggested that the PDO can modulate the climate anomalies resulting from ENSO (Gershunov and Barnett, 1998). In particular, Gershunov and Barnett (1998) found that El Niño signals are stronger and more consistent during the positive phase of PDO, while the La Niña signals are only stronger and consistent during the negative phase of PDO. On the other hand, ENSO (either El Niño or La Niña) usually peaks in December (Tziperman *et al.*, 1998; Ballester *et al.*, 2016). Hence, the impact of PDO is more pronounced during this month. We also compared the *MSLP* and the $WINDS_{850hPa}$ anomalies relative to their long-term means (1961–2008) from November to March to further elaborate why the observed decrease in the mean rainfall are not remarkable in other winter monsoon months during EW2, as shown in Figure 6.18. During November, as shown in Figure 6.18a, anomalous northerly winds can be seen in the vicinity of the Philippines emanating from the mid-latitude anticyclone centered around 115°E and 40°N (i.e., the Siberian High). These anomalous northerlies cool the sea surface of the SCS, which is favorable for the increase in the pressure there and a subsequent development of an anticyclone during December (i.e., the WNPAC), as shown in Figure 6.18b (Wang and Zhang, 2002; Wu *et al.*, 2017a, b). Wu *et al*. (2017a, b) suggested that these anomalous northerlies are induced by the heating anomaly over the central equatorial Pacific (i.e., a Rossby wave response) and advection of negative moist enthalpy (dry air; see their Figure 13). Note that the Philippines is also under the influence of a cyclonic circulation anomaly to its east during November. Concurrent with the development of the WNPAC during December is the eastward retreat of this cyclonic circulation anomaly (Wu *et al*., 2017a, b). According to Wu *et al*. (2017a, b), this eastward retreat of the cyclonic anomaly is modulated by the sign reversal (from positive to negative) of the background relative vorticity gradient.

Southerlies/southwesterlies can also be seen above 20°N along 115°E, which substantiates the weakening of the Siberian High and less cold surge activities reaching the Philippines. It is worth mentioning that the *MSLP* change in the vicinity of the Philippines is largest during December compared with the other winter monsoon months. During January, as shown in Figure 6.18c, there is little change in the *MSLP* and a cyclonic circulation can be seen over the Philippines. The anticyclone initially located over the SCS moved northeastward around 35°N and expands eastward along 160°W. Another remarkable feature in January is the cyclonic circulation centered around 170°W and 55°N, which expands and moves southeastward over the northern Pacific in February, as shown in Figure 6.18d. This, in turn, forces the anticyclonic circulation that is initially located northeast of the Philippines to move southwards. During March, as shown in Figure 6.18e, an anomalous anticyclone is prominent over the WNP.

Aside from ENSO, TCs, and the orographic rainfall, the winter monsoon rainfall variability of the country is influenced by other large-scale systems. For example, Pullen *et al.* (2015) reported that the Madden–Julian Oscillation (MJO; intraseasonal) and an intense cold surge (synoptic) contributed to the extreme rainfall event over the Philippines during 2007–2008. Therefore, it would be interesting to examine the interdecadal variations in intraseasonal oscillations and cold surge activities and how they contributed to the shifts in rainfall in future studies. Moreover, several interesting issues still remain unresolved. For instance, are the observed interdecadal changes due to the climate's natural decadal variability or anthropogenically induced? Another important issue is that whether these shifts will be permanent or will still change in the future. In addition, the precise impact of PDO-ENSO interaction on the rainfall of the Philippines needs further investigation; that is, the response of rainfall to the different

phases of PDO during El Niño and La Niña years. Longer and homogenous datasets are needed to address this issue in future studies.

Chapter 7. General conclusions and outlook

7.1. General conclusions

This study comprehensively examined the climatology of the rainfall variability in the Philippines from synoptic to decadal time scales. Six main aims were addressed and restated as follows:

1. To examine the different rainfall producing synoptic-scale systems and their climatology during the pre-summer monsoon season over the Philippines;
2. To investigate the role of the WNPSH on the early summer monsoon break over Luzon Island;
3. To investigate the role of shearlines on the winter monsoon heavy rainfall events over the Philippines;
4. To detect whether the summer monsoon season of the Philippines has an interdecadal shift in the mid-1990s;
5. To determine potential interdecadal shifts in rainfall during the winter monsoon season;
6. To determine the possible mechanisms that are inducing these interdecadal shifts in rainfall during the summer and winter monsoon seasons.

In order to address the aforementioned objectives, this dissertation first examined the climatology of the wet and dry conditions in the pre-summer monsoon season of the Philippines that are less emphasized in previous works. Using the *OLR* and winds at 925 hPa ($WINDS_{925hPa}$), intermittent convective events (wet cases; Type W), which accounts for about 23 % of the total pre-summer monsoon days from 1979 to 2012,

were identified from April 1 to the monsoon onset defined by the PAGASA, the country's official weather bureau. The differences between the Type W and dry cases (Type D) are presented. Then, the synoptic conditions associated with the Type W cases are sub-divided into two sub-types based on the wind conditions, the (1) westerly $WINDS_{925hPa}$ intrusion over Luzon Island (Type W_W), and (2) enhanced easterly $WINDS_{925hPa}$ (Type W_E). A subset of Type W_E cases (Type W_{EDef}), which features an eastward propagating cold front north of Luzon Island and an intensifying anticyclone to its west originating from the eastern Tibetan Plateau and their differences were also examined. These two opposing circulations interact with the WNPSH over the northern Pacific and the easterlies over Luzon Island, and forms a deformation zone to the north. The confluence region of this deformation zone (i.e., the shearline), where the cold front interacts with the warm and humid air brought by the easterly $WINDS_{925hPa}$, lies over Luzon Island and contributes to the convective activities during the pre-summer monsoon over this region. The results also show that mid-latitude disturbances such as cold fronts besides the easterlies along the southern flank of the WNPSH, contribute to the convection during the pre-summer monsoon season over the Philippines. This is the first attempt to clarify such phenomenon and document the role of deformation zones as another synoptic-scale convective system during the pre-summer monsoon season of the country.

The impact of the WNPSH on rainfall is not limited during the pre-summer monsoon season. We demonstrated in Chapter 3 that the WNPSH tended to intrude Luzon Island in early summer, which induced a monsoon break in rainfall over this region. The climatology of the first post-onset monsoon break was examined. We found that this break is more remarkable in stations located over the northwest and central Luzon Island. Composite analysis of the large-scale circulation features during

the monsoon break period showed that the westward extension of the WNPSH induced unfavorable background conditions for synoptic-scale disturbances over Luzon Island. The westward extension of the WNPSH could have been facilitated, through a cloud-radiation feedback process, by the enhanced rainfall and cloudiness during the onset period. In particular, the enhanced rainfall during the onset period leads to the cooling of the atmosphere, while the enhanced cloudiness leads to a decrease in the incoming solar radiation. These changes lead to the increase in the sea level pressure and subsequent decrease in rainfall around Luzon Island that favors the westward extension of the WNPSH. With the occurrence of the monsoon break in early summer, the seasonal march of the summer monsoon over the Philippines can be divided into three phases: (1) the monsoon onset phase, which occurs between mid to late May under the influence of the westerly/southwesterly winds, (2) the monsoon break phase, when rainfall decreases over Luzon Island in early June, and (3) the monsoon revival phase, when rainfall increases again due to the intrusion of monsoon westerlies over the Philippines. This chapter showed the complex features of the summer monsoon onset and the impact of the WNPSH on the local climate of the Philippines in early summer.

The role of deformation zones, as demonstrated in Chapter 2 is more common during the winter monsoon season. In fact, we found that the shearlines along the axis of dilatation of these deformation zones induces heavy rainfall events (HRFs), especially over the southern Philippines. In Chapter 4, an HRF event that occurred on January 2017 (JAN2017), was examined first. Then, the climatology of non-TC related winter HRFs were examined. This is the first attempt to examine the climatological impact of non-TC related winter HRF events over the Philippines. We found that the JAN2017 HRF event was due to the interaction of the shearline and a westward propagating cyclonic circulation over the Mindanao Island (southern Philippines).

Using the flood reports archived by the Dartmouth Flood Observatory (DFO) and synoptic weather charts from 1979–2017, 34 non-TC related HRF events were identified over the Philippines, in which 25 cases (74 %) occurred over Mindanao Island. Focusing on these 25 cases and using composite analysis, we found a westward propagating cyclonic circulation anomaly over Mindanao Island (Mindanao vortex) and the circulation features in the composites resemble those found in the JAN2017 HRF event. Based on the composites, the Mindanao vortex intensified briefly over Mindanao Island and only progressed west/southwestward when both the southerly winds and the vorticity stretching weaken. This study clarified how cold fronts over the north Pacific together with a westward propagating tropical cyclonic vortex induced winter HRF events over the Philippines.

For the interdecadal variability of rainfall, a robust interdecadal shift was identified in the summer monsoon rainfall of the country around the mid-1990s that is most remarkable from early August to early September. These findings were presented in Chapter 5. Moreover, the results revealed a robust interdecadal shift around 1993/1994 from early August to early September, which corresponds to the peak summer rainy season over the Philippines. The average daily rainfall during 1994–2008 (ES2) was significantly lower than that during 1979–1993 (ES1). This decreased rainfall during ES2 favored the westward extension of the WNPSH, which led to the weakened monsoon westerlies and enhanced moisture flux divergence over the Philippines. The westward intrusion of the WNPSH also induced unfavorable background conditions for TC activity and other synoptic-scale disturbances as substantiated by the suppressed *PKE* in the vicinity of the Philippines. Using numerical simulations, Xiang *et al.* (2013) demonstrated that the enhanced rainfall around August induces the cooling of the sea surface temperature over the WNP, which, subsequently induces an increase in the sea

level pressure and enhanced low-level divergence that favors the intensification of the WNPSH. Therefore, this mechanism, which is referred to as the local convection-wind-evaporation-SST (CWES) feedback, can potentially explain why the decrease in rainfall is most remarkable between August and September.

Another objective of this dissertation is to identify a similar interdecadal shift in rainfall during the winter monsoon season of the Philippines, as presented in Chapter 6. The robust interdecadal shifts during winter were detected around 1976/1977 and 1992/1993. Furthermore, these shifts are most remarkable during December. The analysis period was carried out from 1961 to 2008 and was divided into three epochs: 1961–1976 (EW1), 1977–1992 (EW2), and 1993–2008 (EW3). The mean rainfall and its interannual variability were significantly suppressed during EW2 compared with the two adjacent epochs. The shift around 1976/1977 is related to the PDO shift from a negative phase to a positive phase and featured an El Niño-like SST change of the Pacific basin, while the 1992/1993 shift featured a La Niña-like SST change. A weaker low-level easterly wind, decreased moisture transport, and decreased TC activity contributed in suppressing the mean rainfall during EW2. The El Niño-like SST change and the weakening of the East Asian winter monsoon during EW2 partly contributed in suppressing the interannual variability of December rainfall in the Philippines. Although the rainfall shift during December before 1976/1977 appears symmetric to the shift after 1992/1993 (i.e., reversed), some notable differences in their corresponding circulation features were also noted. For instance, the warming was observed over the Indian Ocean since the 1960's, which is probably a manifestation of climate change. In addition, the WNPSH is stronger during EW3 compared with EW1. This enhancement of the WNPSH after the 1970s was also noted in previous studies (e.g., Yun *et al*., 2010).

It is interesting to note that the interdecadal shift during the peak summer monsoon season around 1993/1994 is almost coincident with the December shift around 1992/1993. In addition, both summer and winter interdecadal shifts feature the westward shift of the WNPSH, which is a common feature of La Niña years (Wu *et al*., 2004). However, the monthly epochal differences of SST from June to September, as shown in Figure 5.12, did not show significant cooling over the central Pacific, although significant warming were found over the western Pacific. A similar SST warming over the western Pacific were found around 1992/1993 during December, as shown in Figure 6.12b, besides the significant cooling over the central Pacific. The westward extension of the WNPSH in summer induces bifurcation of the monsoon westerlies promoting enhanced divergence and weaker monsoon trough, not favorable for synoptic-scale activities and less TC landfall over the Philippines. In contrast, the westward extension of the WNPSH during winter facilitates stronger winter monsoon and more landfalling TCs over the country.

The overall findings of this dissertations highlight the complexity of the pre-summer, summer and winter monsoon seasons of the Philippines. While the interannual variability of rainfall in the country and the impact of synoptic-scale systems such as TCs are well documented, the impact of shearlines, which is another rainfall-producing synoptic-system besides the easterlies from the southern flank of the WNPSH during the pre-summer monsoon season, were documented for the first time. This study is also the first to clarify the climatological impact of shearlines in inducing HRF events during the winter monsoon season of the Philippines. The local impact of the WNPSH in the early summer monsoon season was also examined for the first time. Specifically, its role in inducing a monsoon break following the summer monsoon onset over the Philippines were investigated. The interdecadal shifts in rainfall during both the

summer and winter monsoon seasons and the mechanisms inducing these shifts were further clarified. Contrary to most previous studies that used boreal summer or winter mean fields in decadal-to-interdecadal climate change studies, we demonstrated that the shifts in the summer and winter monsoon rainfall over the Philippines are more robust and remarkable at the sub-seasonal scale.

7.2. Outlook

There are still many issues left unaddressed in this manuscript that requires further investigations. It was stated in Chapter 1 that this study is only limited from synoptic to decadal time scales. In fact, not all of the processes between these time scales were completely analyzed in this study. Rainfall variability occurs over a wide range of spatial and temporal spectrum and the inter-relationship between the scales makes it more complicated. For instance, the decadal-scale variabilities modulate the interannual variabilities, the sub-seasonal variabilities depend on the nature of the interannual-scale variabilities, etc. Hence, further investigations are required.

The intermittent convective events during the pre-summer monsoon season was only viewed as a synoptic-scale phenomenon in Chapter 2. The contribution of the localized thunderstorms on the pre-summer monsoon convection have yet to be investigated. How the shearlines can affect the onset detection of the summer monsoon over the Philippines is also an interesting issue. In addition, we did not examine the thermodynamic aspects of the impact of shearlines on the rainfall of the Philippines. In particular, temporal changes in the convective instability should also be examined in future works. The precise controlling mechanism for the zonal displacement of the WNPSH in early summer is still unclear since most of the numerical simulations cannot correctly simulate its vertical structure.

The important role of ISOs on the rainfall variability of the Philippines is also less emphasized in previous studies. How the ISO induces the break in early summer is an important question that needs to be addressed. Recently, some studies found significant shifts in the ISO of the summer and winter monsoon rainfall over the WNP (e.g., Kajikawa *et al*., 2009; Kajikawa and Wang, 2012; Nguyen-Le and Matsumoto, 2016; Yamaura and Kajikawa, 2016). For example, Kajikawa and Wang (2012) suggested the possible contribution of the enhanced ISO in inducing an advanced summer monsoon onset over the SCS after the mid-1990s. Most of these aforementioned studies linked these changes in the ISO with the mean state change in SST over the Pacific basin in the mid to late 1990s. However, what mechanism maintains the mean state change in SST is still unclear. The role of the changes in ISO on the interdecadal shifts found in this study should be explored in future studies.

The shifting of PDO from a negative phase to a positive phase in inducing the shift around 1976/1977 during December is significant. However, no significant shift in the PDO index was found around 1992/1993, suggesting that another mechanism induces this shift. This should be clarified further in future studies. In addition, how the PDO affects the local climate of the Philippines, in general, has yet to be clarified. As noted in Chapter 1, Villafuerte *et al.* (2014) found inconclusive results regarding the impact of PDO on extreme rainfall in the Philippines. The availability of homogenous and longer historical data set is one of the major challenges in determining the precise mechanism on how the PDO affects the local climate of the country. Furthermore, we only explored the role of the changes in the dynamical aspects of the large-scale circulation features on the interdecadal shifts during the summer and winter monsoon seasons. The role of the changes in the thermodynamics (i.e., radiation, convective stability, etc.) on these interdecadal shifts have yet to be explored.

The role of extra-tropical systems such as cold surge activities in inducing the changes in the mean rainfall during the winter monsoon season is another interesting topic that requires further investigation. While several studies (e.g., Pullen *et al.*, 2015) found that cold surges can induce heavy rainfall over the Philippines, most of these studies are based on specific cases and its climatological impact on the rainfall and long-term trends have yet to be examined. Moreover, it was noted in Chapter 6 that the interannual variability of rainfall during December was significantly reduced during EW2 (i.e., the variance is smaller compared with the two adjoining epochs). A closer inspection of the December rainfall time series, as shown in Figure 6.3b, further reveals that the maximum rainfall values during EW1 and EW3 are almost similar in magnitude. The minimum rainfall values between the three epochs are also almost similar in magnitude. Although we have noted some of the differences between EW1 and EW3 in Chapter 6, it is also interesting to examine their similarities in future works. In particular, a comparison of the atmospheric conditions and SST during the maximum rainfall years between EW1 and EW3 as well as those during the minimum rainfall years should be performed.

Finally, the performance of state-of-the-art numerical models in simulating these synoptic to decadal time scale variabilities is also of great interest. Accurately simulating the timing of the shifts during the summer and winter monsoon seasons has profound implications for the management of water resources in the country.

Bibliography

Akasaka, I. 2010. Interannual variations in seasonal march of rainfall in the Philippines. *Int. J. Climatol.* **30**: 1301–1314, doi:10.1002/joc.1975.

_____, Kubota, H., Matsumoto, J., Cayanan, E.O., de Guzman, R.G., Hilario, F.D. 2018. Seasonal march patterns of the summer rainy season in the Philippines and their long-term variability since the late twentieth century. *Prog. Earth. Planet Sci.* **5**: 20, doi:10.1186/s40645-018-0178-5.

_____, Morishima, W., Mikami, T. 2007. Seasonal march and its spatial difference of rainfall in the Philippines. *Int. J. Climatol.* **27**: 715–725, doi:10.1002/joc.1428.

Asuncion, J.F., Jose, A.M. 1980. A study of the characteristics of the northeast and southwest monsoons in the Philippines. *NRCP Assisted Project*, pp. 29 (available from PAGASA archives).

Bagtasa, G. 2017. Contribution of tropical cyclones to rainfall in the Philippines. *J. Clim.* **30**: 3621–3633, doi:10.1175/JCLI-D-16-0150.1.

Ballester, J., Petrova, D., Bordoni, S., Cash, B., García-Díez, M., Rodó, X. 2016. Sensitivity of El Niño intensity and timing to preceding subsurface heat magnitude. *Sci. Rep.* **6**: 36344, doi:10.1038/srep36344.

Bates, B.C., Chandler, R.E., Browman, A.W. 2012. Trend estimation and change point detection in individual climatic series using flexible regression methods. *J. Geophys. Res. Atmos.* **117**: D16, doi:10.1029/2011JD017077.

Cabanerit, J. 2016. Interaction between a shearline and the inter-tropical convergence zone in northwestern coast of Venezuela (25 November heavy rainfall event), Available at: https://www.wpc.ncep.noaa.gov/international/internal/PRESENTATIONS/ID_201607_Julio_Canaerit_Venezuela.pdf.

Cayanan, E.O., Chen, T., Argete, J., Ten, M., Nilo, P. 2011. The effect of tropical cyclones on southwest monsoon rainfall in the Philippines. *J. Meteor. Soc. Jpn.* **89**: 123–139, doi:10.2151/jmsj.2011-A08.

Chan, J.C.L., Wang, Y., Xiu, J. 2000. Dynamic and thermodynamic characteristics associated with the onset of the 1998 South China Sea summer monsoon. *J. Meteor. Soc. Jpn.* **78**: 367–380, doi:10.1175/1520-0442(2004)017<0699:doscsm>2.0.co;2.

Chang, C.P., Chen, G.T.J. 1995. Tropical circulations associated with southwest monsoon onset and westerly surges over the South China Sea. *Mon. Wea. Rev.* **123**: 3254–3267, doi:10.1175/15200493(1995)123<3254:tcawsm>2.0.co;2.

_____, Wang, Z., McBride, J., Liu, C.H. 2005. Annual cycle of southeast Asia-maritime continent rainfall and the asymmetric monsoon transition. *J. Clim.* **18**: 287–301, doi:10.1175/JCLI-3257.1.

Chen, J., Wu, R., Wen, Z. 2012. Contribution of the South China Sea tropical cyclones to an increase in Southern China rainfall around 1993. *Adv. Atmos. Sci.* **29**: 585–598, doi:10.1007/s00376-011-1181-6.

Chen, T.C. 1985. Global water vapor flux and maintenance during FGGE. *Mon. Wea. Rev*. **113**: 1801–1819, doi:10.1175/1520-0493(1985)113<1801:gwvfam>2.0.co;2.

_____, Wang S.Y., Yen, M.C., Clark, A.J. 2008. Are tropical cyclones less effectively formed by easterly waves in the western North Pacific than in the north Atlantic? *Mon. Wea. Rev.* **136**: 4527–4540, doi:10.1175/2008MWR2149.1.

_____, Tsay, J.D., Matsumoto, J., Alpert, J. 2017. Impact of summer monsoon westerlies in the South China Sea tropical cyclone genesis in May. *Weather Forecast.* **32**: 925–947, doi:10.1175/WAF-D-16-0189.1.

_____, _____, Matsumoto, J., Alpert, J. 2015a. Development and formation mechanism of the Southeast Asian winter heavy rainfall events around the South China Sea. Part I: Formation and propagation of cold surge vortex. *J. Clim.* **28**: 1417–1443, doi:10.1175/JCLI-D-14-00170.1.

_____, _____, Matsumoto, J., Alpert, J. 2015b. Development and formation mechanism of the southeast Asian winter heavy rainfall events around the South China Sea. Part II: Multiple interactions. *J. Clim.* **28**: 1444–1464, doi:10.1175/JCLI-D-14-00171.1.

_____, _____, Yen, M.C., Matsumoto, J. 2013. The winter rainfall of Malaysia. *J. Clim.* **26**: 936–958, doi:10.1175/JCLI-D-12-00174.1.

_____, _____, _____, _____. 2012. Interannual variation of the late fall rainfall in central Vietnam. *J. Clim*. **25**: 392–413, doi:10.1175/jcli-d-11-00068.1.

_____, Wang, S.Y., Huang, W.R., Yen, M.C. 2004. Variation of the East Asian summer monsoon rainfall. *J. Clim.* **17**: 744–762, doi:10.1175/1520 0442(2004)017<0744:
VOTEAS>2.0.CO;2.

Choi, J.W., Cha, Y., Kim, H.D. 2017. Interdecadal variation of precipitation days in August in the Korean Peninsula. *Dyn. Atmos. Oceans* **77**: 74–88, doi:10.1016/j.dynatmoce.
2016.10.003.

_____, Lee, S.W., Lim, B.H., Kim, B.J. 2016. Interdecadal change of winter precipitation over southern China in late 1990s. *J. Meteor. Soc. Jpn.* **94**: 197–213, doi:10.2151/jmsj.2016-011.

Choi, K.S., Wu, C.C., Cha, E.J. 2010. Change of tropical cyclone activity by Pacific-Japan teleconnection pattern in the western North Pacific. *J. Geophys. Res. Atmos.* **115**: doi:10.1029/2010JD013866.

Christidis, N., Betts, R.A., Stott, P.A. 2019. The extremely wet March of 2017 in Peru. *Bull*. *Amer*. *Meteor*. *Soc*. **100**: S31–S35, doi:10.1175/bams-d-18-0110.1.

Cinco, T.A., de Guzman, R.G., Hilario, F.D., Wilson, D.M. 2014. Long-term trends and extremes in observed daily precipitation and near surface air temperature in the Philippines for the period 1951–2010. *Atmos. Res.* **145**: 12–26, doi:10.1016/j.atmosres.2014.03.025.

_____, _____, Ortiz, A.M., Delfina, R.J., Lasco, R.D., Hilario, F.D., Juanillo, E.L., Barba, R., Ares, E.D. 2016. Observed trends and impacts of tropical cyclones in the Philippines. *Int. J. Climatol.* **36**: 4638–4650, doi:10.1002/joc.4659.

Compo, G.P., Kiladis, G.N., Webster, P.J. 1999. The horizontal and vertical structure of the east Asian winter monsoon pressure surges. *Q. J. Roy. Meteor. Soc.* **125**: 29–54, doi:10.1256/smsqj.55302.

Cook, B.I., Buckley, B.M. 2009. Objective determination of monsoon season onset, withdrawal, and length. *J. Geophys. Res. Atmos.* **114**: D23, doi:10.1029/2009JD012795.

Coronas, J. 1920. The climate and weather of the Philippines, 1903 to 1918. Weather Bureau, Bureau of Printing: Manila, Philippines, pp. 1–195.

Corporal-Lodangco, I.L., Leslie, L.M. 2016. Cluster analysis of Philippine tropical cyclone climatology. *J. Climatol. Weather Forecasting*, **4**: 152, doi:10.4172/2332-2594.
1000152.

Cruz, F.T., Narisma, G.T., Villafuerte, M.Q., Chua, K.C., Olaguera, L.M. 2013. A climatological analysis of the southwest monsoon rainfall in the Philippines. *Atmos. Res.* **122**: 609–616, doi:10.1016/j.atmosres.2012.06.010.

Dado, J.M.B., Takahashi, H.G. 2017. Potential impact of sea surface temperature on rainfall over the western Philippines. *Prog. Earth Planet. Sci.* 4: 23, doi:10.1186/
s40645-017-0137-6.

Ding, Y. 1992. Summer monsoon rainfalls in China. *J. Meteor. Soc. Jpn.* **70**: 373–396, doi:10.2151/jmsj1965.70.1b_373.

_____, Sun, Y., Wang, Z., Zhu, Y., Song, Y. 2009. Interdecadal variation of summer precipitation in east China and its association with decreasing Asian summer monsoon. Part II: Possible causes. *Int. J. Climatol.* **29**: 1926–1944, doi:10.1002/
joc.1759.

_____, Wang, Z., Sun, Y. 2008. Interdecadal variation of summer precipitation in east China and its association with decreasing Asian summer monsoon. Part I: Observed evidences. *Int. J. Climatol*. **28**: 1139–1161, doi:10.1002/joc.1615.

Du, Y., Yang, L., Xie, S.P. 2011. Tropical Indian Ocean influence on northwest Pacific tropical cyclones in summer following strong El Nino. *J. Clim.* **24**: 315–322, doi:10.1175/2010JCLI3890.1.

Efron, B., Tibshirani, R.J. 1993. *An introduction to the bootstrap*, Chapman and Hall, New York, USA, pp. 220–234, ISBN: 0–412–04231–2.

Endo, N., Matsumoto, J., Lwin, T. 2009. Trends in precipitation extremes over southeast Asia. *SOLA*. **5**: 168–171, doi:10.2151/sola.2009-043.

Faustino-Eslava, D.V., Yumul, G.P., Servando, N.T., Dimalanta, C.B. 2011. The January 2009 anomalous precipitation associated with the 'Tail-End of the Cold Front' weather system in northern and eastern Mindanao (Philippines): Natural hazards, impacts and risk reductions. *Global and Planetary Change* **76**: 85–94, doi:10.1016/j.gloplacha.2010.12.009.

Flores, J.F., Balagot, V.F. 1969. Climate of the Philippines. In Arakawa H. (ed.), *Climates of Northern and Eastern Asia*, World Survey of Climatology, 8, Elsevier, Amsterdam, pp. 159–213.

Fu, J.J., Li, S.L., Luo, D.H. 2009. Impact of global SST on decadal shift of East Asian summer climate. *Adv. Atmos. Sci.* **26**: 192–201, doi:10.1007/s00376-009-0192-z.

Fudeyasu, H., Iizuka, S., Matsuura, T. 2006. Impact of ENSO on landfall characteristics of tropical cyclones over the western North Pacific during summer monsoon season. *Geophys. Res. Lett.* **33**: 21, doi:10.1029/2006GL027449.

Fukutomi, Y., Yasunari, T. 1999. 10–25-day intraseasonal variations of rainfall and circulation over East Asia and western North Pacific during early summer. *J. Meteor. Soc. Jpn.* **77**: 753–769, doi:10.2151/jmsj1965.77.3_753.

_____, _____. 2002. Tropical-extratropical interaction associated with the 10–25-day oscillation over the western Pacific during the northern summer. *J. Meteor. Soc. Jpn.* **80**: 311–331, doi:10.2151/jmsj.80.311.

Gerpacio, R.V., Labios, J.D., Labios, R.V., Diangkinay, E.I. 2004. Maize in the Philippines: Production Systems, Constraints, and Research Priorities. CIMMYT: Mexico, pp. 1–38, ISBN: 970–648–123–0.

Gershunov, A., Barnett, T.P. 1998. Interdecadal modulation of ENSO teleconnections. *Bull. Amer. Meteor. Soc.*, **79**: 2715–2726, doi:10.1175/1520-0477(1998)079 <2715: IMOET>2.0.CO;2.

Gill, A.E. 1980. Some simple solutions for heat-induced tropical circulation. *Q. J. Royal Meteor. Soc.* **106**: 447–462, doi:10.1002/qj.49710644905.

Gong, D.Y., Ho, C.H. 2002. Shift in the summer rainfall over the Yangtze River valley in the late 1970s. *Geophys. Res. Lett.* **29**: 10, doi:10.1029/2001GL0145.

Goswami, B.N. 2006. The Asian monsoon: interdecadal variability. In: Wang B. (ed) *The Asian Monsoon*, Springer: Berlin, Heidelberg, pp. 295–327, ISBN: 978–3–540–40610–5.

Ha, K.J., Ha, E. 2006. Climatic change and interannual fluctuations in the long-term record of monthly precipitation for Seoul. *Int. J. Climatol*. **26**: 607–618, doi:10.1002/
joc.1272.

_____, Yun, K.S., Jhun, J.G., Li, J. 2009. Circulation changes associated with the interdecadal shift of Korean August rainfall around late 1960s. *J. Geophys. Res. Atmos.* **114**: D4, doi:10.1029/2008JD011287.

Ha, Y., Zhong, Z. 2015. Decadal change in tropical cyclone activity over the South China Sea around 2002/03. *J. Clim.* **28**: 5935–5951, doi:10.1175/JCLI-D-14-00769.1.

Hartmann, B., Wendler, G. 2005. The significance of the 1976 Pacific climate shift in the climatology of Alaska. *J. Clim.* **18**: 4824–4839, doi:10.1175/JCLI3532.1.

Hattori, M., Mori, S., Matsumoto, J. 2011. The cross-equatorial northerly surge over the maritime continent and its relationship to precipitation patterns. *J. Meteor. Soc. Jpn.* **89**: 27–47, doi:10.2151/jmsj.2011-A02.

He, H., Yang, J., Gong, D., Mao, R., Wang, Y., Gao, M. 2015. Decadal changes in tropical cyclone activity over the western North Pacific in the late 1990s. *Clim. Dyn.* **45**: 3317–3329, doi:10.1007/s00382-015-2541-1.

Hirasawa, N., Kato, K., Takeda, T. 1995. Abrupt change in the characteristics of the cloud zone in subtropical East Asia around the middle of May. *J. Meteor. Soc. Jpn.* **73**: 221–239, doi:10.2151/jmsj1965.73.2_221.

Hirata, H., Kawamura, R. 2014. Scale interaction between typhoons and the North Pacific subtropical high and associated remote effects during the Baiu/Mei-yu season. *J. Geophys. Res. Atmos.* **119**: 5157–5170, doi:10.1002/2013JD021430.

Hoell, A., Perlwitz, J., Dewes, C., Wolter, K., Rangwala, I., Quan, X.W., Eischeid, J. 2019. Anthropogenic contributions to the intensity of the 2017 United States northern Great Plains drought. *Bull*. *Amer*. *Meteor*. *Soc*. **100**: S19–S24, doi: 10.1175/bams-d-18-0127.1.

Holland, G.J. 1993. Ready Reckoner—Chapter 9, *Global guide to tropical cyclone forecasting*, WMO/TC-No.560, Report No. TCP-31, World Meteorological Organization, Geneva, Switzerland, 32 pp.

Huang, R., Sun, F. 1992. Impacts of tropical western Pacific on the East Asian summer monsoon. *J. Meteor. Soc. Jpn.* **70**: 243–256, doi:10.2151/jmsj1965.70.1B_243.

Huffman, G.J., Bolvin, D.T. 2015. Real time TRMM multi-satellite precipitation analysis dataset documentation. *NASA Tech. Doc*. Greenbelt, MD, USA, 51 pp.

_____, Adler, R.F., Bolvin, D.T., Nelkin, E.J. 2010. The TRMM multi-satellite precipitation analysis (TMPA). In: Gebremichael M., Hossain F. (eds) *Satellite rainfall applications for surface hydrology*, Springer, Dordrecht, pp. 3–22, doi: 10.1007/978-90-481-2915-7_1.

Hung, C.W., Hsu, H.H. 2008. The first transition of the Asian summer monsoon, intraseasonal oscillation, and Taiwan Mei-yu. *J. Clim.* **21**: 1552–1568, doi:10.1175/2007JCLI1457.1.

_____, Kao, P.K. 2010. Weakening of the winter monsoon and abrupt increase of winter rainfalls over northern Taiwan and southern China in the early 1980s. *J. Clim.* **23**: 2357–2367, doi:10.1175/2009JCLI3182.1.

Inoue, T., Matsumoto, J. 2007. Abrupt climate changes observed in late August over central Japan between 1983 and 1984. *J. Clim.* **20**: 4957–4967, doi:10.1175/JCLI4217.1.

Jacques-Coper, M., Garreaud, R.D. 2015. Characterization of the 1970s climate shift in South America. *Int. J. Climatol.* **35**: 2164–2179, doi:10.1002/joc.4120.

Jia, X., Ge, J. 2017. Interdecadal changes in the relationship between ENSO, EAWM, and the winter precipitation over China at the end of the twentieth century. *J. Clim.* **30**: 1923–1937, doi:10.1175/JCLI-D-16-0422.1.

Kajikawa, Y., Wang, B. 2012. Interdecadal change of the South China Sea summer monsoon onset. *J. Clim.* **25**: 3207–3218, doi:10.1175/JCLI-D-11-00207.1.

_____, Yasunari, T. 2005. Inter-annual variability of the 10–25- and 30–60-day variation over the South China Sea during boreal summer. *Geophys. Res. Lett.* **32**: L04710, doi:10.1029/2004GL021836.

_____, _____, Wang, B. 2009. Decadal change in intraseasonal variability over the South China Sea. *Geophys. Res. Lett.* **36**: 6, doi:10.1029/2009GL037174.

_____, _____, Yoshida, S., Fujinami, H. 2012. Advanced Asian summer monsoon onset in recent decades. *Geophys. Res. Lett.* **39**: 3, doi:10.1029/2011GL050540.

Kanamitsu, M., Ebisuzaki, W., Woollen, J., Yan, S.K., Hnilo, J.J., Fiorino, M., Potter, G.L. 2002. NCEP-DOE AMIP-II Reanalysis (R-2). *Bull. Amer. Meteor. Soc.* **83**: 1631–1643, doi:10.1175/BAMS-83-11-1631.

Kawatani, Y., Ninomiya, K., Tokioka, T. 2008. The north Pacific subtropical high characterized separately for June, July, and August: zonal displacement associated with submonthly variability. *J. Meteor. Soc. Jpn.* **86**: 505–530, doi:10.2151/
jmsj.86.505.

Kemball-Cook, S., Wang, B. 2001. Equatorial waves and air-sea interaction in the boreal summer intraseasonal oscillation. *J. Clim*. **14**: 2923–2942, doi:10.1175/1520-0442
(2001)014<2923:EWAASI>2.0.CO;2.

Kiguchi, M., Matsumoto, J. 2005. The rainfall phenomena during the pre-monsoon period over the Indochina Peninsula in the GAME-IOP year, 1998. *J. Meteor. Soc. Jpn.* **83**: 89–106, doi:10.2151/jmsj.83.89.

_____, _____, Kanae, S., Oki, T. 2016. Pre-monsoon rain and its relationship with monsoon onset over the Indochina Peninsula. *Front. Earth Sci.* **4**: 42, doi:10.3389.
feart.2016.00042.

Kikuchi, K., Wang, B. 2010. Formation of tropical cyclones in the northern Indian Ocean associated with the two types of tropical intraseasonal oscillation modes. *J. Meterol. Soc. Jpn.* **88**: 475–496, doi:10.2151/jmsj.2010-313.

_____, _____, Kajikawa, Y. 2012. Bimodal representation of tropical intraseasonal oscillation. *Clim. Dyn.* **38**: 1989–2000, doi:10.1007/s00382-011-1159-1.

Kim, J.H., Wu, C.C., Sui, C.H., Ho, C.H. 2012. Tropical cyclone contribution to interdecadal change in summer rainfall over South China in the early 1990s. *Terr. Atmos. Ocean. Sci.* **23**: 49–58, doi:10.3319/TAO.2011.08.26.01(A).

Kim, W.M., Jhun, J.G., Ha, K.J., Kimoto, M. 2011. Decadal changes in climatological intraseasonal fluctuation of subseasonal evolution of summer precipitation over the Korean Peninsula in the mid-1990s. *Adv. Atmos. Sci.* **28**: 591–600, doi:10.1007/
s00376-010-0037-9.

Kintanar, R.L. 1984. *Climate of the Philippines*; PAGASA: Quezon City, Philippines, 38 pp.

Kobayashi, S., Ota, Y., Harada, Y., Ebita, A., Moriya, M., Onoda, H., Onogi, K., Kamahori, H., Kobayashi, C., Endo, H., Miyaoka, H., Takahashi, K. 2015. The JRA-55 Reanalysis: General specifications and basic characteristics. *J. Meteor. Soc. Jpn.* **93**: 5–48, doi:10.2151/jmsj.2015–001.

Kubota, H., Chan, J.C.L. 2009. Interdecadal variability of tropical cyclone landfall in the Philippines from 1902 to 2005. *Geophys. Res. Lett.* **36**: L12802, doi:10.1029/
2009GL038108.

_____, Kosaka, Y., Xie, S.P. 2016. A 117-year long index of the Pacific-Japan pattern with application to interdecadal variability. *Int. J. Climatol.* **36**: 1575–1589, doi:10.1002/joc.4441.

_____, Shirooka, R., Matsumoto, J., Cayanan, E.O., Hilario, F.D. 2017. Tropical cyclone influence on the long-term variability of the Philippines summer monsoon onset. *Prog. Earth Planet. Sci.* **4**: 1–12, doi:10.1186/s40645-017-0138-5.

_____, Wang, B. 2009. How much do tropical cyclones affect seasonal and interannual rainfall variability over the western North Pacific? *J. Clim.* **22**: 5495–5510, doi:10.1175/2009JCLI2646.1.

Kwon, M., Jhun, J.G., Ha, K.J. 2007. Decadal change in East Asian summer monsoon circulation in the mid-1990s. *Geophys. Res. Lett.* **34**: 21, doi:10.1029/2007GL031977.

_____, _____, Wang, B., An, S.I., Kug, J.S. 2005. Decadal change in relationship between East Asian and WNP summer monsoons. *Geophys. Res. Lett.* **32**: 16, doi:10.1029/2005GL023026.

Lau, K.H., Lau, N.C. 1990. Observed structure and propagation characteristics of tropical summer-time synoptic-scale disturbances. *Mon. Wea. Rev.* **118**: 1888–1913, doi:10.1175/1520-0493(1990)118<1888:osapco>2.0.co;2.

_____, Yang, G.J., Shen, S.H. 1988. Seasonal and intra-seasonal climatology of summer monsoon rainfall over East Asia. *Mon. Wea. Rev.* **116**: 18–37, doi:10.1175/1520–0493(1988)116<0018:SAICOS>2.0.CO;2.

_____, Yang, S. 1997. Climatology and interannual variability of the southeast Asian summer monsoon. *Adv. Atmos. Sci.* **14**: 141–162, doi:10.1007/s00376-997-0016-y.

Li, H.Y., Lin, Z.H., Chen, H. 2009. Interdecadal variability of spring precipitation over south China and its associated atmospheric water vapor transport. *Atmos. Oceanic Sci. Lett.* **2**: 113–118, doi:10.1080/16742834.2009.11446783.

Liebmann, B., Smith, C.A. 1996. Description of a complete (interpolated) outgoing longwave radiation dataset. *Bull. Amer. Meteor. Soc.* **77**: 1275–1277.

Lin, H., Wang, B. 2002. The time-space structure of the Asian-Pacific summer monsoon: a fast annual cycle view. *J. Clim.* **15**: 2001–2019, doi:10.1175/1520-0442(2002)
015<2001:TTSSOT>2.0.CO;2.

Liu, K.S., Chan, J.C.L. 2013. Inactive period of western North Pacific tropical cyclone activity in 1998–2011. *J. Clim.* **26**: 2614–2630, doi:10.1175/JCLI-D-12-00053.1.

Liu, Y., Huang, G., Huang, R. 2011. Interdecadal variability of summer rainfall in eastern China detected by Lepage test. *Theor. Appl. Climatol.* **106**: 481–488, doi:10.1007/s00704-011-0442-8.

Lohar, D., Pal, B. 1995. The effect of irrigation on premonsoon season precipitation over South West Bengal, India. *J. Clim.* **10**: 2567–2570, doi:10.1175/1520-0442(1995)
008<2567:teoiop>2.0.co;2.

Lu, R., Dong, B. 2001. Westward extension of the north Pacific subtropical high in summer. *J. Meteor. Soc. Jpn.* **79**: 1229–1241, doi:10.2151/jmsj.79.1229.

Luo, M., Lin, L. 2017. Objective determination of the onset and withdrawal of the South China Sea summer monsoon. *Atmos. Sci. Lett.* **18**: 276–282, doi:10.1002/asl.753.

Luo, X., Zhang, Y. 2015. Interdecadal change in the seasonality of rainfall variation in South China. *Theor. Appl. Climatol.* **119**: 1–11, doi:10.1007/s00704-013-1088-5.

Lyon, B., Camargo, S.J. 2009. The seasonally varying influence of ENSO on rainfall and tropical cyclone activity in the Philippines. *Clim. Dyn.* **32**: 125–141, doi:10.1007/
s00382-008-0380-z.

_____, Cristi, H., Verceles, E.R., Hilario, F.D., Abastillas, R. 2006. Seasonal reversal of the ENSO rainfall signal in the Philippines. *Geophys. Res. Lett.* **33**: L24710, doi:10.1029/2006GL028182.

Mallakpour, I., Villarini, G.A. 2016. Simulation study to examine the sensitivity of the Pettitt test to detect abrupt changes in mean. *Hydrolog. Sci. J.* **61**: 245–254, doi:10.1080/02626667.2015.1008482.

Maloney, E.D., Dickinson, M.J. 2003. The intraseasonal oscillation and the energetics of summertime tropical western North Pacific synoptic-scale disturbances. *J. Atmos. Sci.* **60**: 2153–2168, doi:10.1175/1520-0469(2003)060<2153:TIOATE>2.0.CO;2.

Mantua, N.J., Hare, S.R. 2002. The Pacific decadal oscillation. *J. Oceanogr.* **58**: 35–44, doi:10.1023/A:10158206.

_____, _____, Zhang, Y., Wallace, J.M., Francis, R.C. 1997. A pacific interdecadal climate oscillation with impacts on salmon production. *Bull. Amer. Meteor. Soc.* **78**: 1069–1079, doi:10.1175/1520-0477(1997)078<1069:APICOW>2.0.CO;2.

Matsumoto, J. 1992. The seasonal changes in Asian Australian monsoon regions. *J. Meteor. Soc. Jpn.* **70**: 257–273, doi:10.2151/jmsj1965.70.1B_257.

_____. 1995. Rainfall climatology over the Asian monsoon region, In: Murai S. (ed) *Toward global planning of sustainable use of the earth*, Elsevier, Amsterdam, pp. 419–422.

_____. 1997. Seasonal transition of summer rainy season over Indochina and adjacent monsoon region. *Adv. Atmos. Sci.* **14**: 231–245, doi:10.1007/s00376-997-0022-0.

Matsuyama, H., Marengo, J.A., Obregon, G.O., Nobre, C.A. 2002. Spatial and temporal variabilities of rainfall in tropical South America as derived from Climate Prediction Center Merged Analysis of Precipitation. *Int. J. Climatol.* **22**: 175−195, doi:10.1002/joc.724.

Mattesson, D.S., James, N.A. 2014. A nonparametric approach for multiple change point analysis of multivariate data. *J. Amer. Stat. Assoc.* **109**: 334–345, doi:10.1080/ 01621459.2013.849605.

Moron, V., Lucero, A., Hilario, F., Lyon, B., Robertson, A.W., DeWitt, D. 2009. Spatio-temporal variability and predictability of summer monsoon onset over the Philippines. *Clim. Dyn*. **33**: 1159, doi:10.1007/s00382-008-0520-5.

Murakami, T., Matsumoto, J. 1994. Summer monsoon over the Asian continent and western North Pacific. *J. Meteor. Soc. Jpn.* **72**: 719–745, doi:10.2151/ jmsj1965.72.5_719.

Nakazawa, T. 1992. Seasonal phase lock of intraseasonal variation during the Asian summer monsoon. *J. Meteor. Soc. Jpn.* **70**: 597–745, doi:10.2151/ jmsj1965.70.1B_597.

Nitta, T. 1987. Convective activities in the tropical western Pacific and their impact on the northern hemisphere summer circulation. *J. Meteor. Soc. Jpn.* **65**: 373–393, doi:10.2151/jmsj1965.65.3_373.

_____, Yamada, S. 1989. Recent warming of the tropical sea surface temperature and its relationship to the northern hemisphere circulation. *J. Meteor. Soc. Jpn.* **67**: 375–383, doi:10.2151/jmsj1965.67.3_375.

Nguyen-Le, D., Matsumoto, J. 2016. Delayed withdrawal of the autumn rainy season over central Vietnam in recent decades. *Int. J. Climatol.* **36**: 3002–3019, doi:10.1002/
joc.4533.

_____, _____, Ngo-Duc, T. 2014. Climatological onset date of summer monsoon in Vietnam. *Int. J. Climatol.* **34**: 3237–3250, doi:10.1002/joc.3908.

Okada, Y., Yamazaki, K. 2012. Climatological evolution of the Okinawa Baiu and differences in large-scale features during May and June. *J. Clim.* **25**: 6287–6303, doi:10.1175/JCLI-D.-11-00631.1.

Olaguera, L.M., Matsumoto, J. 2019. A climatological study of the wet and dry conditions in the pre-summer monsoon season of the Philippines. *Int. J. Climatol.* Manuscript under review.

_____, _____, Kubota, H., Cayanan, E.O., Hilario, F.D. 2019a. A climatological analysis of the monsoon break following the summer monsoon onset over Luzon Island, Philippines. *Int. J. Climatol.* Manuscript under review.

_____, _____, Dado, J.M., Narisma, G. 2019b. Non-tropical cyclone related winter heavy rainfall events over the Philippines: Climatology and mechanism. *Asia-Pac. J. Atmos. Sci.* Manuscript under review.

_____, _____, _____, Inoue, T., Cayanan, E.O., Hilario, F.D. 2018a. Abrupt climate shift in the mature rainy season of the Philippines in the mid-1990s. *Atmosphere,* **9**: 350, doi:10.3390/atmos9090350.

_____, _____, _____, _____, _____, _____. 2018b. Interdecadal shifts in the winter monsoon rainfall of the Philippines. *Atmosphere,* **9**: 464, doi:10.3390/atmos9120464.

Orgill, M. 1967. Some aspects of the onset of the summer monsoon over South East Asia. Report to U.S.Army, Contract DA28-043-AMC-01303(E). Colorado State University, Ft. Collins, Colorado, USA, 75 pp.

Pettitt, A.N. 1979. A non-parametric approach to the change-point problem. *J. Roy. Stat. Soc.* **28**: 126–135, doi:10.2307/23456729.

Philippine Statistics Authority. 2016. *Selected Statistics on Agriculture*, Available at http://countrystat.psa.gov.ph, Last accessed on 02 February 2017.

Porio, E., Dator-Bercilla, J., Narisma, G., Cruz, F., Yulo-Loyzaga, A. 2019. Drought and urbanization: The case of the Philippines. In: Ray B., Shaw R. (eds) *Urban Drought.* Springer, Singapore, pp. 183–208, doi:10.1007/978-981-10-8947-3_12.

Pullen, J., Gordon, A.L., Flatau, M., Doyle, J.D., Villanoy, C., Cabrera, O. 2015. Multiscale influences on extreme winter rainfall in the Philippines. *J. Geophys. Res. Atmos.* **120**: 3292–3309, doi:10.1002/2014JD022645.

Rajeevan, M., Gadgil, S., Bhate J. 2010. Active and break spells of the Indian summer monsoon. *J. Earth Syst. Sci.* **119**: 229–247, doi:10.1007/s12040-010-0019-4.

Ramage, C.S. 1952. Variation of rainfall over South China through the west season. *Bull. Amer. Meteor. Soc.* **33**: 308–311, doi:10.1175/1520-0477-33.7.308.

_____. 1971. *Monsoon meteorology*, Academic Press, New York, 296 pp.

Rayner, N.A., Parker, D.E., Horton, E.B., Folland, C.K., Alexander, L.V., Rowell, D.P., Kent, E.C., Kaplan, A. 2003. Global analysis of sea surface temperature, sea ice, and night marine air temperature since the late nineteenth century. *J. Geophys. Res. Atmos.* **108**: D14, doi:10.1029/2002JD002670.

Roberts, M.G., Dawe, D., Falcon, W.P., Naylor, R.L. 2009. El Nino-Southern Oscillation impacts on rice production in Luzon, the Philippines. *J. Appl. Meteor. Climatol.* **48**: 1718–1724, doi:10.1175/2008JAMC1628.1.

Ropelewski, C.F., Halpert, M.S. 1987. Global and regional scale precipitation patterns associated with the El Niño/Southern Oscillation. *Mon. Wea. Rev.* **115**: 1606–1626, doi:10.1175/1520-0493(1987)115<1606:GARSPP>2.0.CO;2.

Salarijazi, M., Akhond-Ali, A.M., Adib, A., Daneshkhah, A. 2012. Trend and change-point detection for the annual stream-flow series of the Karun River at the Ahvaz hydrometric station. *Afr. J. Agric. Res.* **32**: 4540–4552, doi:10.5897/AJAR12.650.

Saunders, M.A., Chandler, R.E., Merchant, C.J., Roberts, F.P. 2000. Atlantic hurricanes and NW Pacific typhoon: ENSO spatial impacts on occurrence and landfall. *Geophys. Res. Lett.* **27**: 1147–1150, doi:10.1029/1999GL010948.

Seiki, A., Takayabu, Y.N. 2007. Westerly wind bursts and their relationship with intraseasonal variations and ENSO. Part II: Energetics over the western and central Pacific. *Mon. Wea. Rev.* **135**: 3346–3361. doi:10.1175/MWR3503.1.

Sen Roy, S., Goodrich, G.B., Balling Jr., R.C. 2003. Influence of El Niño/Southern Oscillation, Pacific Decadal Oscillation, and local sea-surface temperature anomalies on peak season monsoon precipitation in India. *Clim. Res.* **25**: 171–178, doi:10.1002/joc.2065.

So, C.H., Chan, J.C.L. 1997. Regional and synoptic-scale features associated with inactive periods of the summer monsoon over South China. *Adv. Atmos. Sci.* **14**: 223–230, doi:10.1007/s00376-997-0021-1.

Stocker, T.F, Qin, D., Plattner, G.K., Tignor, M., Allen, S.K., Boschung, J., Nauels, A., Xia, Y., Bex, B., Midgley, P.M. 2013. The physical science basis: contribution of Working Group I to the Fifth Assessment Report of the Intergovernmental Panel on Climate Change. Cambridge University Press, Cambridge United Kingdom and New York, USA, 1535 pp.

Stone, R.J. 2010. Comments on "Observed trends in indices of daily temperature extremes in South America 1960–2000". *J. Clim.* **24**: 2880–2883, doi:10.1175/2011JCLI3662.1.

Takahashi, H. G. 2011. Long-term changes in rainfall and tropical cyclone activity over South and Southeast Asia. *Adv. Geosci.* **30**: 17–22, doi:105194/adgeo-30-17-2011.

_____, Fukutomi, Y., Matsumoto, J. 2011. The impact of long-lasting northerly surges of the East Asian winter monsoon on tropical cyclogenesis and its seasonal march. *J. Meteor. Soc. Jpn*. **89**: 181–200, doi:10.2151/jmsj.2011-a12.

_____, Yasunari, T. 2006. A climatological monsoon break in rainfall over Indochina—A singularity in the seasonal march of the Asian summer monsoon. *J. Clim*. **19**: 1545–1556, doi:10.1175/JCLI3724.1.

_____, _____. 2008. Decreasing trend in rainfall over Indochina during the late summer monsoon: Impact of tropical cyclones. *J. Meteor. Soc. Jpn.* **86**: 429–438, doi:10.2151/jmsj.86.429.

Tao, S., Chen, L. 1987. A review of recent research on the East Asian summer monsoon in China. In: Chang C.P., Krishnamurti T.N. (eds) *Monsoon Meteorology*, Oxford University Press, London, pp. 60–92.

Trenberth, K.E. 1990. Recent observed interdecadal climate changes in the northern hemisphere. *Bull. Amer. Meteor. Soc.* **71**: 988–993, doi:10.1175/1520-0477(1990)071<0988:ROICCI>2.0.CO;2.

Tziperman, E., Cane, M.A., Zebiak, S.E., Xue, Y., Blumenthal, B. 1998. Locking of El Nino's peak time to the end of the calendar year in the delayed oscillator picture of ENSO. *J. Clim*. **11**: 2191–2199, doi:10.1175/1520-0442(1998)011<2191:

LOENOS>2.0.CO;2.

Ueda, H. 2005. Air-sea coupled process involved in stepwise seasonal evolution of the Asian summer monsoon. *Geogr. Rev. Jpn.* **78**: 825–841, doi:10.4157/grj.78.825.

_____, Yasunari, T. 1996. Maturing process of the summer monsoon over the Western North Pacific: A coupled ocean/atmosphere system. *J. Meteor. Soc. Jpn.* **74**: 493–508, doi:10.215/jmsj1965.74.4_493.

_____, _____, Kawamura, R. 1995. Abrupt seasonal change of large-scale convective activity over the western Pacific in the northern summer. *J. Meteor. Soc. Jpn.* **73**: 795–809, doi:10.2151/jmsj1965.73.4_795.

Villafuerte, M.Q. II, Juanillo E.L., Hilario F.D. 2017. Climatic insights on academic calendar shift in the Philippines. *Phil. J. Science.* **146**: 267–276; ISSN 0031–7683.

_____, Matsumoto, J., Akasaka, I., Takahashi, H.G., Kubota, H., Cinco, T.A. 2014. Long-term trends and variability of rainfall extremes in the Philippines. *Atmos. Res.* **137**: 1–13, doi:10.1016/j.atmosres.2013.09.021.

_____, _____, Kubota, H. 2015. Changes in extreme rainfall in the Philippines (1911–2010) linked to global mean temperature and ENSO. *Int. J. Climatol.* **35**: 2033–2044, doi:10.1002/joc.4105.

Vincent, L.A., Zhang, X., Wang, X.L. 2011. Reply to the comments on "Observed trends in indices of daily temperature extremes in South America 1960–2000". *J. Clim.* **24**: 2884–2887, doi:10.1175/2011JCLI3786.1.

Wang, B. 1995. Interdecadal change in El Niño onset in the last four decades. *J. Clim.* **8**: 267–285, doi:10.1175/1520-0442(1995)008<0267:ICIENO>2.0.CO;2.

_____, An, S.I. 2001. Why the properties of El Niño changed during the late 1970s. *Geophys. Res. Lett.* **28**: 3709–3712, doi:10.1029/2001GL012862.

_____, Chan, J.C. 2002. How strong ENSO events affect tropical storm activity over the western North Pacific. *J. Clim.* **13***:* 1643–1658, doi:10.1175/1520-0442(2002)
015<1643:HSEEAT>2.0.CO;2.

_____, Ding, Q., Fu, X., Kang, I.S., Jin, K., Shukla, J., Doblas-Reyes, F. 2005. Fundamental challenge in simulation and prediction of summer monsoon rainfall. *Geophys. Res. Lett.* **32**: L15711, doi:10.1029/2005GL022734.

_____, Lin, H. 2002. Rainy season of the Asian-Pacific summer monsoon. *J. Clim.* **15**: 386–398, doi:10.1175/1520-0442(2002)015<0386:RSOTAP>2.0.CO;2.

_____, _____, Zhang, Y., Lu, M.M. 2004. Definition of South China Sea monsoon onset and commencement of the East Asian summer monsoon. *J. Clim.* **17**: 699–710, doi:10.1175/1520-0442(2004)017<0699:doscsm>2.0.co;2.

_____, Xu, X. 1997. Northern Hemisphere summer monsoon singularities and climatological intraseasonal oscillation. *J. Clim.* **10**: 1071–1085, doi:10.1175/1520-0442(1997)010<1071. NHSMSA>2.9.CO;2.

_____, Zhang, Q. 2002. Pacific-East Asian teleconnection. Part II: How the Philippine Sea anomalous anticyclone is established during El Niño development. *J. Clim.* **15**: 3252–3265, doi:10.1175/1520-0442(2002)015<3252:PEATPI>2.0.CO;2.

Wang, H., He, S. 2012. Weakening relationship between East Asian winter monsoon and ENSO after mid-1970s. *Chin. Sci. Bull.* **57**: 3535–3540, doi:10.1007/s11434-012-5285-x.

Wang, H.J. 2001. Weakening of the Asian monsoon circulation after the end of 1970s. *Adv. Atmos. Sci.* **18**: 376–386, doi:10.1007/BF02919316.

Wang, L., Chen, W. 2015. An intensity index for the East Asian winter monsoon. *J. Clim.* **27**: 2361–2374, doi:10.1175/JCLI-D-13-00086.1.

_____, _____, Huang, R. 2008. Interdecadal modulation of PDO on the impact of ENSO on the East Asian winter monsoon. *Geophys. Res. Lett.* **35**: L20702, doi:10.1029/2008GL035287.

_____, Huang, R., Wu, R. 2013. Interdecadal variability in tropical cyclone frequency over the South China Sea and its association with the Indian Ocean sea surface temperature. *Geophys. Res. Lett.* **40**: 768–771, doi:10.1002/GRL.50171.

Wang, T., Yang, H., Yang, D., Wang, Y. 2018. Quantifying the streamflow response to frozen ground degradation in the source region of the Yellow River within the Budyko framework. *J. Hydrol.* **558**: 301–313, doi:10.1016/j.hydrol.2018.01.050.

Wheeler, M.C., Hendon, H.H. 2004. An all-season real-time multivariate MJO index: development of an index for monitoring and prediction. *Mon. Wea. Rev.* **132**: 1917–1932, doi:10.1175/1520-0493(2004)132<1917:aarmmi>2.0.co;2.

Wilks, D.S. 2011. *Statistical Methods in the Atmospheric Sciences*, 3rd ed.; Academic Press: Oxford; Waltham, MA, pp. 143–144; ISBN 978-0-12-385022-5.

Wu, B., Zhou, T., Li, T. 2017a. Atmospheric dynamic and thermodynamic processes driving the western North Pacific anomalous anticyclone during El Niño. Part I: Maintenance mechanisms. *J. Clim.* **30**: 9621–9635, doi:10.1175/JCLI-D-16-0489.1.

_____, _____, _____. 2017b. Atmospheric dynamic and thermodynamic processes driving the western North Pacific anomalous anticyclone during El Niño. Part II: Formation processes. *J. Clim.* **30**: 9637–9650, doi:10.1175/JCLI-D-16-0495.1.

Wu, C.C., Cheung, K.K., Lo, Y.Y. 2009. Numerical study of the rainfall event due to the interaction of Typhoon Babs (1998) and the northeasterly monsoon. *Mon. Wea. Rev.* **137**: 2049–2064, doi:10.1175/2009mwr2757.1.

Wu, L., Zhiping, W., Ronghui, H., Renguang, W. 2012. Possible linkage between the monsoon trough variability and the tropical cyclone activity over the western North Pacific. *Mon. Wea. Rev.* **140**: 140–150.doi:10.1175/MWR-D-11-00078.1.

Wu, M.C., Chang, W.L., Leung, W.M. 2004. Impacts of El Niño-Southern Oscillation events on tropical cyclone landfalling activity in the western North Pacific. *J. Clim.* **17**: 1419–1428, doi:10.1175/1520-0442(2004)017<1419:IOENOE>2.0.CO;2.

Wu, R. 2002. Processes for the northeastward advance of the summer monsoon over the western North Pacific. *J. Meteor. Soc. Jpn.* **80**: 67–83, doi:10.2151/jmsj.80.67.

_____, Wang, B. 2000. Inter-annual variability of the summer monsoon onset over the western North Pacific and the underlying processes. *J. Clim.* **13**: 2483–2501, doi:10.1175/1520-0442(2000)013<2483:IVOSMO>2.0.CO:2.

_____, _____. 2001. Multi-stage onset of the summer monsoon over the western North Pacific. *Clim. Dyn.* **17**: 277–289, doi:10.1007/s003820000118.

_____, Wen, Z., Yang, S., Li, Y. 2010. An interdecadal change in Southern China summer rainfall around 1992/1993. *J. Clim.* **23**: 2389–2403, doi:10.1175/2009JCLI3336.1.

Xiang, B., Wang, B. 2013. Mechanisms for the advanced Asian summer monsoon onset since the mid-to-late 1990s. *J. Clim.* **26**: 1993–2009, doi:10.1175/JCLI-D-12-00445.

_____, _____, Yu, W., Xu, S. 2013. How can anomalous western North Pacific subtropical high intensify in late summer. *Geophys. Res. Lett.* **40**: 2349–2354, doi:10.1002/grl.50431.

Xie, P., Arkin, P. 1997. Global precipitation: A 17-year monthly analysis based on gauge observations, satellite estimates, and numerical model outputs. *Bull. Amer. Meteor. Soc.* **78**: 2539–2558, doi:10.1175/1520-0477(1997)078<2539:GPAYMA>
2.0.CO;2.

Xu, K., Lu, R. 2018. Decadal change of the western North Pacific summer monsoon break around 2002/2003. *J. Clim.* **31**: 177–193, doi:10.1175/JCLI-D-16-0739.1.

Xu, S., Wang, B. 2014. Enhanced western North Pacific tropical cyclone activity in May in recent years. *Clim. Dyn.* **42**: 2555–2563, doi:10.1007/s00382-013-1921-7.

Yamaura, T., Kajikawa, Y. 2016. Decadal change in the boreal summer intraseasonal oscillation. *Clim. Dyn.* **45**: 3003–3014, doi:10.1007/s00382-016-3247-8.

Yanai, M., Li, C., Song, Z. 1992. Seasonal heating of the Tibetan Plateau and its effects on the evolution of the Asian summer monsoon. *J. Meteor. Soc. Jpn.* **70**: 319–351, doi:10.2151/jmsj1965.70.1B_319.

Yang, L., Du, Y., Wang, C., Wang, X. 2015. Impact of intraseasonal oscillation on the tropical cyclone track in the South China Sea. *Clim. Dyn.* **44**: 1505–1519, doi:10.1007/s00382-014-2180-y.

Yeh, C.F., Wang, J., Yeh, H.F., Lee, C.H. 2015. Spatial and temporal streamflow trends in northern Taiwan. *Water* **7**:634–651, doi:10.3390/w7020634.

Yin, Y., Liu, H., Yi, H., Liu, W. 2015. Spatiotemporal variation and abrupt change analysis of temperature from 1960 to 2012 in the Huang-Huai-Hai Plain, China. *Adv. Meteor.* **2015**: 1–11, doi:10.1155/2015/643493.

Yokoi, S., Matsumoto, J. 2008. Collaborative effects of cold surge and tropical depression-type disturbance on heavy rainfall in central Vietnam. *Mon. Wea. Rev.* **136**: 3275–3287, doi:10.1175/2008mwr2456.1.

Yuan, F., Chen, W. 2013. Roles of the tropical convective activities over different regions in the earlier onset of the South China Sea summer monsoon after 1993. *Theor. Appl. Climatol.* **13**: 175–185, doi:10.1007/s00704-012-0776-x.

Yumul, G.P., Cruz, N.A., Servando, N.T., Dimalanta, C.B. 2011. Extreme weather events and related disasters in the Philippines, 2004-08: a sign of what climate change will mean? *Disasters* **35**: 362–382, doi:10.1111/j.1467-7717.2010.01216.x.

_____, Dimalanta, C.B., Servando, N.T., Cruz, N.A. 2013. Abnormal weather events in 2009, increased precipitation and disastrous impacts in the Philippines. *Climatic Change* **118**: 715–727, doi:10.1007/s10584-012-0661-8.

Yun, K.S., Seo, K.H., Ha, K.J. 2010. Interdecadal change in the relationship between the ENSO and the intraseasonal oscillation in East Asia. *J. Clim.* **23**: 3599–3612, doi:10.1175/2010JCLI3431.1.

Zhang, L., Karnauskas, K.B. 2017. The role of tropical interbasin SST gradients in forcing Walker circulation trends. *J. Clim.* **30**: 499–508, doi:10.1175/JCLI-D-16-0349.1.

Zhang, W., Graf, H.F., Leung, Y., Herzog, M. 2012. Different El Niño types and tropical cyclone landfall in East Asia. *J. Clim.* **25**: 6510–6523, doi:10.1175/JCLI-D-11-00488.1.

Zhang, Z., Chan, J.C.L., Ding, Y. 2004. Characteristics, evolution, and mechanisms of the summer monsoon onset over Southeast Asia. *Int. J. Climatol.* **24**: 1461–1482, doi:10.1002/joc.1082.

Zhou, B., Cui, X. 2008. Hadley circulation signal in the tropical cyclone frequency over the western North Pacific. *J. Geophys. Res. Atmos.* **113**: D16, doi:10.1029/2007JD009156.

Zhou, L.T., Wu, R. 2015. Interdecadal variability of winter precipitation in northwest China and its association with the north Atlantic SST change. *Int. J. Climatol.* **35**: 1172–1179, doi:10.1002/joc.4047.

Zhu, Y., Wang, H., Zhou, W., Ma, J. 2011. Recent changes in the summer precipitation pattern in East Asia and the background circulation. *Clim. Dyn.* **36**: 1463–1473, doi:10.1007/s00382-010-0852-9.

FIGURES

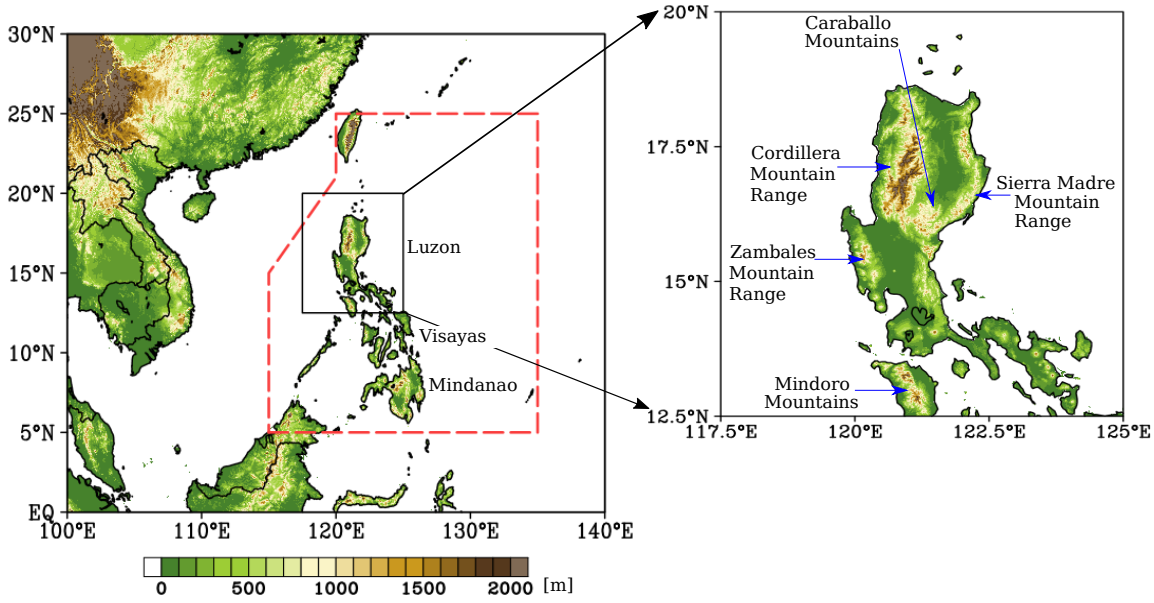

Figure 1.1. The Philippines and its topography (m) from the Global 30-Arc-Second elevation data set (GTOPO30). The dashed red lines demarcate the Philippine Area of Responsibility (PAR). The figure on the right shows the enlarged map of Luzon Island and its major mountain ranges.

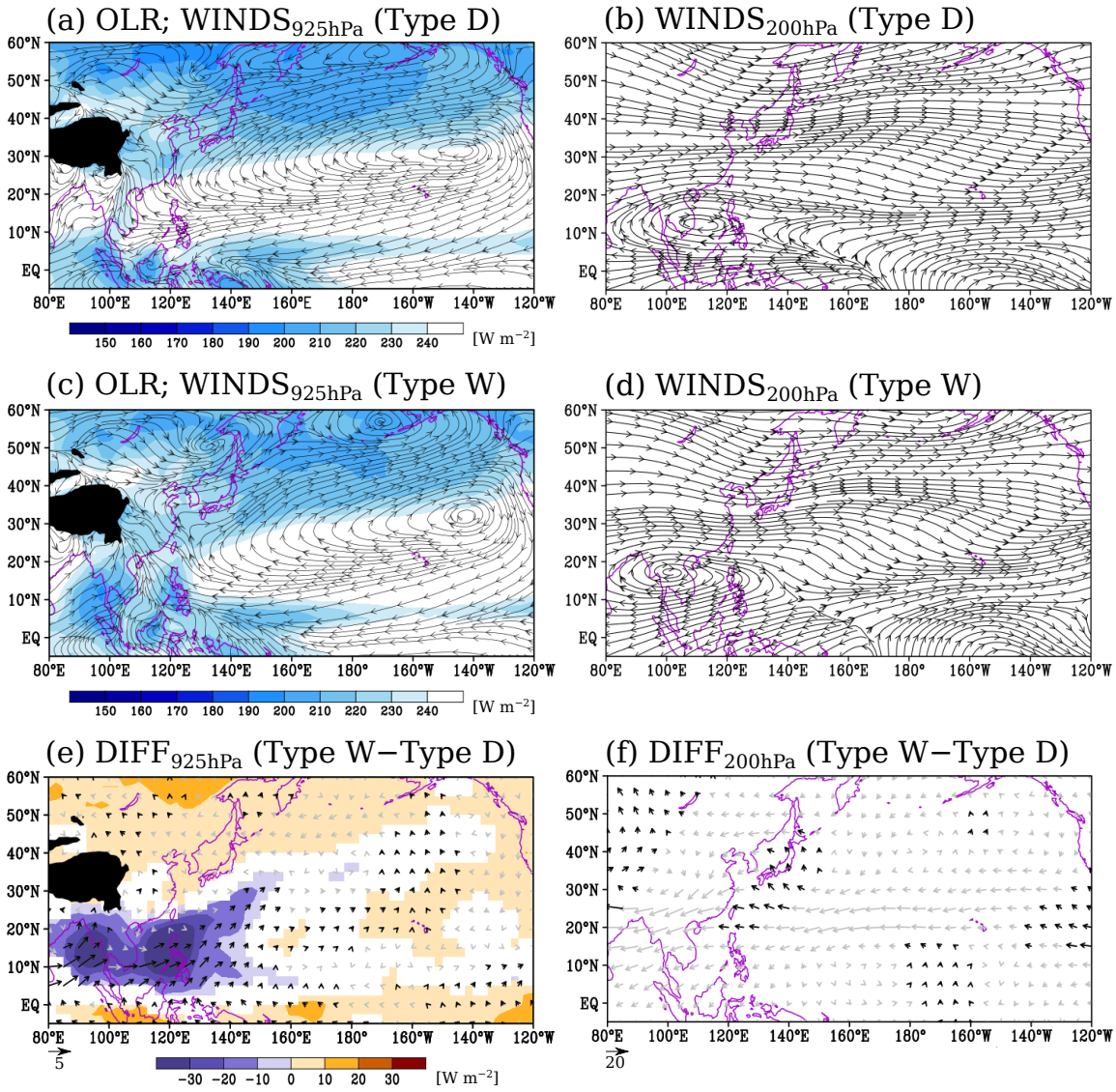

Figure 2.1. Spatial distribution of Outgoing Longwave Radiation (*OLR*; shades; W m^{-2}) and winds at 925 hPa (*WINDS$_{925hPa}$*) and 200 hPa (*WINDS$_{200hPa}$*) (streams; m s^{-1}) for: Type D (a, b); Type W (c, d); and their difference (e, f). Shaded areas in (e) and bold vectors in (e) and (f) indicate significant differences at the 95 % confidence level by Student's *t*-test. The scale of the vectors in (e) and (f) are 5 and 20 m s^{-1}, respectively.

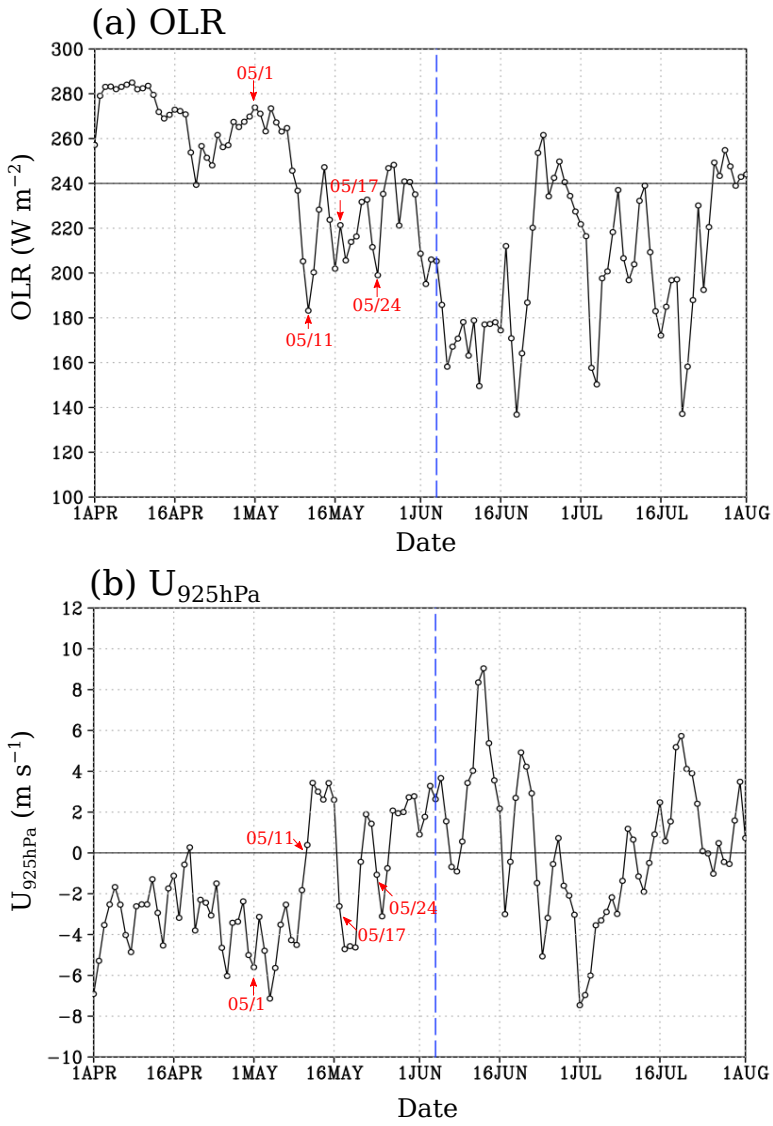

Figure 2.2. Times series of area-averaged: (a) Outgoing Longwave Radiation (*OLR*; W m^{-2}); and (b) zonal wind at 925 hPa (U_{925hPa}; m s^{-1}) over Luzon Island (120–122.5°E and 12.5–22°N) for the year 1981. The dashed blue vertical line indicates the onset of the summer monsoon on June 4, defined by the Philippine Atmospheric, Geophysical and Astronomical Services Administration (PAGASA). The four dates (month/day) shown in red fonts denote the four case studies discussed in Section 2.3.

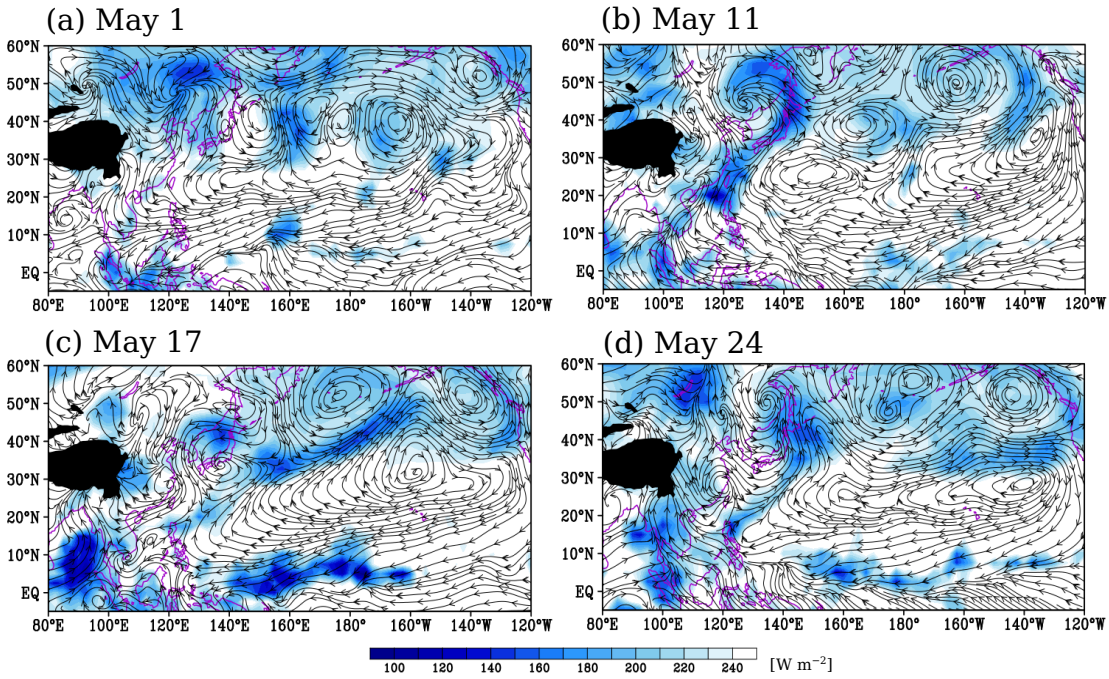

Figure 2.3. Spatial distribution of Outgoing Longwave Radiation (*OLR*; shades; W m^{-2}) and winds at 925 hPa (streams; m s^{-1}) for: (a) May 1; (b) May 11; (c) May 17; and (d) May 24 in the year 1981.

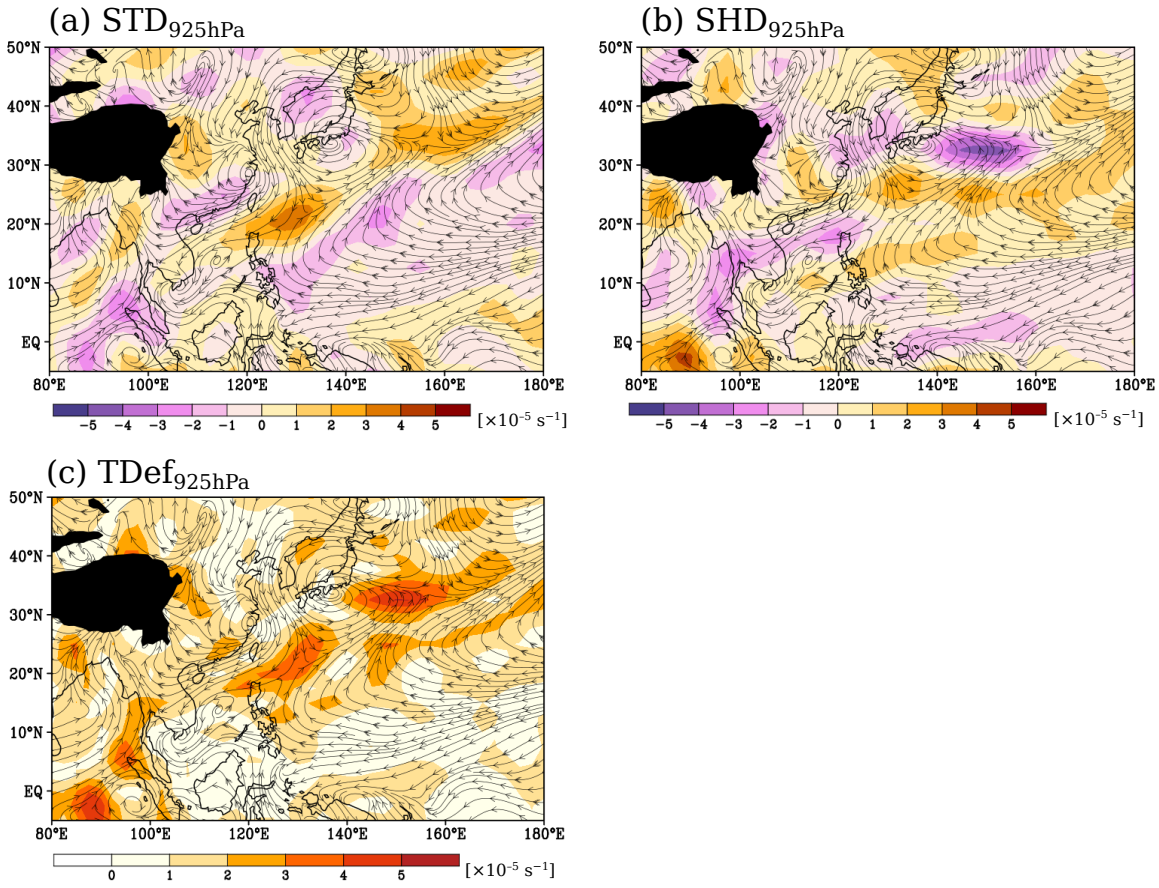

Figure 2.4. Spatial distribution of the: (a) stretching deformation (STD_{925hPa}; shades; $\times 10^{-5}$ s^{-1}); (b) shearing deformation (SHD_{925hPa}; $\times 10^{-5}$ s^{-1}); and (c) total deformation ($TDef_{925hPa}$; $\times 10^{-5}$ s^{-1}) superimposed with the winds at 925 hPa (streams; m s^{-1}) on May 17, 1981.

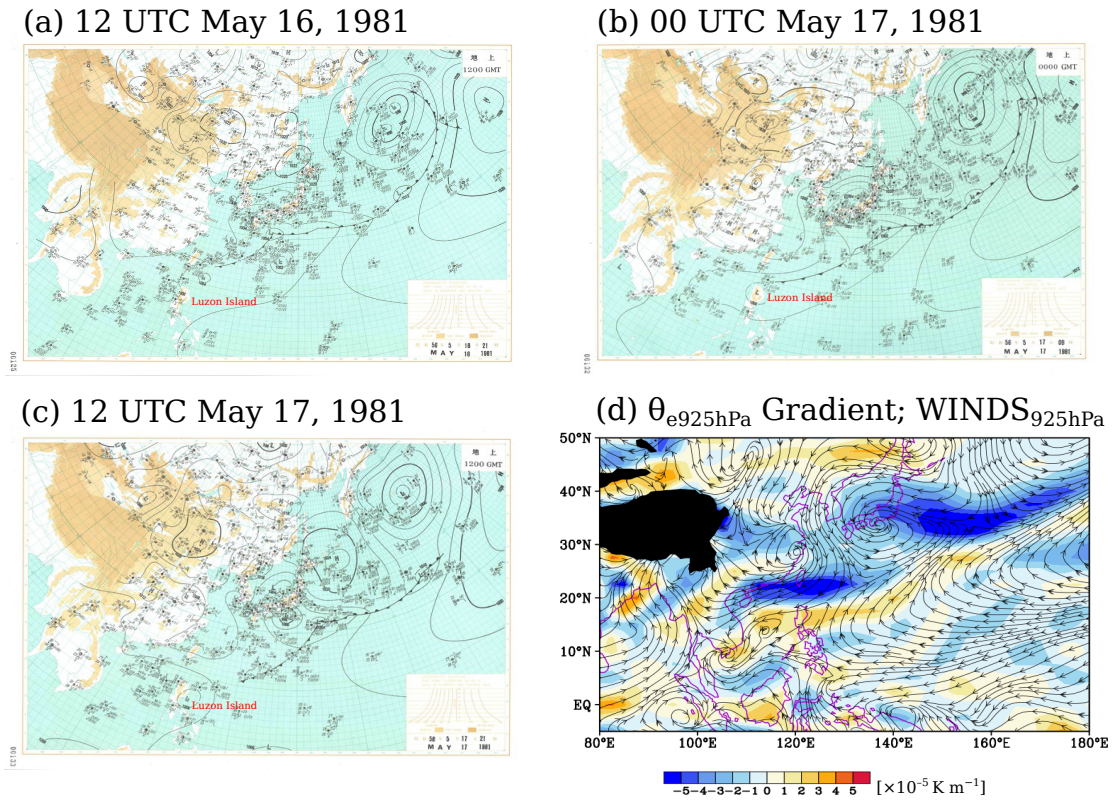

Figure 2.5. Surface weather charts from the Japan Meteorological Agency on: (a) 12 UTC May 16, 1981; (b) 00 UTC May 17, 1981; and (c) 12 UTC May 17, 1981. (d) Averaged daily meridional equivalent potential temperature gradient at 925 hPa (θe_{925hPa}; shades; $\times 10^{-5}$ K m^{-1}) and winds at 925 hPa ($WINDS_{925hPa}$; streams; m s^{-1}).

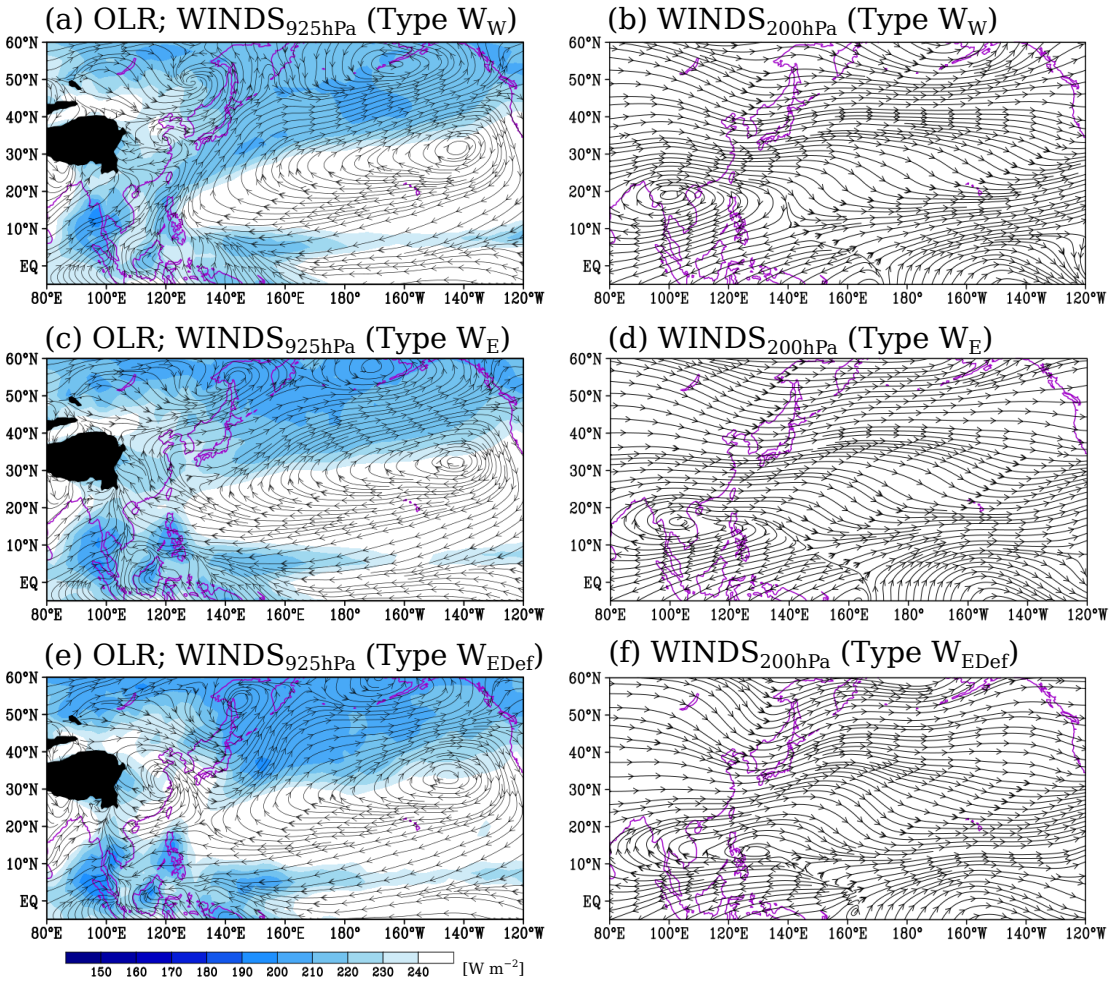

Figure 2.6. Spatial distribution of Outgoing Longwave Radiation (*OLR*; shades; W m^{-2}) and winds at 925 hPa (*WINDS$_{925hPa}$*) and 200 hPa (*WINDS$_{200hPa}$*) (streams; m s^{-1}) for: Type W$_W$ (a, b); Type W$_E$ (c, d); and Type W$_{ED}$ (e, f).

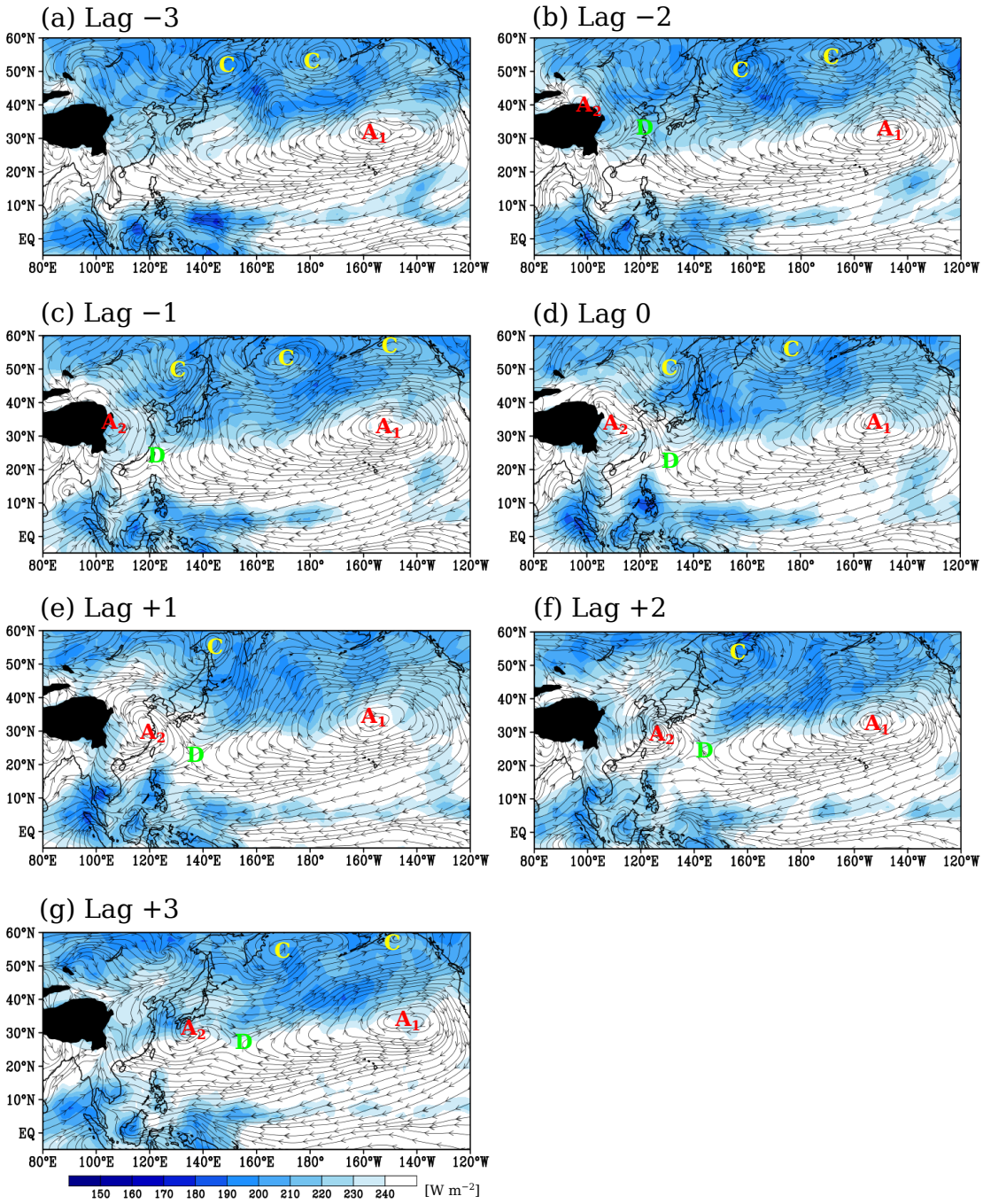

Figure 2.7. Composites of Outgoing Longwave Radiation (*OLR*; shades; W m^{-2}) and winds at 925 hPa (streams; m s^{-1}) for: (a) Lag –3; (b) Lag –2; (c) Lag –1; (d) Lag 0; (e) Lag +1; (f) Lag +2; and (g) Lag +3. The cyclonic and anticyclonic circulations, and deformation zone are denoted as "C", "A", and "D", respectively.

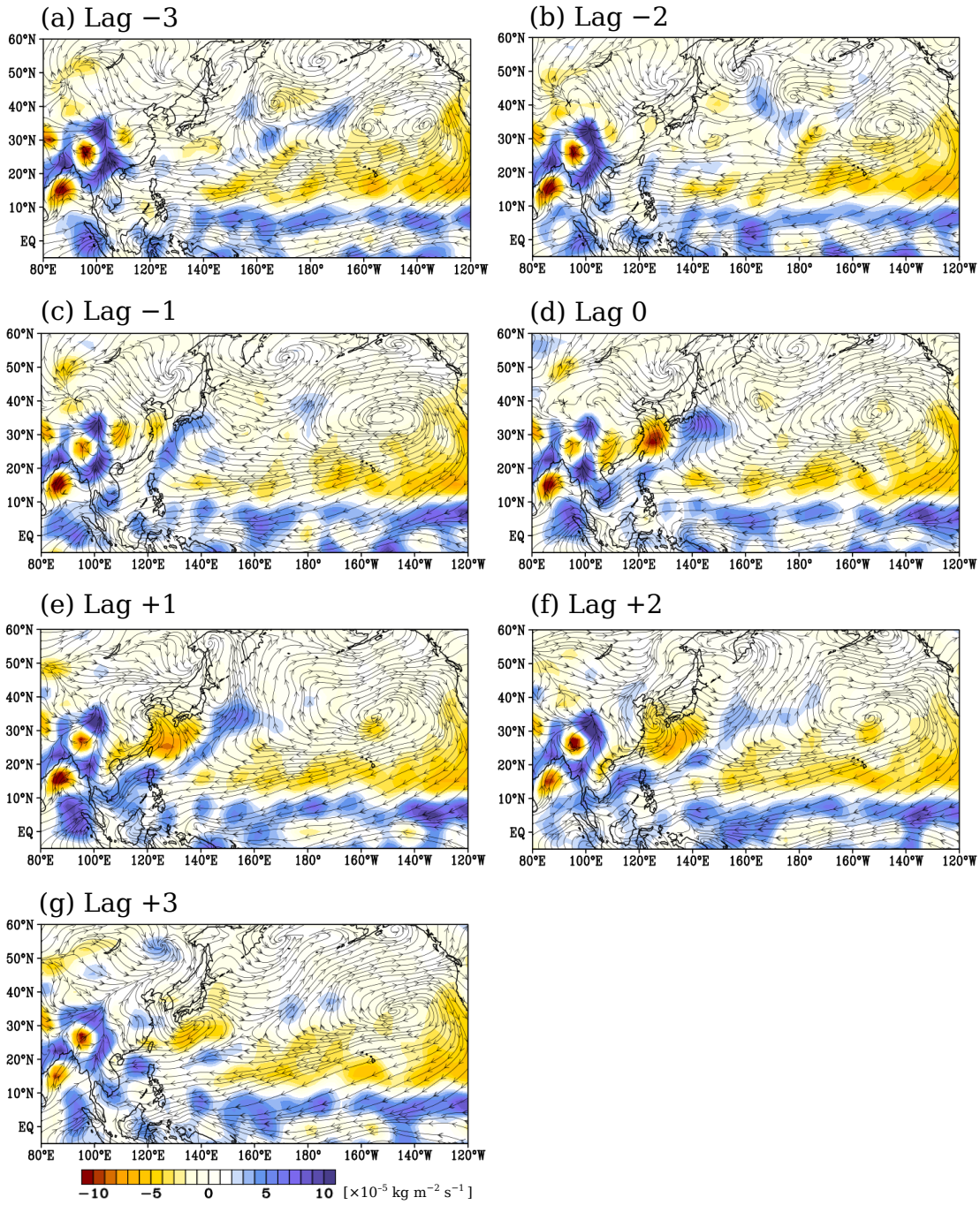

Figure 2.8. As in Fig.2.7 but for the vertically integrated moisture flux (streams; $\times 10^{-4}$ kg m^{-1} s^{-1}) and its convergence (shades; $\times 10^{-4}$ kg m^{-2} s^{-1}).

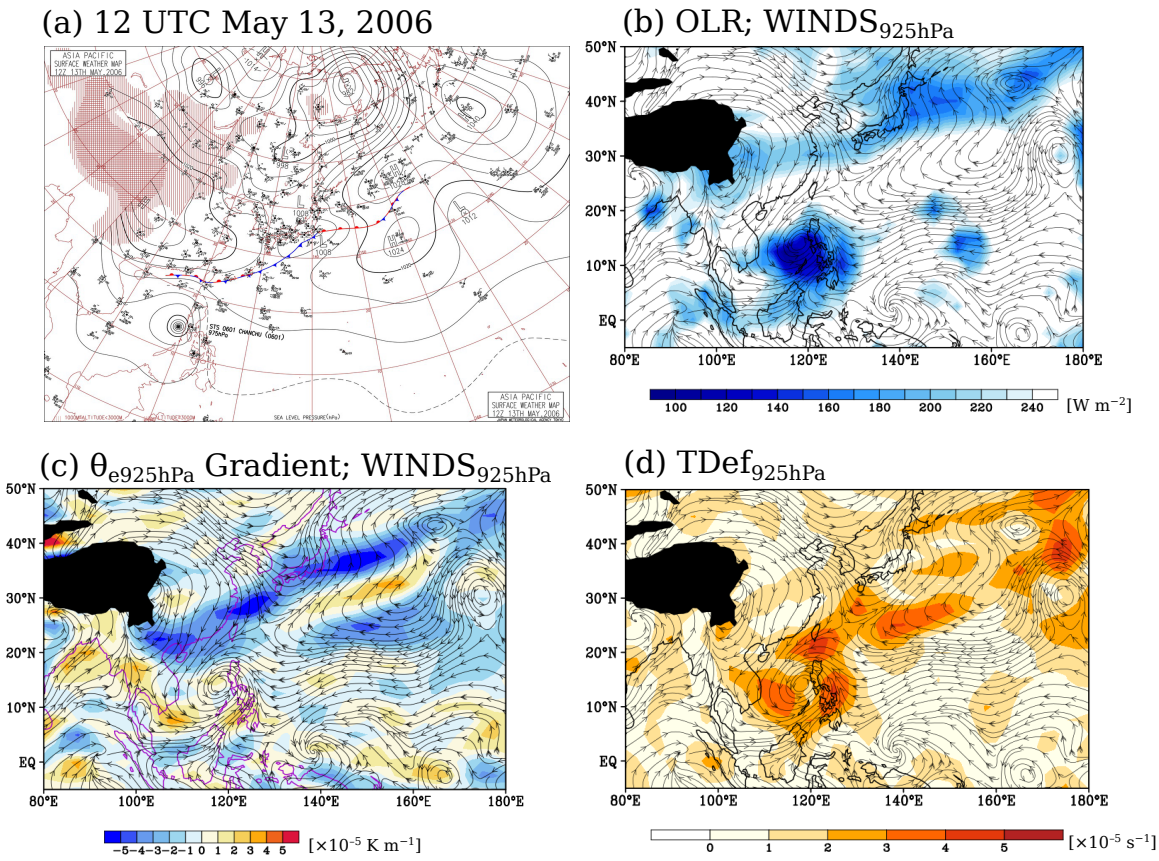

Figure 2.9. Surface weather chart from the Japan Meteorological Agency on 12 UTC May 13, 2006. (b) As in (a) but for the daily averaged Outgoing Longwave Radiation (*OLR*; shades; W m^{-2}) and winds at 925 hPa (*WINDS*$_{925hPa}$; streams; m s^{-1}). (c) As in (b) but for the meridional equivalent potential temperature gradient at 925 hPa (θe_{925hPa}; shades; $\times 10^{-5}$ K m^{-1}). (d) As in (b) but for the total deformation at 925 hPa (*TDef*$_{925hPa}$; shades; $\times 10^{-5}$ s^{-1}).

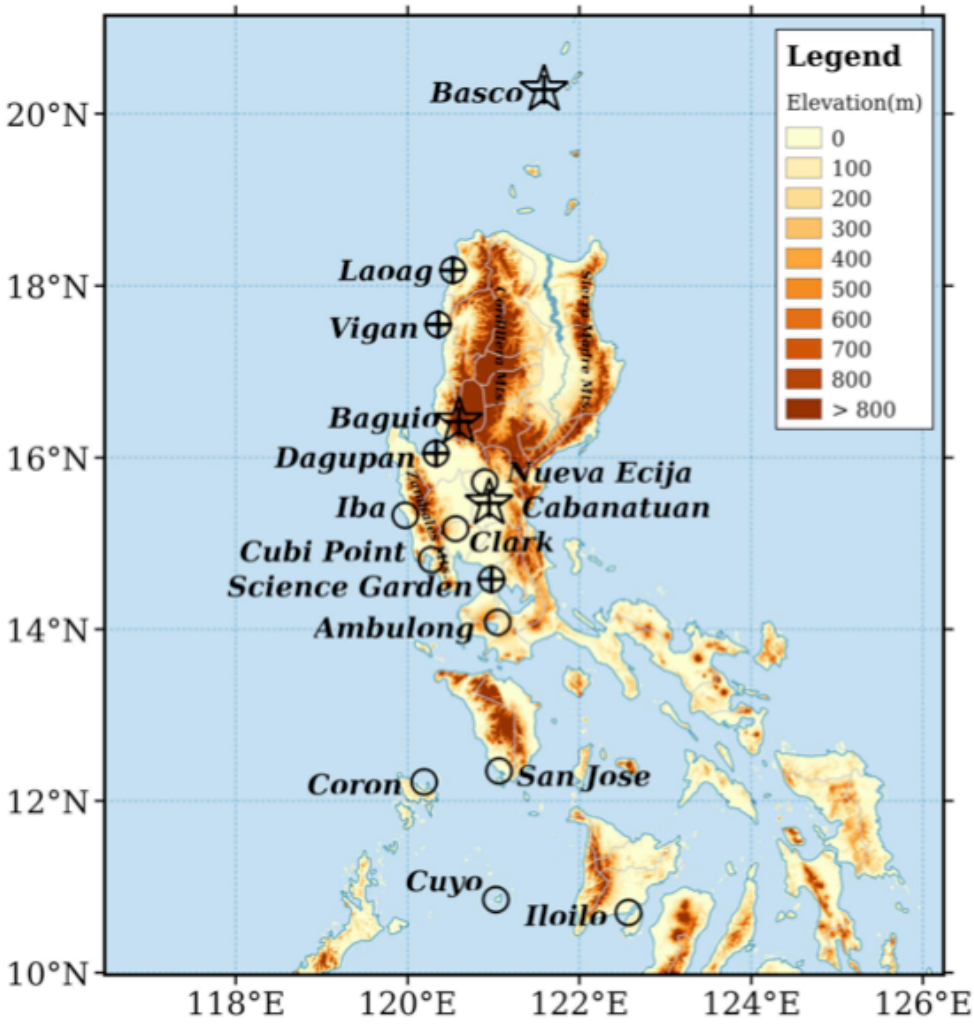

Figure 3.1. Location of the 16 meteorological stations from the Philippine Atmospheric, Geophysical and Astronomical Services Administration (PAGASA) and the topography of the Philippines. The open circles are the stations used by PAGASA in their operational onset, while the stars are the three additional stations used for discussion in this study. The black crosses indicate the seven stations used for the monsoon break detection.

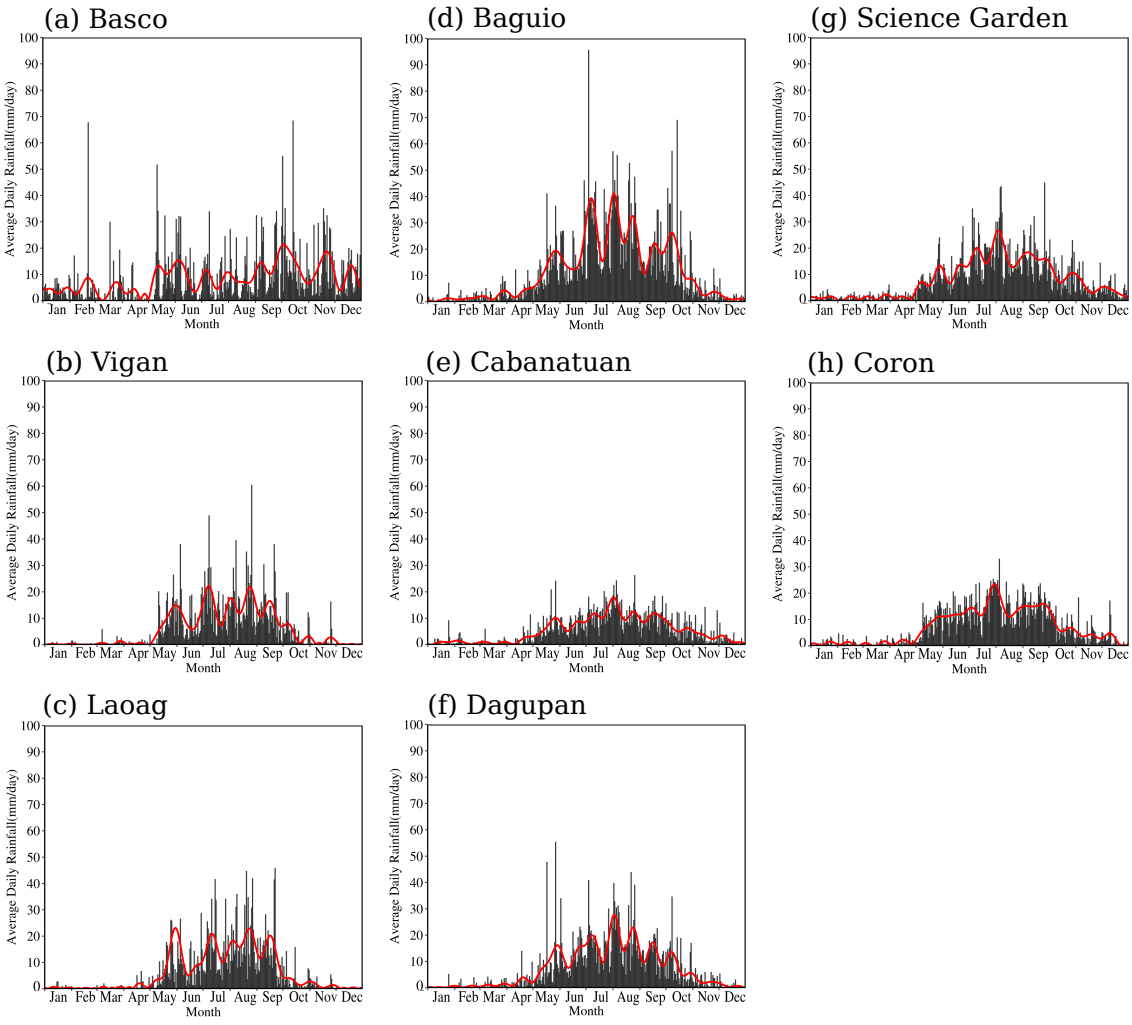

Figure 3.2. Annual variations of daily rainfall climatology (1998–2012) for: (a) Basco; (b) Vigan; (c) Laoag; (d) Baguio; (e) Cabanatuan; (f) Dagupan; (g) Science Garden; and (h) Coron. The red solid line represents the smoothed curve obtained by adding the first 18 Fourier harmonics of the daily rainfall time series.

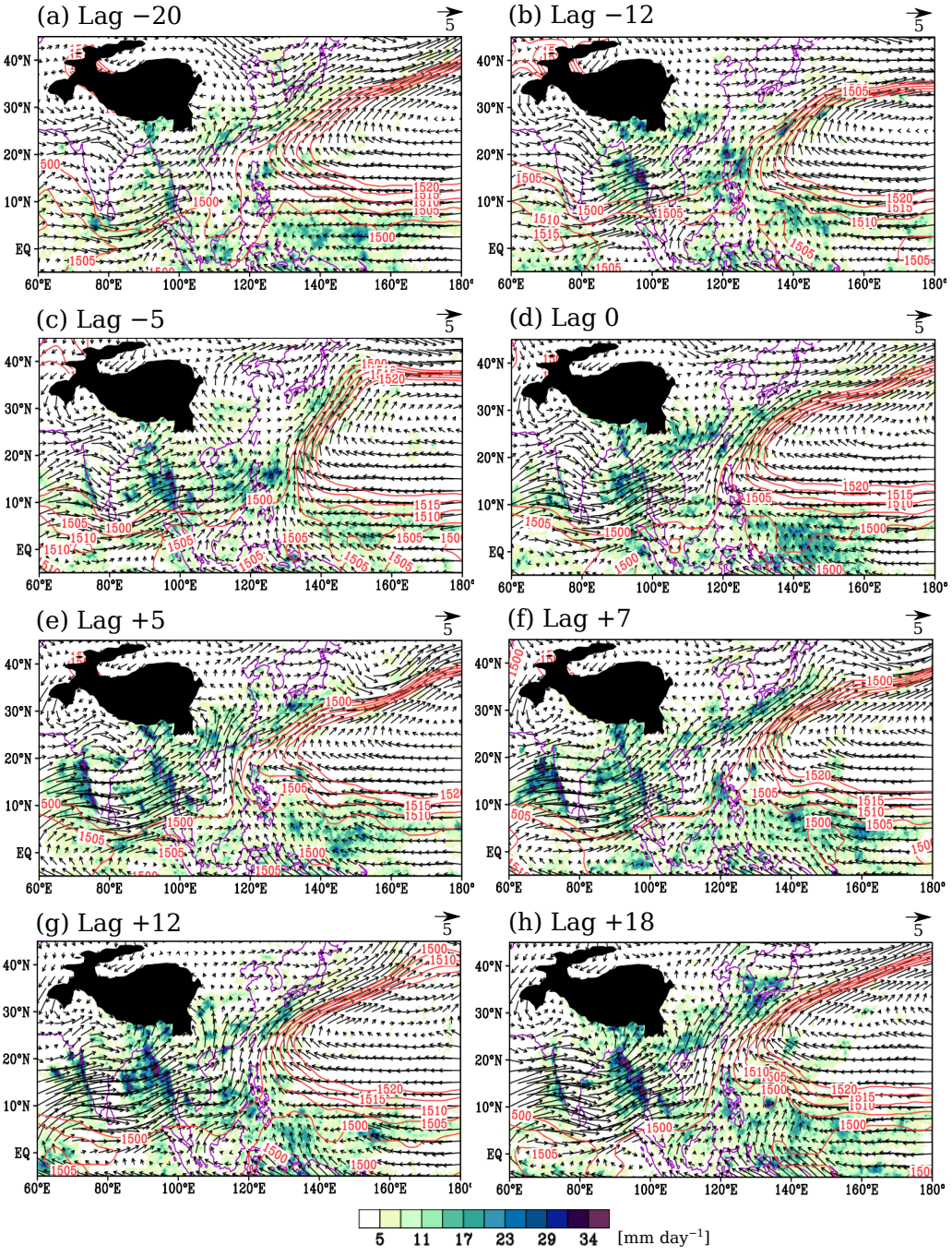

Figure 3.3. Spatial distribution of the lag composites of TRMM rainfall (mm day^{-1}; shaded), 850 hPa *HGT* (HGT_{850hPa}; m; contours), and 850 hPa winds ($WINDS_{850hPa}$; m s^{-1}; vectors) for: (a) Lag –20; (b) Lag –12; (c) Lag –5; (d) Lag 0; (e) Lag +5; (f) Lag +7; (g) Lag +12; and (h) Lag +18. The scale of the wind vectors is 5 m s^{-1}. The contour interval of the HGT_{850hPa} is 5 m between 1, 500 and 1, 520 m.

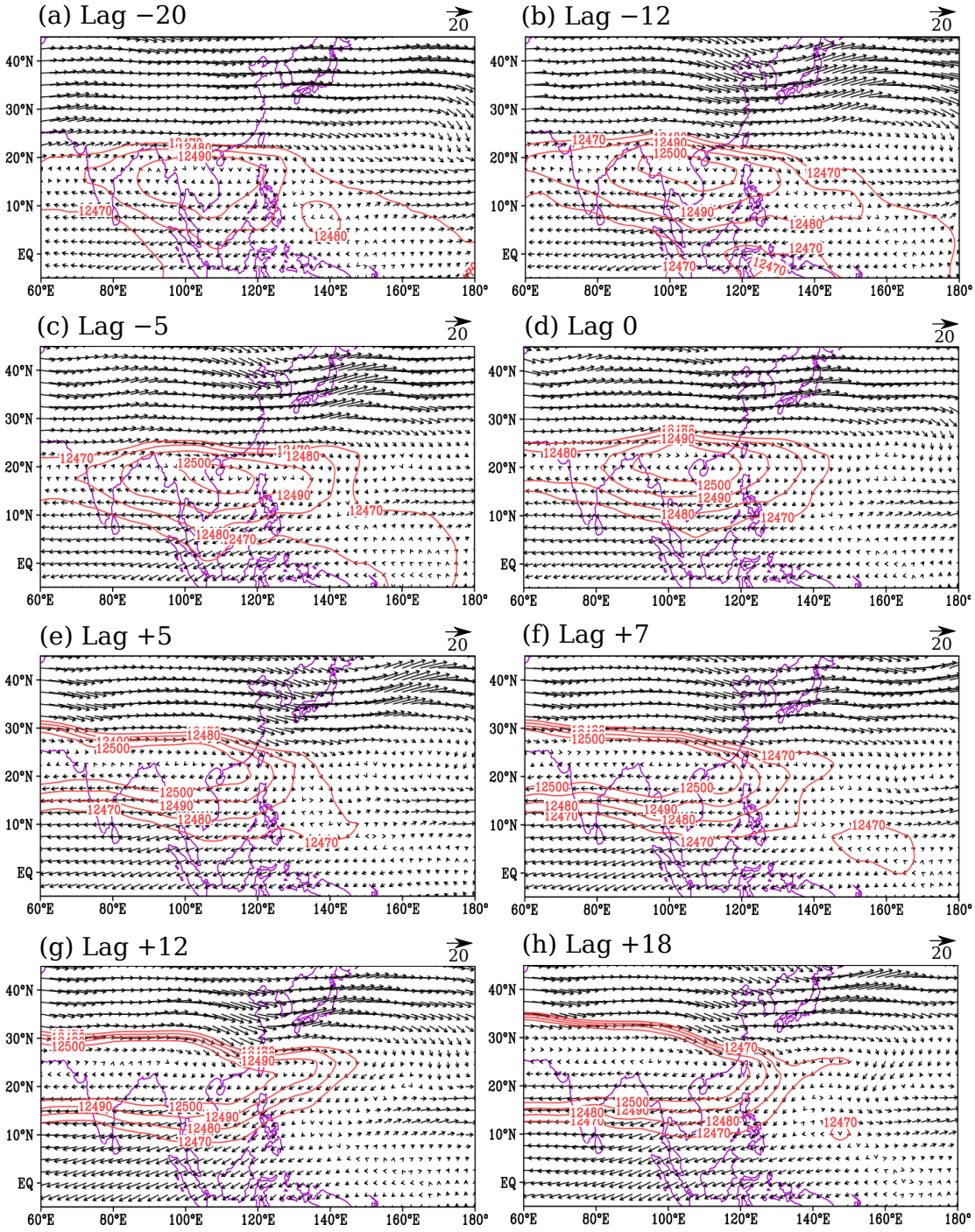

Figure 3.4. As in Fig. 3.3 but for the 200 hPa winds (*WINDS*$_{200hPa}$; vectors; m s^{-1}) and 200 hPa geopotential height (*HGT*$_{200hPa}$) only. The scale of the wind vectors is 20 m s^{-1}. The contour interval of the *HGT*$_{200hPa}$ is 10 m, between 12, 470 and 12, 500 m.

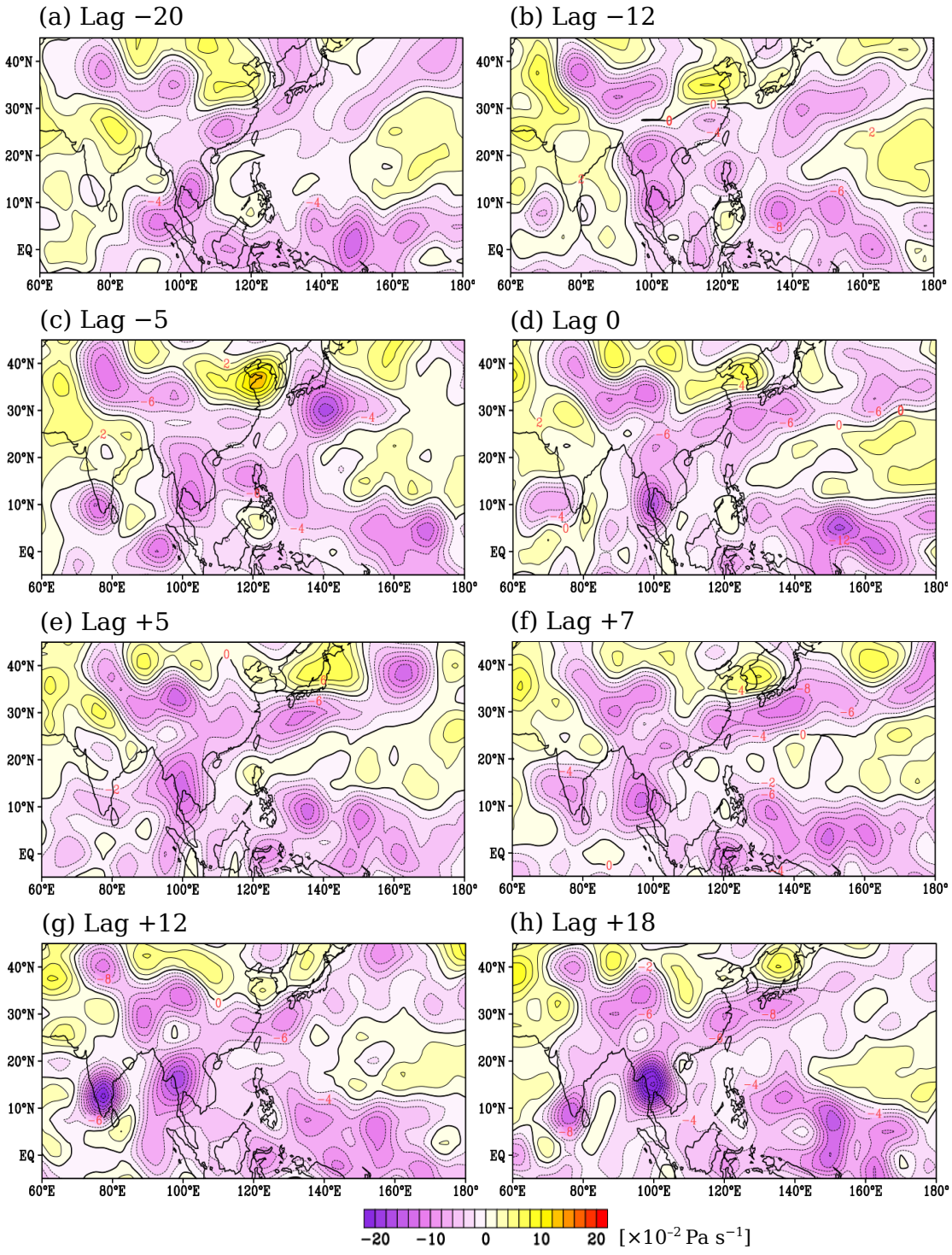

Figure 3.5. As in Fig. 3.3 but for the 500 hPa vertical velocity ($\times 10^{-2}$ Pa s^{-1}). The contour interval is 2×10^{-2} Pa s^{-1}.

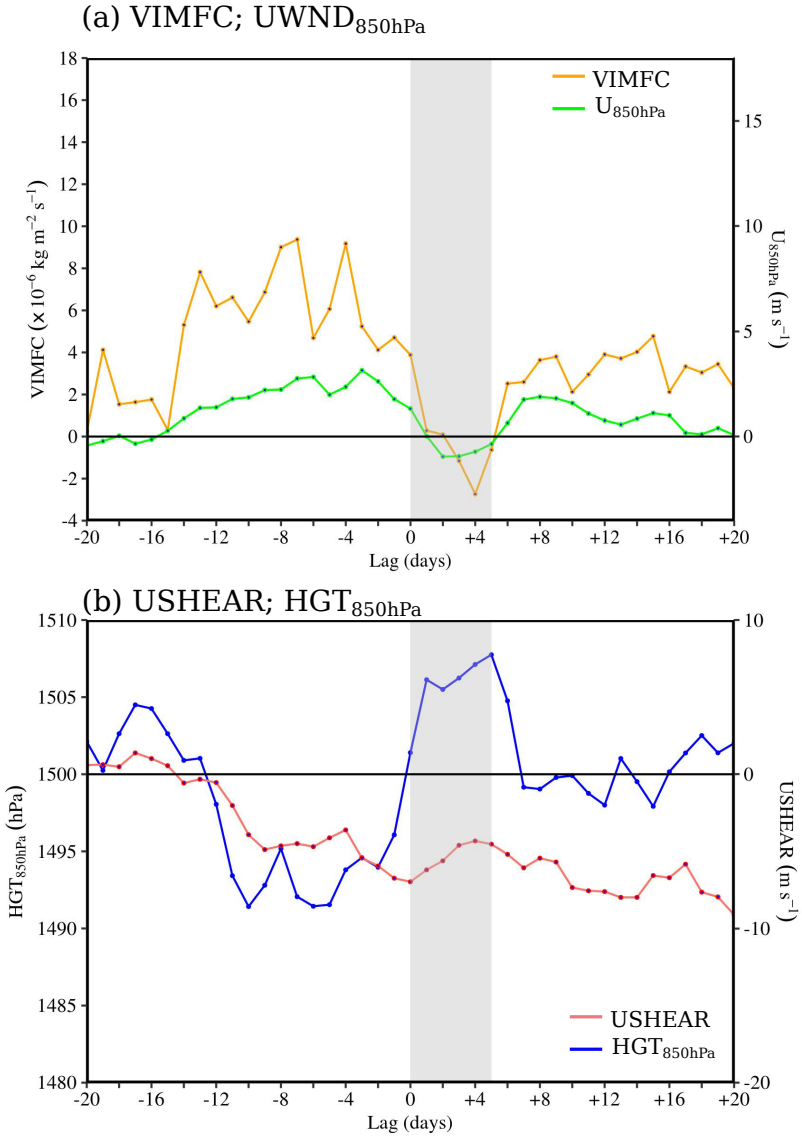

Figure 3.6. Time series of: (a) vertically integrated moisture flux convergence (*VIMFC*; orange line; $\times 10^{-6}$ kg m^{-2} s^{-1}) and zonal wind at 850 hPa (U_{850hPa}; green line; m s^{-1}) over Luzon Island (120–122.5°E., 12.5–22°N). (b) As in (a) but for the geopotential height (HGT_{850hPa}; blue lines; m) and vertical zonal wind shear (*USHEAR*; U_{200hPa} minus U_{850hPa}; red line; m s^{-1}). The solid horizontal line in (a) indicates the 0 *VIMFC* and U_{850hPa}. The solid horizontal line in (b) indicates the 1, 500-m HGT_{850hPa} and 0 *USHEAR*. Shaded lag days indicate the monsoon break period.

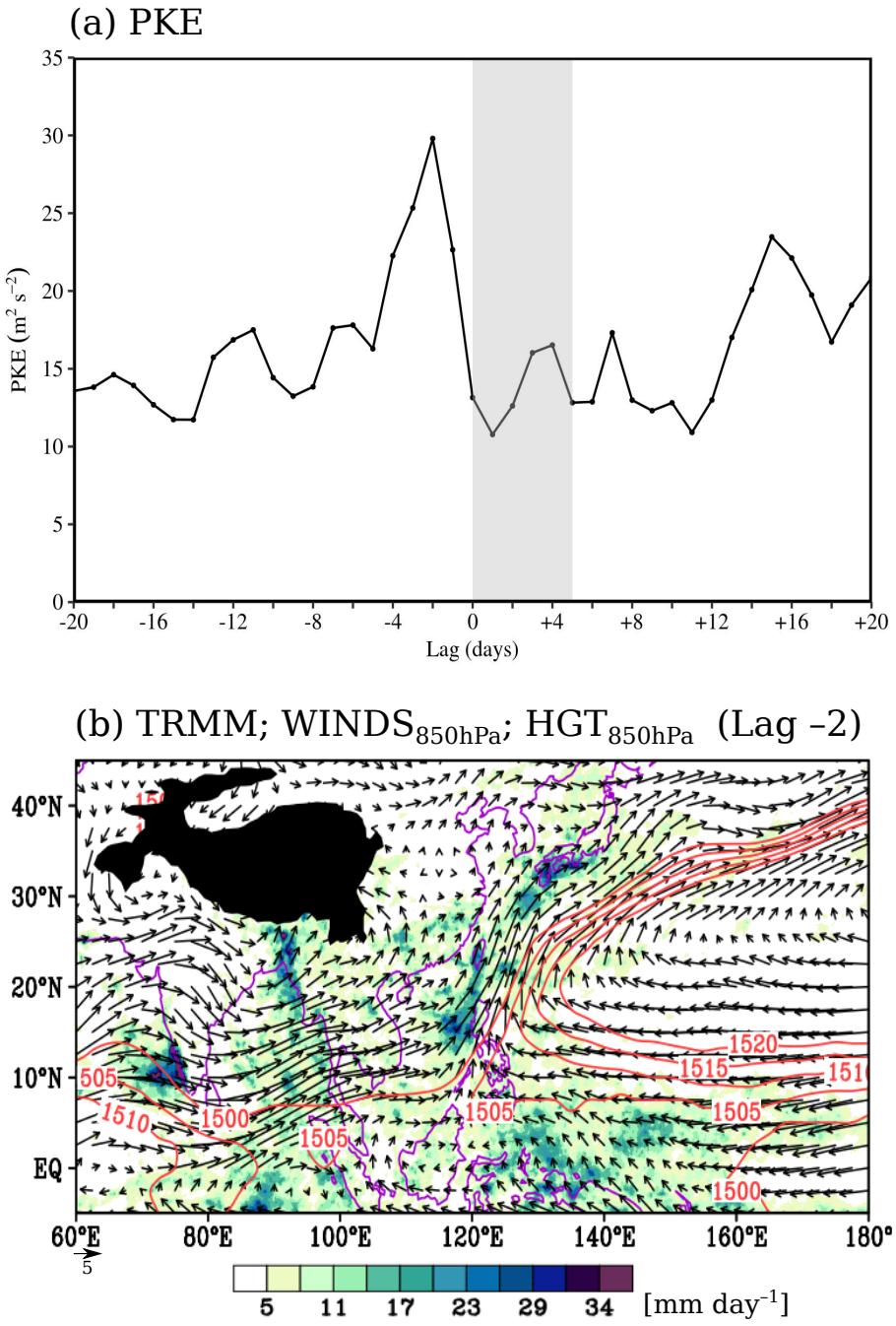

Figure 3.7. (a) As in Fig. 3.6a but for the perturbation kinetic energy (*PKE*; m^2 s^{-2}) only. (b) As in Fig.3.3 but for Lag –2 only.

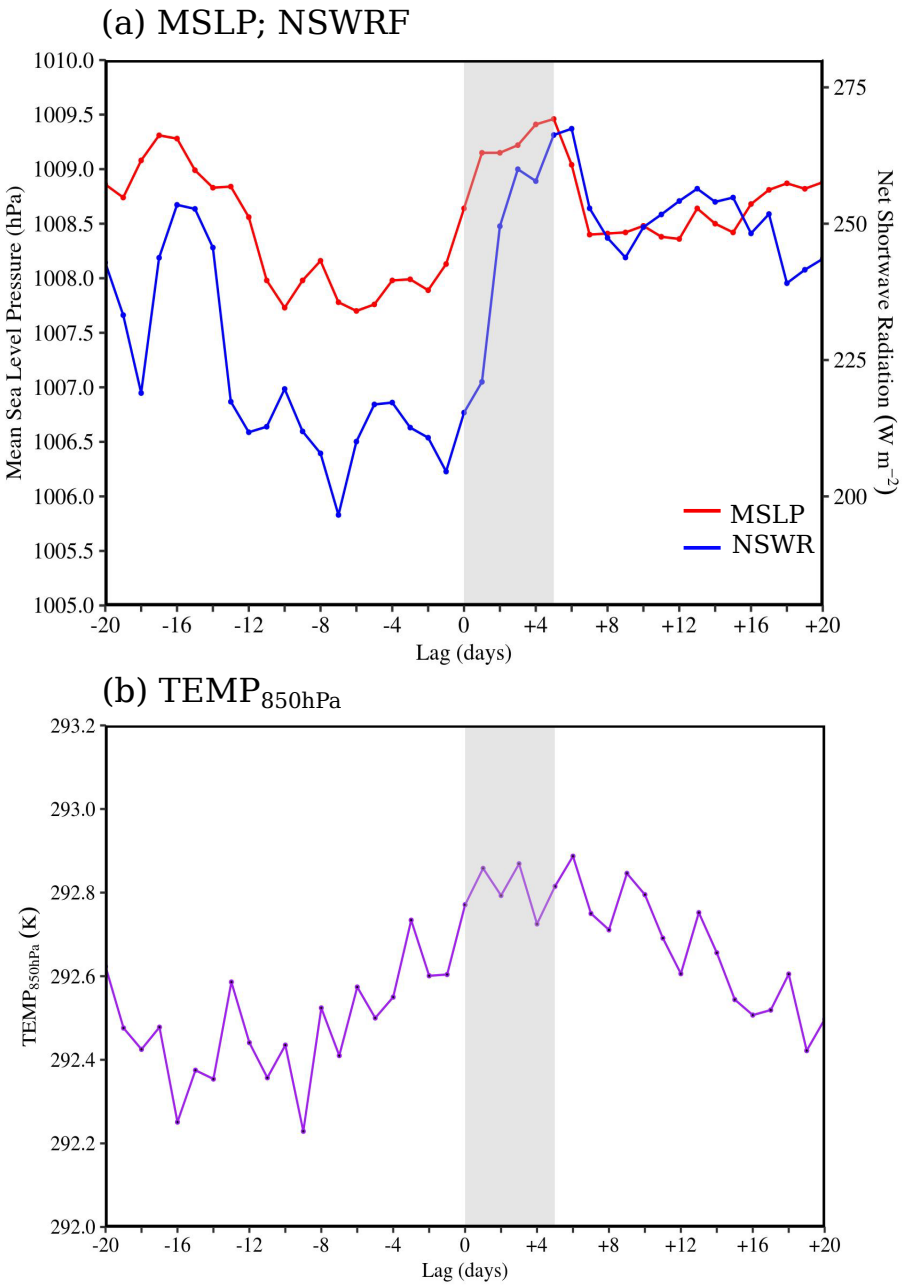

Figure 3.8. (a) Time series of mean sea level pressure (*MSLP*; hPa; red line) and net shortwave radiation (*NSWR*; W m^{-2}; blue line) over Luzon Island (120–122.5°E, 12.5–22°N). (b) As in (a) but for the temperature at 850 hPa only (*TEMP$_{850hPa}$*; K). Shaded lag days indicate the monsoon break period.

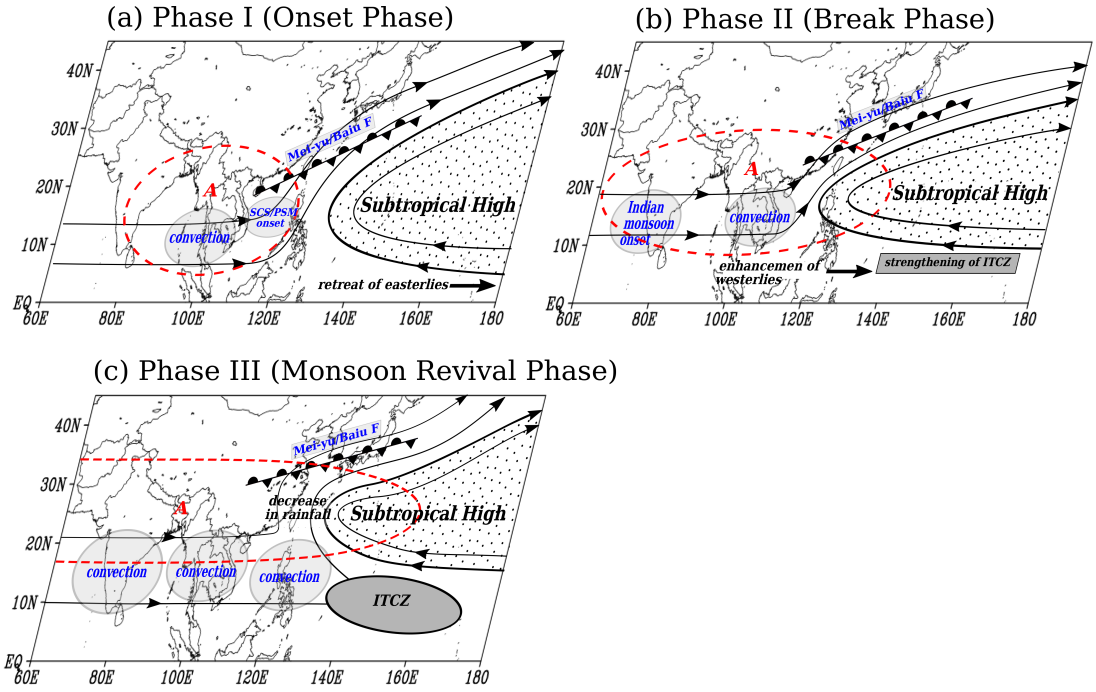

Figure 3.9. Schematic diagram illustrating the three-phase onset process of the summer monsoon over the Philippines: (a) Phase I (Onset Phase; mid to late May); (b) Phase II (Break Phase; early June); and (c) Phase III (Monsoon Revival Phase; mid-June). Phases I, II, and III correspond to the periods before and during Lag –12, Lag 0 to Lag +5, after Lag +5, in Figs. 3.3, 3.4, and 3.5, respectively. Stippled areas correspond to dry areas. The red broken line and "A" indicates the location of the anticyclonic circulation at 200 hPa.

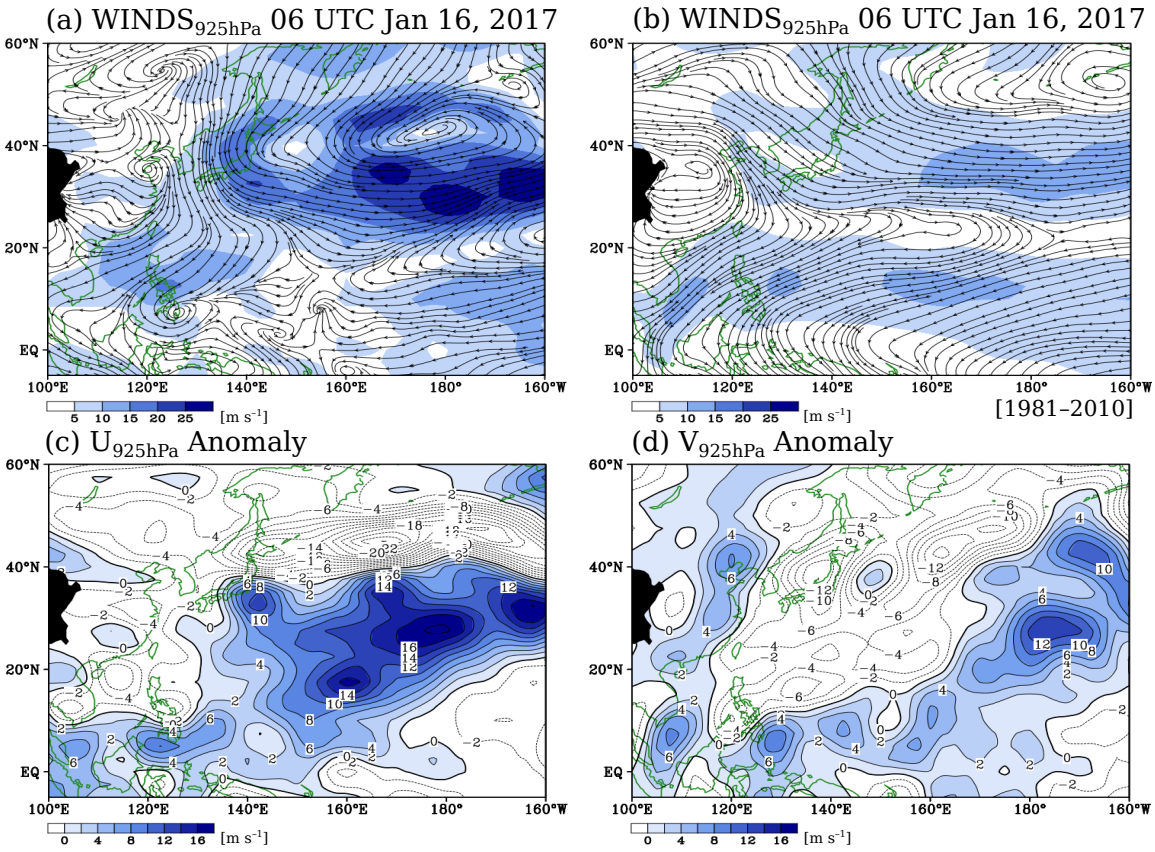

Figure 4.1. Horizontal winds at 925 hPa (*WINDS*$_{925hPa}$; shades and contours; m s^{-1}) on: (a) 06 UTC January 16, 2017; and (b) its corresponding climatology (06 UTC January 16; 1981–2010). Anomalies of the 925 hPa: (c) zonal (*U*$_{925hPa}$; shades and contours; m s^{-1}); and (d) meridional (*V*$_{925hPa}$; shades and contours; m s^{-1}) winds. Shadings in (a) and (b) indicate the magnitude of the *WINDS*$_{925hPa}$. The contour interval in (c) and (d) is 2 m s^{-1}.

(a) 06 UTC Jan 15, 2017

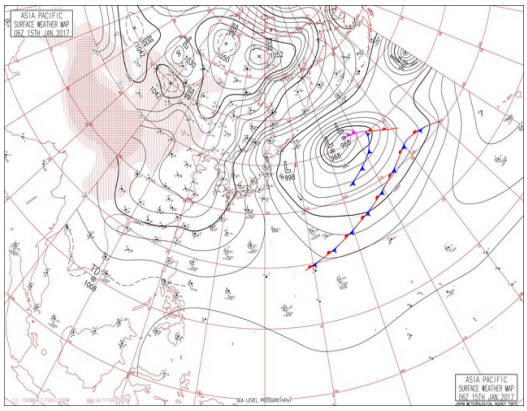

(b) 12 UTC Jan 15, 2017

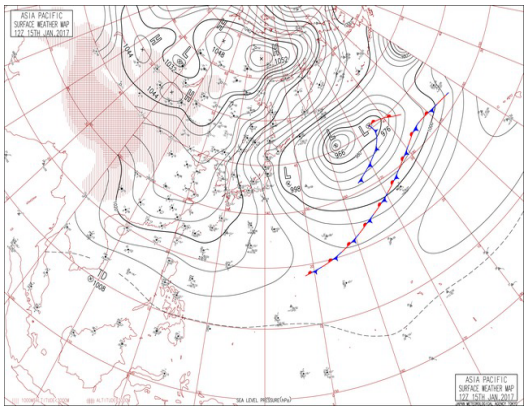

(c) 18 UTC Jan 15, 2017

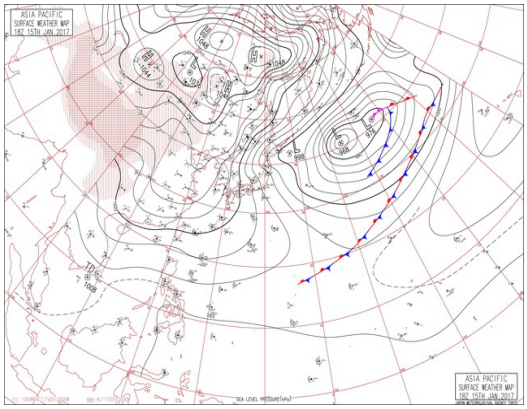

(d) 00 UTC Jan 16, 2017

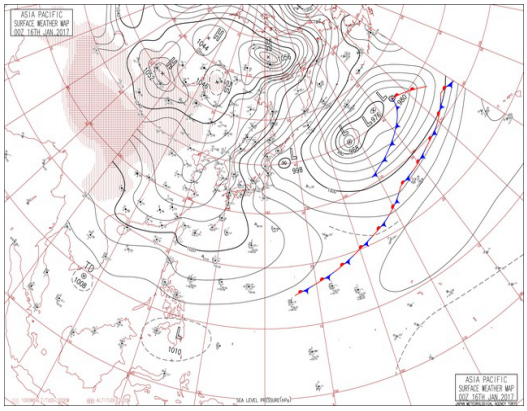

(e) 06 UTC Jan 16, 2017

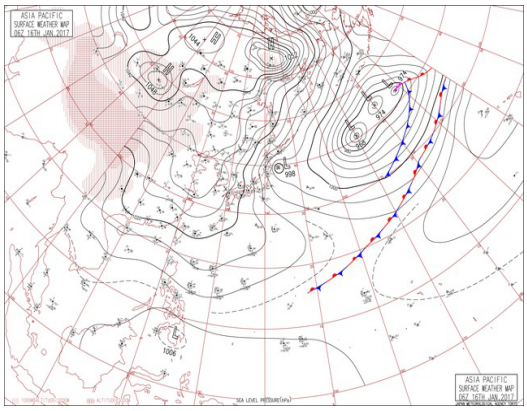

(f) 12 UTC Jan 16, 2017

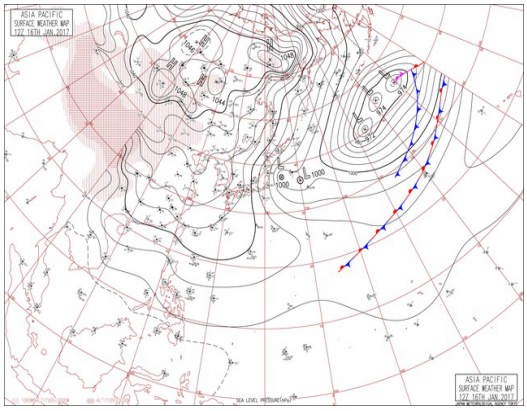

Figure 4.2. Surface weather charts provided by the Japan Meteorological Agency for: (a) 06 UTC January 15, 2017; (b) 12 UTC January 15, 2017; (c) 18 UTC January 15, 2017; (d) 00 UTC January 16, 2017; (e) 06 UTC January 16, 2017; and (f) 12 UTC January 16, 2017.

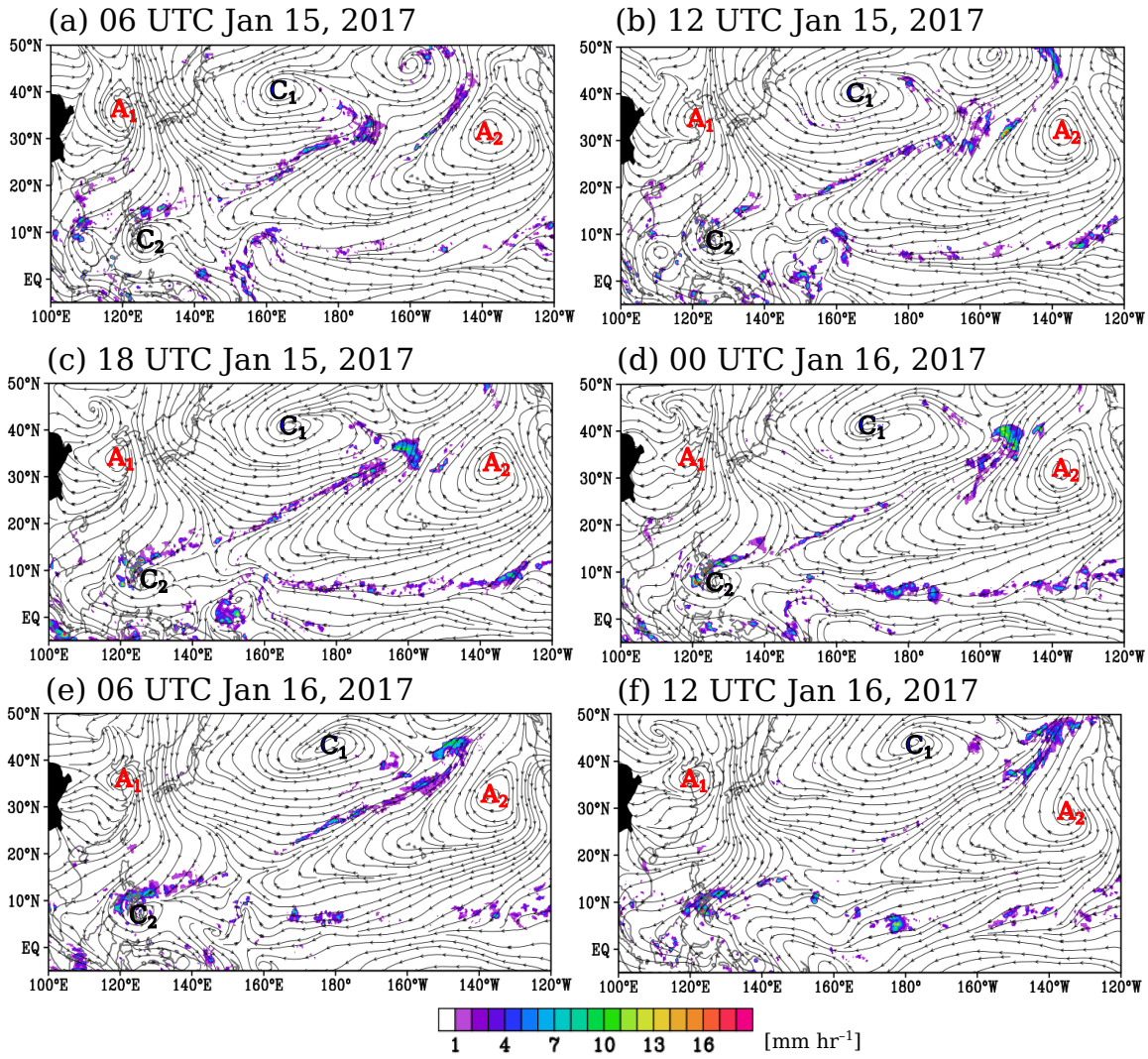

Figure 4.3. As in Fig. 4.2 but for the distribution of rainfall from the Tropical Rainfall Measuring Mission (TRMM) 3B42 version 7 (shades; mm hr^{-1}) and 925 hPa winds (*WINDS*$_{925hPa}$; streams; m s^{-1}). The cyclonic and anticyclonic circulations are denoted as "C" and "A", respectively.

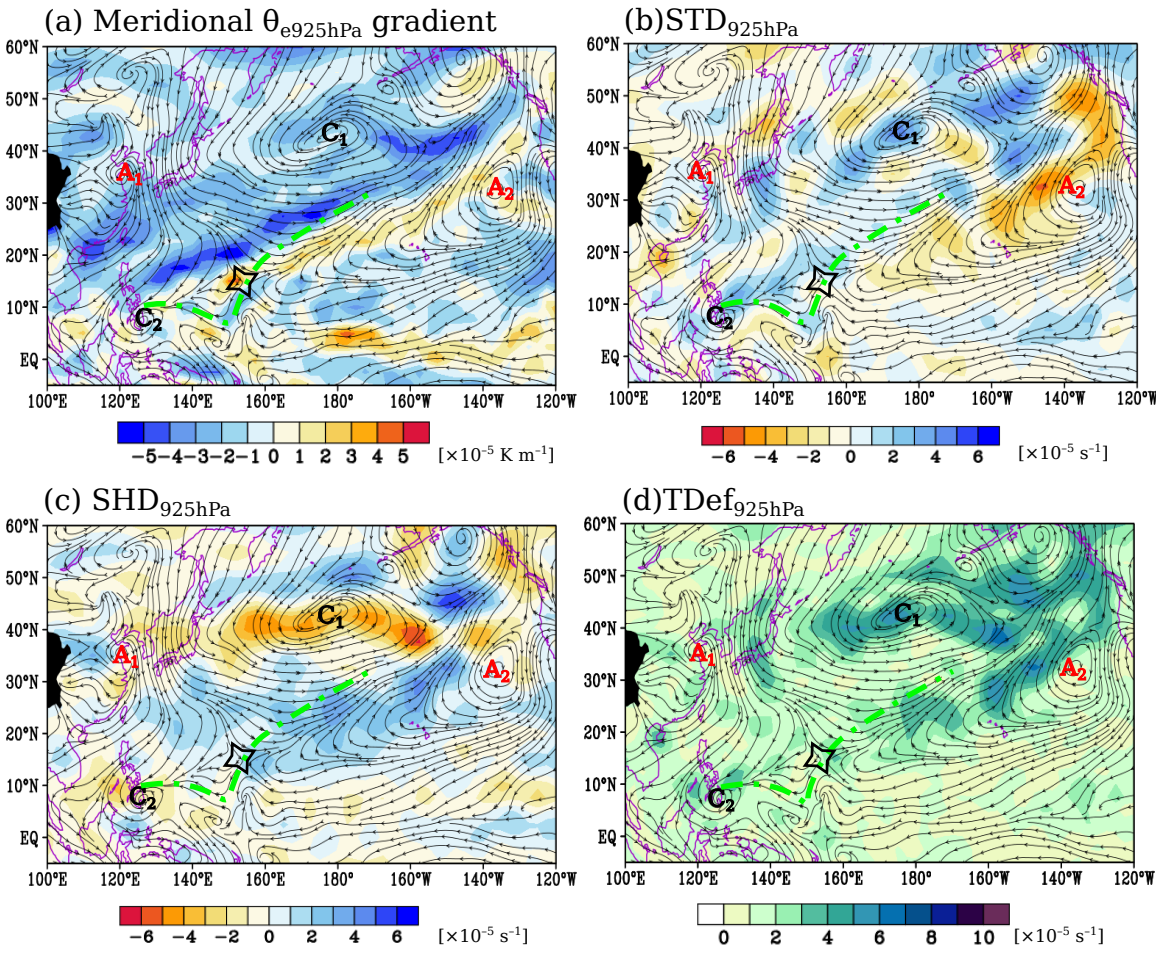

Figure 4.4. Spatial distribution of the 925 hPa: (a) meridional equivalent potential temperature gradient (θe_{925hPa}; shades; × 10^{-5} K m^{-1}); (b) stretching deformation (STD_{925hPa}; shades; × 10^{-5} s^{-1}); (c) shearing deformation (SHD_{925hPa}; shades; × 10^{-5} s^{-1}); and (d) total deformation ($TDef_{925hPa}$; shades; × 10^{-5} s^{-1}) on 06 UTC January 16, 2017. The 925 hPa wind anomalies (streams; m s^{-1}) are superimposed for discussion. The black star indicates the location of the deformation zone. The "A" and "C" are similar to those in Fig. 4.3.

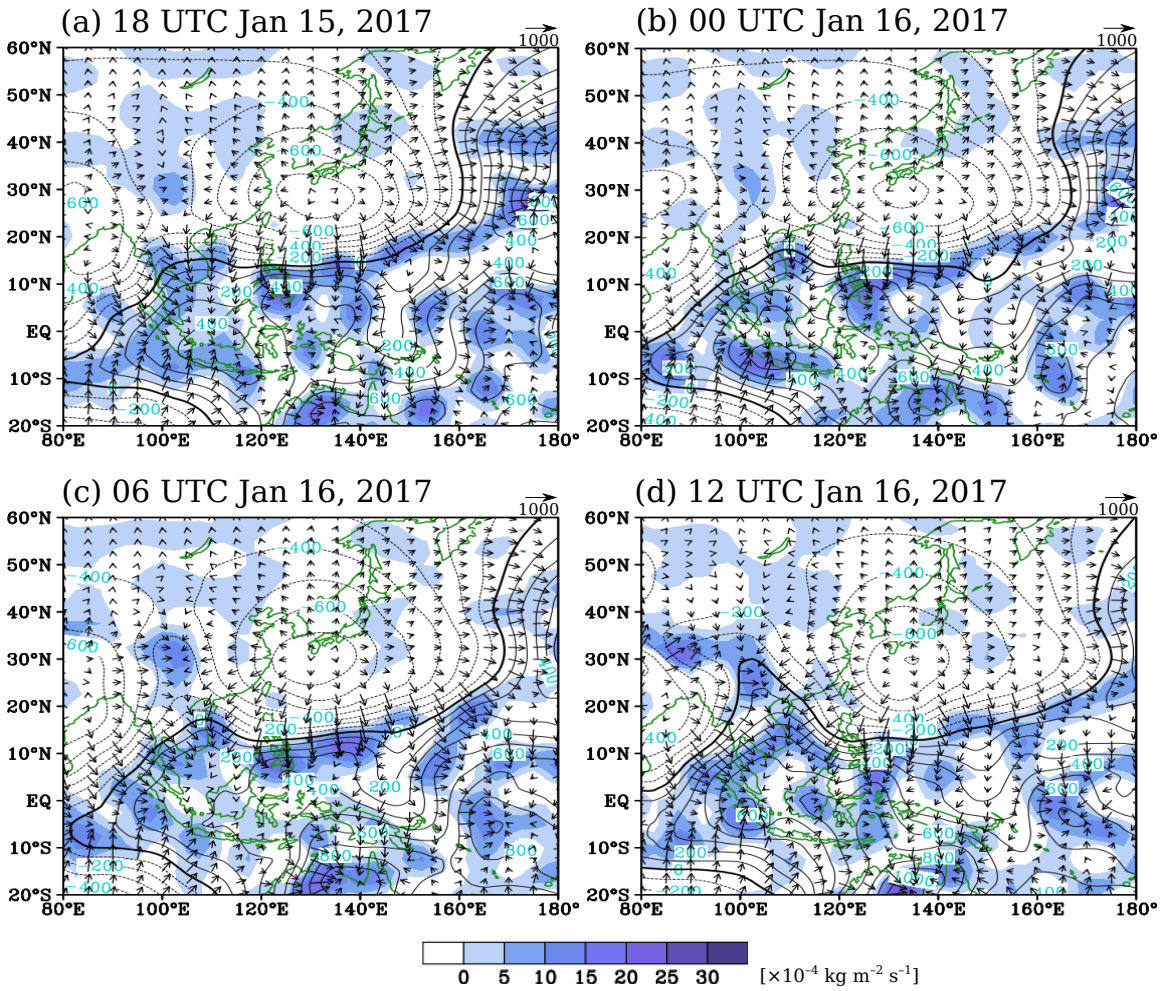

Figure 4.5. Spatial distribution of vertically integrated moisture flux convergence (Q; shades; $\times 10^{-4}$ kg m^{-2} s^{-1}), velocity potential (χ_Q; contours; $\times$ 10^6 kg s^{-1}), and the divergent component of Q (Q_D; vectors; kg m^{-1} s^{-1}) for: (a) 18 UTC January 15, 2017; (b) 00 UTC January 16, 2017; (c) 06 UTC January 16, 2017; and (d) 12 UTC January 16, 2017. The contour interval of χ_Q is 100 $\times$ 10^6 kg s^{-1}, while the scale of the vectors is 1000 kg m^{-1} s^{-1}.

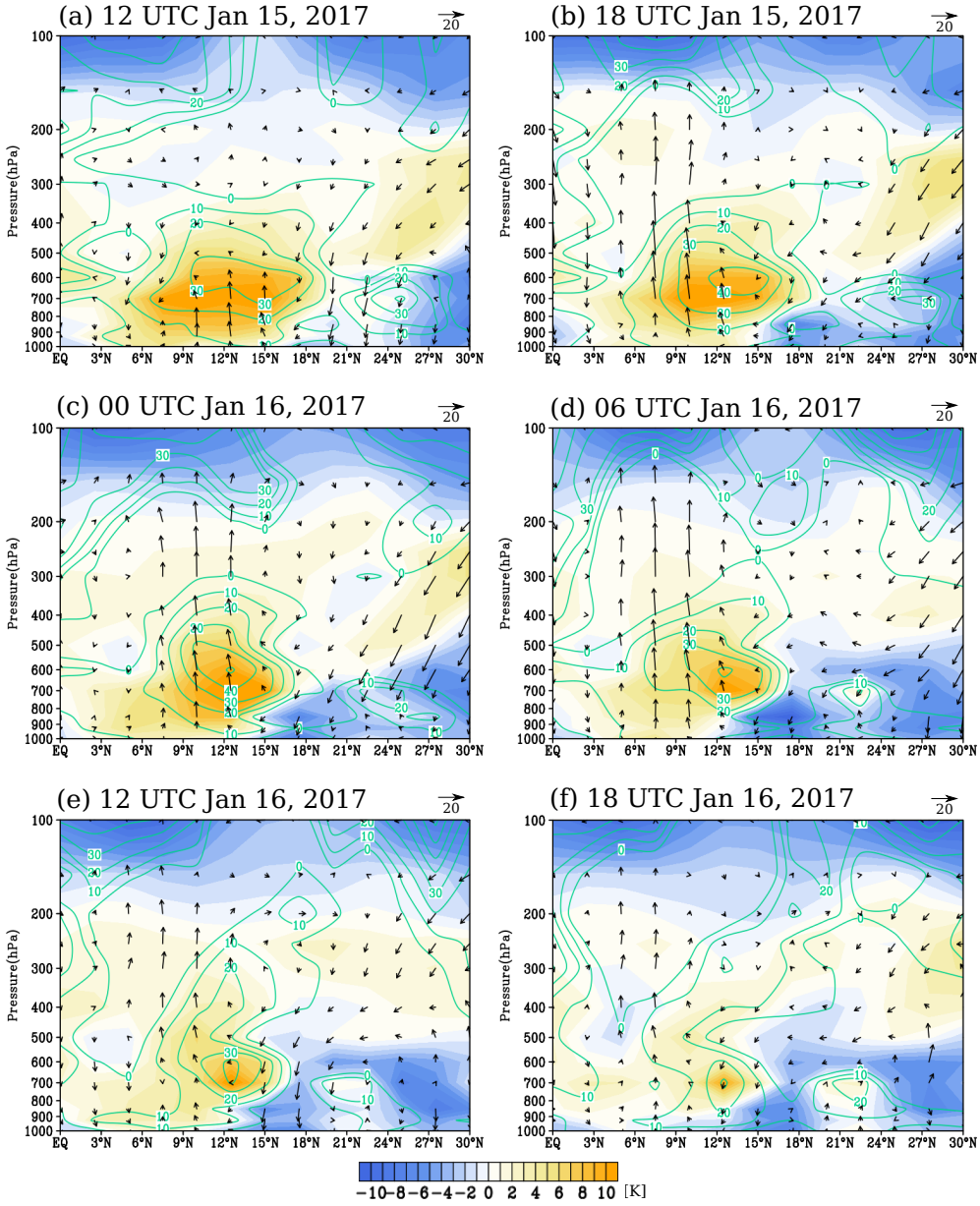

Figure 4.6. Vertical profile of the equivalent potential temperature anomaly (shades; K) and relative humidity anomaly (contours; %) averaged from 122–127°E for: (a) 12 UTC January 15, 2017; (b) 18 UTC January 15, 2017; (c) 00 UTC January 16, 2017; (d) 06 UTC January 16, 2017; (e) 12 UTC January 16, 2017; and (f) 18 UTC January 16, 2017. The vectors are the meridional and vertical velocity anomalies (m s^{-1}; scale is 20 m s^{-1}). The anomalies are relative to the 1981–2010 mean.

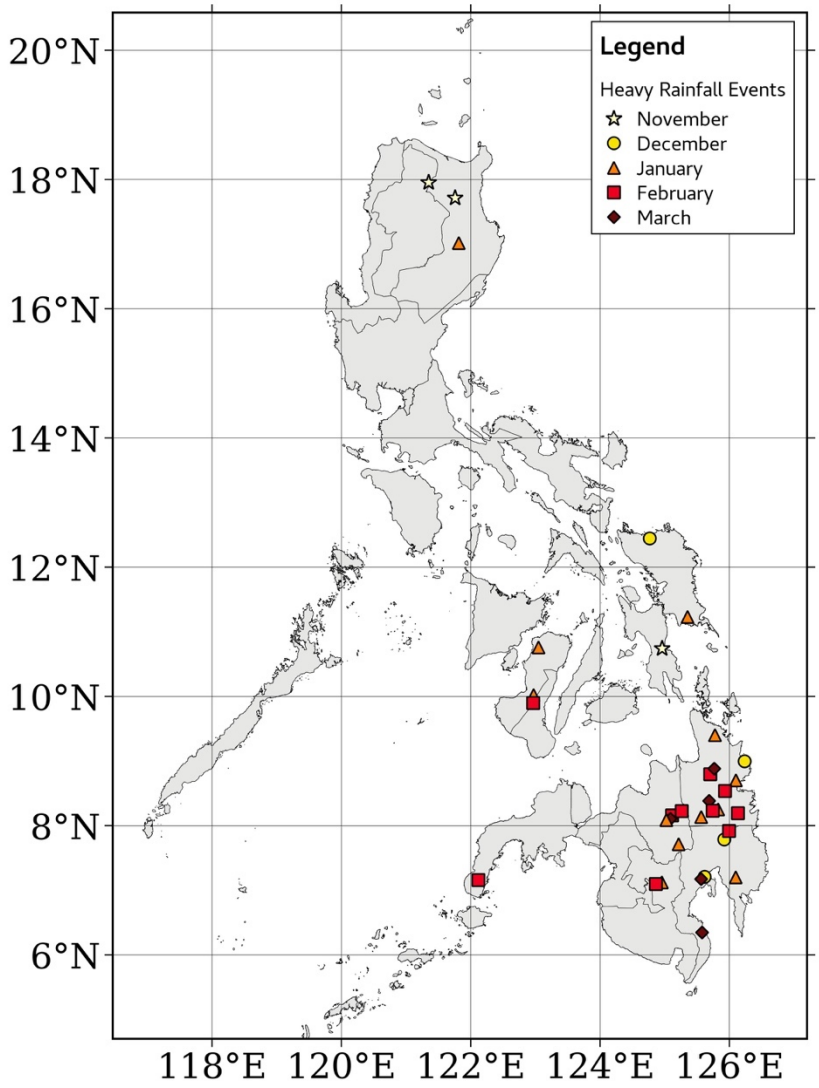

Figure 4.7. The location of the 34 non-tropical cyclone related heavy rainfall/flood (HRF) events from November to March over the Philippines from 1979–2017 based on the Dartmouth Flood Observatory archive.

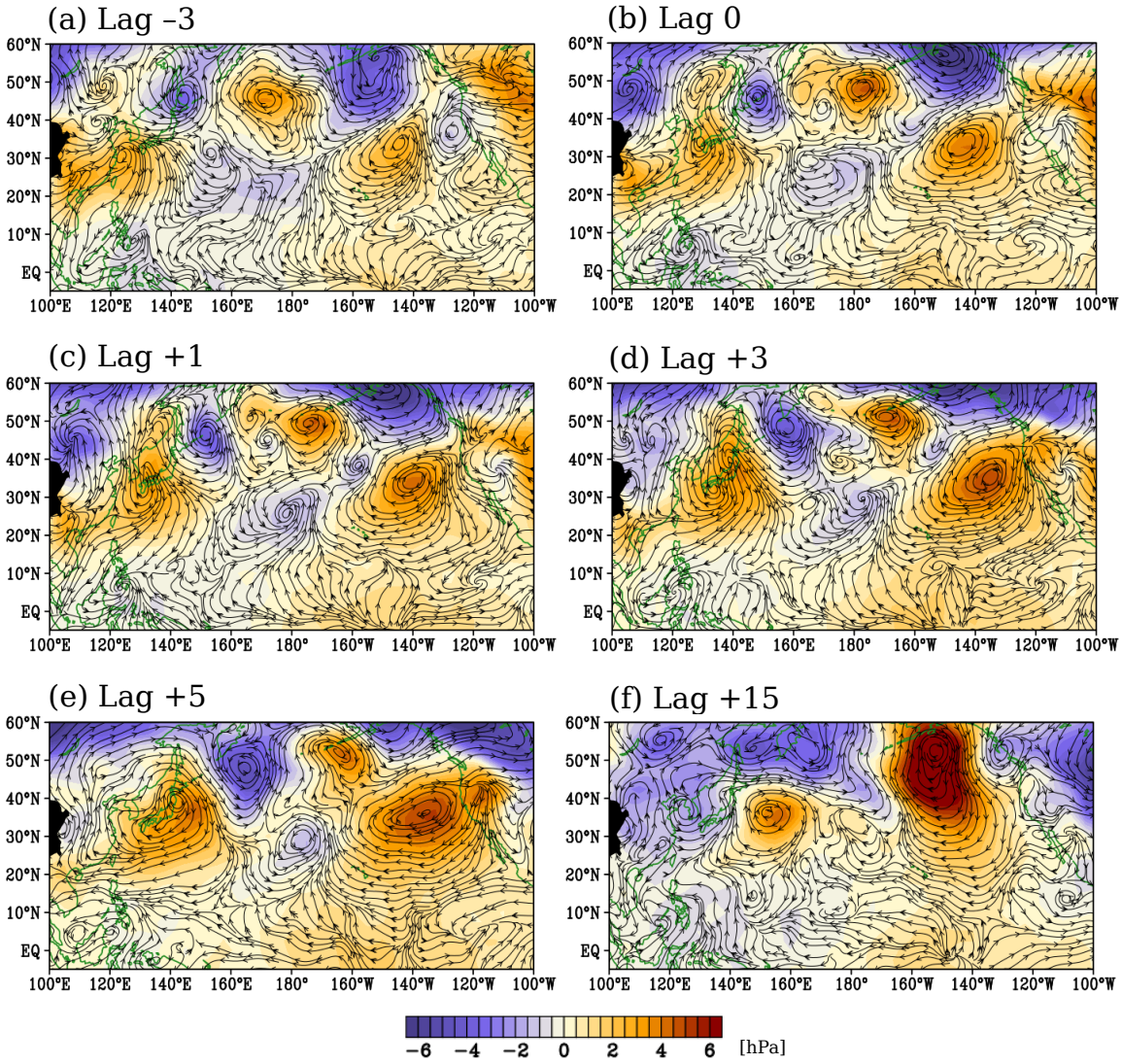

Figure 4.8. Lag composite anomalies of mean sea level pressure (shades; hPa), 925 hPa winds (streams; m s^{-1}) for: (a) Lag –3; (b) Lag 0; (c) Lag +1; (d) Lag +3; (e) Lag +5; and (f) Lag +15. Lag 0 refers to the time when the area-averaged vertically integrated moisture flux convergence (*VIMFC*) of the recorded HRF event over Mindanao Island is maximum. Note that the reanalysis data is 6-hourly so that Lag –3 (+3) means 18 hours before (after) the peak *VIMFC*.

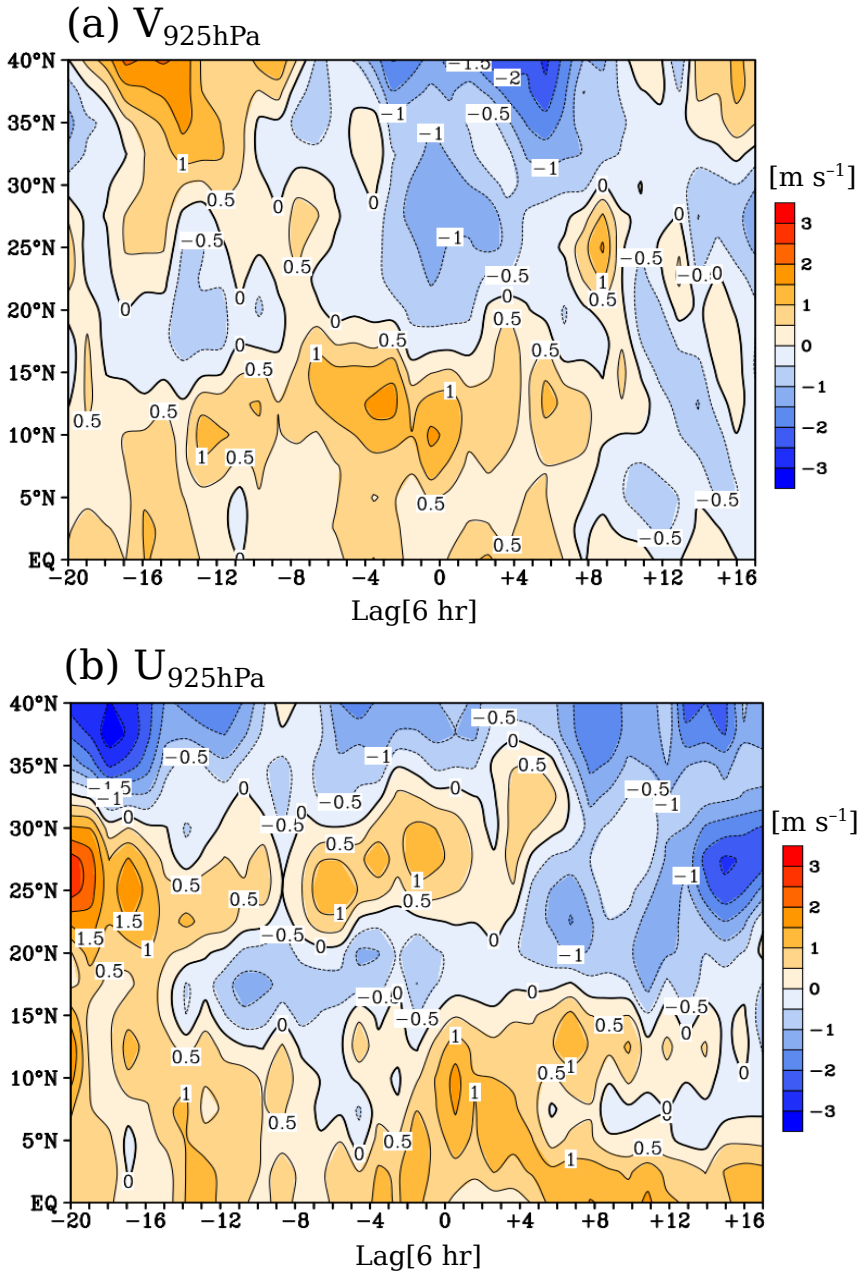

Figure 4.9. Composite anomalies of: (a) 925 hPa meridional wind (V_{925hPa}; shades and contours; m s^{-1}); and (b) 925 hPa zonal winds (U_{925hPa}; shades and contours; m s^{-1}) averaged from 122–127.5°E. The contour interval is 0.5 m s^{-1}.

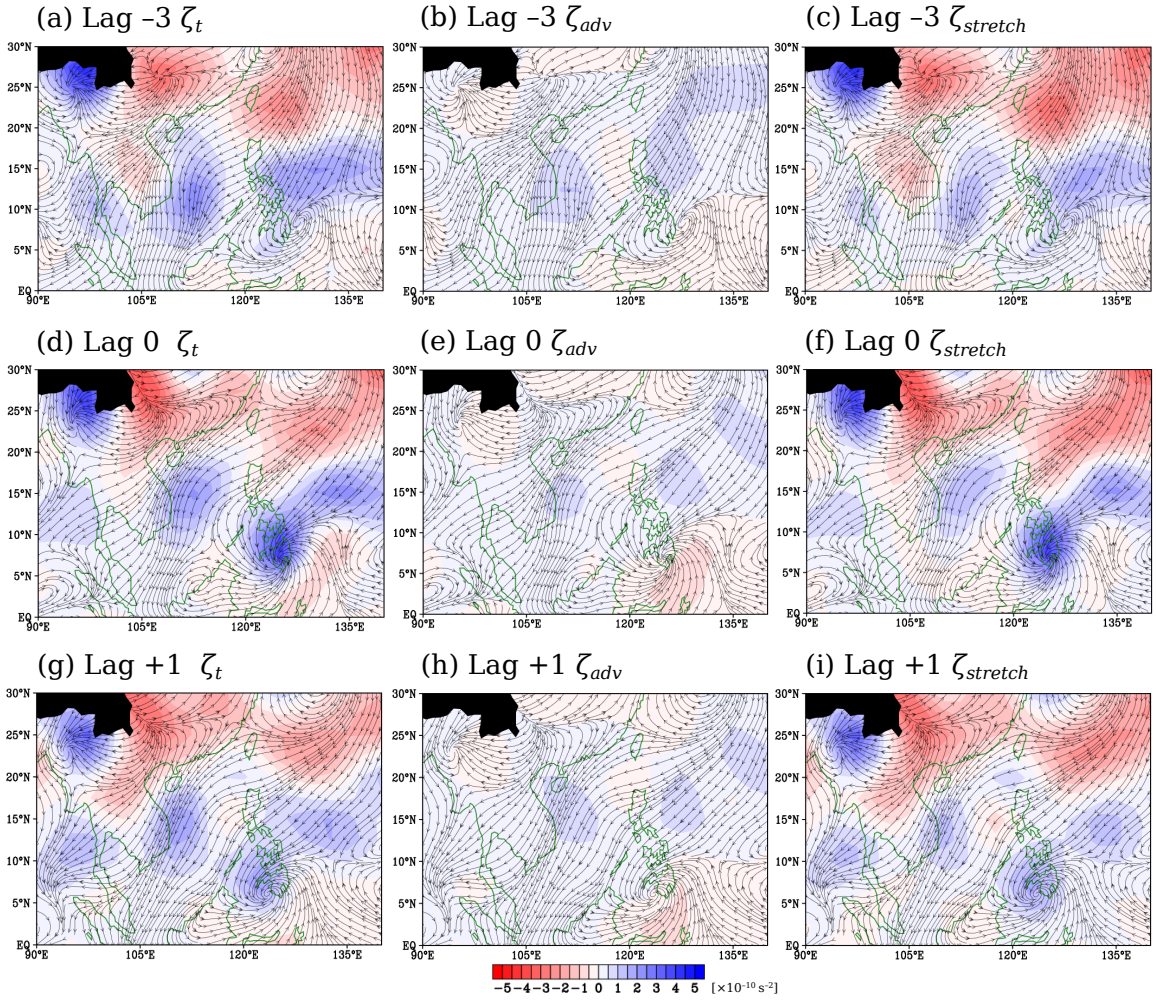

Figure 4.10. Spatial distribution of composite anomalies of vorticity tendency (ζ_t; $\times 10^{-10}$ s^{-2}), its advection term (ζ_{adv}; $\times 10^{-10}$ s^{-2}), and stretching term ($\zeta_{stretch}$; $\times 10^{-10}$ s^{-2}) for: Lag –3 (a, b, c); Lag 0 (d, e, f); and Lag +1 (g, h, i), respectively. The 925 hPa wind anomalies (m s^{-1}) are superimposed for discussion.

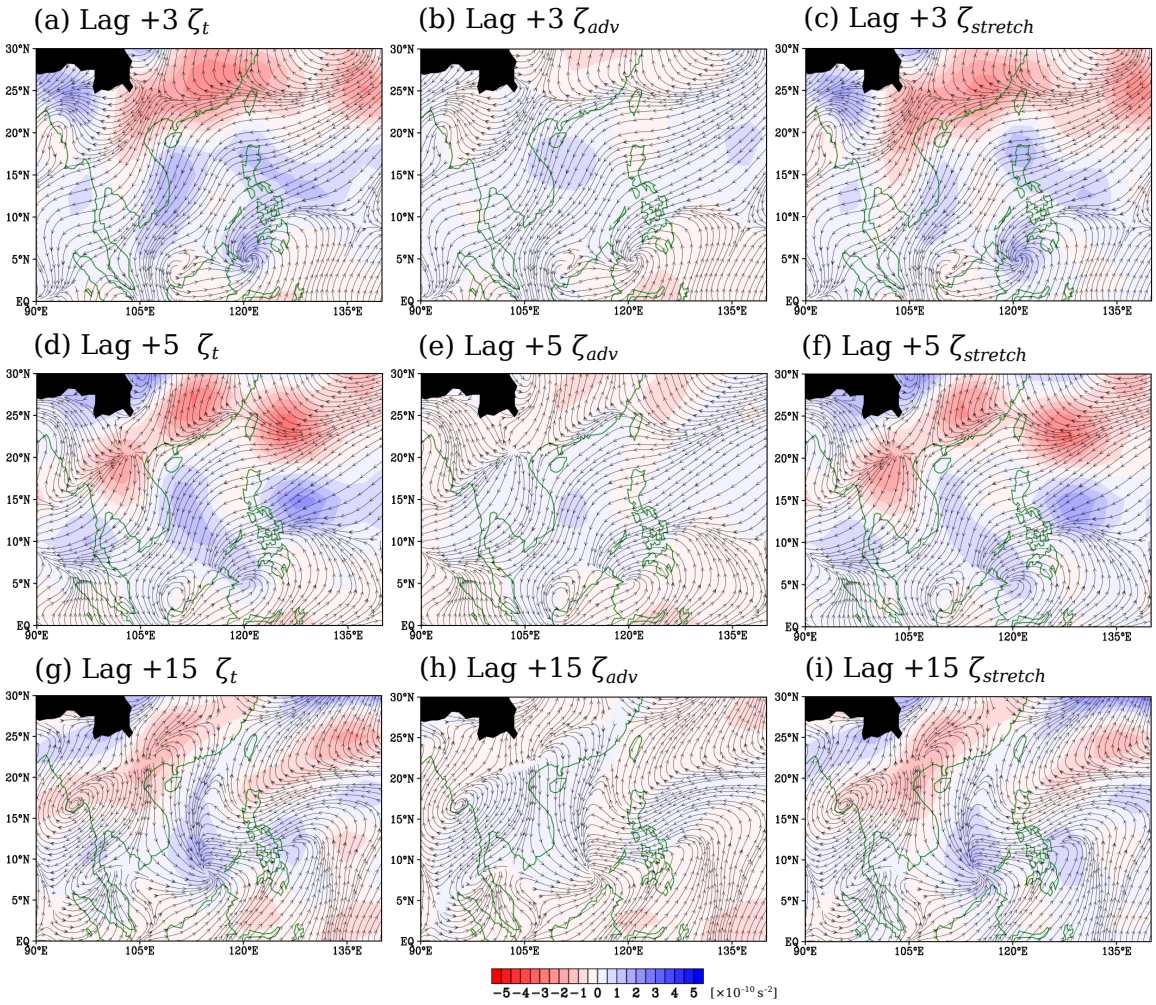

Figure 4.11. As in Fig. 4.10 but for: Lag +3 (a, b, c); Lag +5 (d, e, f); and Lag +15 (g, h, i).

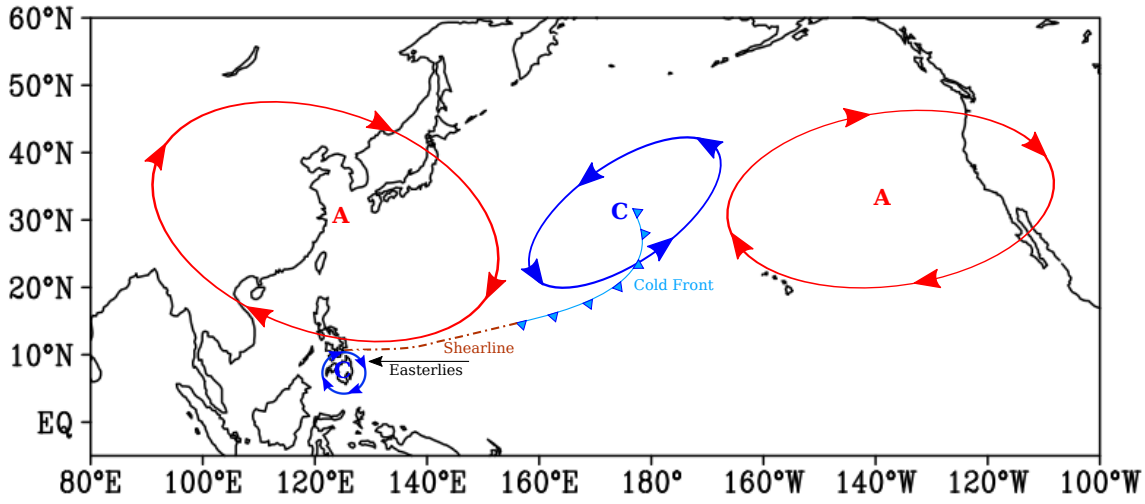

Figure 4.12. Schematic diagram of the possible mechanism leading to the winter HRF over the Mindanao Island (southern Philippines). The cyclonic and anticyclonic circulations are denoted as "C" and "A", respectively. The dot-dashed line indicates the location of the shearline.

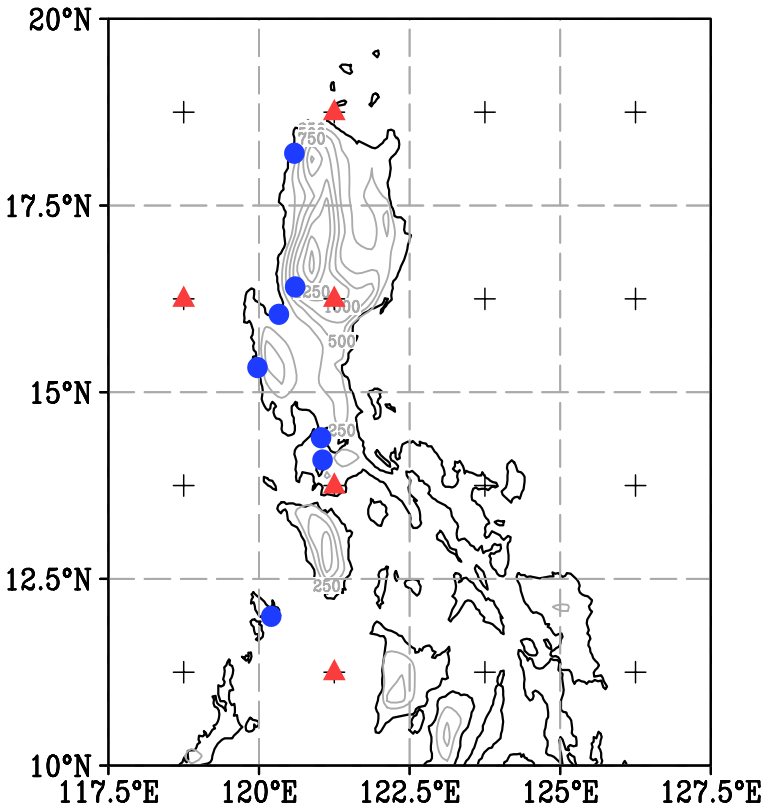

Figure 5.1. Location of the seven meteorological stations of the Philippine Atmospheric, Geophysical and Astronomical Services Administration (PAGASA; blue circles), Climate Prediction Center Merged Analysis of Precipitation (CMAP) grid points (+ markings), and the topography of the Philippines above 250 m (gray contour lines). The contour interval of the topography is 250 m. The red triangles indicate the nearest five CMAP grid points to the location of the PAGASA stations.

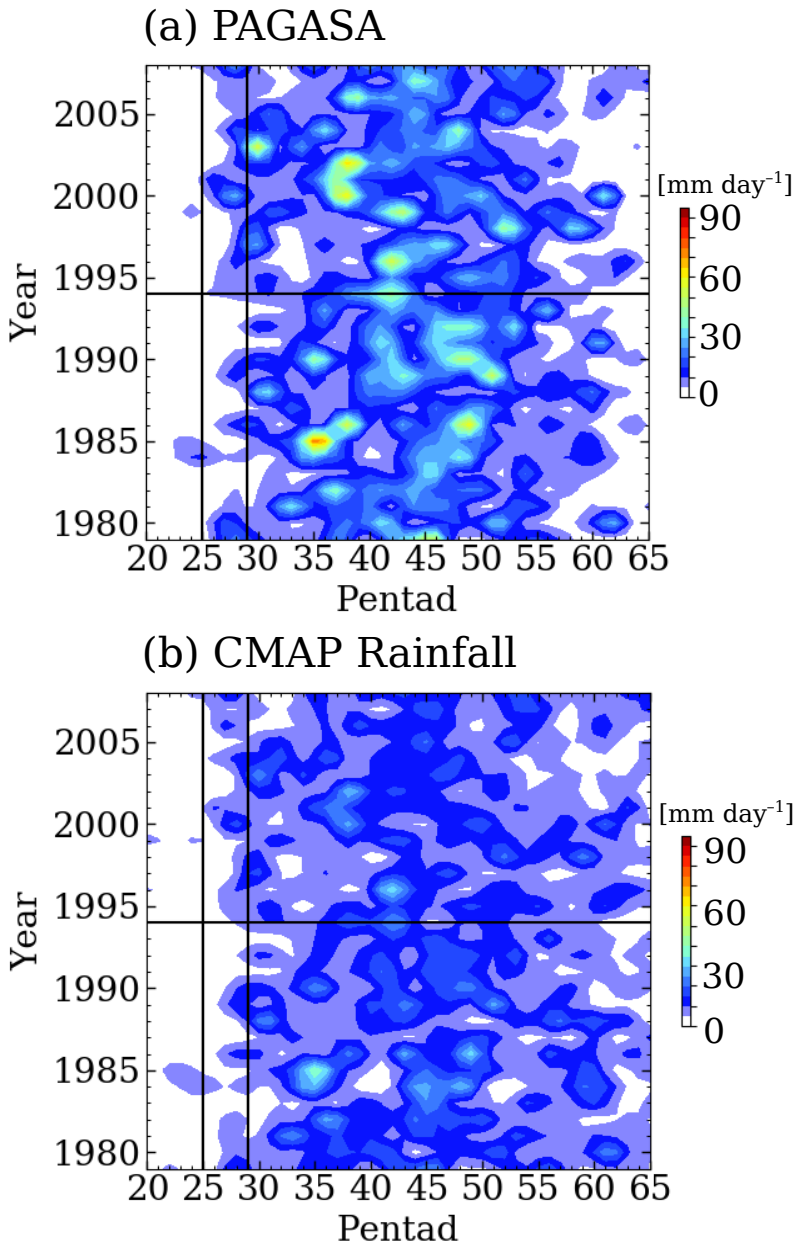

Figure 5.2. Rainfall distribution (mm day^{-1}) from 1979–2008 averaged across the: (a) seven PAGASA stations; and (b) five nearest CMAP grid points to the PAGASA stations. The rainfall distributions are smoothed by 1–2–1 filter in both x- and y-axis. The two vertical lines in (a) and (b) indicates P25 (start of May) and P29 (climatological summer monsoon onset based on Akasaka, 2010), respectively. The horizontal lines in (a) and (b) indicate 1994.

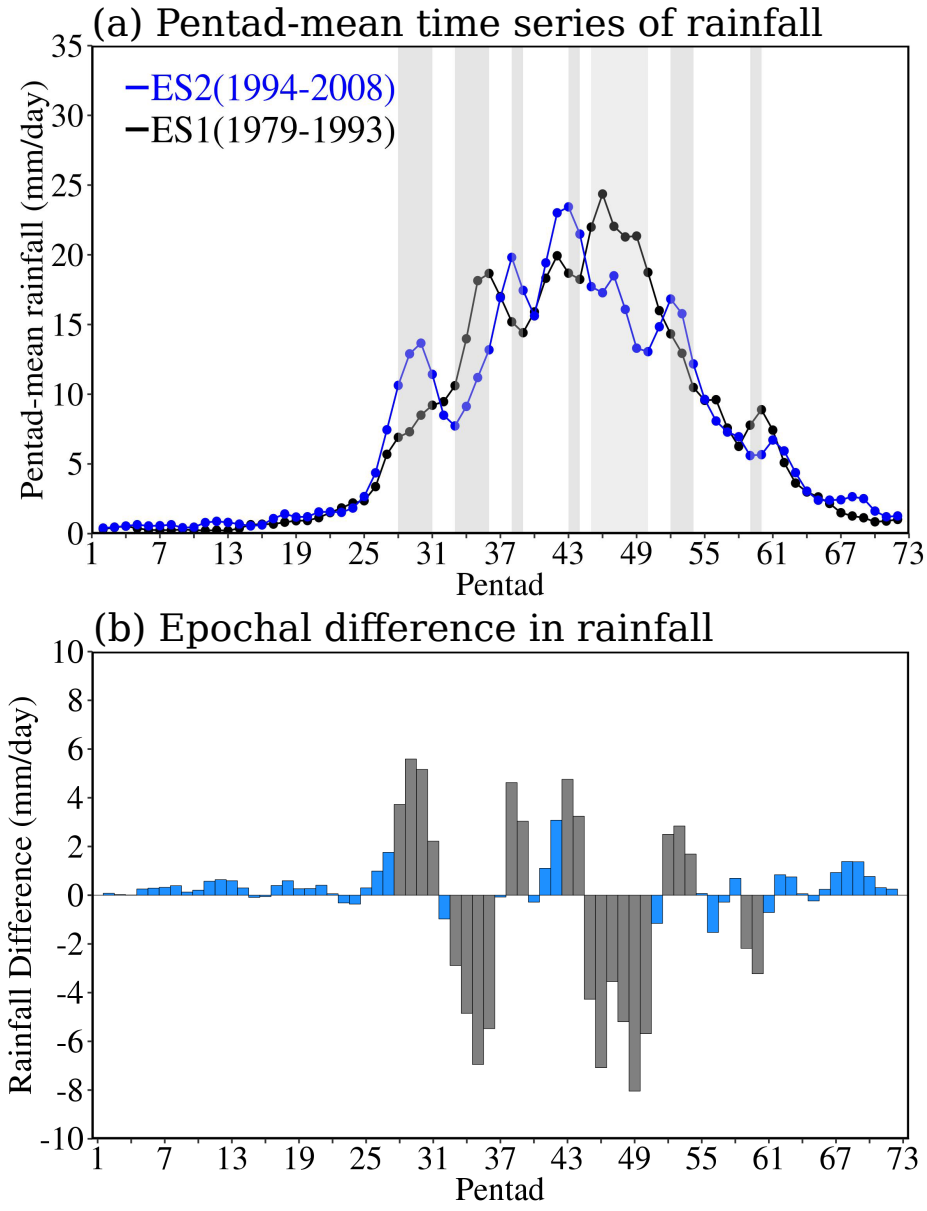

Figure 5.3. (a) Smoothed (1–2–1 filter) pentad-mean rainfall between ES1 (1979–1993) and ES2 (1994–2008) averaged across the seven PAGASA stations on the western coast of the Philippines; and (b) their epochal difference. Shaded pentads in (a) and gray bars in (b) indicate statistically significant difference above the 95 % confidence level using the Student's *t*-test.

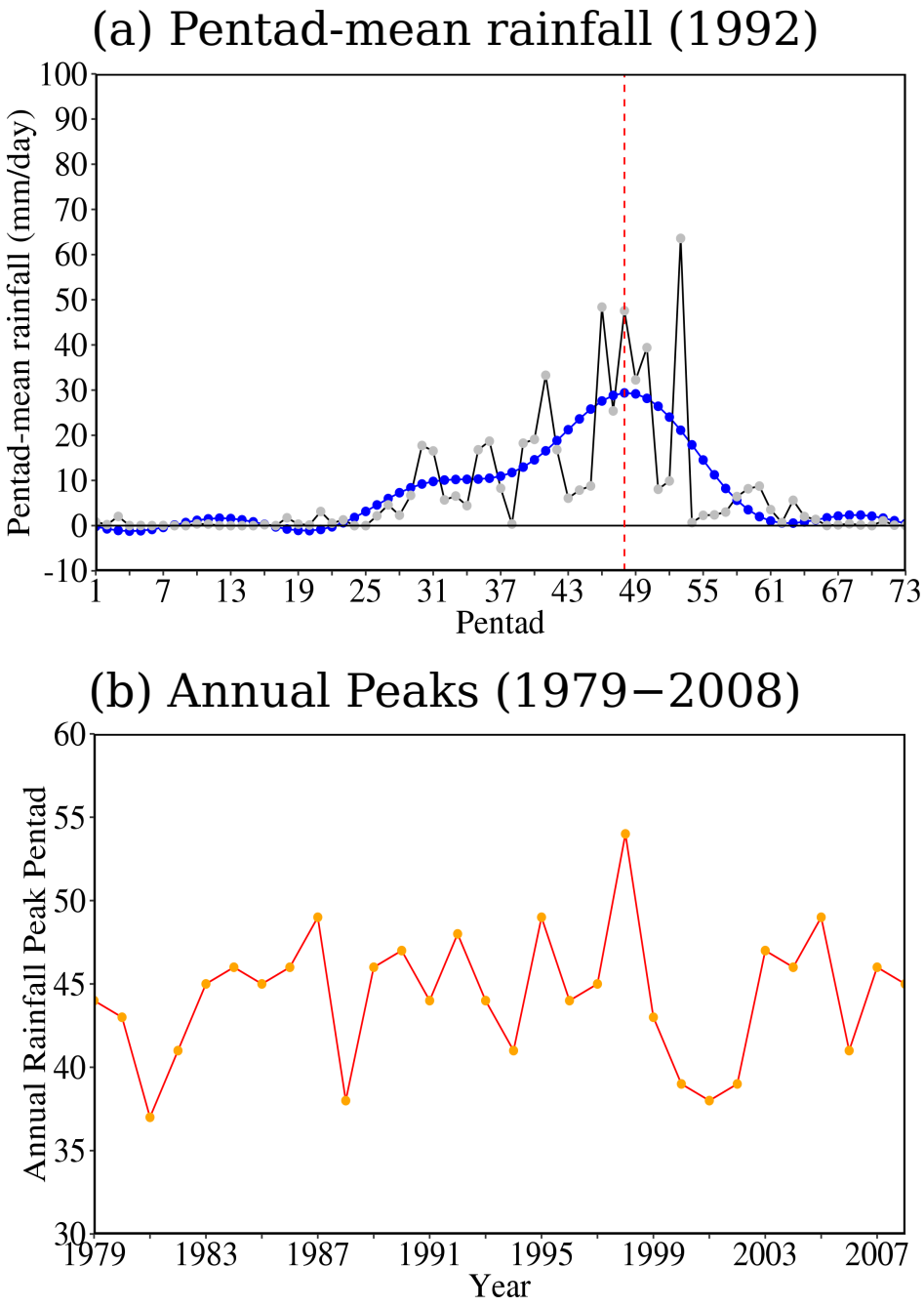

Figure 5.4. (a) Pentad-mean rainfall time series during 1992 (black line; mm day^{-1}) and its equivalent smoothed time series (blue line) obtained by adding the first four Fourier harmonics of the original time series; and (b) time series of annual peak pentads, defined as the maximum of the smoothed time series, from 1979 to 2008.

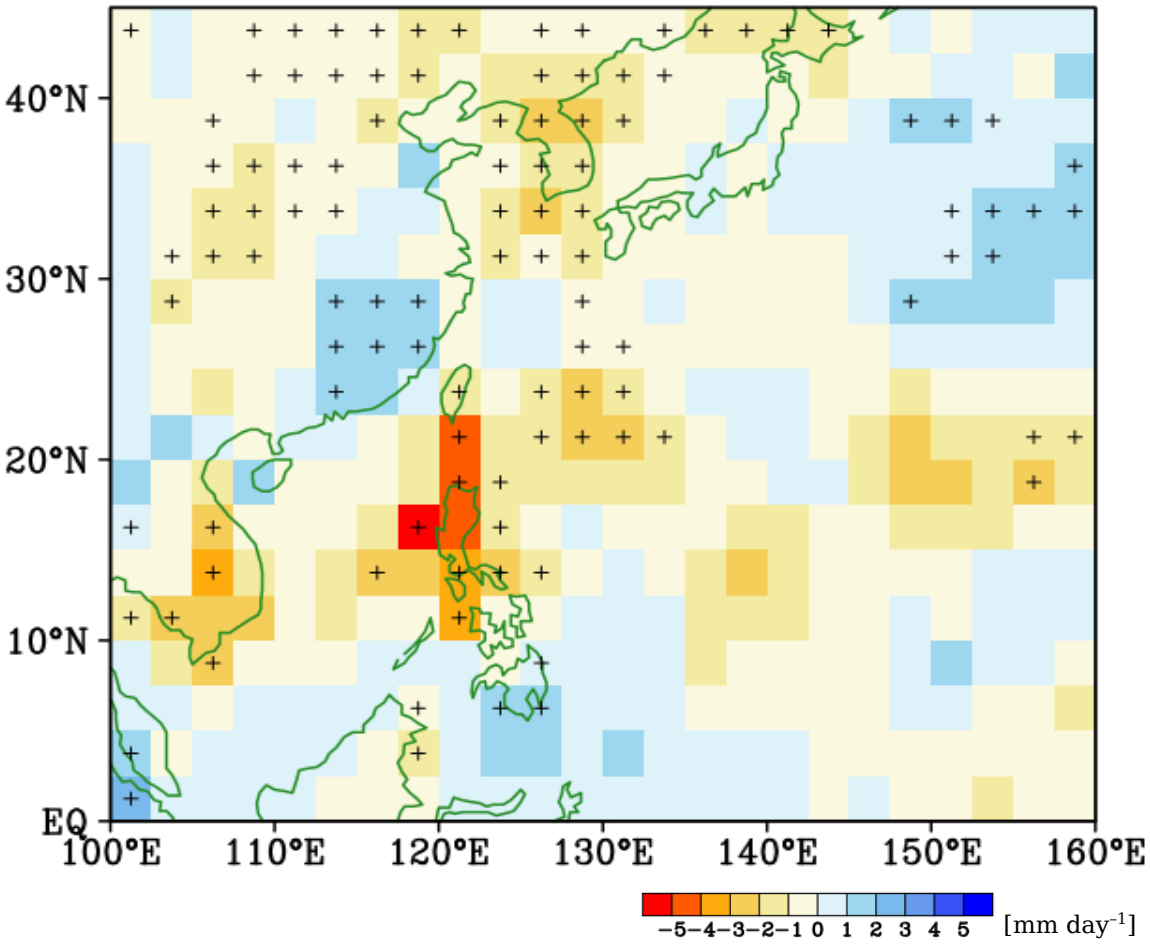

Figure 5.5. Epochal difference (ES2 minus ES1) in the spatially smoothed (1–2–1 filter; both longitudinal and latitudinal direction) CMAP rainfall (mm day^{-1}) during P45–P50. Cross (+) markings indicate statistical significance at the 95 % confidence level.

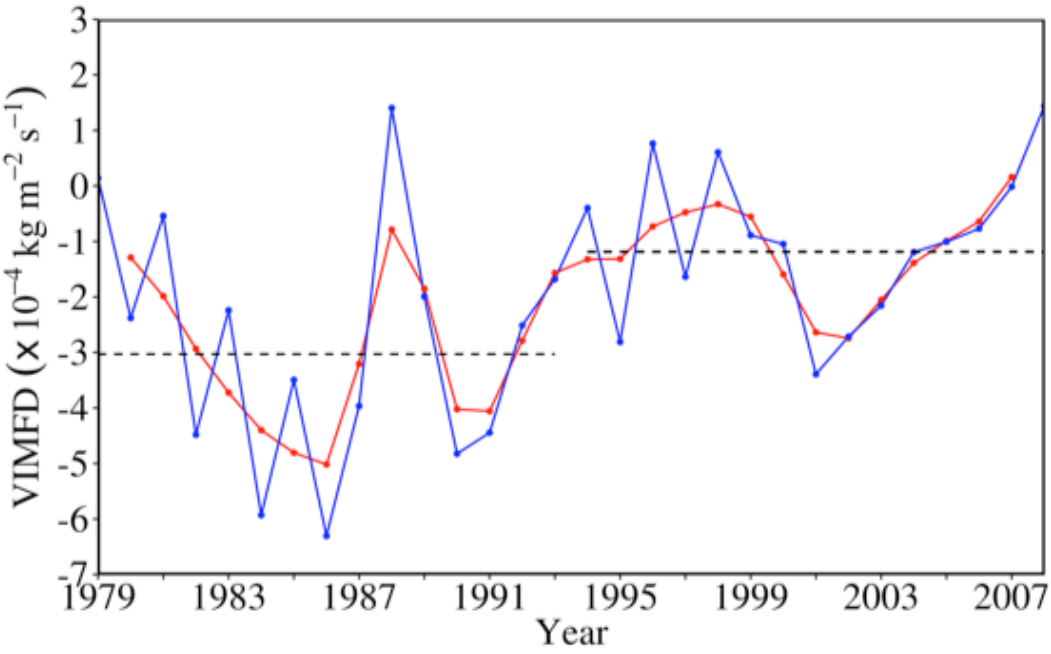

Figure 5.6. Time series of area-averaged vertically integrated moisture flux divergence (*VIMFD*; $\times 10^{-4}$ kg m^{-2} s^{-1}) over 117.5–122.5°E and 10–20°N during P45–P50. The blue (red) line is the unfiltered (1–2–1 filtered) time series. Dashed horizontal lines indicate the epochal means.

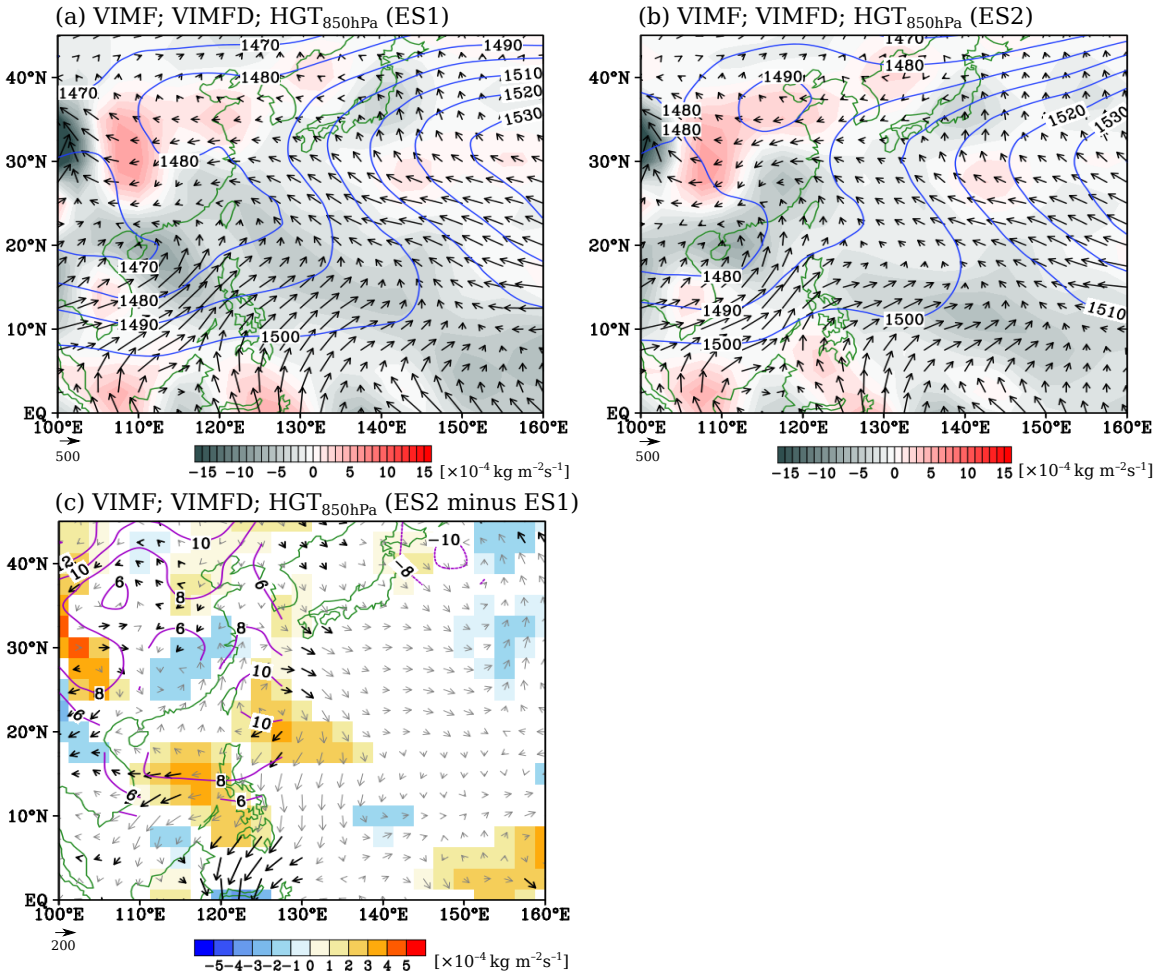

Figure 5.7. Smoothed (1–2–1 filter) vertically integrated moisture flux (*VIMF*; vectors; kg m^{-1} s^{-1}), moisture flux divergence (*VIMFD*; shades; ×10^{-4} kg m^{-2} s^{-1}), and 850 hPa geopotential height (HGT_{850hPa}; contours; m) for P45–P50 during: (a) ES1 (1979–1993); (b) ES2 (1994–2008); and their (c) epochal difference (ES2 minus ES1). (a–c) The contour interval is 10 m. Shaded areas, black arrows, and purple contours in (c) indicate statistical significance at the 95 % confidence level. The scale of the vectors is indicated on the lower-left corner of each figure.

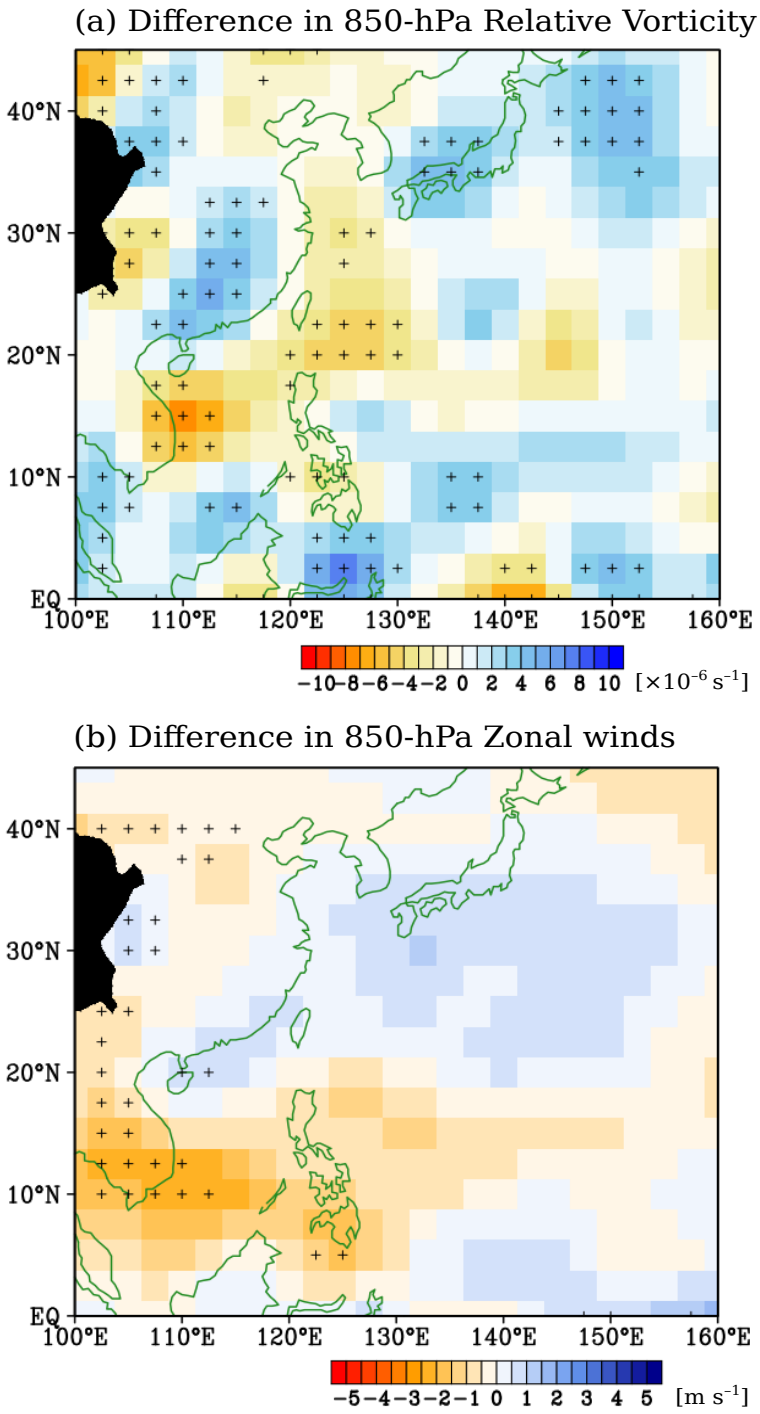

Figure 5.8. Epochal difference (1994–2008 minus 1979–1993) in smoothed (1–2–1 filter): (a) 850 hPa relative vorticity ($\times 10^{-6}$ s^{-1}); and (b) 850 hPa zonal winds (U_{850hPa}; m s^{-1}). Cross (+) markings indicate statistical significance at the 95 % confidence level.

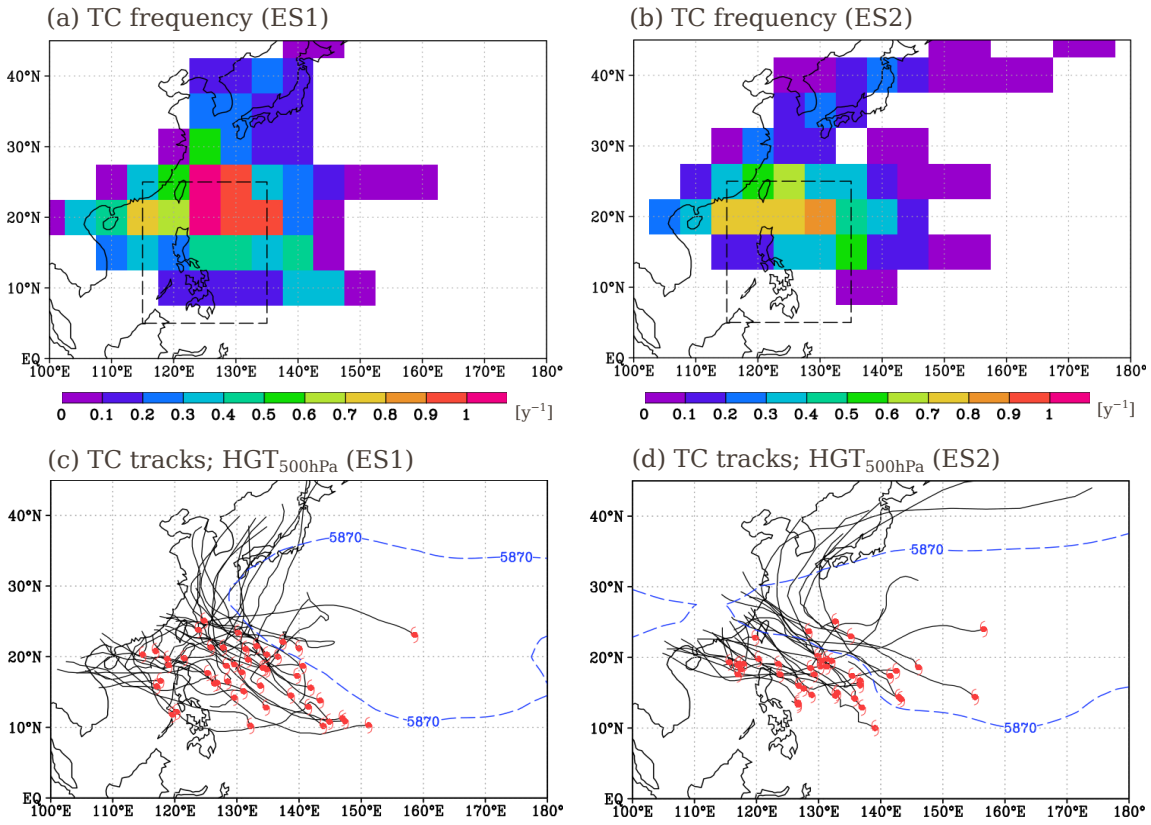

Figure 5.9. Tropical cyclone (TC) track frequency (per year) in P45–P50 interpolated onto a 5° × 5° grid for: (a) ES1 (1979–1993); and (b) ES2 (1994–2008) based on JTWC track dataset. As in (a) but for TC tracks and location of 5, 870-m contour line of the 500 hPa geopotential height (HGT_{500hPa}; dashed blue line) for: (c) ES1; and (d) ES2. Dashed boxes in (a) and (b) indicate the Philippine Area of Responsibility (PAR; 115–135°E and 5–25°N). The genesis locations in (c) and (d) are indicated by the red markings.

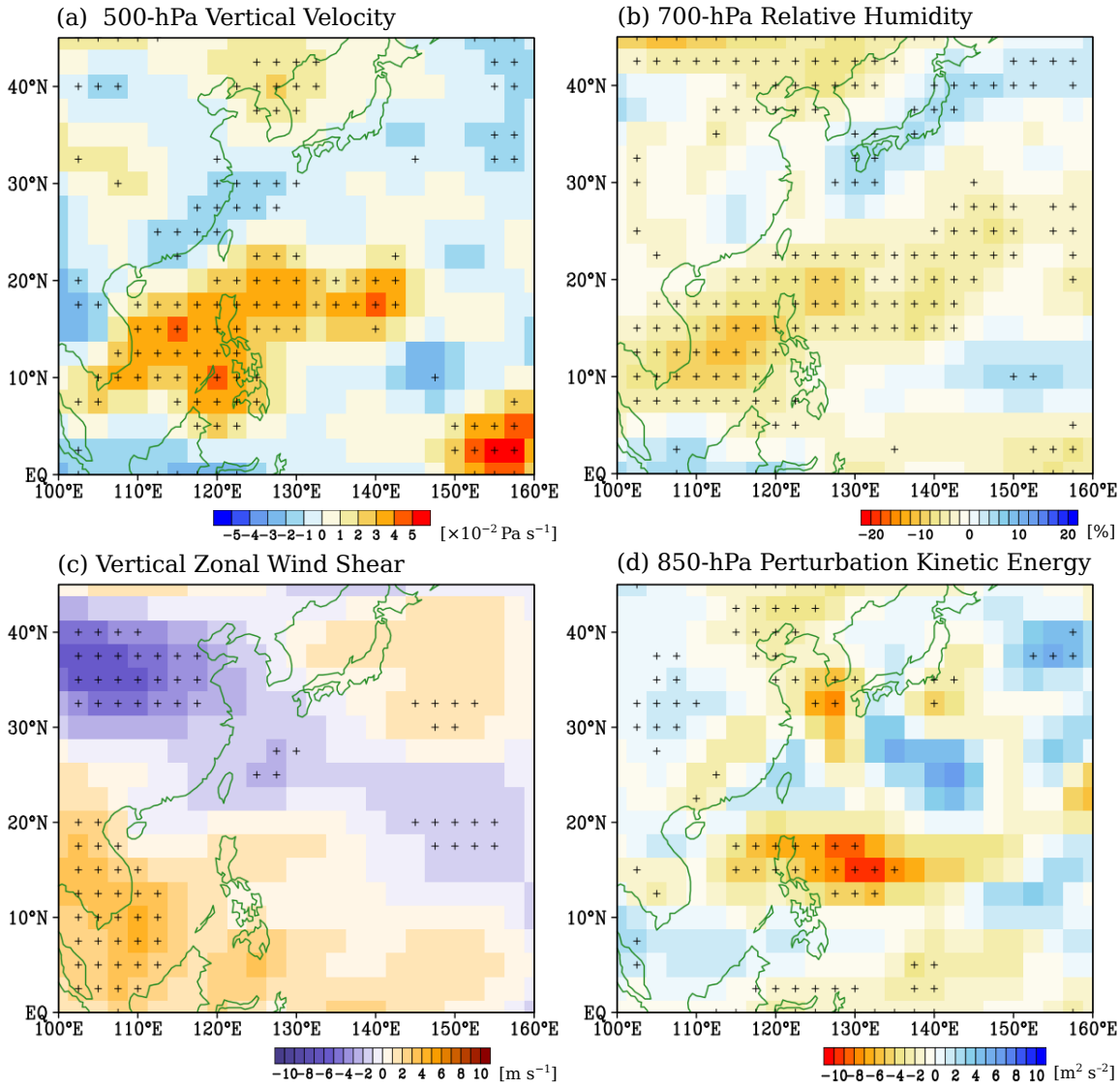

Figure 5.10. As in Fig. 5.5 but for: (a) 500 hPa vertical velocity (ω; $\times 10^{-2}$ Pa s^{-1}); (b) 700 hPa relative humidity (*RHUM*; %); (c) vertical zonal wind shear (U_{200hPa} minus $U_{850hPa;}$ m s^{-1}); and (d) 850 hPa perturbation kinetic energy (*PKE*; m^2 s^{-2}). Cross (+) markings indicate statistical significance at the 95 % confidence level.

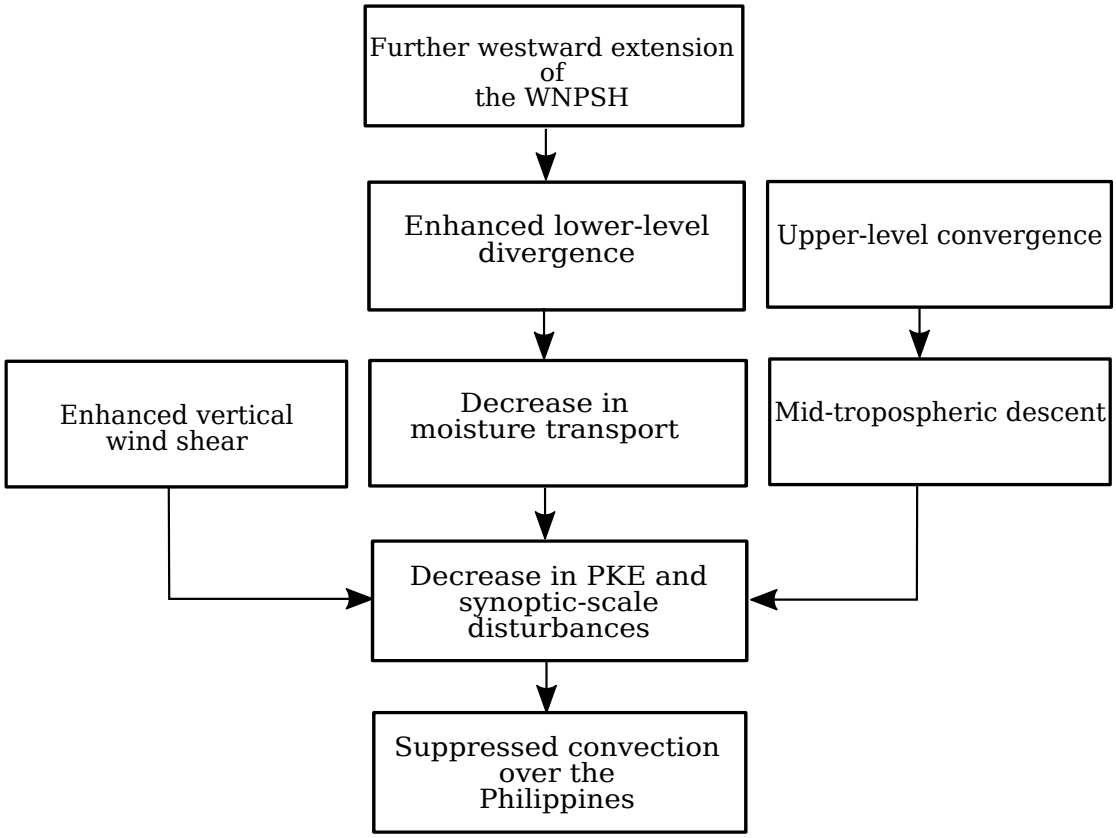

Figure 5.11. Schematic diagram showing the possible mechanism leading to the decrease in rainfall over the Philippines from early August to early September occurring in the mid-1990s (1993/1994).

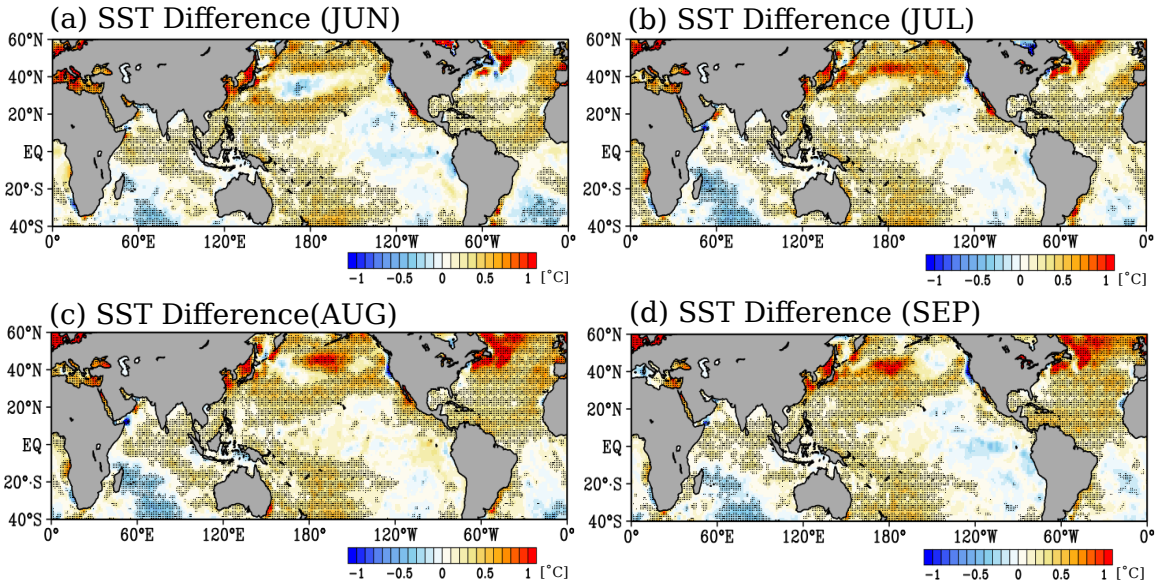

Figure 5.12. Epochal difference (1994–2008 minus 1979–1993) in smoothed sea surface temperature (SST; °C) during: (a) June; (b) July; (c) August; and (d) September. Dotted areas indicate statistical significance at the 95 % confidence level by Student's *t*-test. The SST data came from monthly Hadley Center sea ice and sea surface temperature data set (HadISST version 1.1; Rayner *et al.*, 2003).

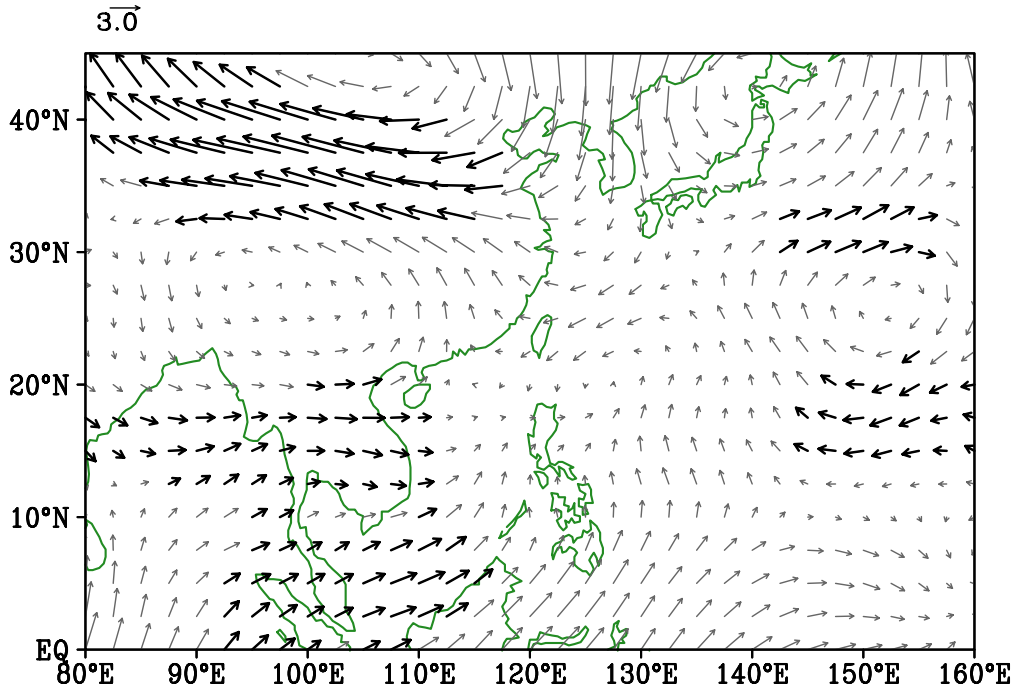

Figure 5.13. Epochal difference (1994–2008 minus 1979–1993) in smoothed (1–2–1 filter) 200 hPa winds (U_{200hPa}). Bold vectors are statistically significant at the 95 % confidence level by Student's *t*-test.

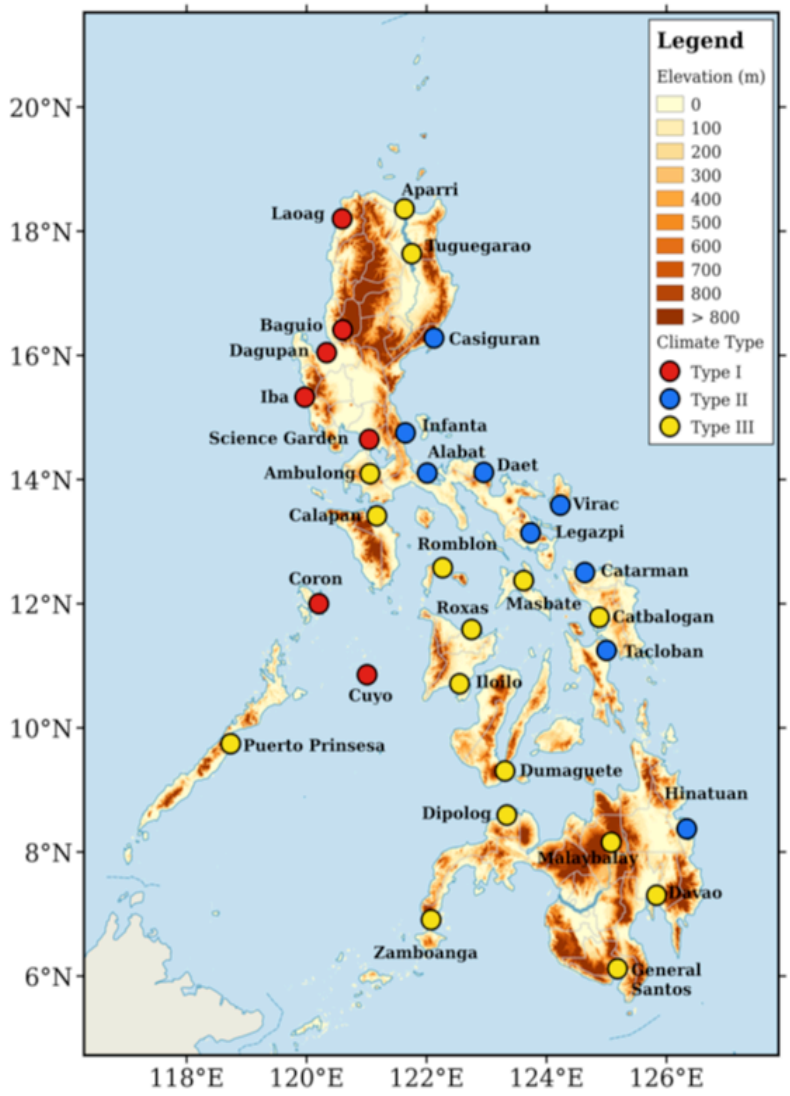

Figure 6.1. The location of the 32 stations from the Philippine Atmospheric, Geophysical and Astronomical Serviced Station (PAGASA) and the topography of the Philippines (shades; m). The colors of the circles indicate the climate types based on Villafuerte *et al*. (2017).

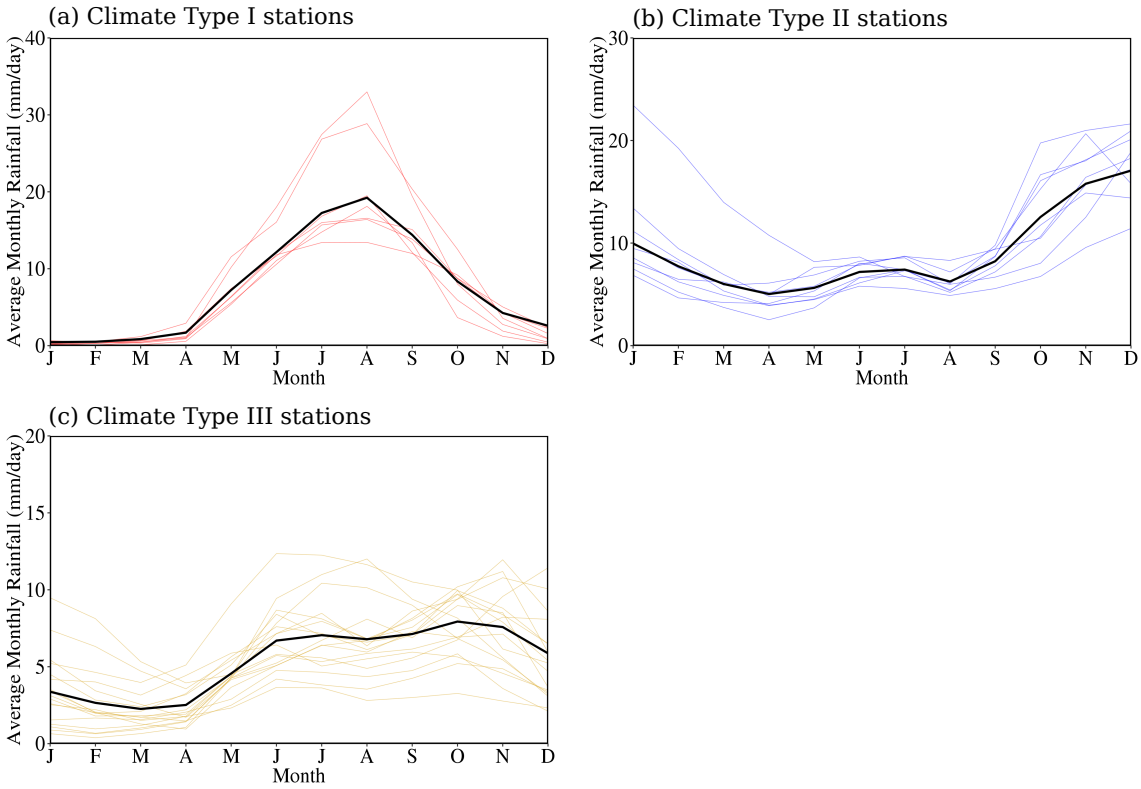

Figure 6.2. Average monthly rainfall (mm day^{-1}) distribution of the stations that belong to: (a) Climate Type I; (b) Climate Type II; and (c) Climate Type III from the period 1961 to 2008. The black solid line in each figure represents the mean rainfall time series of the different stations in each climate type.

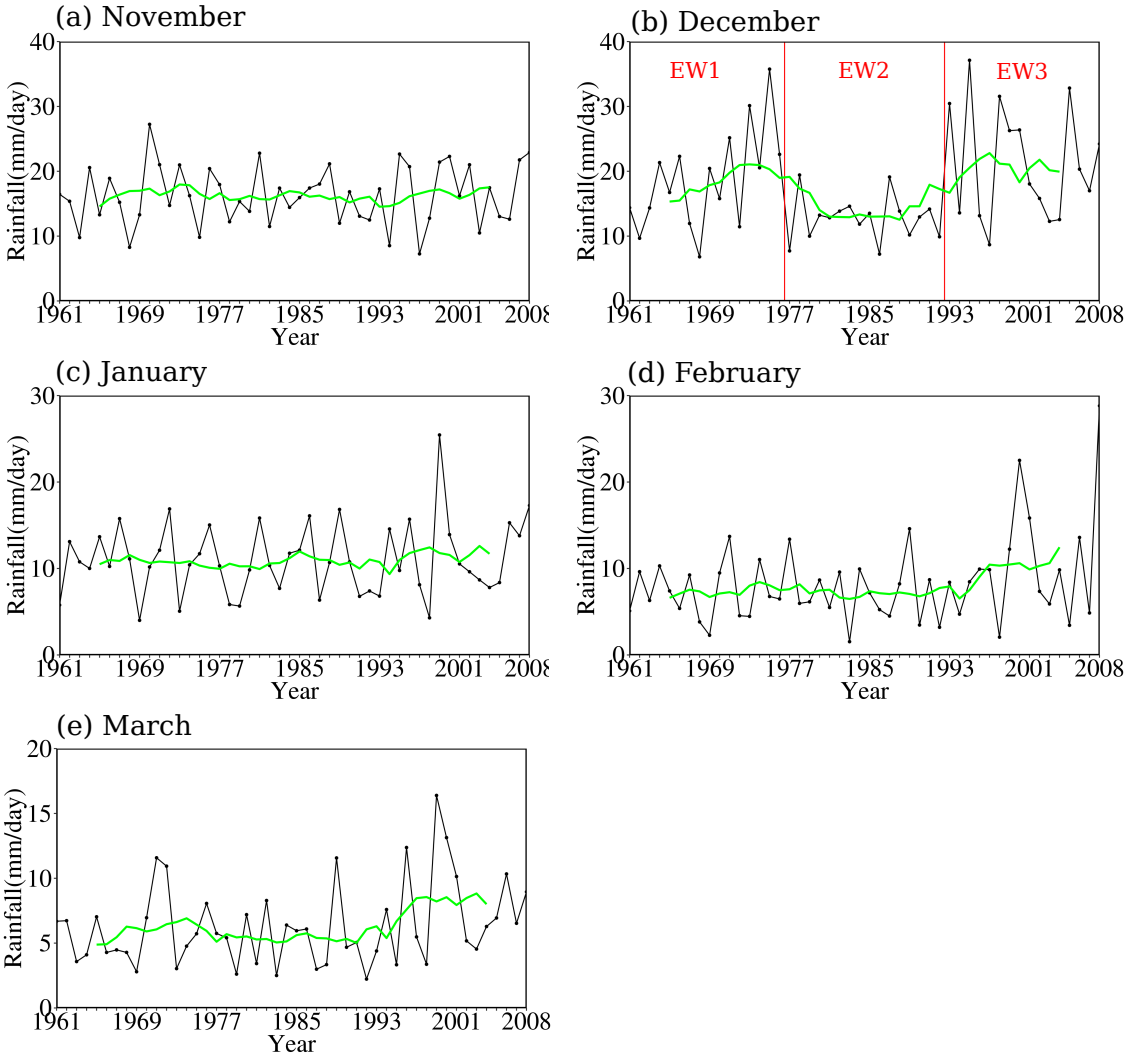

Figure 6.3. Time series of average monthly rainfall (mm day^{-1}) of Climate Type II stations from 1961 to 2008 for: (a) November; (b) December; (c) January; (d) February; and (e) March. The red vertical lines in (b) indicate the significant change points around 1976/1977 and 1992/1993 that divides the time series into three epochs: EW1 (1961–1976); EW2 (1977–1992); and EW3 (1993–2008). The green line indicates the 9-year running average.

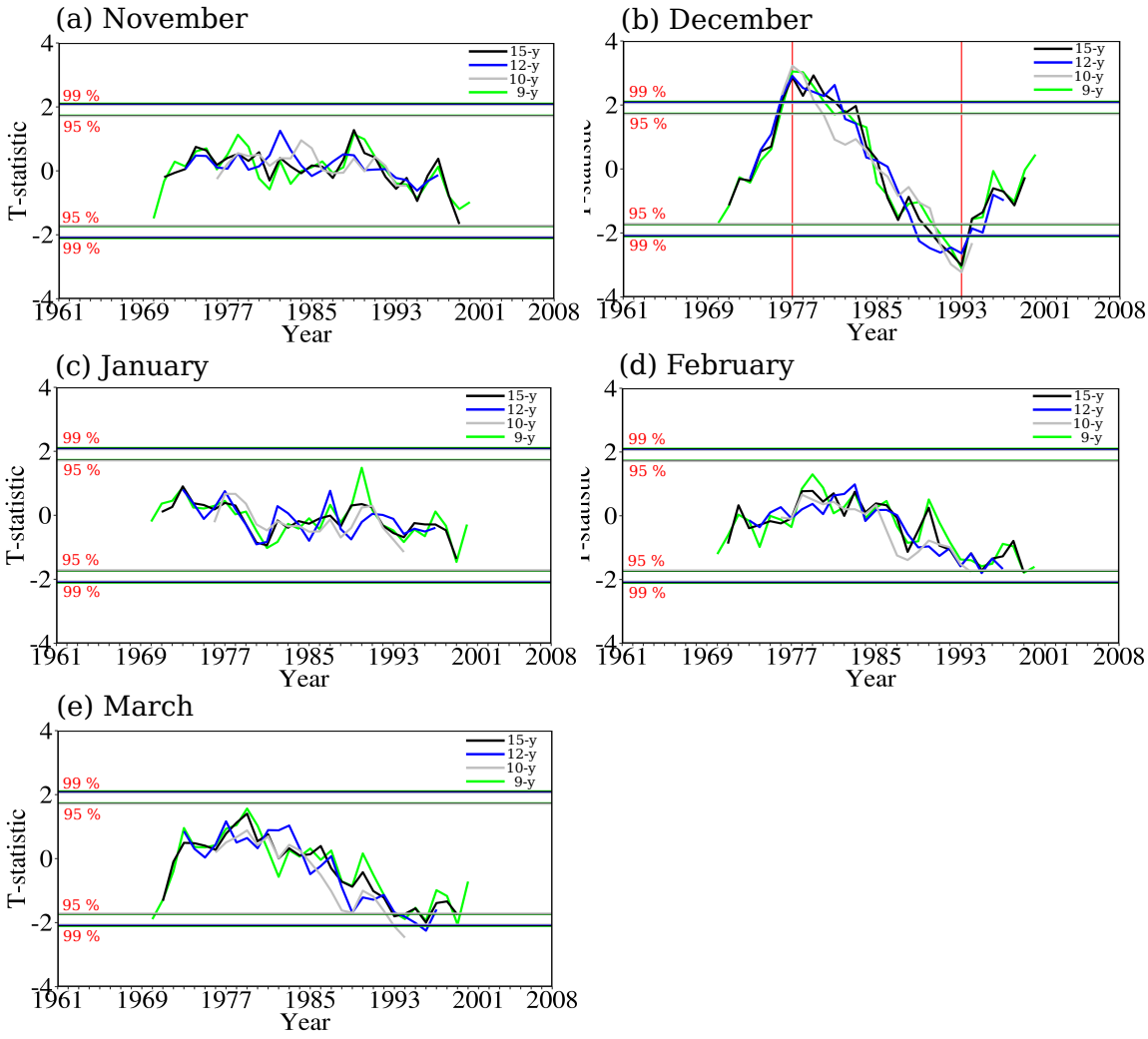

Figure 6.4. Time series of tau statistics from the moving Student's *t*-test with varying time windows for: (a) November; (b) December; (c) January; (d) February; and (e) March. The horizontal lines from (a) to (e) indicate the statistical significance at the 95 % and 99 % confidence level for each time window. The red vertical lines in (b) indicate the significant change points around 1976/1977 and 1992/1993 that divides the time series into three epochs: EW1 (1961–1976); EW2 (1977–1992); and EW3 (1993–2008).

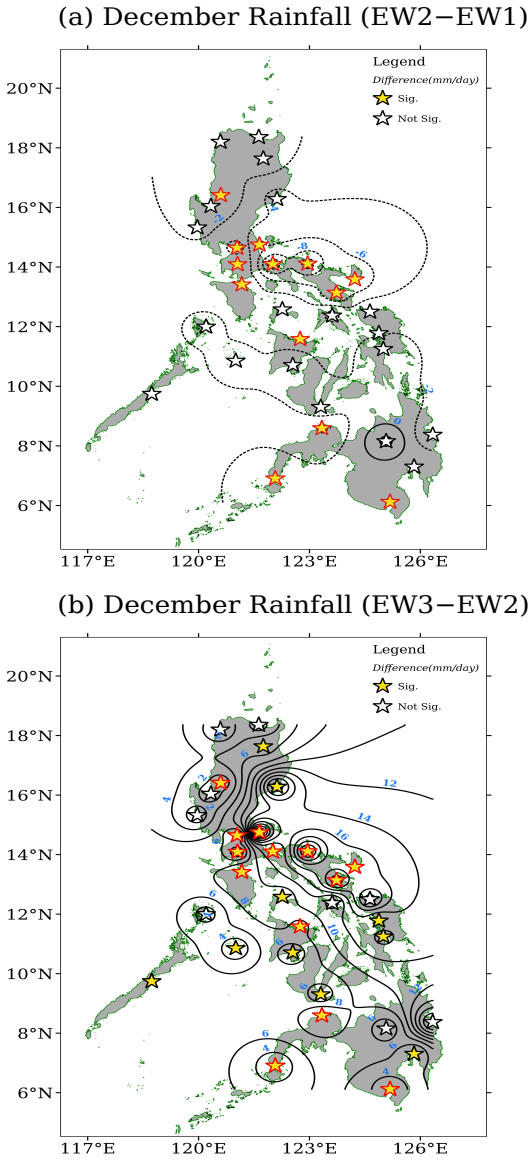

Figure 6.5. Differences in interpolated rainfall (contours) during December between: (a) EW1 (1961–1976) and EW2 (1977–1992) (EW2 minus EW1); and (b) EW2 and EW3 (1993–2008) (EW3 minus EW2) across the 32 PAGASA stations (stars). Negative (positive) contours are indicated by dashed (solid) lines. The contour interval is 2 mm day^{-1}. Yellow shaded stars indicate a significant difference at the 95 % confidence level by bootstrapping. The stars with red outlines indicate the 13 stations with significant difference in both (a) and (b).

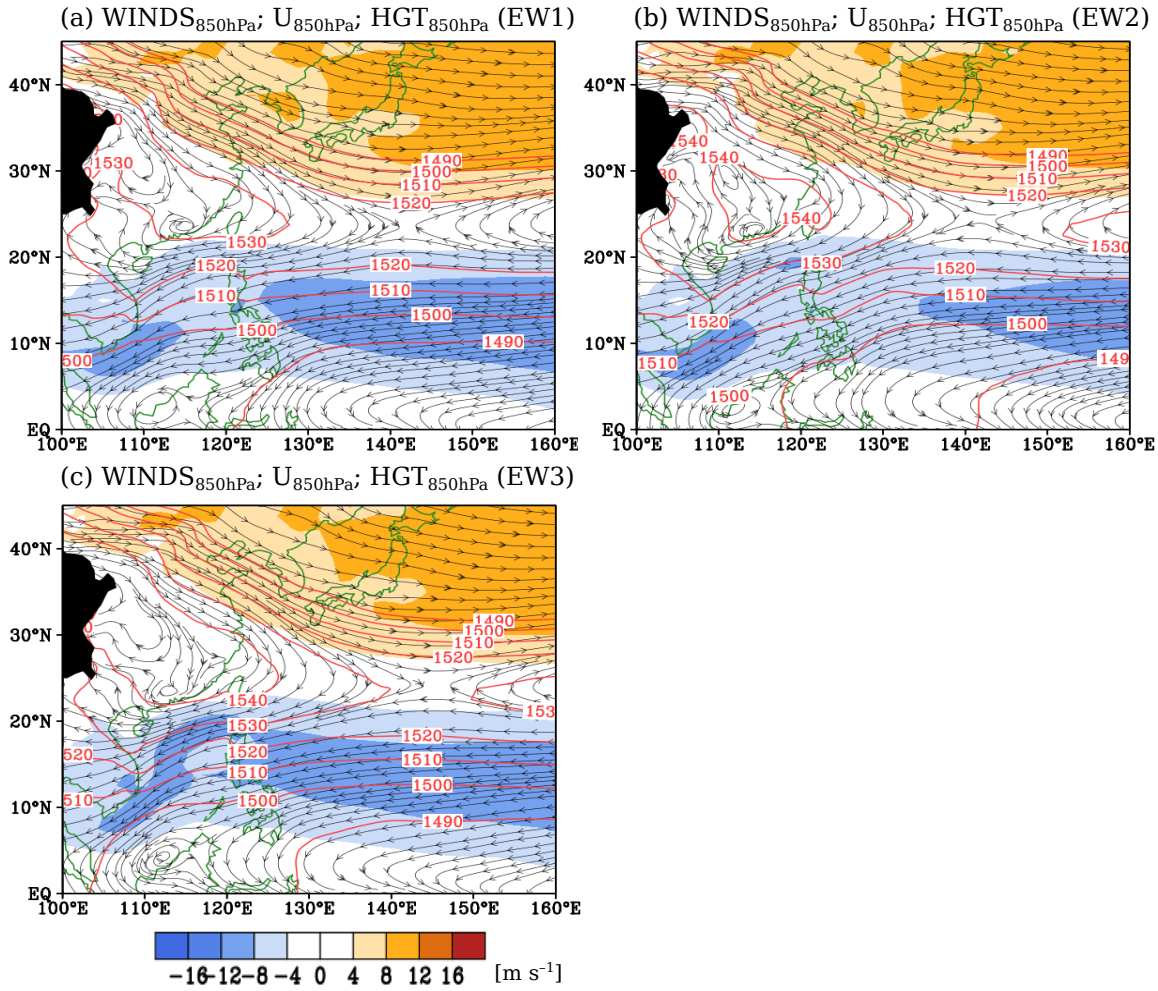

Figure 6.6. The epochal means of 850 hPa winds (*WINDS*$_{850hPa}$; streamlines; m s^{-1}), 850 hPa zonal winds (*U*$_{850hPa}$; shades; m s^{-1}), and 850 hPa geopotential height (*HGT*$_{850hPa}$; contours; m) during December for: (a) EW1 (1961–1976); (b) EW2 (1977–1992); and (c) EW3 (1993–2008). The contour interval is 10 meters.

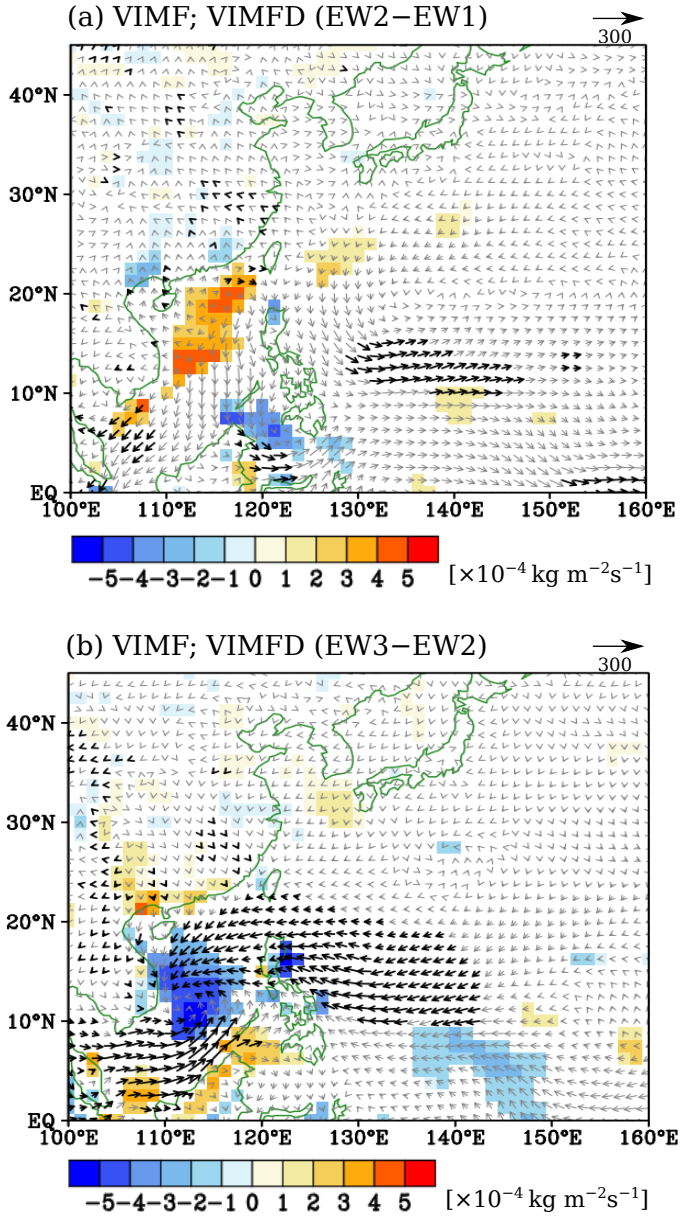

Figure 6.7. The epochal difference in the vertically integrated moisture flux (*VIMF*; vectors; kg m^{-1} s^{-1}) and moisture flux divergence (*VIMFD*; shades; $\times 10^{-4}$ kg m^{-2} s^{-1}) during December between: (a) EW1 (1961–1976) and EW2 (1977–1992) (EW2 minus EW1); and (b) EW2 and EW3 (1993–2008) (EW3 minus EW2). Shaded areas and black vectors indicate statistical significance at the 95 % confidence level by Student's *t*-test. The scale of the wind vectors is indicated on the upper right corner in each plot.

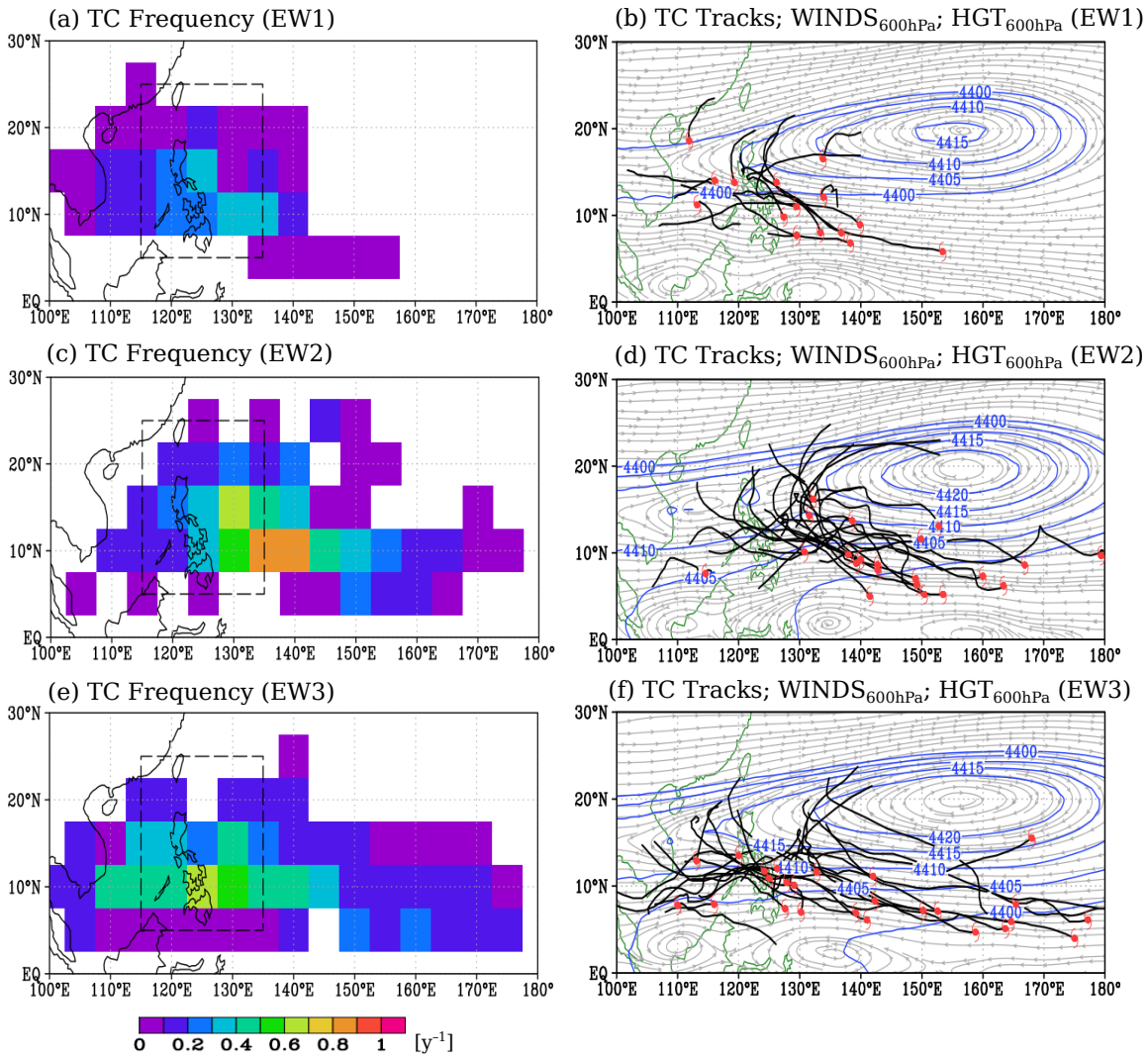

Figure 6.8. Tropical cyclone (TC) track frequency (y^{-1}) interpolated onto a 5° × 5° grid during December, TC tracks (black lines), 600 hPa winds (*WINDS*$_{600hPa}$; gray streamlines; m s^{-1}), and 600 hPa geopotential height (*HGT*$_{600hPa}$; blue contours; m) for: EW1 (1961–1976; a, b); EW2 (1977–1992; c, d); and EW3 (1993–2008; e, f) based on the Joint Typhoon Warning Center (JTWC) track dataset. Dashed boxes in (a), (c), and (e) indicate the Philippine Area of Responsibility (PAR; 115–135°E and 5–25°N). The TC genesis locations in (b), (d), and (f) are indicated by the red markings.

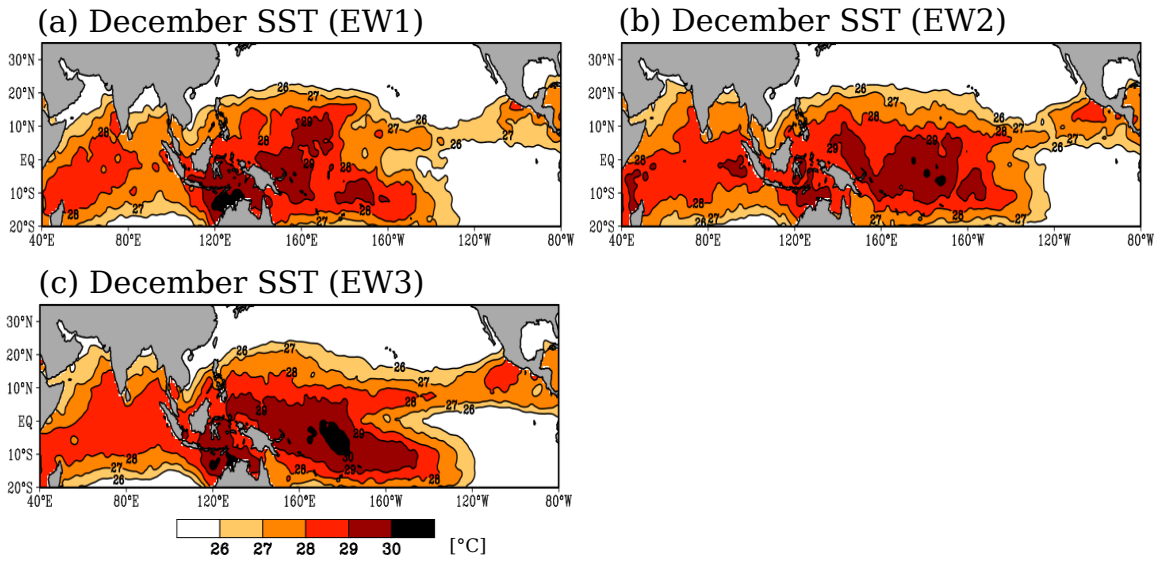

Figure 6.9. Epochal mean of December sea surface temperature (SST; °C) above 26 °C during (a) EW1 (1961–1972); (b) EW2 (1977–1992); and (c) EW3 (1993–2008). The contour interval is 1 °C.

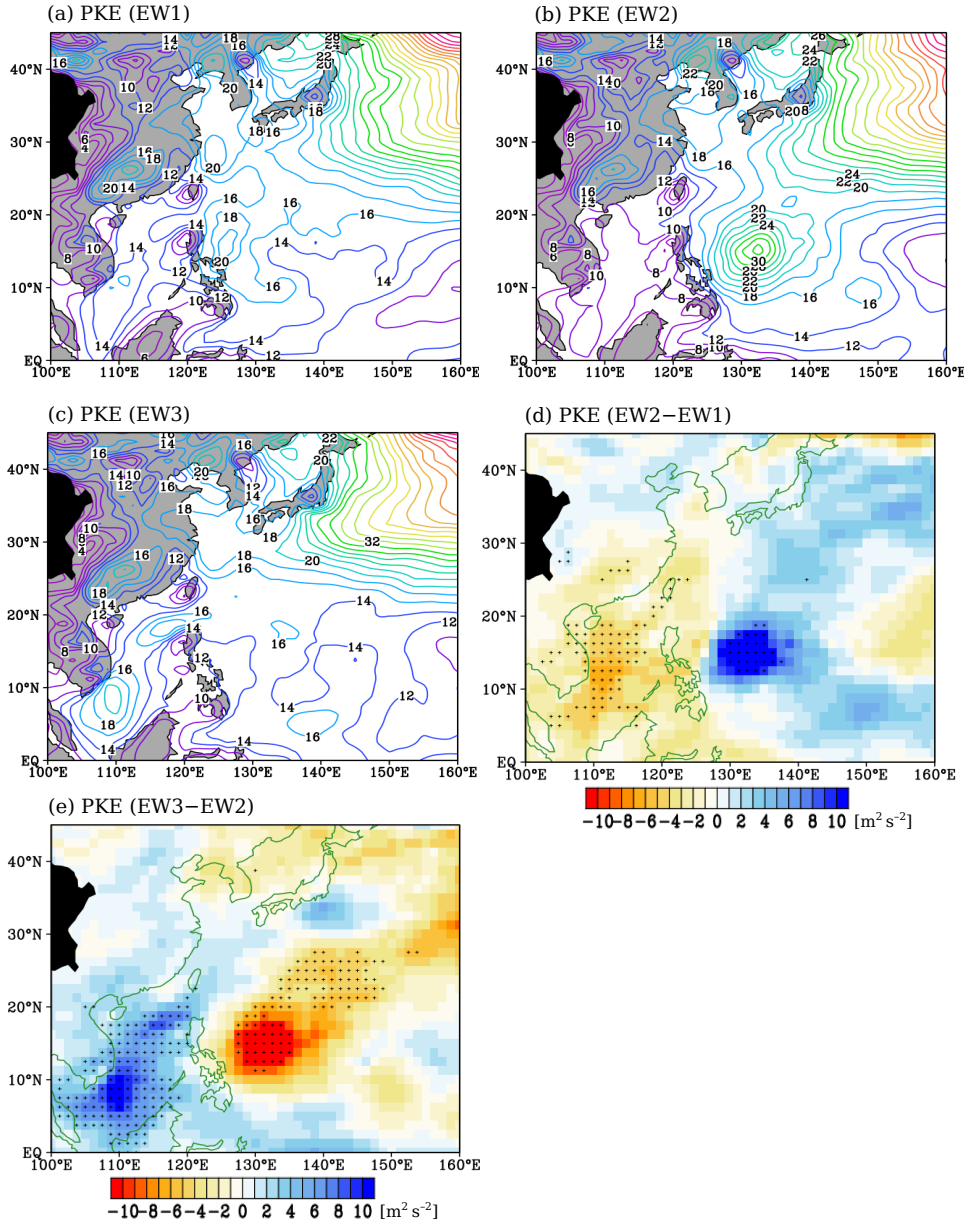

Figure 6.10. Spatial distribution of the mean 850 hPa perturbation kinetic energy (*PKE*; m^2 s^{-2}) during December for: (a) EW1 (1961–1976); (b) EW2 (1977–1992); and (c) EW3 (1993–2008). Epochal difference in *PKE* between (d) EW1 and EW2 (EW2 minus EW1) and (e) EW2 and EW3 (EW3 minus EW2). The contour interval from (a) to (c) is 2 m. Cross markings in (d) and (e) indicate a significant difference at the 95 % confidence level using the Student's *t*-test.

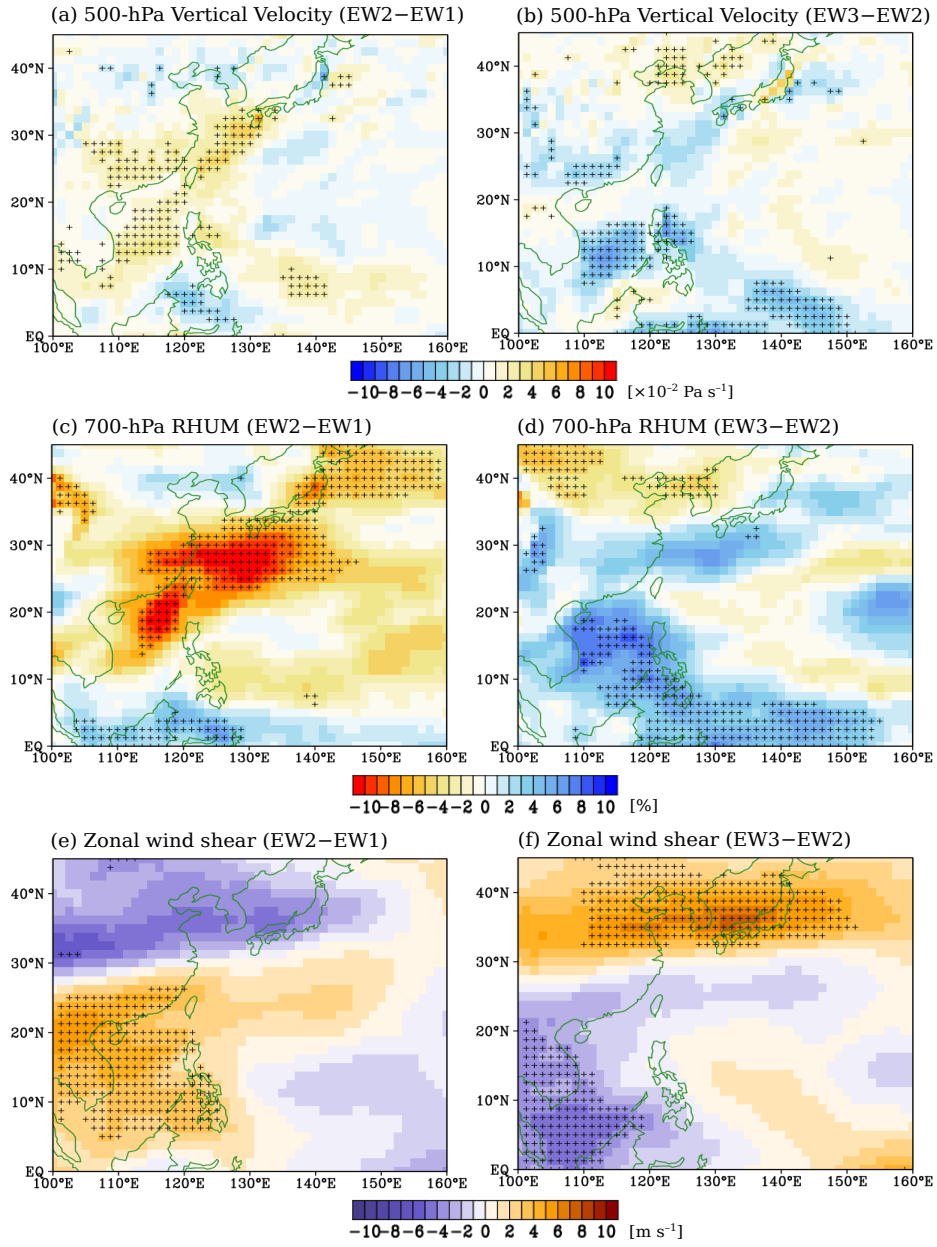

Figure 6.11. Epochal difference in 500 hPa vertical velocity ($\times 10^{-2}$ Pa s^{-1}; a, b), 700 hPa relative humidity (*RHUM*; %; c, d); and vertical zonal wind shear (U_{200hPa} minus U_{850hPa}; m s^{-1}; e, f) during December. Figures 6.11a, c, and e are the differences between EW1 (1961–1976) and EW2 (1977–1992) (EW2 minus EW1). Figures 6.11b, d, and f are the differences between EW2 and EW3 (1993–2008) (EW3 minus EW2). Cross markings indicate statistical significance at the 95 % confidence level using the Student's *t*-test.

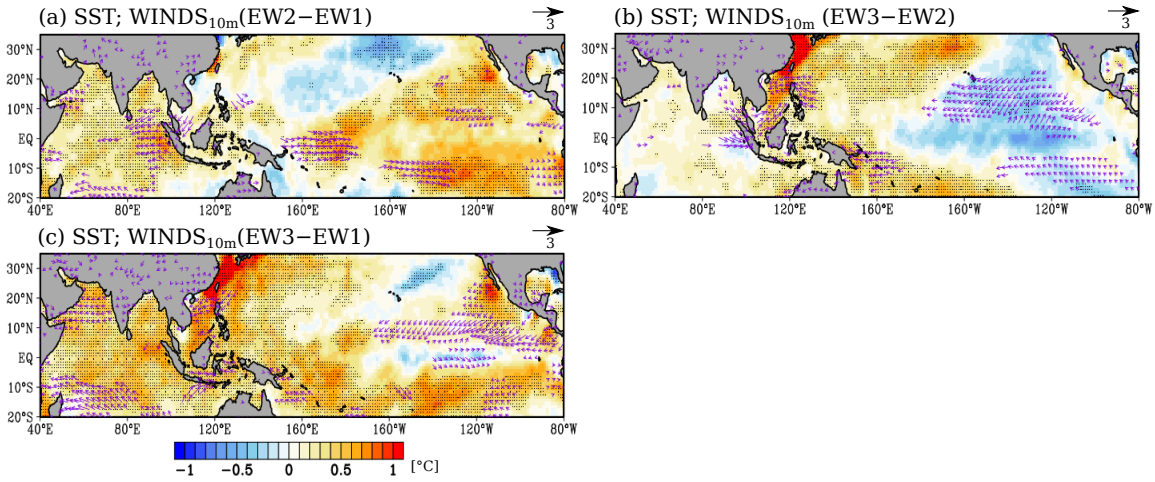

Figure 6.12. Epochal difference in sea surface temperature (SST; °C) and 10-m winds (*WINDS*$_{10m}$; m s^{-1}) in December between: (a) EW1 (1961–1976) and EW2 (1977–1992) (EW2 minus EW1); (b) EW2 and EW3 (1993–2008) (EW3 minus EW2); and (c) EW3 and EW1 (EW3 minus EW1). Stippled areas and vectors in (a), (b), and (c) indicate significant difference at the 95 % confidence level using the Student's *t*-test. The scale of the arrows is indicated on the upper right corner of (a) and (b).

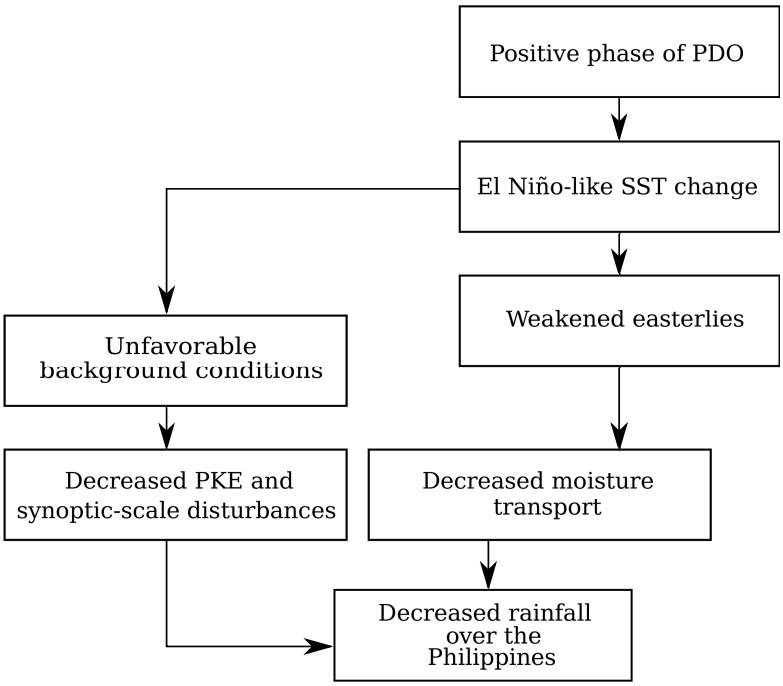

Figure 6.13. Schematic diagram showing the possible mechanisms leading to the decrease in rainfall during December during EW2 (1977–1992) over the Philippines. PDO: Pacific Decadal Oscillation.

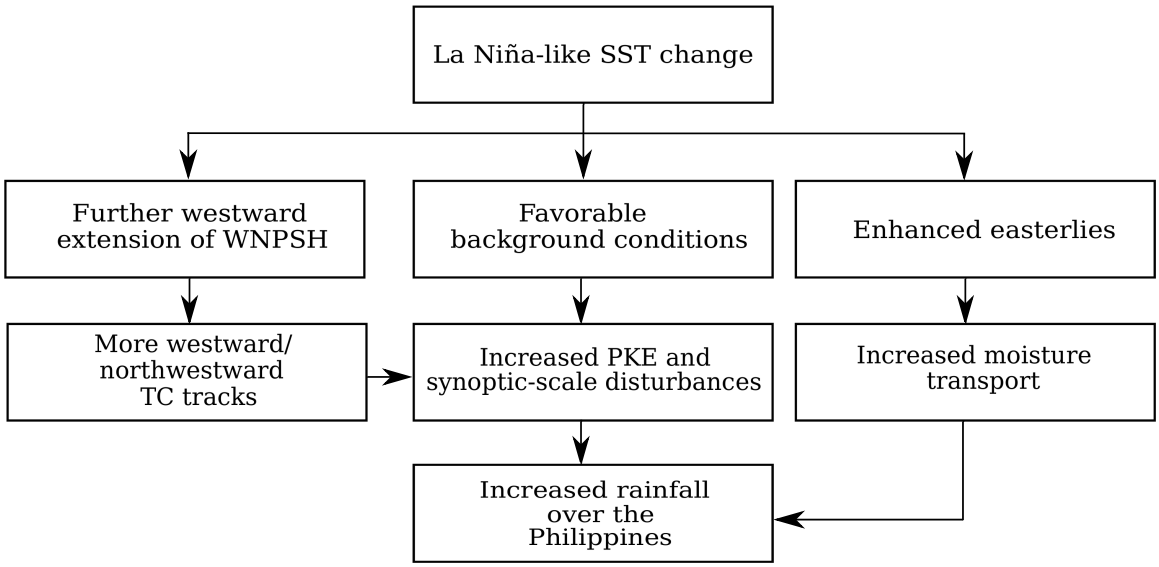

Figure 6.14. As in Fig. 6.13 but for the increase in rainfall during EW3 (1993–2008).

WNPSH: western North Pacific Subtropical High.

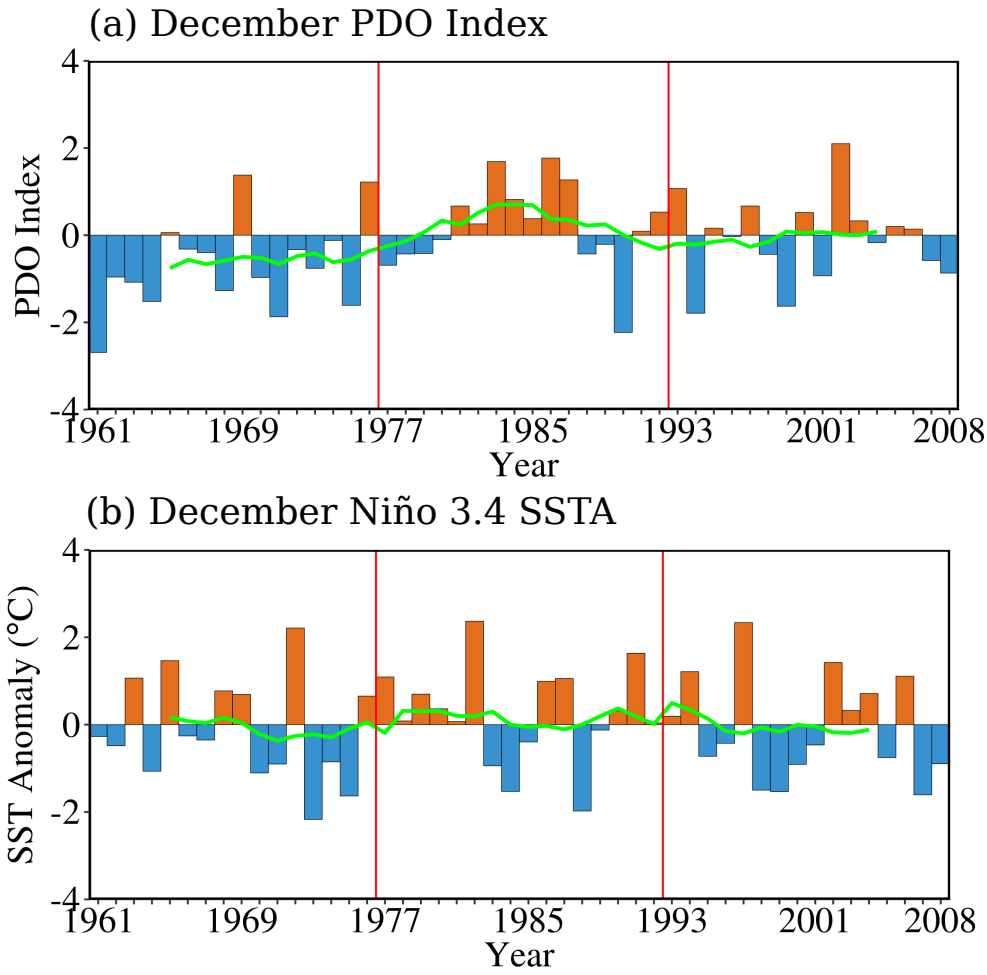

Figure 6.15. Time series of: (a) the December Pacific Decadal Oscillation (PDO); and (b) December SST anomaly (SSTA) over the Niño 3.4 region (5°S–5°N, 170°E–120°W) from the period 1961 to 2008. The green line indicates the 9-year running average. The red vertical lines indicate the change points around 1976/1977 and 1992/1993 based on the December rainfall time series for reference discussion.

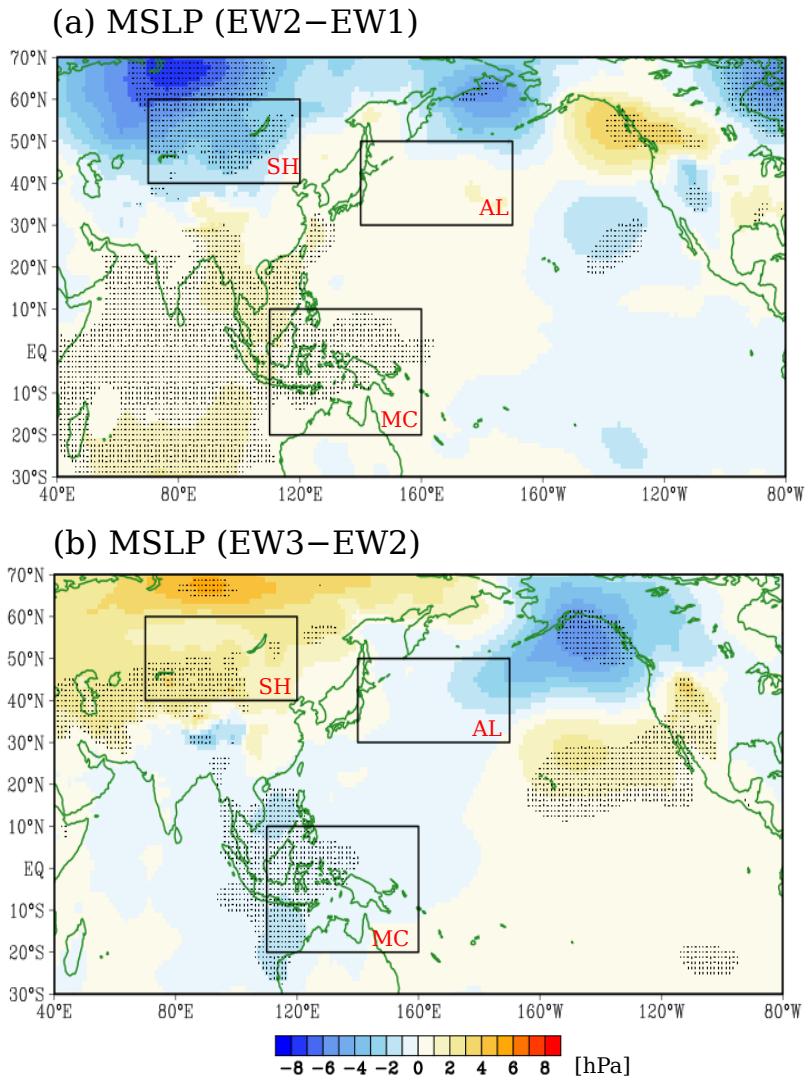

Figure 6.16. Epochal difference in mean sea level pressure (*MSLP*; hPa) during December between: (a) EW1 (1961–1976) and EW2 (1977–1992) (EW2 minus EW1); and (b) EW2 and EW3 (1993–2008) (EW3 minus EW2). Stippled areas indicate statistical significance at the 95 % confidence level using the Student's *t*-test. The boxes indicate the area averaging location for the East Asian winter monsoon index: Siberian high (SH), Aleutian low (AL), and Maritime Continent (MC) low.

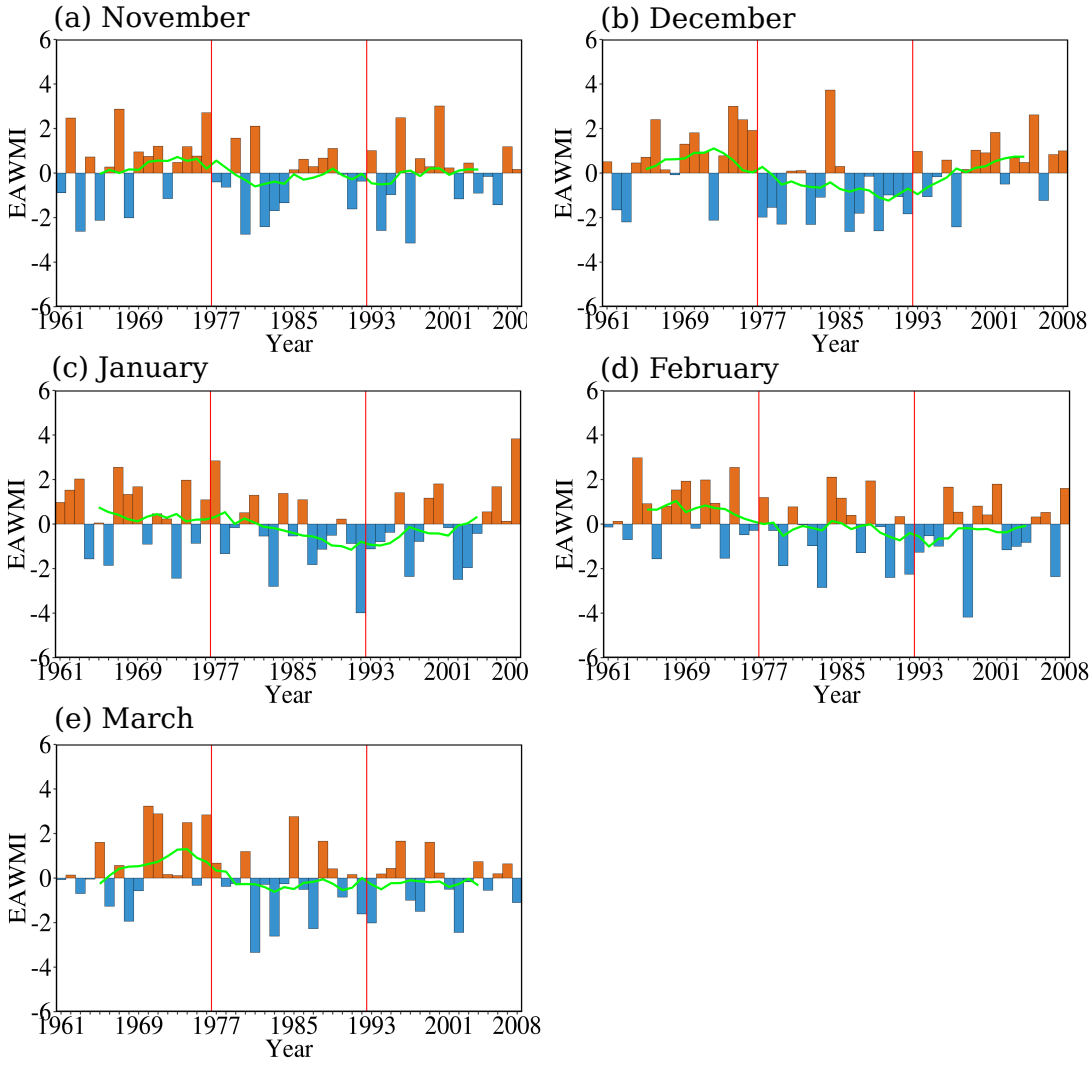

Figure 6.17. Time series of the East Asian winter monsoon index (EAWMI) from 1961 to 2008 for: (a) November; (b) December; (c) January; (d) February; and (e) March. The red vertical lines indicate the change points around 1976/1977 and 1992/1993 based on the December rainfall time series for reference discussion. The green line indicates the 9-yr running average.

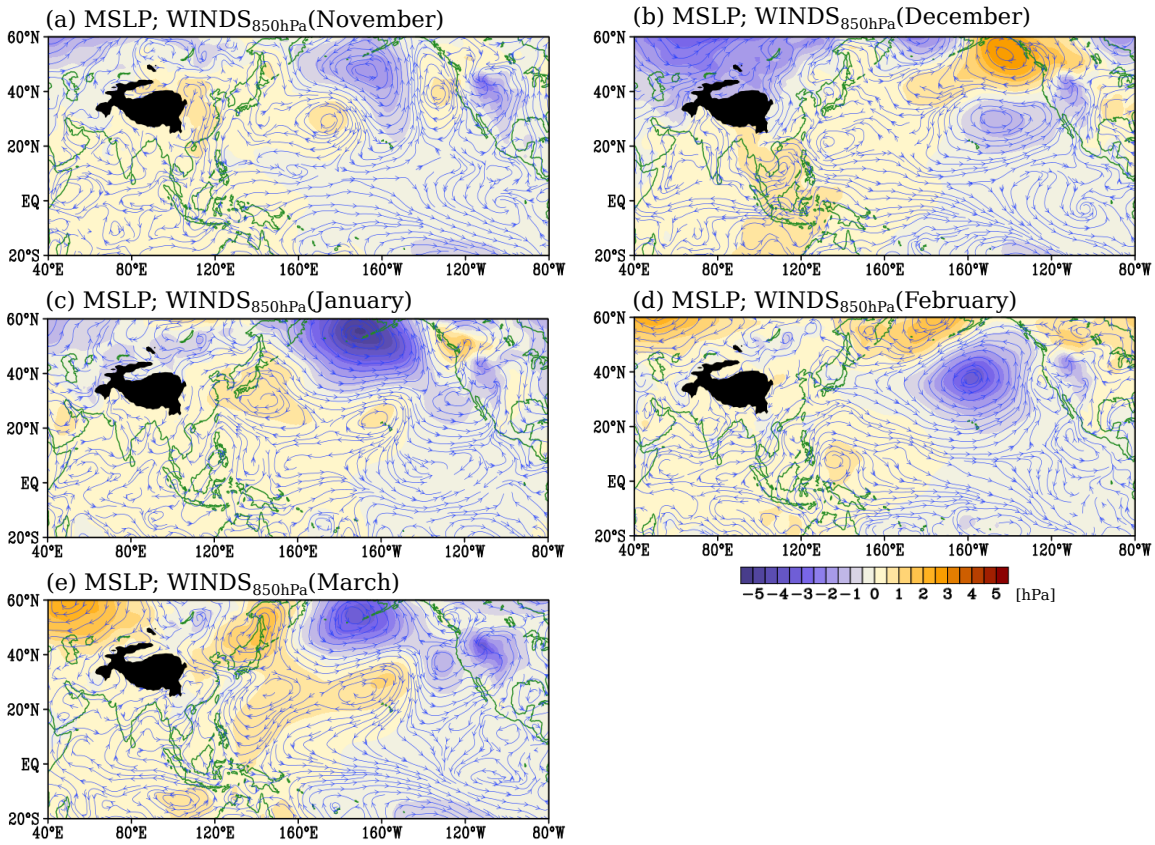

Figure 6.18. Composite anomalies of the mean sea level pressure (*MSLP*; shades; hPa) and 850 hPa winds (*WINDS*$_{850hPa}$; streamlines; m s^{-1}) during EW2 for: (a) November; (b) December; (c) January; (d) February; and (e) March. The anomalies are the deviations from the long-term means (1961–2008).

TABLES

Table 2.1. Classification of the pre-summer monsoon convection over Luzon Island in the Philippines.

Type	**Variables Used**	**Conditions**	**No. of cases (days)**
Type D (Dry days)	*OLR*	*OLR* ≥ 240 W m^{-2}	1459
Type W (Wet days)	*OLR*	*OLR* < 240 W m^{-2}	433
Type W_W (Westerlies)	*OLR*, U_{925hPa}	*OLR* < 240 W m^{-2} U_{925hPa} > 0 m s^{-1}	160
Type W_E (Easterlies)	*OLR*, U_{925hPa}	*OLR* < 240 W m^{-2} U_{925hPa} < 0 m s^{-1}	273
Type W_{EDef}	*OLR*, U_{925hPa}, Deformation parameters at 925 hPa	*OLR* < 240 W m^{-2} U_{925hPa} < 0 m s^{-1} Total Deformation > 0 s^{-1}	52

Table 2.2. List of deformation cases that lasted for at least 2 consecutive days from 1979 to 2012.

Year	Month-Day	Duration (days)
1981	May 17–19	3
1985	April 22–24	3
1986	April 5–7	3
1991	May 28–30	3
1999	April 5–6	2
2000	April 15–16	2
2001	April 25–26	2
2006	May 13–14	2
2008	April 24–26	3
2009	April 25–27	3
2010	April 29–30	2
Average		**2.5**

Table 3.1. Summary of the first post-onset breaks, their duration (days), and timing (days) relative to the onset dates from 1998 to 2012.

Year	First post-onset break	Duration	Number of days relative to the onset
1998	June 3–5	3	11
1999	June 8–12	5	7
2000	May 28–June 2	6	18
2001	May 13–19	7	6
2002	June 10–15	6	18
2003	May 16–21	6	14
2004	May 29–June 1	4	14
2005	June 12–15	4	15
2006	June 28–July 4	7	17
2007	June 3–7	5	9
2008	May 24–May 26	7	13
2009	May 10–13	4	7
2010	June 6–9	4	5
2011	May 31–June 7	8	8
2012	June 21–24	4	23
Average	**June 2**	**5**	**12**

Table 5.1. Summary of change points based on the Pettitt test between the CMAP and PAGASA rainfall datasets.

PERIOD	CMAP	PAGASA
P28–P31	1986/1987	1995/1996*
P33–P36	1992/1993*	1993/1994*
P38–P39	1998/1999	1998/1999
P43–P44	1989/1990	1993/1994*
P45–P50	1993/1994**	1993/1994*
P52–P54	1990/1991	1990/1991*
P59–P60	1999/2000*	1999/2000**

* significant at the 95 % confidence level; ** significant at the 99 % confidence level.

Table 5.2. The seven-station averaged P_{TOTAL}, P_{TC}, and P_{NOTC} for P45–P50 (9 August–7 September) during ES1 (1979–1993) and ES2 (1994–2008).

	ES1 (1979–1993)	**ES2 (1994–2008)**	**Average**
P_{TOTAL} (mm)	651.00	464.11	557.55
P_{TC} (mm)	352.03	160.42	256.22
P_{NOTC} (mm)	298.97	303.69	301.33